Analysis, simulation and control of chaotic behaviour and power electronic converters

ANALYSIS, SIMULATION AND CONTROL OF CHAOTIC BEHAVIOUR IN POWER ELECTRONIC CONVERTERS

by

Ammar Nimer Natsheh

Doctoral Thesis Submitted in partial fulfilment of

the requirements for the award of the degree of

Doctor of Philosophy

of Loughborough University

October, 2008

Supervisor: J. G. Kettleborough

Department of Electronic and Electrical Engineering

ABSTRACT

The thesis describes theoretical and experimental studies on the chaotic behaviour of a peak current-mode controlled boost converter, a parallel two-module peak current-mode controlled DC-DC boost converter, and a peak current-mode controlled power factor correction (PFC) boost converter. The research concentrates on converters which do not have voltage control loops, since the main interest is in the intrinsic mechanism of chaotic behaviour.

These converters produce sub-harmonics of the clock frequency at certain values of the reference current I_{ref} and input voltage V_{in}, and may behave in a chaotic manner, whereby the frequency spectrum of the inductor becomes continuous. Non-linear maps for each of the converters are derived using discrete time modelling and numerical iteration of the maps produce bifurcation diagrams which indicate the presence of sub-harmonics and chaotic operation. In order to check the validity of the analysis, MATLAB/SIMULINK models for the converters are developed.

A comparison is made between waveforms obtained from experimental converters, with those produced by the MATLAB/SIMULINK models of the converters. The experimental and theoretical results are also compared with the bifurcation points predicted by the bifurcation diagrams. The simulated waveforms show excellent agreement, with both the experimental waveforms and the transitions predicted by the bifurcation diagrams.

The thesis presents the first application of a delayed feedback control scheme for eliminating chaotic behaviour in both the DC-DC boost converter and the PFC boost converter. Experimental results and FORTRAN simulations show the effectiveness and robustness of the scheme. FORTRAN simulations are found to be in close agreement with experimental results and the bifurcation diagrams.

A theoretical comparison is made between the above converters controlled using delayed feedback control and the popular slope compensation method. It is shown that delayed

feedback control is a simpler scheme and has a better performance than that for slope compensation.

Keywords: *DC-DC boost converters, AC-DC PFC boost converter, Bifurcation and Chaos theory, and Delayed continuous current feedback controller.*

ACKNOWLEDGEMENTS

First of all, let me express my deepest gratitude to my God for his blessings.

I would like to express my sincere thanks to my supervisor, Mr. Gordon Kettleborough, for his expert guidance, invaluable advice, support, encouragement, and motivation during my PhD study. It is owing to his emphasis on the pragmatic approach by which the research should be carried out that satisfactory results have been achieved in both theoretical and experimental work. I want to thank him for his words of advice on issues related not only to academics but, to life in general. These years in the PhD study were filled with challenging and exciting moments and long evenings in the lab.

My gratitude must go to my Director of Research, Prof. Ivor Smith, for his valuable comments during the research work.

I would also like to express my gratitude to Dr. Natalia Janson, School of Mathematics, for our conceptual discussions on the theory of Chaos, which improved the overall thesis. I am also very grateful to her husband Dr. Alexander Balanov, Department of Physics, for the help with producing the FORTRAN software and his advices with some software under LINUX operating systems.

I would like to thank the Technical Staff of the Department of Electronic and Electrical Engineering for their kind help and advice. In particular, sincere thanks to Mr. Bill Gabb, Mr. Peter Godfrey, and Mr. Chandrakant Mistry.

My deepest gratitude goes to my parents, sisters, and brothers, whose love and support have enabled me to complete this study. I have always cherished the enthusiasm of my father Dr. Nimer, whose scientific prowess has always inspired me to constantly challenge myself and strive hard to achieve this goal. In particular, without my mother's blessings, I could not have achieved whatever little I have today.

Finally, I wish to extend a huge and special thanks to my wife Bahjat and my lovely daughter Rayya for their unconditional support and blessings throughout the years spent at Loughborough. It is this family value and spirit that has given me the strength and motivation throughout my research.

DEDICATION

To my big & small family with love and gratitude
for their patience, moral support, and understanding
during this study

TABLE OF CONTENTS

LIST OF PRINCIPAL SYMBOLS AND ABBREVIATIONS

The following letter symbols are used in this thesis:

L	Inductor
C	Capacitor
R	Load resistor
V_{in}	Input voltage
S	Switch
D	Diode
x	State variable
i_L	Inductor current
v_C	Capacitor voltage
i_{L1}, i_{L2}	Currents through inductors L_1 and L_2 respectively
I_{ref}	Reference current
T	Switching Period
t_n	On-time
t_n'	Off-time
τ_{RC}	Time constant
m_c	Slope of the ramp
m_1	Slope of the increasing inductor current
D_{on}	Switch duty-cycle
$F(t)$	Feedback control force
τ	Time delay
K	Feedback gain
$i_L(t-\tau)$	Delayed inductor current
ω_n	Natural frequency
R_1, R_2	Circuit loop-resistances

The following abbreviations are used:

PFC	Power factor correction
CCM	Continuous conduction mode
DCM	Discontinuous conduction mode
SCM	Slope Compensation Method
DCFM	Delayed Current Feedback Method

CHAPTER 1
INTRODUCTION

1.1 Research Background

The steady-state performance of switched-mode boost converters have been thoroughly investigated, but some aspects of their dynamic behaviour are still not fully understood. Switched-mode converters operating at a fixed switching frequency and employing either peak or average current control have been shown to exhibit sub-harmonic oscillations, with period doubling leading eventually to chaotic behaviour under certain system conditions, whereby the sub-harmonic frequency spectrum is continuous. This behaviour is detrimental, since it results in increased losses, undesirable audible noise, problems with controllability and may cause catastrophic failure of the unit. This thesis is concerned with investigations into the effects of chaos in a single DC/DC boost converter, a two-module parallel input/parallel output DC/DC boost converter and an AC/DC power factor correction (PFC) boost converter. In every case, the converter is operating without an output feedback loop, so that the inherent chaotic behaviour of the converter may be investigated. A robust method for controlling the effects of chaos is presented and this is shown to be effective.

A boost converter has two modes of operation; the continuous conduction mode (CCM), and the discontinuous conduction mode (DCM). The work described in this thesis relates to converters operating in the continuous conduction mode.

The dynamic performance of a converter may be investigated using either numerical or analytical techniques. Numerical methods use either numerical integration algorithms or iterative techniques to produce quantitative results. Although they are accurate, they fail to provide an understanding of the converter behaviour. On the other hand, analytical techniques develop expressions representing the converter operation and provide a qualitative understanding of its performance.

In general, modelling techniques may be classified as continuous or discrete. The most popular continuous-time technique is small signal analysis, whereby the sets of state-space equations for the switched network are replaced by a single set of state-

space equations using state-space averaging [1]. Although averaged models have been employed successfully in many applications, they fail to accurately predict the system behaviour at high frequency [2].

Discrete-time modelling techniques are more accurate and can predict system behaviour in the high frequency region [2]. The switched continuous system is replaced by a discrete-time system that describes the state of the system at the switching frequency. The work described in this thesis is based on these techniques.

DC-DC converters have exhibited several types of nonlinear phenomena including bifurcations and chaos in both the continuous and the discontinuous conduction modes [3-23]. Sub-harmonic instability and chaos has been observed in current-controlled DC-DC boost converters operating in the continuous conduction mode [9, 19]. In these studies, analysis was limited to a single converter. However, modular DC-DC converters are often used in applications where the output current or voltage is shared by two or more modules, to reduce the current or voltage stress on the semiconductors. The system can be parallel-input/parallel-output, or parallel-input/series-output, depending on the connections of the two modules. Al-Mothafar [24] investigated the small-signal and transient behaviour of a two-module parallel-input/series-output DC-DC converter with mutually coupled inductors. However, nonlinear dynamics were not addressed in his paper. In fact, despite the growing popularity of modular converters, their nonlinear dynamic performance has rarely been studied. The work presented in [25-27] describes the nonlinear dynamics in a parallel-input/parallel-output boost converter under a master-slave current-sharing control scheme. One converter has voltage feedback control, while the other has an additional inner current loop that provides the current error information. This is used to adjust the voltage feedback loop and ensure equal sharing of the load current.

This thesis describes the performance of a two-module parallel input/parallel-output boost converter operating under a peak current-mode control scheme, where each module has its own current feedback loop. The unit consists of two boost circuits operating in the continuous-current conduction mode. The effects of tolerances on the values of the energy storage inductors for the two converters are investigated.

A high frequency power factor correction (PFC) boost converter may be used to shape the supply current waveform to meet the arduous statutory requirements of low harmonic content and high power factor. The static conversion properties of this converter have been thoroughly understood since the early 1980s [28-30] and well-known and commercially used by the Unitrode Corporation (Texas Instruments now) in the late 1980s [31-35]. Limited research has been conducted on the chaotic behaviour of this type of converter. The work presented in [36] and [38] investigated the instability of boost PFC converters with average current-mode control, while that described in [37] and [39] investigated the instability under peak current-mode control. Only [36] provided experimental verification of the simulated results, whereas none of the papers provide experimental verification for the peak current-mode control. The current work presents both simulation and experimental results for peak current mode control.

1.2 Thesis Organisation

Chapter 2 describes the operation of a single boost converter and develops an iterative map comprising analytical expressions for the inductor current and the capacitor voltage.

Bifurcation analysis is introduced in Chapter 3 and using the iterative map developed in Chapter 2, the converter behaviour is predicted for various modes of operation using the resulting bifurcation diagram. This is compared with both simulated and experimental results obtained from an experimental converter.

The operation of a two-module boost converter is described in Chapter 4 and both theoretical and experimental results are presented for the converter in Chapter 5, operating under various conditions leading to chaos.

Chapter 6 describes a method for controlling chaos in a single converter, based on the delayed feedback control method developed by Pyragas [43]. The optimum feedback parameters for stability and robustness of control are identified and the scheme is implemented both theoretically and experimentally. MATLAB/SIMULINK models are developed for a converter controlled using both delayed feedback control and the

more common slope compensation method. These are used in Chapter 8 to compare the performance of the two methods.

Chapter 7 presents both a discrete control scheme for the single boost converter and a microcontroller implementation using an ATMEL AT89C51ED2 processor. The software implementation of the microcontroller is described in the chapter.

Chapter 8 presents both experimental and simulated results for the single boost converter using the microcontroller implemented delayed current feedback and the improvement in performance over that of the uncontrolled converter is investigated. The simulated performance of a boost converter using both delayed current feedback and slope compensation are compared.

Chapter 9 describes the operation of an AC/DC PFC boost converter and develops an iterative map for analyzing the circuit behaviour.

The iterative map developed in Chapter 9 is used in Chapter 10 to investigate the performance of the PFC boost converter. An experimental converter was built and this was used to compare the experimental with the simulated performance of the converter.

In Chapter 11, delayed feedback control is again used to control chaos in a PFC boost converter. The scheme is implemented both theoretically and experimentally and is shown to successfully control chaotic behaviour. MATLAB/SIMULINK models are developed for both the slope compensation and delayed feedback control methods and simulations show that the latter method is a more effective approach.

Chapter 12 presents conclusions for the work described in the thesis and suggestions for future work.

The work has resulted in the publication [53-54] of two journal papers "Analysis, simulation and experimental study of chaotic behaviour in parallel-connected DC–DC boost converters" and "Experimental study of controlling chaos in a DC-DC boost converter". Also, a paper was presented [55] to an IEEE International Symposium on

Industrial Electronics at Cambridge University "Control of chaos in a DC-DC boost converter". Two journal papers are in the process of being written and these will be submitted to the IET. The published work is given in Appendix E.

CHAPTER 2

SINGLE BOOST CONVERTER

2.1 Converter Operation

A simplified circuit diagram for a single boost converter is shown in Fig. 2.1. It comprises a controlled switch S , a diode D, an inductor L, a capacitor C, and a load resistor R. The switch is controlled by a current feedback path comprising a fixed frequency clock, a comparator and a flip-flop. The repetitive clock pulse sets the flip-flop, which turns-on the switch. The inductor current increases, storing energy in the magnetic field of the inductor. When the inductor current reaches the reference value I_{ref} , the comparator resets the flip-flop, which turns-off the switch. As a result of Lenz's law, a voltage is induced in the inductor, in such a direction as to try to maintain the current flow. This forward biases the diode D and energy is transferred from the inductor to the capacitor and the load. The magnitude of the reference current determines how much energy is transferred from the input to the output of the converter and consequently the magnitude of the converter output voltage for a given load resistance.

The above circuit operation has two states, depending on whether the controlled switch S is OPEN or CLOSED and these form the basis for the analysis in the next section.

2.2 Iterative Map

To analyse the behaviour of the converter, an iterative map was developed, which requires a difference equation for the system, taking the form

$$x_{n+1} = f(x_n, I_{ref}) \tag{2.1}$$

with

$$x = [i_L \quad v_C]^T \tag{2.2}$$

where i_L is the inductor current and v_C the capacitor voltage.

As mentioned in the previous section, there are two circuit configurations, according to the condition of the switch. Assuming that it is initially closed and neglecting circuit resistance, the inductor current i_L increases linearly until $i_L = I_{ref}$ and any clock pulses arriving prior to this time are ignored. During this interval, the capacitor is providing the energy to the load and the capacitor voltage is decaying. When $i_L = I_{ref}$, the switch opens, and remains open until the arrival of the next clock pulse, at which point it re-closes. During this interval, the energy stored in the inductor is transferred to the capacitor and the load and the capacitor voltage is increasing. Sketches of the waveforms for I_{ref}, i_L and v_C are given in Fig. 2.2.

The two circuit states are treated separately:

***S* Closed**

Diode D blocks at $t = 0$ and the circuit is as shown in Fig. 2.3 (a). Assuming that the switch and inductor resistances are negligible, the circuit equations are

$$L\frac{di_L}{dt} = V_{in} \tag{2.3}$$

$$C\frac{dv_C}{dt} = -\frac{v_C}{R} \tag{2.4}$$

Defining the inductor current i_n at time $t = 0$ and I_{ref} at $t = t_n$, the solution of equation 2.3 is

$$t_n = \frac{L(I_{ref} - i_n)}{V_{in}} \tag{2.5}$$

Defining the capacitor voltage v_n at $t = 0$, the solution of equation 2.4 at $t = t_n$ is

$$v_c(t_n) = v_n e^{-t_n/\tau_{RC}} \tag{2.6}$$

where the time constant $\tau_{RC} = RC$ and t_n is the time at which S opens.

***S* Open**

The switch opens at t_n and D conducts as shown in Fig. 2.3 (b). The circuit equations are now

$$L\frac{di_L}{dt} + v_C = V_{in} \tag{2.7}$$

$$C\frac{dv_C}{dt} + \frac{v_C}{R} = i_L \tag{2.8}$$

Substituting v_C and $\frac{dv_C}{dt}$ from Eq.2.7 into Eq.2.8, results in the second-order differential equation

$$\frac{d^2 i_L}{dt^2} + (\frac{1}{RC})\frac{di_L}{dt} + (\frac{1}{LC})i_L = \frac{V_{in}}{(RLC)} \tag{2.9}$$

The general solution of Eq.2.9 is the sum of the solution of the corresponding homogeneous equation and a particular solution.

The particular solution is obtained by assigning a final value (i_L = constant) in Eq.2.9 after all derivative quantities become zero. Thus

$$i_{Lp}(t) = \frac{V_{in}}{R} \tag{2.10}$$

The solution of the homogeneous equation has a form depending on the roots of the characteristic equation

$$\lambda_{1,2} = -\frac{1}{2RC} \pm \sqrt{\frac{1}{4R^2C^2} - \frac{1}{LC}}$$

or (2.11)

$$\lambda_{1,2} = -\frac{1}{2\tau_{RC}} \pm j\omega$$

where

$$\omega = \sqrt{\frac{1}{LC} - \frac{1}{(2\tau_{RC})^2}} \tag{2.12}$$

Thus, the homogeneous solution is

$$i_{Lh}(t) = e^{-t/2\tau_{RC}}(A_1 \sin \omega t + A_2 \cos \omega t) \tag{2.13}$$

giving the general solution

$$i_L(t) = e^{-t/2\tau_{RC}}(A_1 \sin \omega t + A_2 \cos \omega t) + \frac{V_{in}}{R} \tag{2.14}$$

where the constants A_1 and A_2 are defined by the boundary conditions.

The circuit is described by Eq.2.14 until the next clock pulse arrives, causing the switch to close at time t_n', where

$$t_n' = T[1-(t_n/T)] \tag{2.15}$$

Setting $t=0$ immediately after the switch has opened gives

$$i_L(0) = A_2 + \frac{V_{in}}{R} = I_{ref} \tag{2.16}$$

Thus

$$A_2 = I_{ref} - \frac{V_{in}}{R} \tag{2.17}$$

and

$$v_C(0) = v_n e^{-t_n/\tau_{RC}} = V_{in} - L\frac{di_L}{dt}\Big|_{t=0} \tag{2.18}$$

Using Eq.2.14, and taking the time derivative at $t=0$, gives

$$\frac{di_L}{dt}\Big|_{t=o} = A_1\omega - \frac{A_2}{2\tau_{RC}} \tag{2.19}$$

Solving for A_1

$$A_1 = \frac{\frac{L}{2\tau_{RC}}(I_{ref}') + V_{in} - v_n e^{-t_n/\tau_{RC}}}{\omega L} \tag{2.20}$$

where

$$I_{ref}' = I_{ref} - \frac{V_{in}}{R} \tag{2.21}$$

By definition, $i_{n+1} = i_L(t_n')$, so Eqs.2.14, 2.17, and 2.20 give

$$i_L(t) = e^{-t_n'/2\tau_{RC}}\left[\frac{\frac{L}{2\tau_{RC}}I_{ref}' + V_{in} - v_n e^{-t_n/\tau_{RC}}}{\omega L}\sin\omega t_n' + I_{ref}'\cos\omega t_n'\right] + \frac{V_{in}}{R} \tag{2.22}$$

The derivative $\frac{di_L}{dt}$ is obtained from Eq.2.8 and substituted into Eq.2.7, to give the second-order differential equation in terms of v_C

$$\frac{d^2 v_C}{dt^2} + (\frac{1}{RC})\frac{dv_C}{dt} + (\frac{1}{LC})v_C = \frac{V_{in}}{(LC)} \tag{2.23}$$

The general solution of Eqn.2.23 is the sum of the solution of the corresponding homogeneous equation and a particular solution.

The steady-state solution is given by putting a final value (v_C = constant) in Eq.2.23 after all derivative quantities become zero, thus

$$v_{Cp}(t) = V_{in} \tag{2.24}$$

The solution of the homogeneous equation depends on the roots of the characteristic equation

$$\begin{aligned} \lambda_{1,2} &= -\frac{1}{2RC} \pm \sqrt{\frac{1}{4R^2C^2} - \frac{1}{LC}} \\ \lambda_{1,2} &= -\frac{1}{2\tau_{RC}} \pm j\omega \end{aligned} \tag{2.25}$$

where:

$$\omega = \sqrt{\frac{1}{LC} - \frac{1}{(2\tau_{RC})^2}} \tag{2.26}$$

Thus, the homogeneous solution is

$$v_{Ch}(t) = e^{-t/\tau_{RC}}(B_1 \sin \omega t + B_2 \cos \omega t) \tag{2.27}$$

giving the general solution

$$v_C(t) = e^{-t/\tau_{RC}}(B_1 \sin \omega t + B_2 \cos \omega t) + V_{in} \tag{2.28}$$

where the constants B_1 and B_2 are set by boundary conditions.

Setting $t = 0$ immediately after the switch opens gives

$$v_C(0) = B_2 + V_{in} = v_n e^{-t_n/\tau_{RC}} \tag{2.29}$$

so

$$B_2 = v_n e^{-t_n/\tau_{RC}} - V_{in} \tag{2.30}$$

and

$$i_L(0) = C\frac{dv_C}{dt}\Big|_{t=0} + \frac{v_C}{R} = I_{ref} \tag{2.31}$$

Taking the time derivative of Eq. 2.28 at $t = 0$, gives

$$\frac{dv_C}{dt}\Big|_{t=0} = B_1\omega - \frac{B_2}{2\tau_{RC}} \tag{2.32}$$

from which

$$B_1 = \frac{[\frac{v_n e^{-t_n/\tau_{RC}}}{2\tau_{RC}} - \frac{V_{in}}{2\tau_{RC}} - I'_{ref}/C]}{\omega} \tag{2.33}$$

Since $v_{C(n+1)} = v_C(t'_n)$, from Eqs.2.28, 2.30, and 2.33

$$v_C(t) = V_{in} - e^{-t'_n/2\tau_{RC}}[(\frac{v_n e^{-t_n/\tau_{RC}}}{2\tau_{RC}} - \frac{V_{in}}{2\tau_{RC}} - \frac{I'_{ref}}{C})\frac{\sin\omega t'_n}{\omega} + (V_{in} - v_n e^{-t_n/\tau_{RC}})\cos\omega t'_n] \tag{2.34}$$

Eqns.2.22 and 2.34 comprise a form of mapping for the boost converter, which will be used in chapter 3 to investigate dynamic behaviour of the converter.

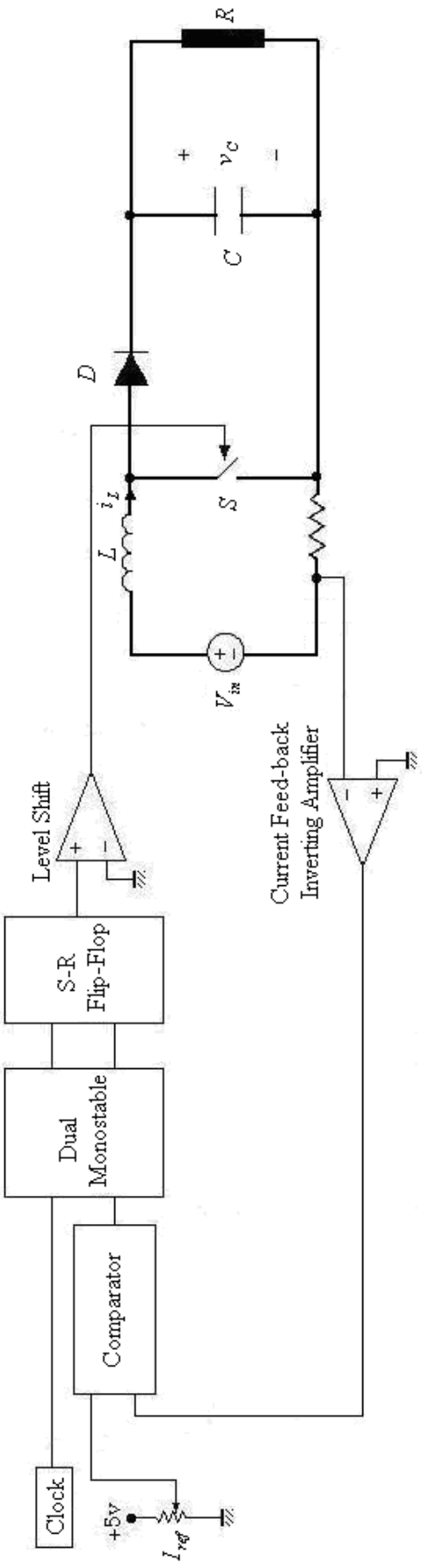

Figure 2.1 Converter circuit diagram.

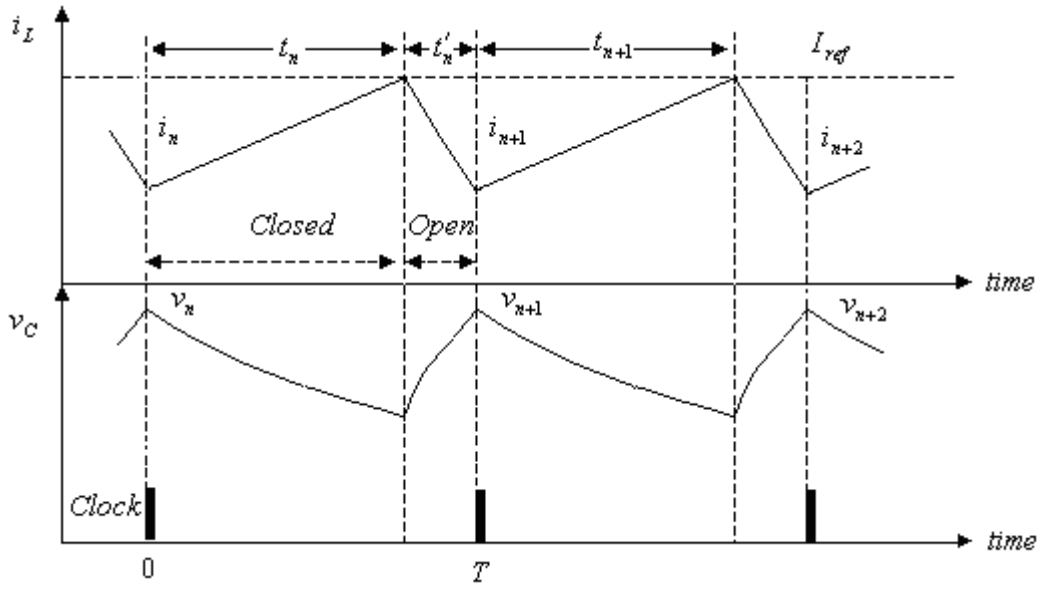

Figure 2.2 Circuit waveforms for Fig. 2.1.

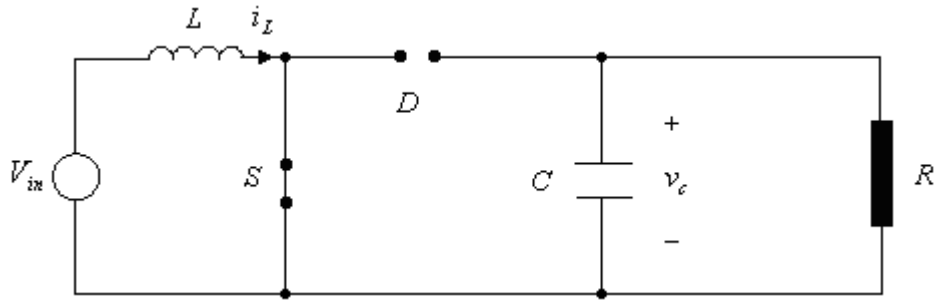

(a) S closed.

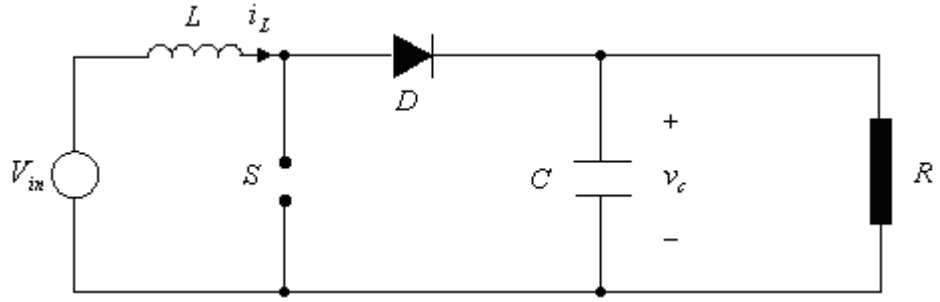

(b) S open.

Figure 2.3 Converter operation.

CHAPTER 3
CHAOS IN A SINGLE BOOST CONVERTER

3.1 Bifurcation Theory and Chaos

Bifurcation theory was originally developed by Poincaré. It is used to indicate the qualitative change in system behaviour, in terms of the number and the type of solutions, under the variation of one or more parameters on which the system depends [40].

In bifurcation theory, the system variables are defined as state variables and control parameters. The relationship between a control parameter and a state variable is called the state-control space. In this space, locations at which bifurcations occur are called bifurcation points. Bifurcations of an equilibrium or fixed-point solution are classified as either *static or dynamic bifurcations*. Examples of static bifurcation are saddle-node, pitch fork, or transcritical bifurcations. *Dynamic bifurcations,* which are also known as Hopf bifurcations, exhibit periodic solutions. With fixed-point solutions, the local stability of the system is determined from the eigenvalues of the Jacobian matrix of the linearized system. With periodic-solutions, the system stability depends on what is known as the Floquet theory and the eigenvalues of the Monodromy matrix that are known in the literature as Floquet or characteristic multipliers. The types of bifurcation are determined from the manner in which the Floquet multipliers leave the unit circle. There are three possible ways for this to happen [40]:

i) If the Floquet multiplier leaves the unit circle through +1, then three possible bifurcations may occur: transcritical, symmetry-breaking, or cyclic-fold bifurcation.
ii) If the Floquet multiplier leaves through -1, a period-doubling (Flip bifurcation) occurs.
iii) If the Floquet multipliers are complex conjugate and leave the unit circle from the real axis, the system exhibits secondary Hopf bifurcation.

A nonlinear system can have a more complicated steady-state behaviour that is not equilibrium, periodic oscillation, or almost-periodic oscillation. Such behaviour is

usually referred to as *Chaos*. Some of these chaotic motions exhibit randomness, despite the deterministic nature of the system [41].

To observe the system dynamics under all the above possible bifurcations, a *bifurcation diagram* may be constructed, which shows the variation of one of the state variables with one of the control parameters. A MATLAB program was written to obtain the bifurcation diagrams for the boost converter. A flowchart for the program is shown in Fig. 3.1 and the program listing is given in Appendix A.1. The parameters used for the study are those obtained from published literature [9] and are given in Table 3.1.

Circuit Components	Values
Switching Period T	$100\mu s$
Input Voltage V_{in}	$10V$
Inductor L	$1mH$
Capacitor C	$10\ \mu F$
Load Resistor R	20Ω

Table 3.1 System parameters.

3.2 Numerical Analysis

The *Bifurcation diagrams* constructed to investigate the system dynamics define the variation of a state variable (v_C or i_L) with a control parameter and relate ($v_{C\,(n+1)}$ or $i_{L\,(n+1)}$) sampled at one instant of switch turn-on, to ($v_{C\,(n)}$ or $i_{L\,(n)}$) at the previous switch turn-on. The MATLAB program required the specification of initial conditions ($v_{C(0)}$ or $i_{L(0)}$) and the reference current I_{ref}. Eqs.2.22 and 2.34 were iterated 750 times. The first 500 iterations were discarded, to eliminate transient conditions and the last 250 were plotted, taking I_{ref} as the bifurcation parameter. I_{ref} was swept from 0.5 to 5.5 A in intervals of 0.05A.

Fig. 3.2 shows the bifurcation diagram for the inductor current as the state-variable, with a supply voltage $V_{in} = 10V$. It is evident from the figure that the system is period-1 until $I_{ref} = 1.68A$. Over this region, the inductor current i_L, has a single

unique value at the instant of every switch turn-on. As an example, consider $I_{ref} = 1.0A$ in Fig. 3.2. The single value of i_L at switch turn-on is i_L = 0.75A. At $I_{ref} = 1.68A$ one of the Floquet multipliers leaves the unit circle through -1, producing a period-doubling bifurcation (period-2). During period-2, the inductor current has two unique values at alternate instants of turn-on. For example, with I_{ref} = 2A, i_L alternates between 1.15 and 1.9A at switch turn-on. As I_{ref} increases further, the system undergoes stable period-3 operation, and eventually becomes chaotic at I_{ref} = 2.7A, with the value of i_L at each turn-on having many values. The diagram indicates that the system is stable for lower values of I_{ref} and becomes unstable as it increases.

Fig. 3.3 shows bifurcation diagrams for the inductor current and the capacitor voltage, with a fixed reference current I_{ref} = 3A, as the input voltage bifurcation parameter V_{in} is swept from 5 to 25V in 1V intervals. It is evident that in these diagrams, the period-doubling route to chaos is from right to left, as opposed to the one obtained when I_{ref} was the control parameter. Thus the system is more stable for higher values of V_{in} and becomes more unstable as V_{in} is reduced.

An interesting comparison may be made between the bifurcation diagrams of Figs. 3.2 and 3.3(a). In the former, the system is chaotic at a value of I_{ref} = 3A, with the inductor current i_L at switch turn-on having many values between 3.0A and 1.5A. In the latter, at a value of V_{in} = 10V, the system is again chaotic, with the inductor current i_L at turn-on again having many values between 3A and 1.5A. In fact, these two cases are the same and constitute a single situation in a 3-dimensional state-control space, with orthogonal axes I_{ref}, i_L and V_{in} assuming the conventional axes x, y and z.

3.3 Experimental Implementation

To verify the theoretically obtained bifurcation diagrams, an experimental converter using the parameters of Table 3.1 was built. The circuit diagram is shown in Fig. 3.4 and a photograph of the hardware is given in Appendix D.1.

A 10 kHz clock signal is obtained using an LM555 integrated circuit. The rising edge of the clock signal triggers a 74HCT123N monostable to drive the set input of an S-R flip flop constructed using 2-input NOR gates and 3-input AND gates. The output of the flip-flop is applied to a 311 comparator, which drives the gate of the MOSFET switch.

The inductor current i_L is sensed using a 0.2Ω non-inductive resistor in series with the source of the MOSFET switch. This signal is amplified using a TL071 connected as an inverting amplifier, and the output is compared with a voltage representing the reference current I_{ref} using a 311 comparator. The output of the comparator resets the flip-flop to generate the drive signal explained in section 2.1.

3.4 MATLAB/SIMULINK Model

A MATLAB/SIMULINK model was developed based on the system equations:

$$\begin{aligned} \frac{di_L}{dt} &= \frac{1}{L}[v_{in} - v_C(1-u_S)] \\ \frac{dv_C}{dt} &= \frac{1}{C}[-\frac{v_C}{R} + i_L(1-u_S)] \end{aligned} \tag{3.1}$$

where u_S takes the value 0 or 1, which modifies Eq.3.1, depending on whether the switch is closed or open.

The structure of the SIMULINK model is given in Fig. 3.5.

3.5 Experimental and Simulated Results

The experimental and simulated inductor current waveforms, harmonic spectra and phase portraits relating the inductor current to the capacitor voltage, for different values of the bifurcation parameter I_{ref} and an input voltage $V_{in} = 10V$ are given in Figs. 3.6 to 3.8.

Fig. 3.6 shows the results for period-1 operation with $I_{ref} = 1A$. The experimental inductor current of Fig. 3.6(a) shows steps at the instances at which the MOSFET switch turns-on and turns-off. This is due to differential noise in the circuit. The

value of i_L at the instant of switch turn-on is 0.7A, which compares favourably with the bifurcation diagram of Fig 3.2. The predominant harmonic is the fundamental (10 kHz) with an observable second harmonic (20 kHz). The experimental phase portrait of Fig. 3.6(c) shows the characteristic period-1 single loop trajectory. The channel 1 and channel 2 inputs to the oscilloscope are AC coupled to eliminate the DC offsets in the signals, otherwise the phase portrait would be very small.

Fig. 3.7 shows the results for period-2 operation with $I_{ref} = 1.7A$. The two values of i_L at turn-on are 1.1A and 1.35A, which again agree with the bifurcation diagram of Fig. 3.2. The period-2 sub-harmonic is clearly seen in both the experimental and simulated harmonic spectra, and it is evident that the sub-harmonic is larger than the fundamental. The phase portrait has the characteristic period-2 trajectory.

Fig. 3.8 shows results for chaotic behaviour with $I_{ref} = 3A$. As expected, the value of i_L at turn-on is unpredictable and the sub-harmonic frequency spectrum has become continuous. The magnitude of the fundamental (the nominal switching frequency) in the experimental spectrum is small.

All the results are in good agreement with the theoretically obtained bifurcation diagram and the phase portraits corresponding to these three cases clearly demonstrate period-1, period-2, and chaotic behaviour. The harmonic spectrum in the chaotic region is continuous, unlike that for period-1, which contains a fundamental component. The results of Figs 3.6 to 3.8 also show good agreement with those obtained from the MATLAB/SIMULINK model, giving confidence in the model's ability to predict chaotic behaviour in the converter.

The inductor current and capacitor voltage waveforms, with different values of the bifurcation parameter V_{in} and a fixed reference current (I_{ref} = 3A) are given in Figs. 3.9 to 3.11. Fig. 3.9 shows the results for period-1 operation with $V_{in} = 20V$. In this case, the value of i_L is 2.2A and v_C is 35V at the instant of switch turn-on, which agrees with the bifurcation diagrams of Figs. 3.3(a) and (b) respectively.

Fig. 3.10 shows the results for period-2 operation with $V_{in} = 17V$. In this case, i_L alternates between 1.9A and 2.7A and v_C alternates between 30V and 33V at switch turn-on. Fig. 3.11 shows results for chaotic behaviour with $V_{in} = 10V$. Again, the figures are in good agreement and agree with the bifurcation diagrams of Fig. 3.3.

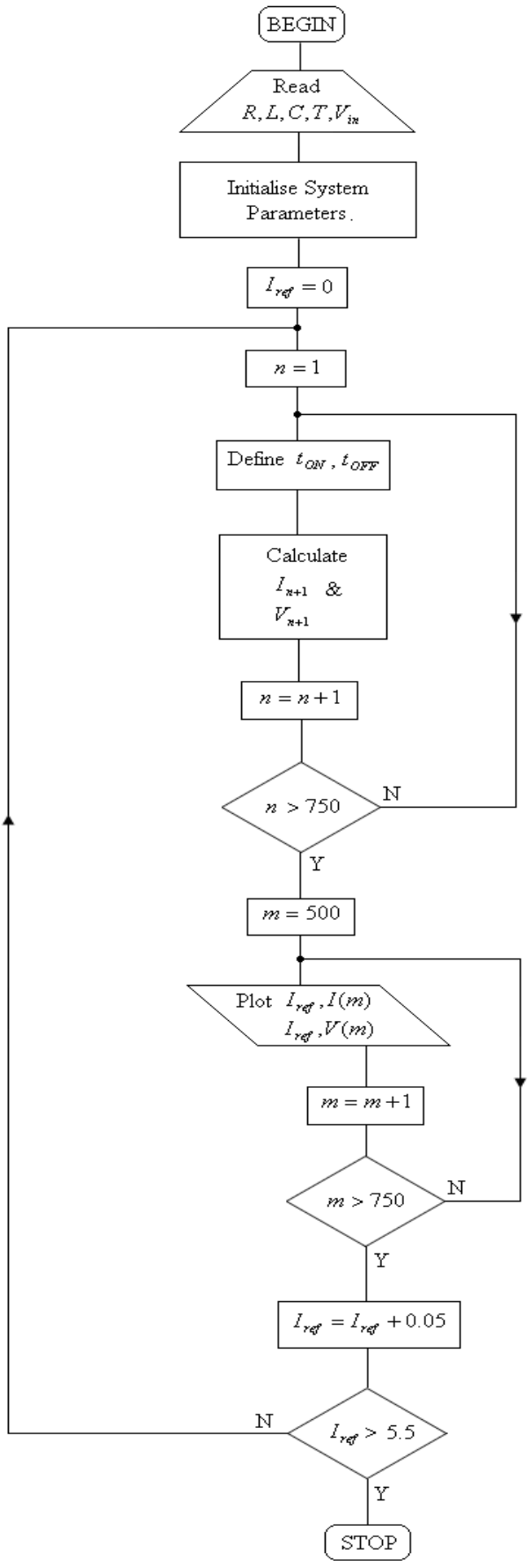

Figure 3.1 Bifurcation program flowchart.

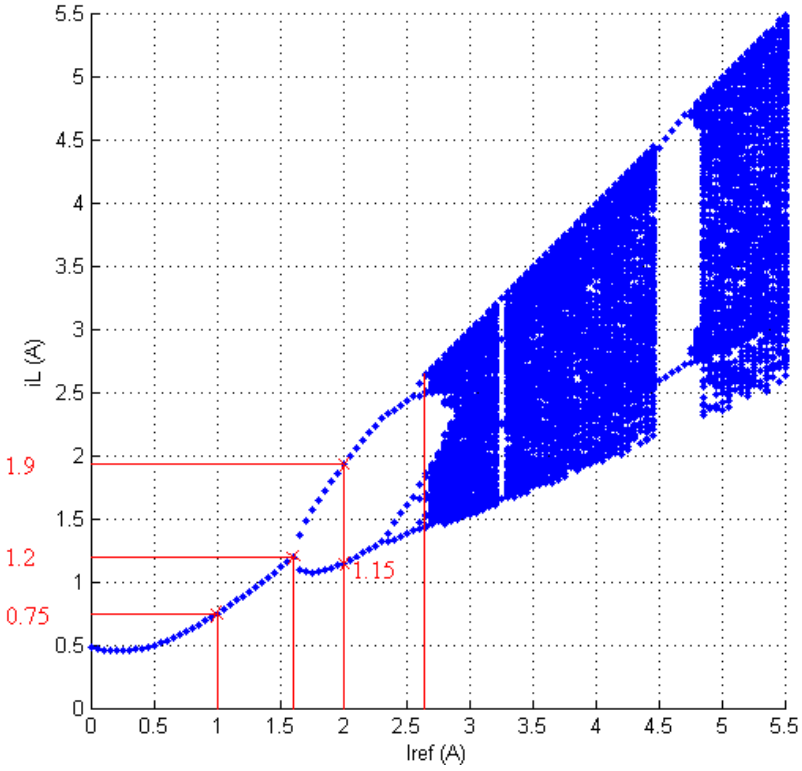

Figure 3.2 Bifurcation diagram for i_L with I_{ref} as the control parameter $V_{in} = 10V$.

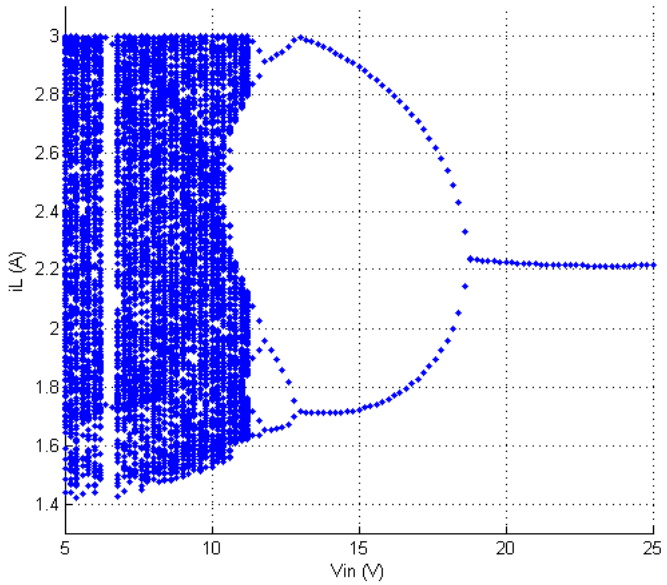

(a)

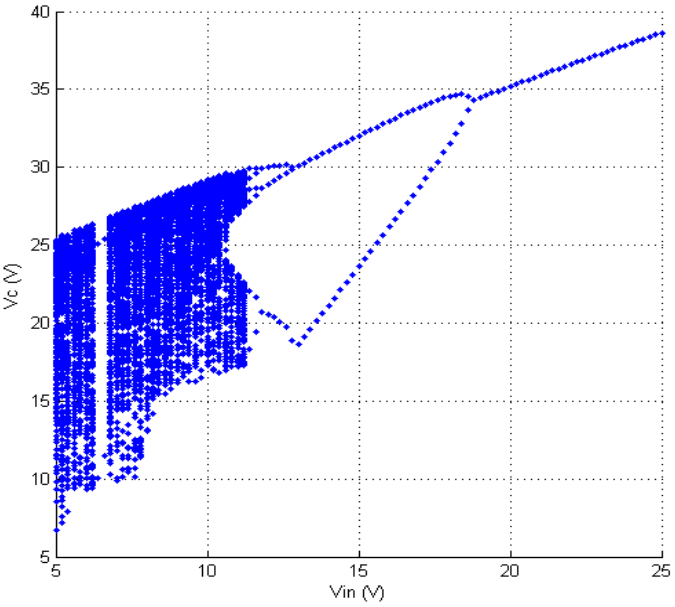

(b)

Figure 3.3 Bifurcation diagrams for i_L and v_C with V_{in} as the control parameter ($I_{ref} = 3\text{A}$).

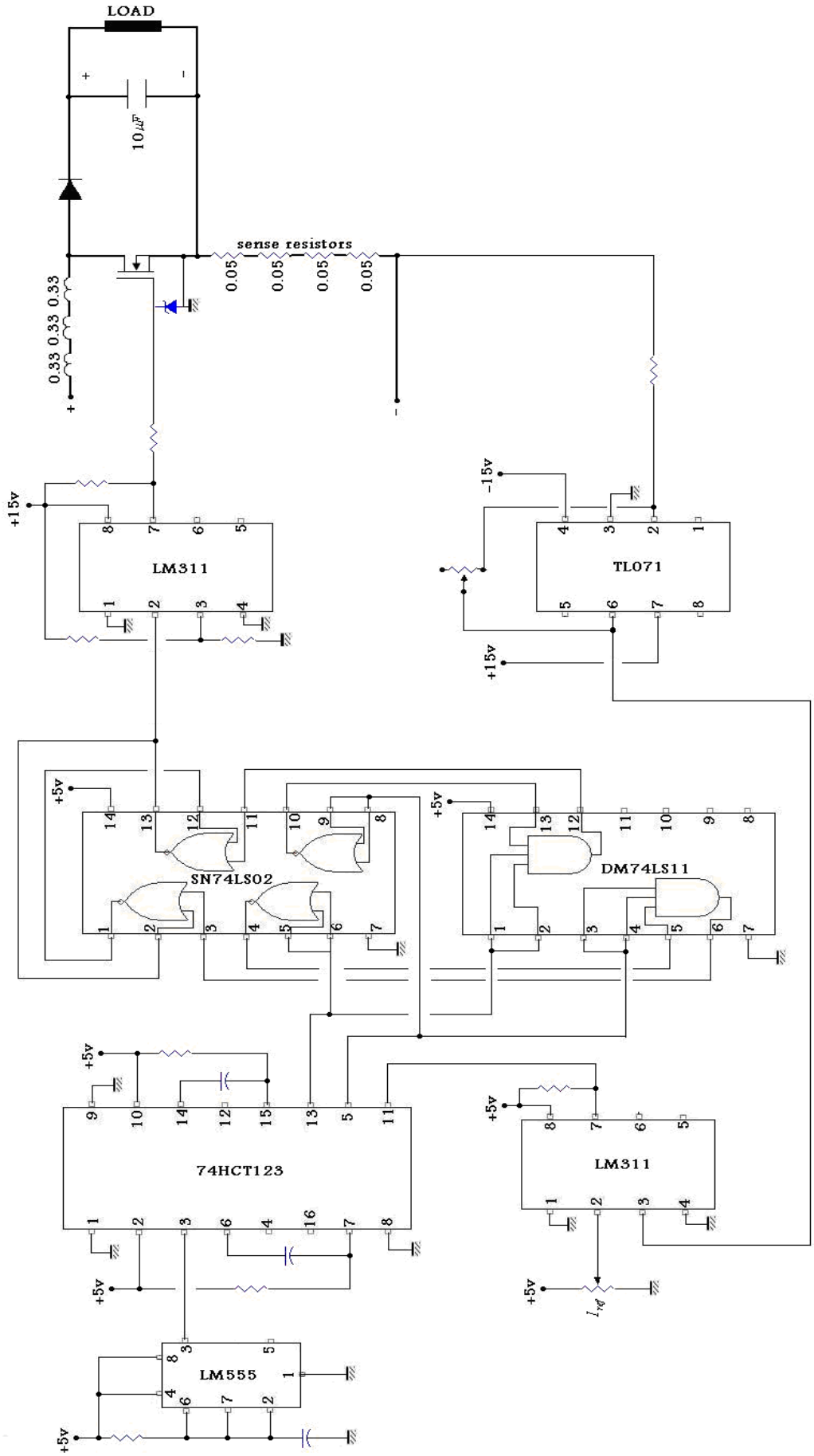

Figure 3.4 Single boost converter hardware.

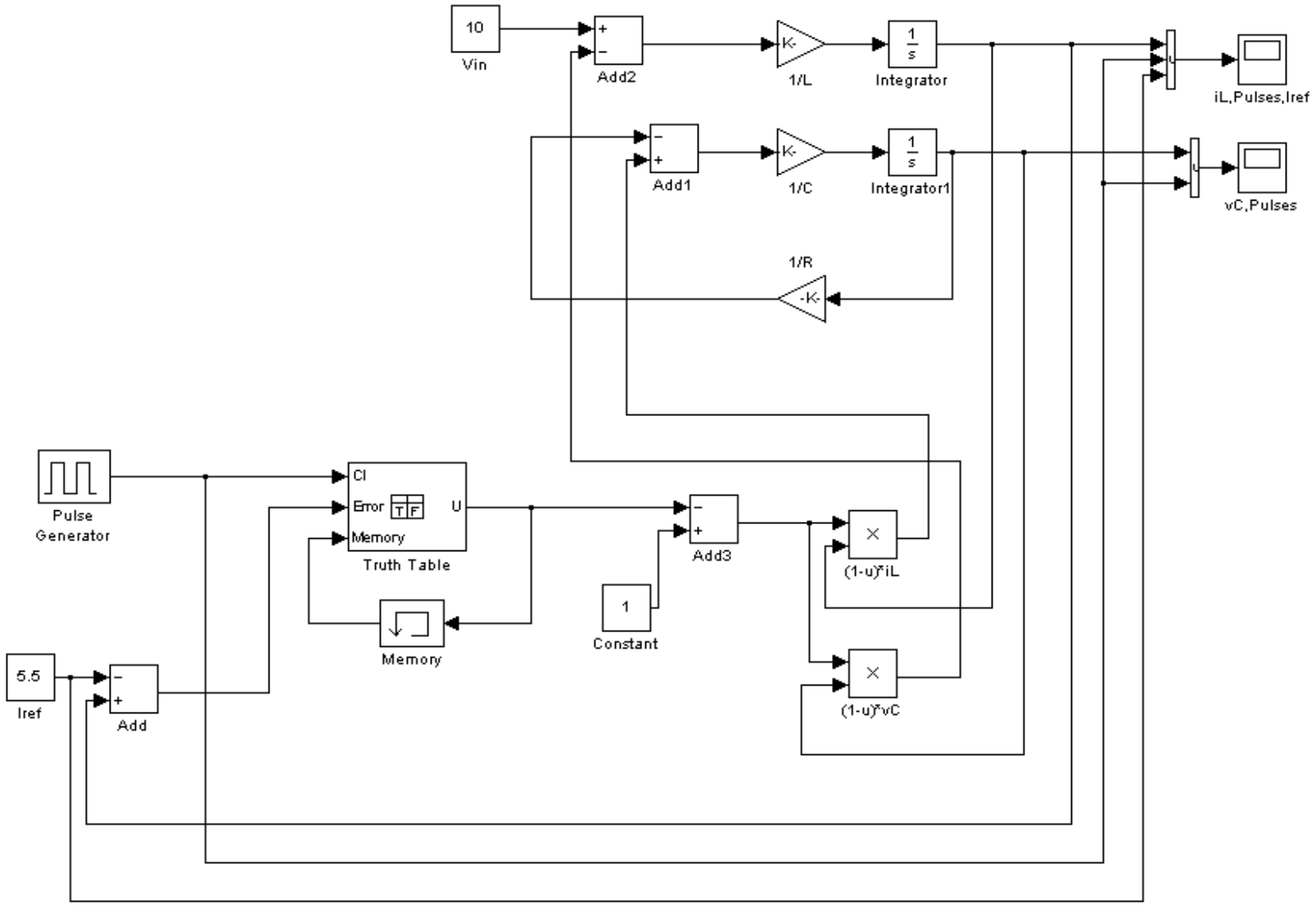

Figure 3.5 MATLAB/SIMULINK model for a single boost converter.

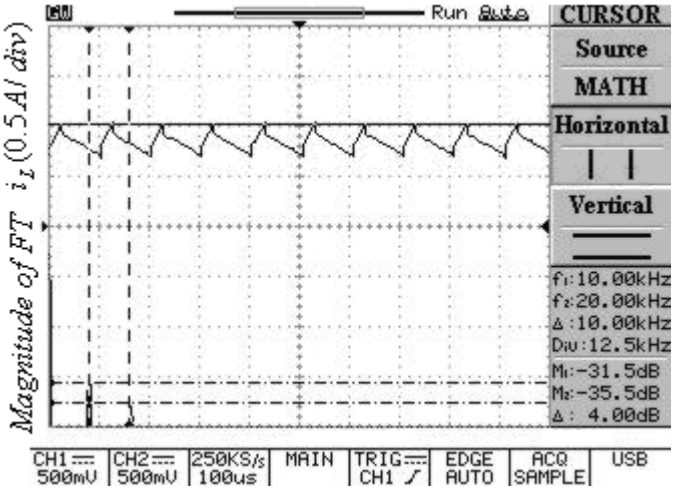

(a) Experimental inductor current and frequency spectrum (1A/V).

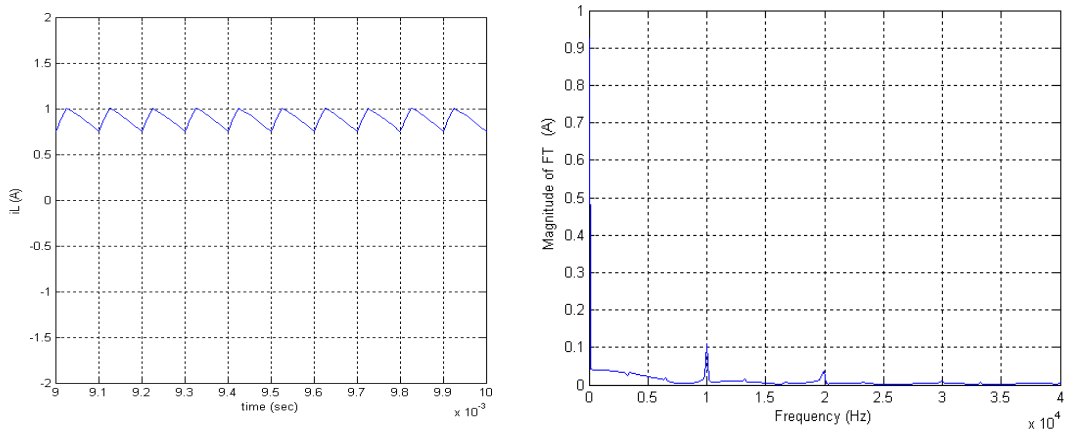

(b) Simulated inductor current and frequency spectrum.

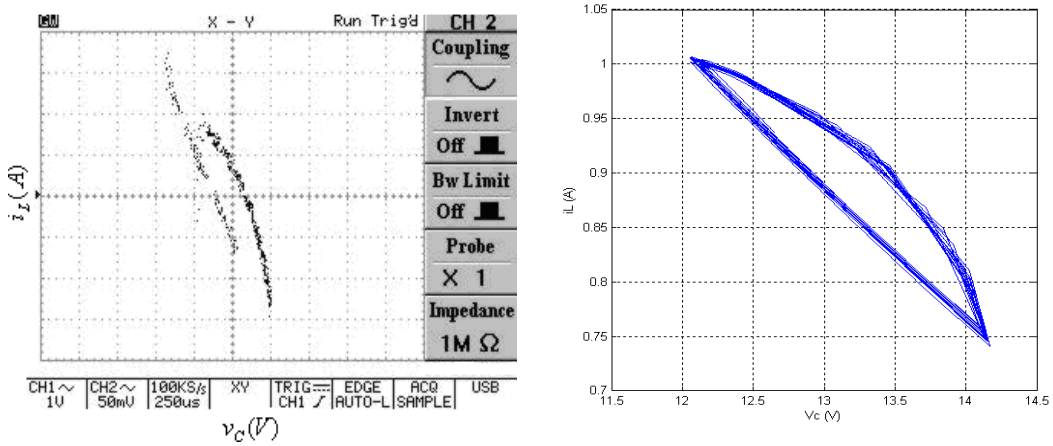

(c) Experimental and simulated phase portrait.

{**Left**: experimental, CH2 (1A/V), **right**: simulated}.

Figure 3.6 Period-1 at $I_{ref} = 1A$.

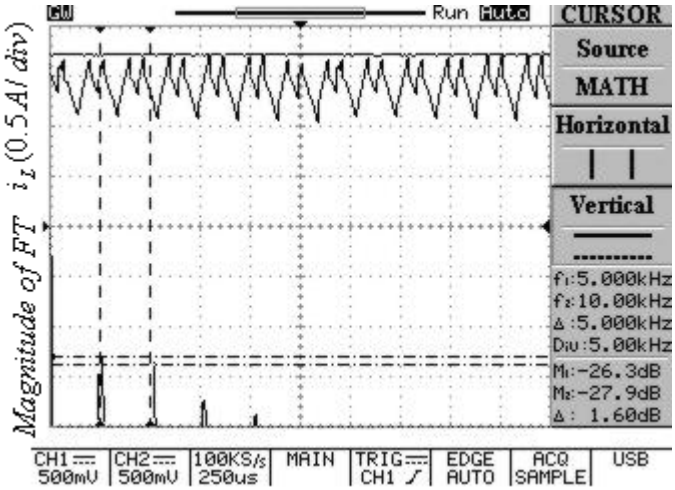

(a) Experimental inductor current and frequency spectrum (1A/V).

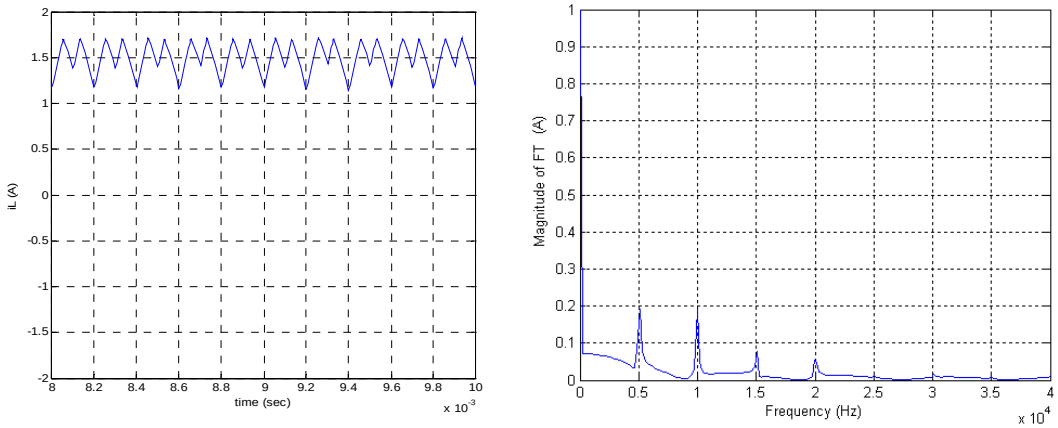

(b) Simulated inductor current and frequency spectrum.

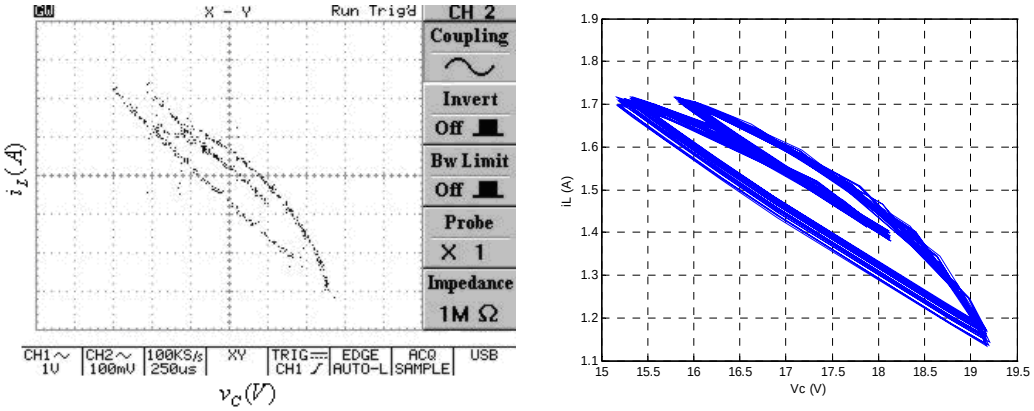

(c) Experimental and simulated phase portrait.

{**Left**: experimental, CH2 (1A/V), **right**: simulated}.

Figure 3.7 Period-2 at $I_{ref} = 1.7A$.

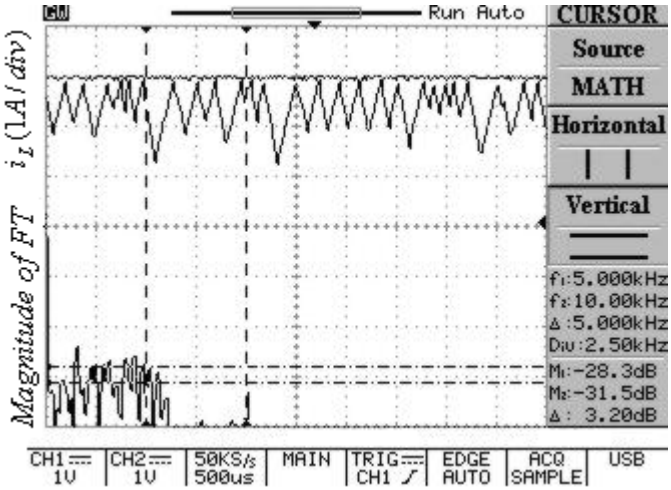

(a) Experimental inductor current and frequency spectrum (1A/V).

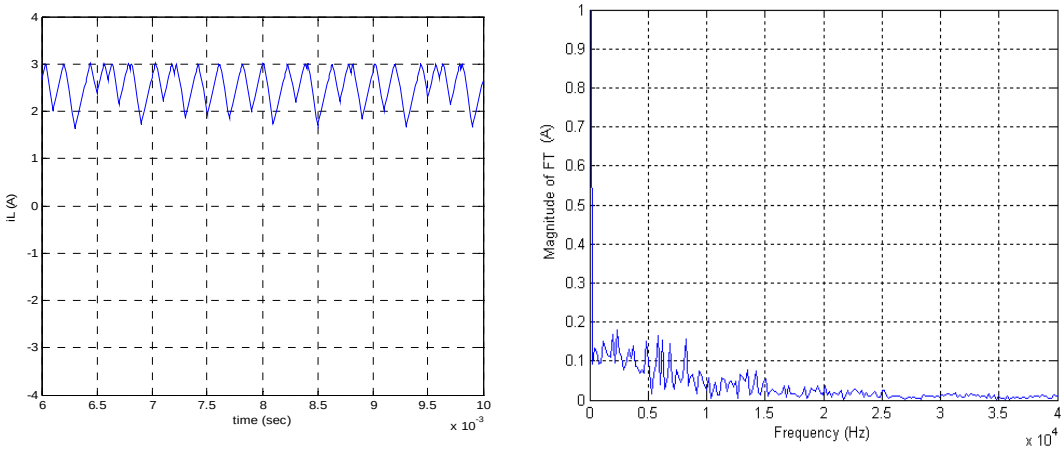

(b) Simulated inductor current and frequency spectrum.

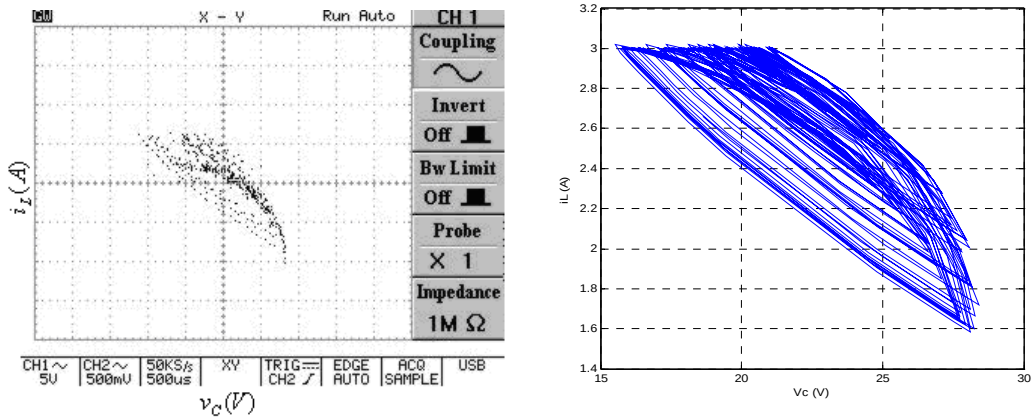

(c) Experimental and simulated phase portrait.

{**Left**: experimental, CH2 (1A/V), **right**: simulated}.

Figure 3.8 Chaotic at $I_{ref} = 3A$.

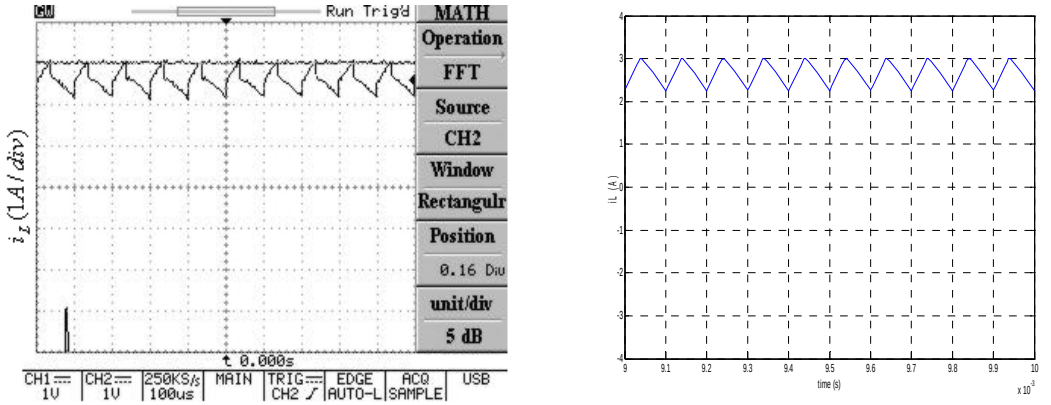

(a) Experimental and simulated inductor current.

{**Left**: experimental (1A/V), **right**: simulated}.

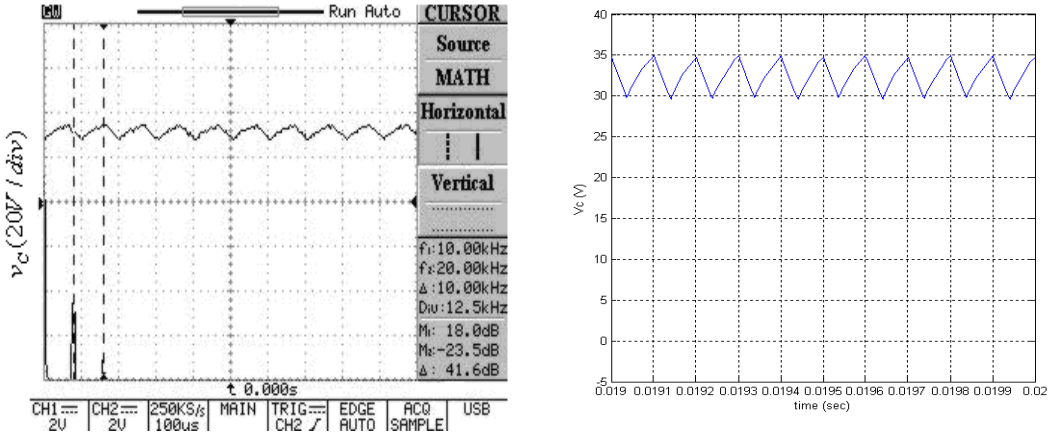

(b) Experimental and simulated capacitor voltage.

{**Left**: experimental, **right**: simulated}.

Figure 3.9 Period-1 at $V_{in} = 20V$.

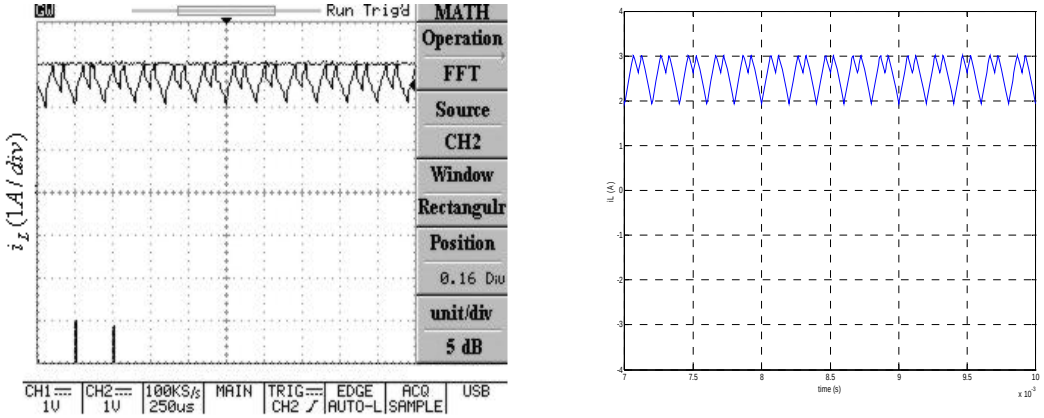

(a) Experimental and simulated inductor current.

{**Left**: experimental (1A/V), **right**: simulated}.

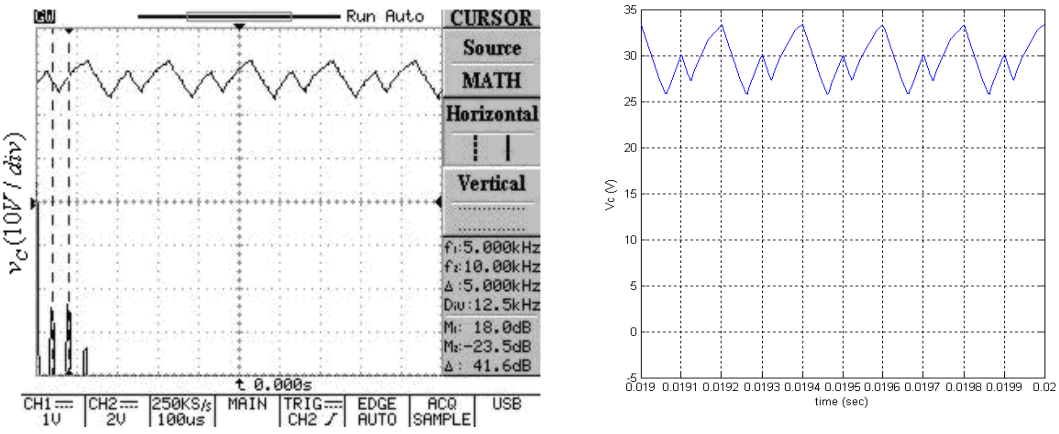

(b) Experimental and simulated capacitor voltage.

{**Left**: experimental, **right**: simulated}.

Figure 3.10 Period-2 at $V_{in} = 17V$.

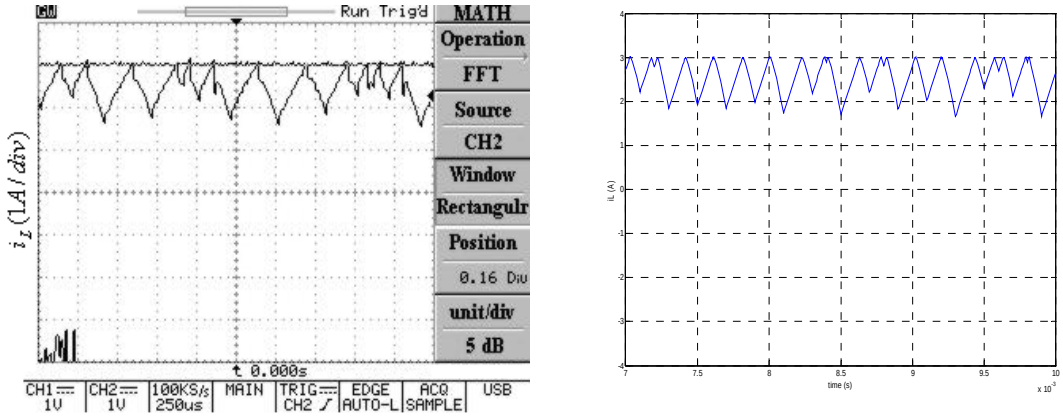

(a) Experimental and simulated inductor current.

{**Left**: experimental (1A/V), **right**: simulated}.

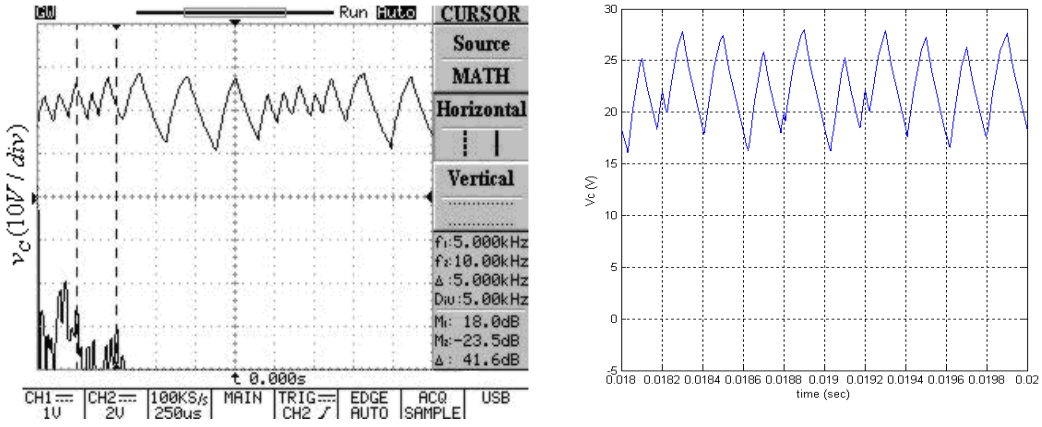

(b) Experimental and simulated capacitor voltage.

{**Left**: experimental, **right**: simulated}.

Figure 3.11 Chaotic at $V_{in} = 10V$.

CHAPTER 4
TWO-MODULE BOOST CONVERTER

4.1 Operation of the Two-Module Boost Converter

A simplified circuit diagram for the parallel input / parallel output boost converter is shown in Fig. 4.1. The operation of each module is similar to that of the single boost converter described in section 2.1.

The circuit has four states, depending on whether S_1 and S_2 are open, S_1 open and S_2 closed, S_1 closed and S_2 open, or S_1 and S_2 are closed. When S_1 and S_2 are closed, the inductor currents increase and any clock pulses to reset the flip-flop during these periods are ignored. S_1 and S_2 open when i_1 and i_2 respectively reach the reference current and i_1 and i_2 decrease. S_1 and S_2 re-close on the arrival of the next clock pulse. Assuming a general situation, in which L_1 and L_2 have different values due to component tolerance, the circuit waveforms are as shown in Fig. 4.2.

4.2 Iterative Map

A difference equation for the system takes the form

$$x_{n+1} = f(x_n, I_{ref}) \tag{4.1}$$

where

$$x = \begin{bmatrix} v_C & i_{L1} & i_{L2} \end{bmatrix}^T \tag{4.2}$$

with i_{L1} and i_{L2} respectively the inductor currents, and v_C the capacitor voltage.

$$\dot{x} = \begin{bmatrix} \dot{v}_C & \dot{i}_{L1} & \dot{i}_{L2} \end{bmatrix}^T \tag{4.3}$$

$$\dot{x} = \begin{cases} A_1 x + B_1 v_i; & nT \le t < nT + d_1 T \quad (S_1\text{''}ON\text{''}, S_2\text{''}ON\text{''}) \\ A_2 x + B_2 v_i; & nT + d_1 T \le t < nT + d_2 T \quad (S_1\text{''}OFF\text{''}, S_2\text{''}ON\text{''}) \quad (L_1 < L_2) \\ A_3 x + B_3 v_i; & nT + d_2 T \le t < (n+1)T \quad (S_1\text{''}OFF\text{''}, S_2\text{''}OFF\text{''}) \end{cases} \tag{4.4}$$

where

$$A_1 = \begin{bmatrix} -1/RC & 0 & 0 \\ 0 & 0 & 0 \\ 0 & 0 & 0 \end{bmatrix}, \; A_2 = \begin{bmatrix} -1/RC & 1/C & 0 \\ -1/L_1 & 0 & 0 \\ 0 & 0 & 0 \end{bmatrix},$$

$$A_3 = \begin{bmatrix} -1/RC & 1/C & 1/C \\ -1/L_1 & 0 & 0 \\ -1/L_2 & 0 & 0 \end{bmatrix}, B_1 = B_2 = B_3 = \begin{bmatrix} 0 \\ 1/L_1 \\ 1/L_2 \end{bmatrix}$$

$$d_1 T = t_{c1} = \frac{L_1 (I_{ref} - i_{L1_{(n)}})}{v_i}$$

$$T - t_{c1} = t_{d1}$$

$$d_2 T = t_{c2} = \frac{L_2 (I_{ref} - i_{L2_{(n)}})}{v_i}$$

$$T - t_{c2} = t_{d2}$$

Using fixed point iteration (successive substitution) [42]:

$$x_{n+1} = \phi_3(T - d_2 T).\phi_2(d_2 T - d_1 T).\phi_1(d_1 T).\left[x_n + \int_{nT}^{(n+d_1)T} \phi_1(nT - \tau) B_1 v_i d\tau \right] + \phi_3(T - d_2 T).$$

$$\phi_2(d_2 T - d_1 T).\left[\int_{(n+d_1)T}^{(n+d_2)T} \phi_2(nT + d_1 T - \tau) B_2 v_i d\tau \right] + \phi_3(T - d_2 T).\left[\int_{(n+d_2)T}^{(n+1)T} \phi_3(nT + d_2 T - \tau) B_3 v_i d\tau \right] \tag{4.5}$$

where

$$\phi_j(\xi) = 1 + \sum_{K=1}^{\infty} \frac{1}{K!} A_j{}^K \xi^K \tag{4.6}$$

for $j = 1,2,3$ and 1 is the identity matrix.

so

$$\phi_1(d_1 T) = \phi_1(t_{c1}) = 1 + \left[A_1 t_{c1} + \frac{1}{2} A_1{}^2 t_{c1}{}^2 + \frac{1}{6} A_1{}^3 t_{c1}{}^3 + \cdots \right] = \begin{bmatrix} 1 - \frac{t_{c1}}{RC} + \frac{t_{c1}{}^2}{2R^2 C^2} & 0 & 0 \\ 0 & 1 & 0 \\ 0 & 0 & 1 \end{bmatrix} \tag{4.7}$$

$$\phi_2(d_2 T - d_1 T) = \phi_2(t_{c2} - t_{c1}) = 1 + \left[A_2 (t_{c2} - t_{c1}) + \frac{1}{2} A_2{}^2 (t_{c2} - t_{c1})^2 + \frac{1}{6} A_2{}^3 (t_{c2} - t_{c1})^3 + \cdots \right]$$

$$= \begin{bmatrix} 1-\frac{(t_{c2}-t_{c1})}{RC}+\frac{(t_{c2}-t_{c1})^2}{2}(\frac{1}{R^2C^2}-\frac{1}{L_1C}) & \frac{(t_{c2}-t_{c1})}{C}+\frac{(t_{c2}-t_{c1})^2}{2}(-\frac{1}{RC^2}) & 0 \\ -\frac{(t_{c2}-t_{c1})}{L_1}+\frac{(t_{c2}-t_{c1})^2}{2}(\frac{1}{RL_1C}) & 1+\frac{(t_{c2}-t_{c1})^2}{2}(-\frac{1}{L_1C}) & 0 \\ 0 & 0 & 1 \end{bmatrix} \quad (4.8)$$

$$\phi_3(T-d_2T)=\phi_3(t_{d2})=1+\left[A_3t_{d2}+\frac{1}{2}A_3{}^2t_{d2}{}^2+\frac{1}{6}A_3{}^3t_{d2}{}^3+\cdots\right]=$$

$$\begin{bmatrix} 1-\frac{t_{d2}}{RC}+\frac{t_{d2}{}^2}{2}(\frac{1}{R^2C^2}-\frac{1}{L_1C}-\frac{1}{L_2C}) & \frac{t_{d2}}{C}+\frac{t_{d2}{}^2}{2}(-\frac{1}{RC^2}) & \frac{t_{d2}}{C}+\frac{t_{d2}{}^2}{2}(-\frac{1}{RC^2}) \\ -\frac{t_{d2}}{L_1}+\frac{t_{d2}{}^2}{2}(\frac{1}{RL_1C}) & 1+\frac{t_{d2}{}^2}{2}(-\frac{1}{L_1C}) & \frac{t_{d2}{}^2}{2}(-\frac{1}{L_1C}) \\ -\frac{t_{d2}}{L_2}+\frac{t_{d2}{}^2}{2}(\frac{1}{RL_2C}) & \frac{t_{d2}{}^2}{2}(-\frac{1}{L_2C}) & 1+\frac{t_{d2}{}^2}{2}(-\frac{1}{L_2C}) \end{bmatrix} \quad (4.9)$$

and

$$\phi_1(nT-\tau)=1+\left[A_1(nT-\tau)+\frac{1}{2}A_1{}^2(nT-\tau)^2+\frac{1}{6}A_1{}^3(nT-\tau)^3+\cdots\right]=$$

$$\begin{bmatrix} 1-\frac{(\mathrm{nT}-\tau)}{\mathrm{RC}}+\frac{(\mathrm{n}^2\mathrm{T}^2+\tau^2-2\mathrm{nT}\tau)}{2\mathrm{R}^2\mathrm{C}^2} & 0 & 0 \\ 0 & 1 & 0 \\ 0 & 0 & 1 \end{bmatrix} \quad (4.10)$$

$$\phi_2(nT+d_1T-\tau)=1+\left[A_2(nT+t_{c1}-\tau)+\frac{1}{2}A_2{}^2(nT+t_{c1}-\tau)^2+\frac{1}{6}A_2{}^3(nT+t_{c1}-\tau)^3+\cdots\right]=$$

$$\begin{bmatrix} 1-\frac{(nT+t_{c1}-\tau)}{RC}+\frac{U_1}{2}(\frac{1}{R^2C^2}-\frac{1}{L_1C}) & \frac{(nT+t_{c1}-\tau)}{C}-\frac{U_1}{2RC^2} & 0 \\ -\frac{(nT+t_{c1}-\tau)}{L_1}+\frac{U_1}{2RL_1C} & 1-\frac{U_1}{2L_1C} & 0 \\ 0 & 0 & 1 \end{bmatrix} \quad (4.11)$$

$$\phi_3(nT+d_2T-\tau)=1+\left[A_3(nT+t_{c2}-\tau)+\frac{1}{2}A_3{}^2(nT+t_{c2}-\tau)^2+\frac{1}{6}A_3{}^3(nT+t_{c2}-\tau)^3+\cdots\right]=$$

$$\begin{bmatrix} 1-\frac{(nT+t_{c2}-\tau)}{RC}+\frac{U_2}{2}(\frac{1}{R^2C^2}-\frac{1}{L_1C}-\frac{1}{L_2C}) & \frac{(nT+t_{c2}-\tau)}{C}-\frac{U_2}{2RC^2} & \frac{(nT+t_{c2}-\tau)}{C}-\frac{U_2}{2RC^2} \\ -\frac{(nT+t_{c2}-\tau)}{L_1}+\frac{U_2}{2RL_1C} & 1-\frac{U_2}{2L_1C} & -\frac{U_2}{2L_1C} \\ -\frac{(nT+t_{c2}-\tau)}{L_2}+\frac{U_2}{2RL_2C} & -\frac{U_2}{2L_2C} & 1-\frac{U_2}{2L_2C} \end{bmatrix} \tag{4.12}$$

where

$$U_1=(nT+t_{c1}-\tau)^2=(nT+t_{c1})^2+\tau^2-2(nT+t_{c1})\tau \tag{4.13}$$

$$U_2=(nT+t_{c2}-\tau)^2=(nT+t_{c2})^2+\tau^2-2(nT+t_{c2})\tau \tag{4.14}$$

so

$$\int_{nT}^{(n+d_1)T}\phi_1(nT-\tau)B_1v_i d\tau=\begin{bmatrix} 0 \\ t_{c1}/L_1 \\ t_{c2}/L_2 \end{bmatrix}v_i \tag{4.15}$$

$$\int_{(n+d_1)T}^{(n+d_2)T}\phi_2(nT+t_{c1}-\tau)B_2v_i d\tau=\begin{bmatrix} -\frac{(t_{c2}^{\ 2}-t_{c1}^{\ 2})}{2L_1C}-\frac{(t_{c2}^{\ 3}-t_{c1}^{\ 3})}{6RL_1C^2} \\ \frac{(t_{c2}-t_{c1})}{L_1}-\frac{(t_{c2}^{\ 3}-t_{c1}^{\ 3})}{6L_1^{\ 2}C} \\ \frac{(t_{c2}-t_{c1})}{L_2} \end{bmatrix}v_i \tag{4.16}$$

$$\int_{(n+d_2)T}^{(n+1)T}\phi_3(nT+t_{c2}-\tau)B_3v_i d\tau=\begin{bmatrix} -\frac{t_{d2}^{\ 2}}{2L_1C}-\frac{t_{d2}^{\ 3}}{6RL_1C^2}-\frac{t_{d2}^{\ 2}}{2L_2C}-\frac{t_{d2}^{\ 2}}{6RL_2C} \\ \frac{t_{d2}}{L_1}-\frac{t_{d2}^{\ 3}}{6L_1^{\ 2}C}-\frac{t_{d2}^{\ 3}}{6L_1L_2C} \\ \frac{t_{d2}}{L_2}-\frac{t_{d2}^{\ 3}}{6L_2^{\ 2}C}-\frac{t_{d2}^{\ 3}}{6L_1L_2C} \end{bmatrix}v_i \tag{4.17}$$

and

$$\phi_3(T-d_2T).\phi_2(d_2T-d_1T)=\begin{bmatrix} k_{11} & k_{12} & k_{13} \\ k_{21} & k_{22} & k_{23} \\ k_{31} & k_{32} & k_{33} \end{bmatrix} \tag{4.18}$$

$$\phi_3(T-d_2T).\phi_2(d_2T-d_1T).\phi_1(d_1T)=\begin{bmatrix} k_{11}(1-\frac{t_{c1}}{RC}+\frac{{t_{c1}}^2}{2R^2C^2}) & k_{12} & k_{13} \\ k_{21}(1-\frac{t_{c1}}{RC}+\frac{{t_{c1}}^2}{2R^2C^2}) & k_{22} & k_{23} \\ k_{31}(1-\frac{t_{c1}}{RC}+\frac{{t_{c1}}^2}{2R^2C^2}) & k_{32} & k_{33} \end{bmatrix} \quad (4.19)$$

where

$$k_{11}=\left(1-\frac{t_{d2}}{RC}+\frac{{t_{d2}}^2}{2}(\frac{1}{R^2C^2}-\frac{1}{L_1C}-\frac{1}{L_2C})\right)\left(1-\frac{(t_{c2}-t_{c1})}{RC}+\frac{(t_{c2}-t_{c1})^2}{2}(\frac{1}{R^2C^2}-\frac{1}{L_1C})\right)+$$
$$\left(\frac{t_{d2}}{C}+\frac{{t_{d2}}^2}{2}(-\frac{1}{RC^2})\right)\left(-\frac{(t_{c2}-t_{c1})}{L_1}+\frac{(t_{c2}-t_{c1})^2}{2}(\frac{1}{RL_1C})\right)$$

$$k_{21}=\left(-\frac{t_{d2}}{L_1}+\frac{{t_{d2}}^2}{2}(\frac{1}{RL_1C})\right)\left(1-\frac{(t_{c2}-t_{c1})}{RC}+\frac{(t_{c2}-t_{c1})^2}{2}(\frac{1}{R^2C^2}-\frac{1}{L_1C})\right)+$$
$$\left(1+\frac{{t_{d2}}^2}{2}(-\frac{1}{L_1C})\right)\left(-\frac{(t_{c2}-t_{c1})}{L_1}+\frac{(t_{c2}-t_{c1})^2}{2}(\frac{1}{RL_1C})\right)$$

$$k_{31}=\left(-\frac{t_{d2}}{L_2}+\frac{{t_{d2}}^2}{2}(\frac{1}{RL_2C})\right)\left(1-\frac{(t_{c2}-t_{c1})}{RC}+\frac{(t_{c2}-t_{c1})^2}{2}(\frac{1}{R^2C^2}-\frac{1}{L_1C})\right)+$$
$$\left(\frac{{t_{d2}}^2}{2}(-\frac{1}{L_2C})\right)\left(-\frac{(t_{c2}-t_{c1})}{L_1}+\frac{(t_{c2}-t_{c1})^2}{2}(\frac{1}{RL_1C})\right)$$

$$k_{12}=\left(1-\frac{t_{d2}}{RC}+\frac{{t_{d2}}^2}{2}(\frac{1}{R^2C^2}-\frac{1}{L_1C}-\frac{1}{L_2C})\right)\left(\frac{(t_{c2}-t_{c1})}{C}+\frac{(t_{c2}-t_{c1})^2}{2}(-\frac{1}{RC^2})\right)+$$
$$\left(\frac{t_{d2}}{C}+\frac{{t_{d2}}^2}{2}(-\frac{1}{RC^2})\right)\left(1+\frac{(t_{c2}-t_{c1})^2}{2}(-\frac{1}{L_1C})\right)$$

$$k_{22}=\left(-\frac{t_{d2}}{L_1}+\frac{{t_{d2}}^2}{2}(\frac{1}{RL_1C})\right)\left(\frac{(t_{c2}-t_{c1})}{C}+\frac{(t_{c2}-t_{c1})^2}{2}(-\frac{1}{RC^2})\right)+$$
$$\left(1+\frac{{t_{d2}}^2}{2}(-\frac{1}{L_1C})\right)\left(1+\frac{(t_{c2}-t_{c1})^2}{2}(-\frac{1}{L_1C})\right)$$

$$k_{32}=\left(-\frac{t_{d2}}{L_2}+\frac{{t_{d2}}^2}{2}(\frac{1}{RL_2C})\right)\left(\frac{(t_{c2}-t_{c1})}{C}+\frac{(t_{c2}-t_{c1})^2}{2}(-\frac{1}{RC^2})\right)+$$
$$\left(\frac{{t_{d2}}^2}{2}(-\frac{1}{L_2C})\right)\left(1+\frac{(t_{c2}-t_{c1})^2}{2}(-\frac{1}{L_1C})\right)$$

$$k_{13} = \left(\frac{t_{d2}}{C} + \frac{{t_{d2}}^2}{2}(-\frac{1}{RC^2}) \right)$$

$$k_{23} = \left(\frac{{t_{d2}}^2}{2}(-\frac{1}{L_1 C}) \right)$$

$$k_{33} = \left(1 + \frac{{t_{d2}}^2}{2}(-\frac{1}{L_2 C}) \right)$$

so

$$\phi_3(T-d_2T).\phi_2(d_2T-d_1T).\phi_1(d_1T).\left[\int_{nT}^{(n+d_1)T} \phi_1(nT-\tau) B_1 v_i d\tau \right] = \begin{bmatrix} k_{12}\frac{t_{c1}}{L_1} + k_{13}\frac{t_{c1}}{L_2} \\ k_{22}\frac{t_{c1}}{L_1} + k_{23}\frac{t_{c1}}{L_2} \\ k_{32}\frac{t_{c1}}{L_1} + k_{33}\frac{t_{c1}}{L_2} \end{bmatrix} v_i \qquad (4.20)$$

$$\phi_3(T-d_2T).\phi_2(d_2T-d_1T).\left[\int_{(n+d_1)T}^{(n+d_2)T} \phi_2(nT+d_1T-\tau) B_2 v_i d\tau \right] = \begin{bmatrix} N_1 \\ N_2 \\ N_3 \end{bmatrix} v_i \qquad (4.21)$$

$$\phi_3(T-d_2T).\left[\int_{(n+d_2)T}^{(n+1)T} \phi_3(nT+d_2T-\tau) B_3 v_i d\tau \right] = \begin{bmatrix} M_1 \\ M_2 \\ M_3 \end{bmatrix} v_i \qquad (4.22)$$

where

$$N_1 = k_{11}\left(-\frac{({t_{c2}}^2 - {t_{c1}}^2)}{2L_1 C} - \frac{({t_{c2}}^3 - {t_{c1}}^3)}{6RL_1 C^2} \right) + k_{12}\left(\frac{(t_{c2}-t_{c1})}{L_1} - \frac{({t_{c2}}^3 - {t_{c1}}^3)}{6{L_1}^2 C} \right) + k_{13}\frac{(t_{c2}-t_{c1})}{L_2}$$

$$N_2 = k_{21}\left(-\frac{({t_{c2}}^2 - {t_{c1}}^2)}{2L_1 C} - \frac{({t_{c2}}^3 - {t_{c1}}^3)}{6RL_1 C^2} \right) + k_{22}\left(\frac{(t_{c2}-t_{c1})}{L_1} - \frac{({t_{c2}}^3 - {t_{c1}}^3)}{6{L_1}^2 C} \right) + k_{23}\frac{(t_{c2}-t_{c1})}{L_2}$$

$$N_3 = k_{31}\left(-\frac{({t_{c2}}^2 - {t_{c1}}^2)}{2L_1 C} - \frac{({t_{c2}}^3 - {t_{c1}}^3)}{6RL_1 C^2} \right) + k_{32}\left(\frac{(t_{c2}-t_{c1})}{L_1} - \frac{({t_{c2}}^3 - {t_{c1}}^3)}{6{L_1}^2 C} \right) + k_{33}\frac{(t_{c2}-t_{c1})}{L_2}$$

$$M_1 = \left(1 - \frac{t_{d2}}{RC} + \frac{{t_{d2}}^2}{2}(\frac{1}{R^2C^2} - \frac{1}{L_1 C} - \frac{1}{L_2 C}) \right).\left(-\frac{{t_{d2}}^2}{2L_1 C} - \frac{{t_{d2}}^3}{6RL_1 C^2} - \frac{{t_{d2}}^2}{2L_2 C} - \frac{{t_{d2}}^2}{6RL_2 C} \right) +$$

$$\left(\frac{t_{d2}}{C} + \frac{{t_{d2}}^2}{2}(-\frac{1}{RC^2}) \right).\left(\frac{t_{d2}}{L_1} - \frac{{t_{d2}}^3}{6{L_1}^2 C} - \frac{{t_{d2}}^3}{6L_1 L_2 C} \right) +$$

$$\left(\frac{t_{d2}}{C}+\frac{{t_{d2}}^2}{2}(-\frac{1}{RC^2})\right).\left(\frac{t_{d2}}{L_2}-\frac{{t_{d2}}^3}{6{L_2}^2C}-\frac{{t_{d2}}^3}{6L_1L_2C}\right)$$

$$M_2=\left(-\frac{t_{d2}}{L_1}+\frac{{t_{d2}}^2}{2}(\frac{1}{RL_1C})\right).\left(-\frac{{t_{d2}}^2}{2L_1C}-\frac{{t_{d2}}^3}{6RL_1C^2}-\frac{{t_{d2}}^2}{2L_2C}-\frac{{t_{d2}}^2}{6RL_2C}\right)+$$

$$\left(1+\frac{{t_{d2}}^2}{2}(-\frac{1}{L_1C})\right).\left(\frac{t_{d2}}{L_1}-\frac{{t_{d2}}^3}{6{L_1}^2C}-\frac{{t_{d2}}^3}{6L_1L_2C}\right)+$$

$$\left(\frac{{t_{d2}}^2}{2}(-\frac{1}{L_1C})\right).\left(\frac{t_{d2}}{L_2}-\frac{{t_{d2}}^3}{6{L_2}^2C}-\frac{{t_{d2}}^3}{6L_1L_2C}\right)$$

$$M_3=\left(-\frac{t_{d2}}{L_2}+\frac{{t_{d2}}^2}{2}(\frac{1}{RL_2C})\right).\left(-\frac{{t_{d2}}^2}{2L_1C}-\frac{{t_{d2}}^3}{6RL_1C^2}-\frac{{t_{d2}}^2}{2L_2C}-\frac{{t_{d2}}^2}{6RL_2C}\right)+$$

$$\left(\frac{{t_{d2}}^2}{2}(-\frac{1}{L_2C})\right).\left(\frac{t_{d2}}{L_1}-\frac{{t_{d2}}^3}{6{L_1}^2C}-\frac{{t_{d2}}^3}{6L_1L_2C}\right)+$$

$$\left(1+\frac{{t_{d2}}^2}{2}(-\frac{1}{L_2C})\right).\left(\frac{t_{d2}}{L_2}-\frac{{t_{d2}}^3}{6{L_2}^2C}-\frac{{t_{d2}}^3}{6L_1L_2C}\right)$$

So

$$x_{n+1}=\phi_3(T-d_2T).\phi_2(d_2T-d_1T).\phi_1(d_1T).\left[x_n+\int_{nT}^{(n+d_1)T}\phi_1(nT-\tau)B_1v_i\,d\tau\right]+\phi_3(T-d_2T).$$

$$\phi_2(d_2T-d_1T).\left[\int_{(n+d_1)T}^{(n+d_2)T}\phi_2(nT+d_1T-\tau)B_2v_i\,d\tau\right]+\phi_3(T-d_2T).\left[\int_{(n+d_2)T}^{(n+1)T}\phi_3(nT+d_2T-\tau)B_3v_i\,d\tau\right]=$$

$$\begin{bmatrix}v_{C_{(n+1)}}\\ i_{L1_{(n+1)}}\\ i_{L2_{(n+1)}}\end{bmatrix}=\begin{bmatrix}k_{11}\left(1-\frac{t_{c1}}{RC}+\frac{{t_{c1}}^2}{2R^2C^2}\right) & k_{12} & k_{13}\\ k_{21}\left(1-\frac{t_{c1}}{RC}+\frac{{t_{c1}}^2}{2R^2C^2}\right) & k_{22} & k_{23}\\ k_{31}\left(1-\frac{t_{c1}}{RC}+\frac{{t_{c1}}^2}{2R^2C^2}\right) & k_{32} & k_{33}\end{bmatrix}\begin{bmatrix}v_{C_{(n)}}\\ i_{L1_{(n)}}\\ i_{L2_{(n)}}\end{bmatrix}+\begin{bmatrix}k_{12}\frac{t_{c1}}{L_1}+k_{13}\frac{t_{c1}}{L_2}+N_1+M_1\\ k_{22}\frac{t_{c1}}{L_1}+k_{23}\frac{t_{c1}}{L_2}+N_2+M_2\\ k_{32}\frac{t_{c1}}{L_1}+k_{33}\frac{t_{c1}}{L_2}+N_3+M_3\end{bmatrix}v_i$$

(4.23)

Eqn.4.23 comprises one form of the mapping for the two-module converter, which will be described in Chapter 5.

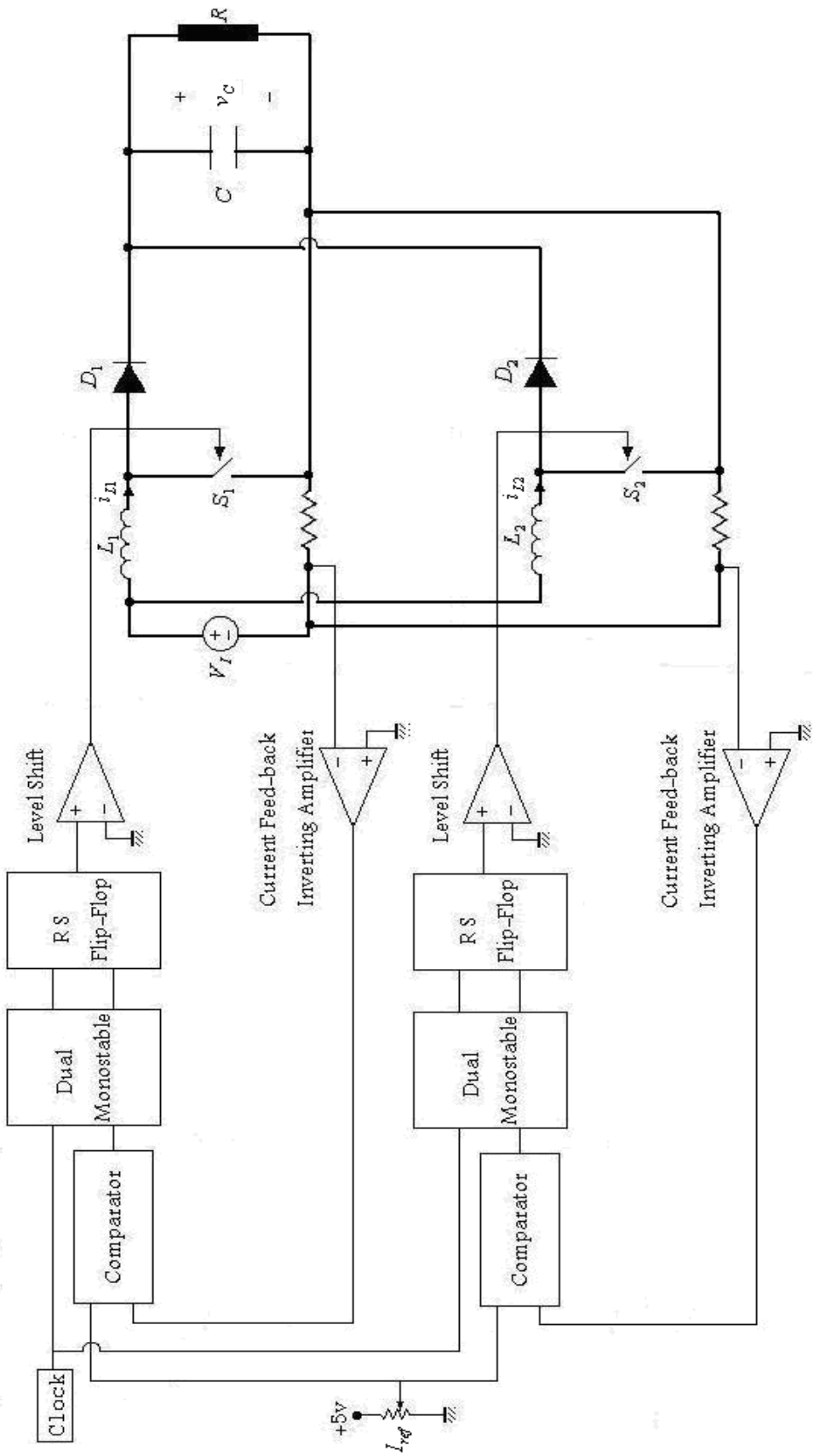

Figure 4.1 Simplified circuit diagram.

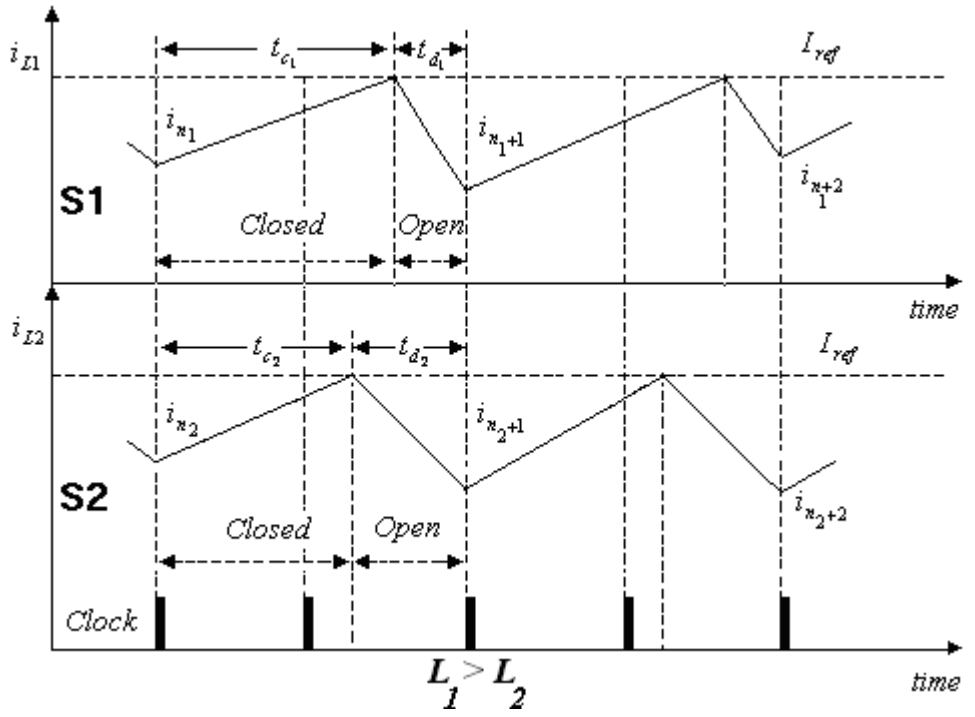

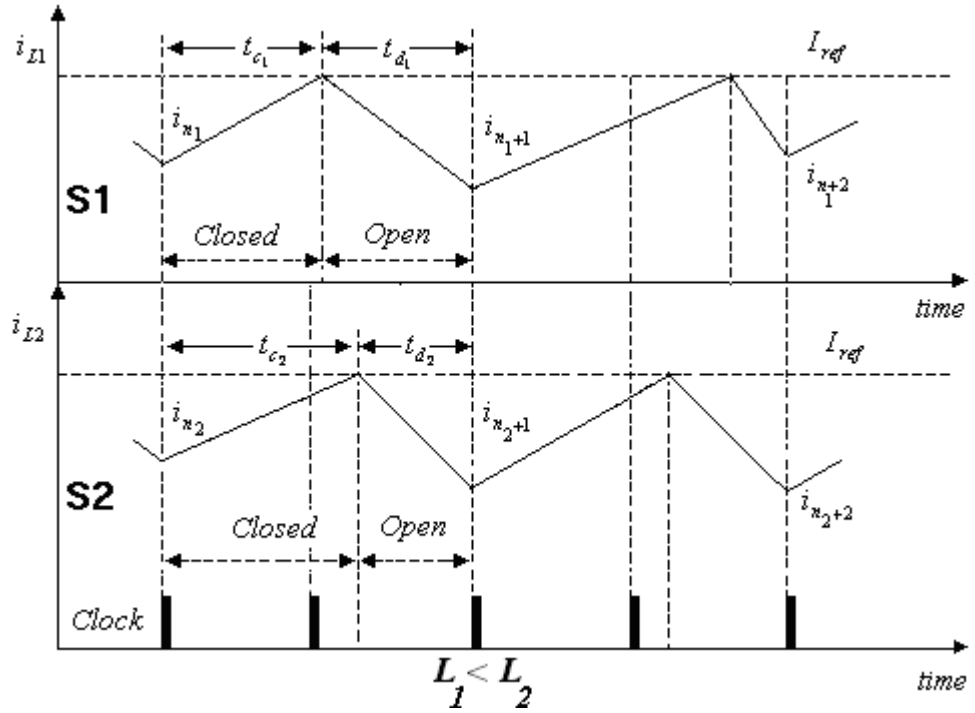

Figure 4.2 Circuit waveforms of Fig. 4.1 with different inductors.

CHAPTER 5
CHAOS IN A TWO-MODULE BOOST CONVERTER

5.1 Numerical Analysis

A MATLAB program was written to produce bifurcation diagrams for a two-module boost converter, with different values for the energy storage inductor L_2. A flowchart for the program is given in Fig. 5.1 and the program listing is given in Appendix A.2. The nominal parameters used for the simulations are based on those published in [9] and are given in Table 5.1.

Circuit Components	Values
Switching Period T	$100\mu s$
Input Voltage V_{in}	$10V$
Inductor L_1 (nominal)	$1mH$
Inductor L_2	$1.1mH, 0.9mH, 1.0mH$
Capacitor C	$20\,\mu F$
Load Resistor R	$20\,\Omega$

Table 5.1 System parameters.

To obtain the bifurcation diagrams, initial conditions $(v_{C(0)}, i_{1(0)}, i_{2(0)})$ were specified and Eq.4.23 was iterated 750 times, taking I_{ref} as the bifurcation parameter. As with the single converter, the first 500 values were discarded to eliminate transients and the last 250 values were plotted.

Figs. 5.2(a) to (c) show the bifurcation diagrams for the total input current to the two module converter with L_1 = 1.0mH and three different values for L_2. Figs. 5.3(a) to (c) show the individual bifurcation diagrams for the two inductor currents in the three different cases. Some interesting and unexpected results are evident in Fig. 5.3. The bifurcation diagrams for the individual inductor currents appear to be "synchronised", with bifurcations occurring at the same values of I_{ref}. For instance, Fig. 5.3(a) shows that both converters operate in period-1 up to about 0.95A, at which point a bifurcation doubling occurs. As I_{ref} increases further, each converter becomes

chaotic at the same value of I_{ref}. The same phenomenon occurs in Figs. 5.3(b) and (c).

Although paralleling converters appears to synchronise the points at which bifurcations occur, the magnitudes of the currents at these points are different. For instance, at the period-1/period-2 boundary (I_{ref} = 0.95A) in Fig. 5.3(a), $i_{L1} = 0.52A$, whereas $i_{L2} = 0.57A$. At the period-1/period-2 boundary (I_{ref} = 0.97A) in Fig. 5.3(b), $i_{L1} = 0.53A$, whereas $i_{L2} = 0.48A$, etc. Furthermore, the bifurcation diagram for the single converter with $L = 1mH$, shown in Fig. 3.2, is considerably different from those of the paralleled converter with $L_1 = L_2 = 1mH$, shown in Fig. 5.3(c).

This "synchronisation" phenomenon of paralleled converters was valid over a range of $\pm 10\%$ of the nominal inductance value (1.0mH), which is much larger than the manufacturing tolerances for these inductors. This behaviour could simplify the control of chaos in paralleled converters, since the paralleled units could be considered as an entity.

5.2 Experimental Implementation

An experimental two-module converter was designed and built, based on the parameters of Table 5.1. The circuit is shown in Fig. 5.4 and the operation of each module is similar to that of the single boost converter explained in Chapter 3 (section 3.3). A photograph of the converter hardware is shown in Appendix D.2.

5.3 MATLAB/SIMULINK Model

A MATLAB/SIMULINK model was developed based on the system equations:

$$\begin{aligned}
\frac{di_{L1}}{dt} &= \frac{1}{L_1}[v_{in} - v_C(1-u_{S1})] \\
\frac{di_{L2}}{dt} &= \frac{1}{L_2}[v_{in} - v_C(1-u_{S2})] \\
\frac{dv_C}{dt} &= \frac{1}{C}[-\frac{v_C}{R} + i_{L1}(1-u_{S1}) + i_{L2}(1-u_{S2})]
\end{aligned} \tag{5.1}$$

where u_{S1} and u_{S2} again take the value 0 or 1 depending on whether the switches 1 or 2 are closed or open. The structure of the SIMULINK model is given in Fig. 5.5.

5.4 Experimental and Simulation Results (Unbalanced Inductors)

The inductor current waveforms, harmonic spectra and phase portraits for the two-module boost converter with $(L_1 = 1mH, L_2 = 1.1mH)$ and $(L_1 = 1mH, L_2 = 0.9mH)$, for different values of the bifurcation parameter I_{ref} are shown in Figs. 5.6 to 5.13.

Figs. 5.6 and 5.10 show the results for period-1 operation with $I_{ref} = 0.8A$, Figs. 5.7 and 5.11 show the results for period-2 operation with $I_{ref} = 1A$ and Figs. 5.8 and 5.12 show results for the chaotic behaviour with $I_{ref} = 1.3A$. The phase portraits for the three values of reference current are shown in Figs. 5.9 and 5.13. As with the phase portraits for the single converter, the oscilloscope inputs were AC coupled, to eliminate DC components in the waveforms. The experimental and simulated results are in good agreement and agree with the bifurcation diagrams of Fig 5.3.

5.5 Experimental and Simulation Results (Balanced Inductors)

The inductor current waveforms, harmonic spectra and phase portraits for the balanced two-module boost converter $(L_1 = L_2 = 1mH; i_{L1} = i_{L2})$, with different values of the bifurcation parameter I_{ref} are shown in Figs. 5.14 to 5.16. Fig. 5.14 shows period-1 operation with $I_{ref} = 0.9A$, Fig. 5.15 shows period-2 operation with $I_{ref} = 1.2A$. (Note the large 5kHz component in the inductor current frequency spectrum). Fig. 5.16 shows results for the chaotic behaviour with $I_{ref} = 1.7A$. Again, the experimental and simulated results are in good agreement and agree with the bifurcation diagrams for the balanced module as shown in Fig. 5.3(c).

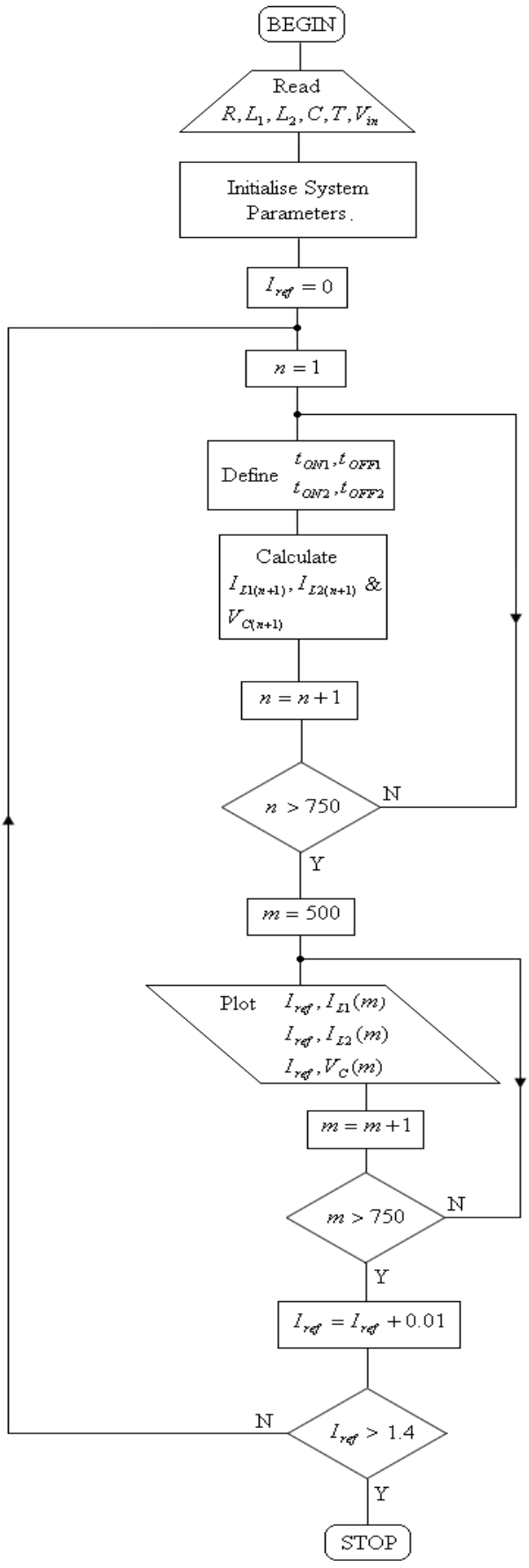

Figure 5.1 Bifurcation program flowchart.

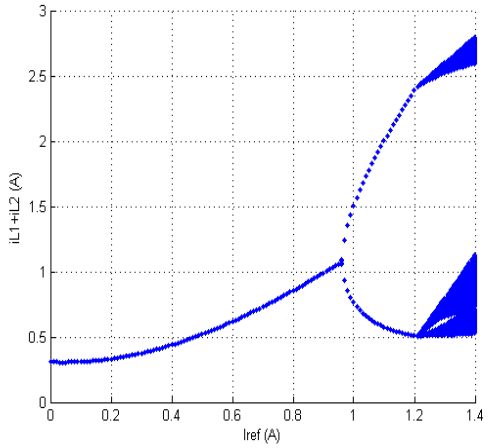

(a) $L_1 = 1mH, L_2 = 1.1mH$.

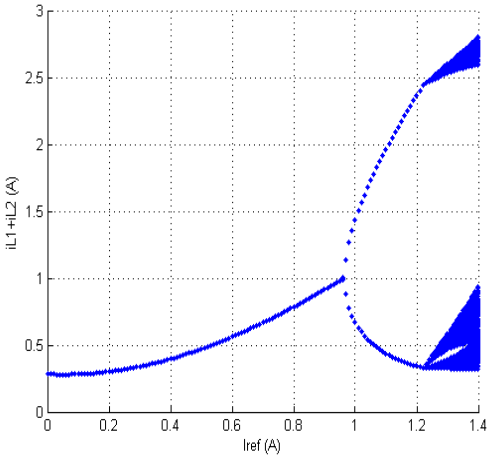

(b) $L_1 = 1mH, L_2 = 0.9mH$.

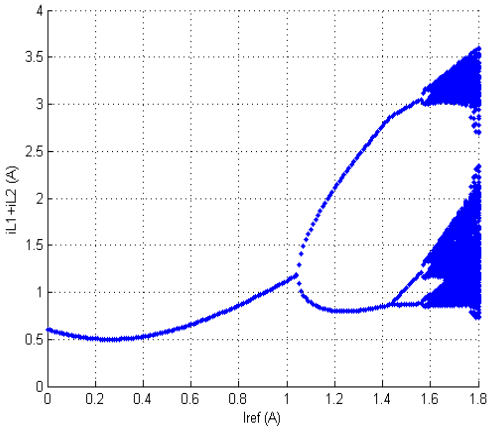

(c) $L_1 = L_2 = 1mH$.

Figure 5.2 Overall bifurcation diagrams relating the total input current to I_{ref} .

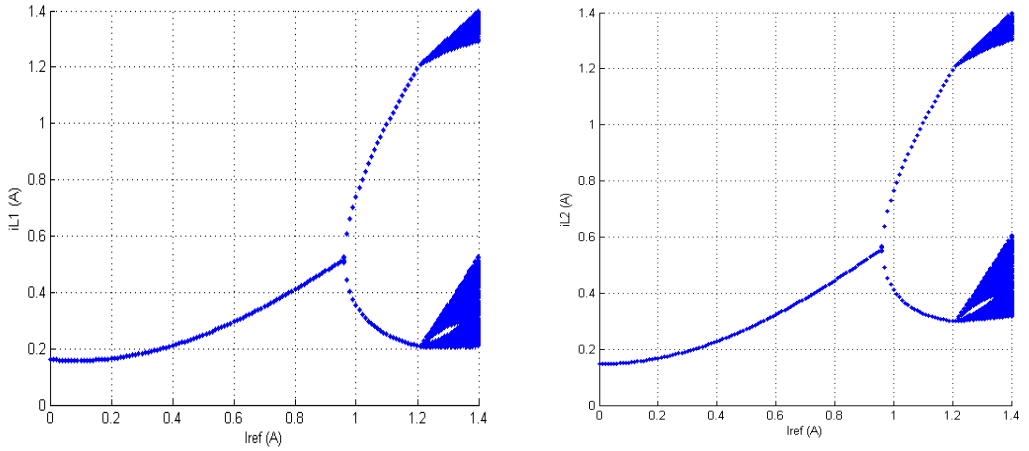

(a) (Left) $L_1 = 1mH$, **(Right)** $L_2 = 1.1mH$.

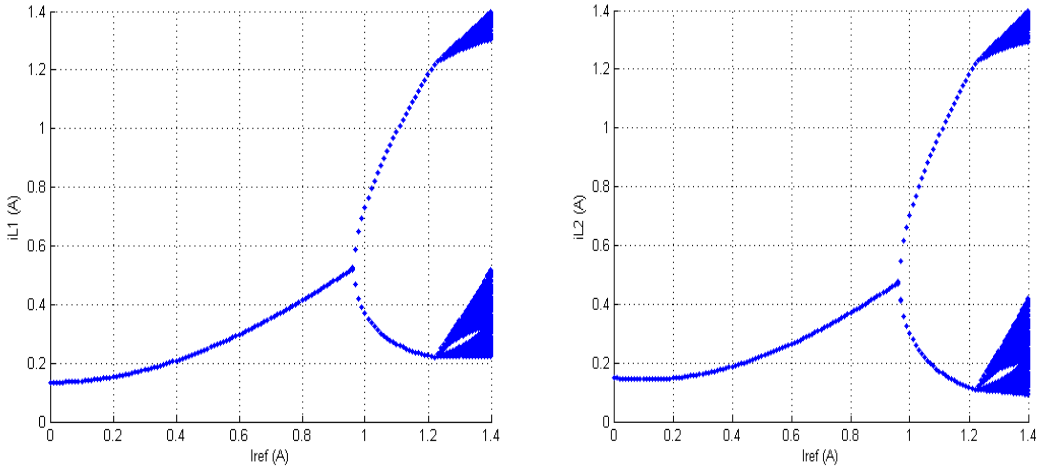

(b) (Left) $L_1 = 1mH$, **(Right)** $L_2 = 0.9mH$.

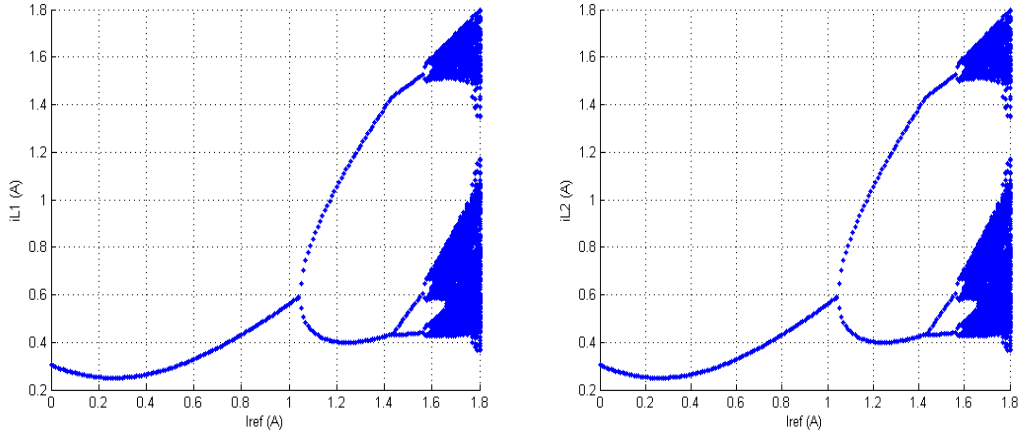

(c) (Left) $L_1 = 1mH$, **(Right)** $L_2 = 1mH$.

Figure 5.3 Individual converter bifurcation diagrams relating i_{L1} and i_{L2} to I_{ref} .

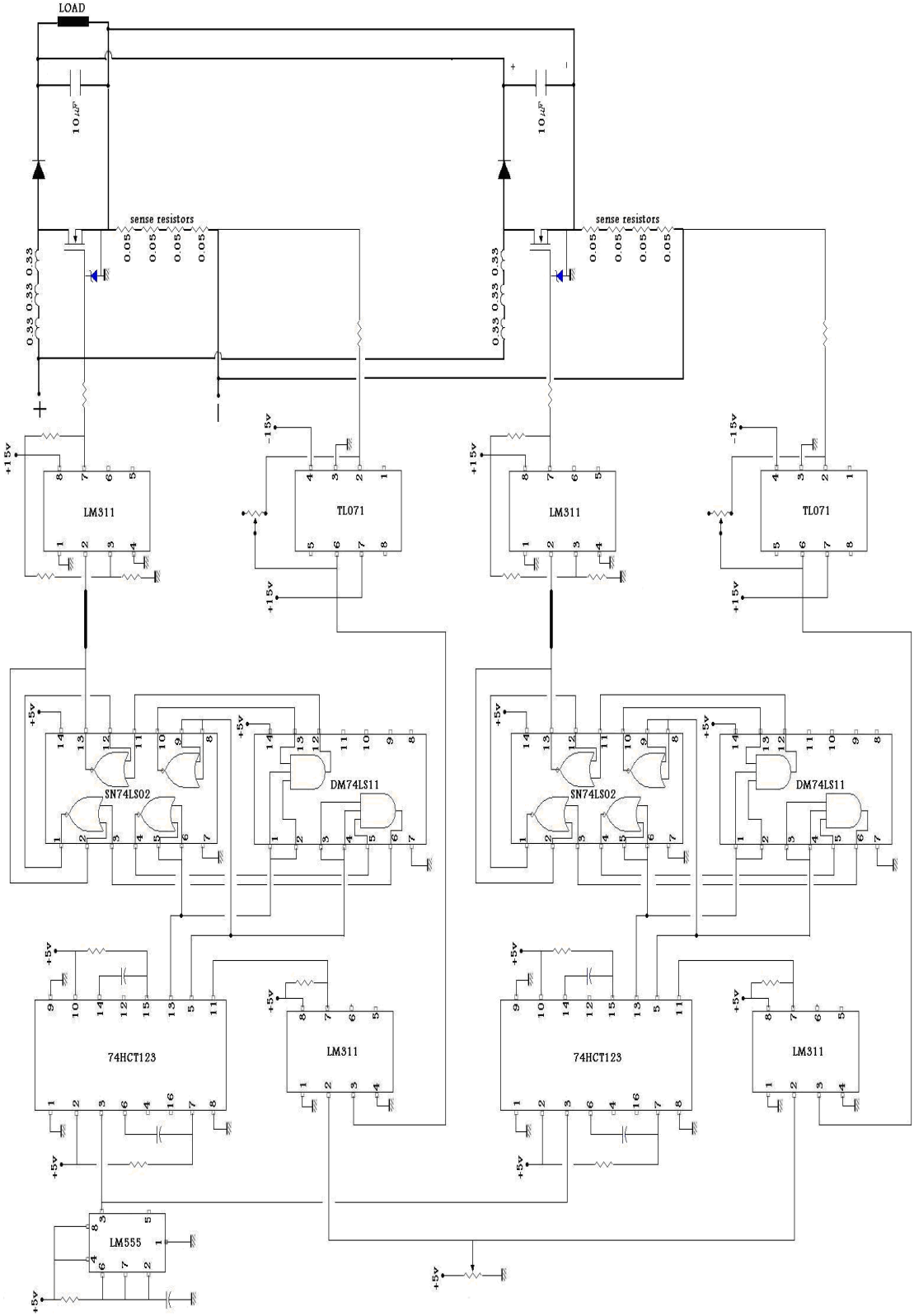

Figure 5.4 Two-module converter hardware.

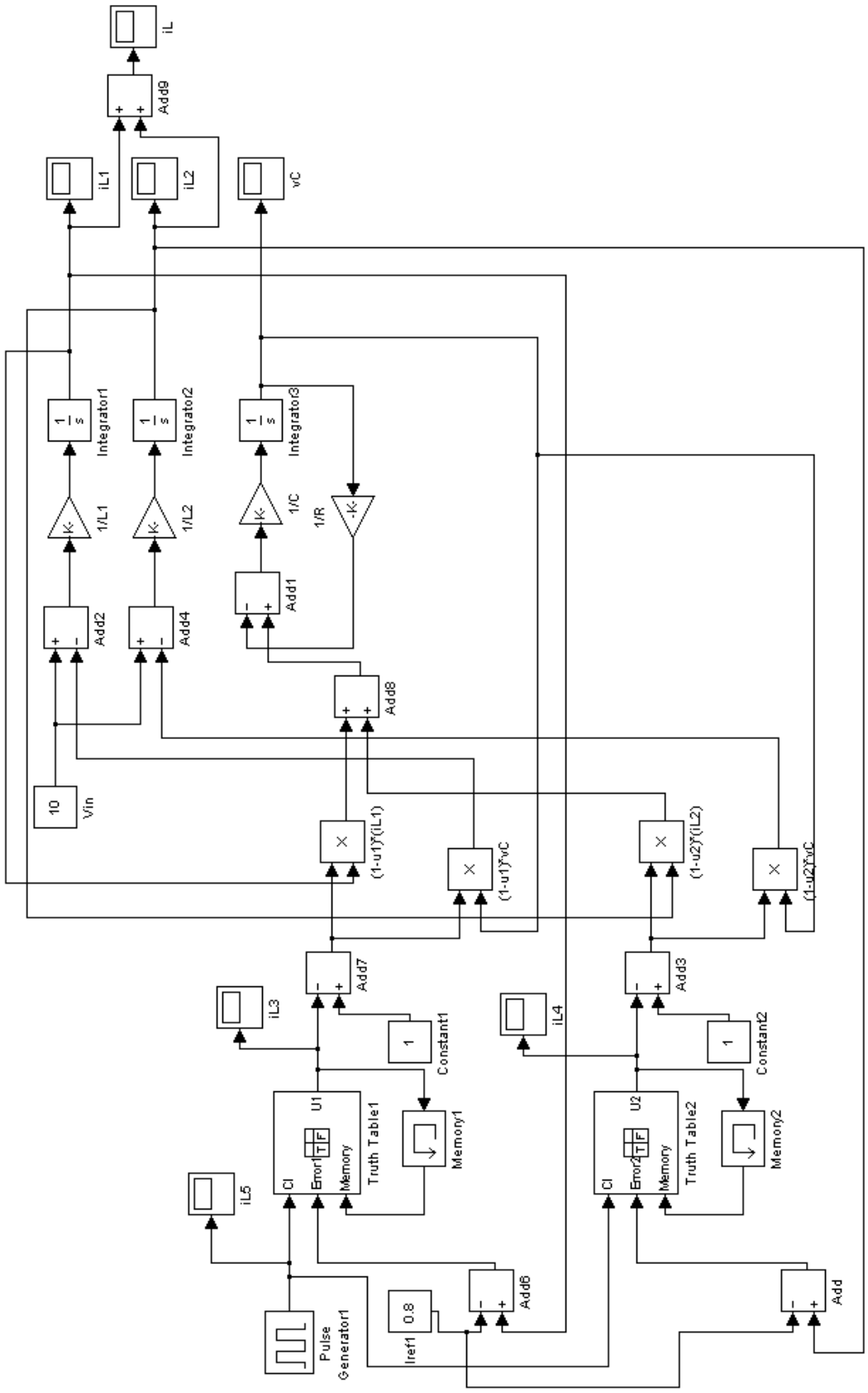

Figure 5.5 MATLAB/SIMULINK model for the two-module converter.

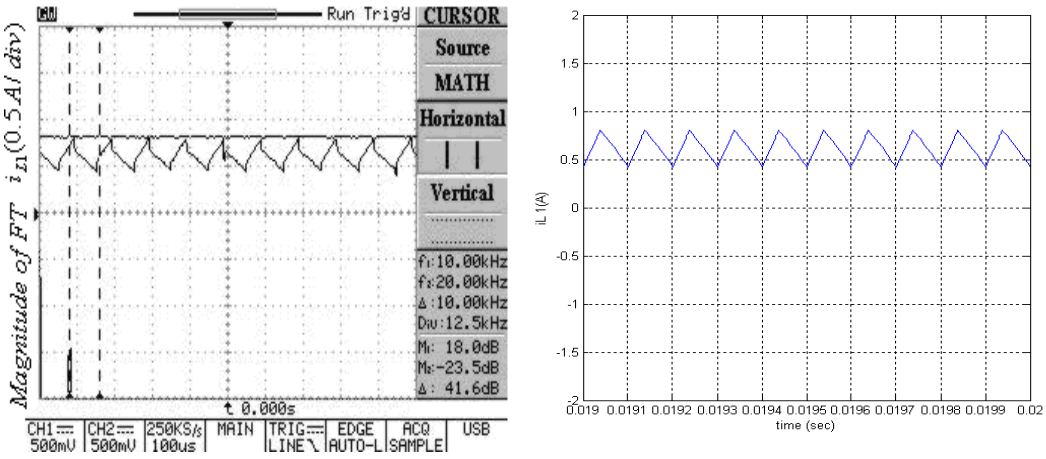

(a) Experimental and simulated results for i_{L1}.

{**Left**: experimental (1A/V), **right**: simulated}.

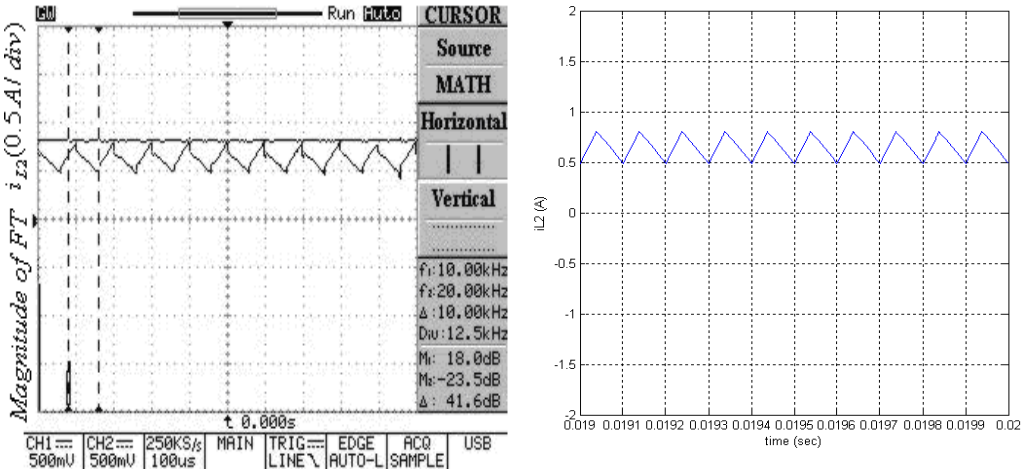

(b) Experimental and simulated results for i_{L2}.

{**Left**: experimental (1A/V), **right**: simulated}.

Figure 5.6 Period-1 with $L_1 = 1mH, L_2 = 1.1mH$ at $I_{ref} = 0.8A$.

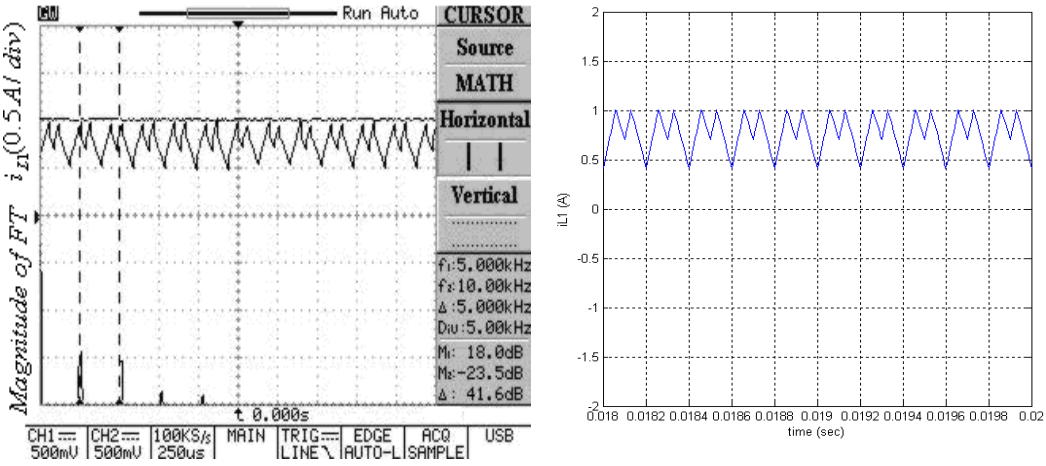

(a) Experimental and simulated results for i_{L1}.

{**Left**: experimental (1A/V), **right**: simulated}.

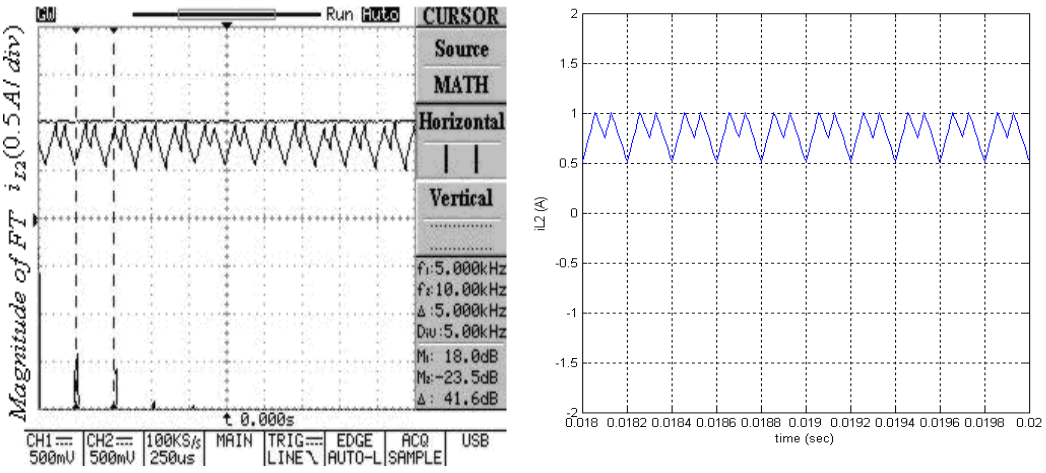

(b) Experimental and simulated results for i_{L2}.

{**Left**: experimental (1A/V), **right**: simulated}.

Figure 5.7 Period-2 with $L_1 = 1mH, L_2 = 1.1mH$ at $I_{ref} = 1A$.

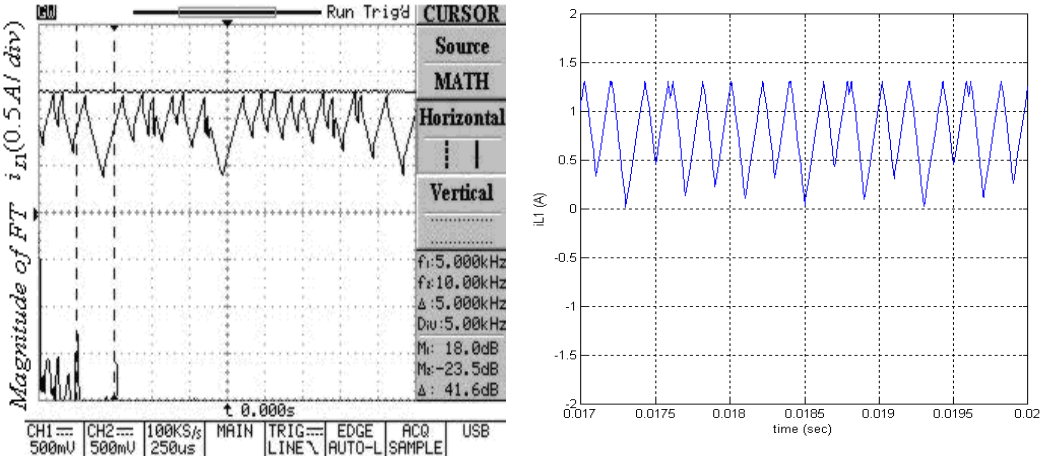

(a) Experimental and simulated results for i_{L1}.

{**Left**: experimental (1A/V), **right**: simulated}.

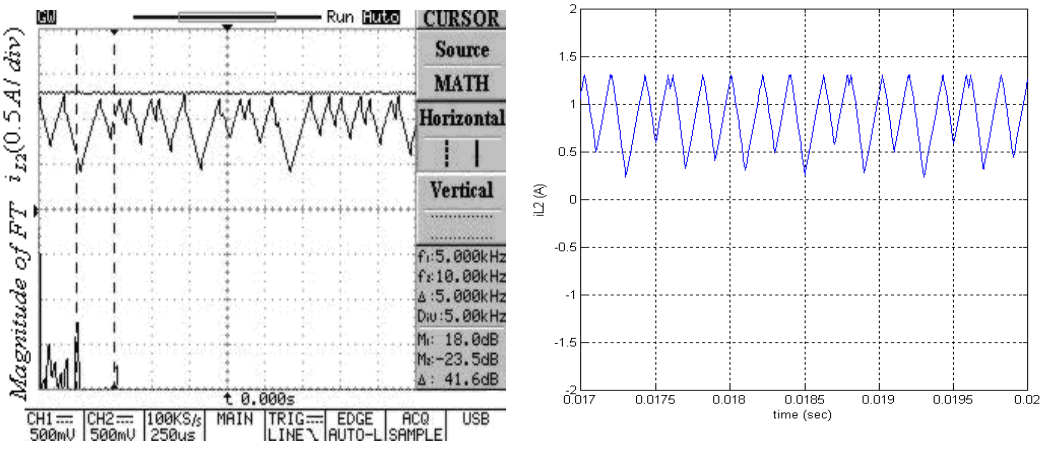

(b) Experimental and simulated results for i_{L2}.

{**Left**: experimental (1A/V), **right**: simulated}.

Figure 5.8 Chaotic with $L_1 = 1mH, L_2 = 1.1mH$ at $I_{ref} = 1.3A$.

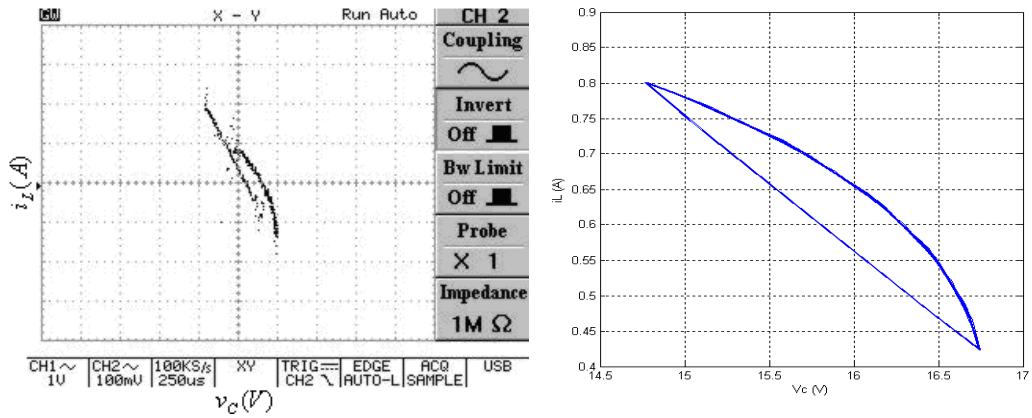

(a) Period-1 at $I_{ref} = 0.8A$

{**Left**: experimental CH2 (1A/V), **right**: simulated}.

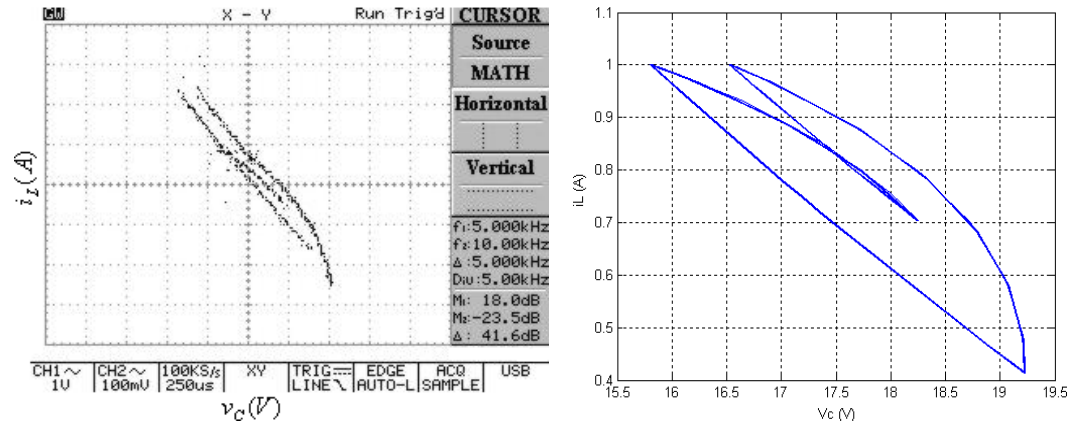

(c) Period-2 at $I_{ref} = 1A$

{**Left**: experimental CH2 (1A/V), **right**: simulated}.

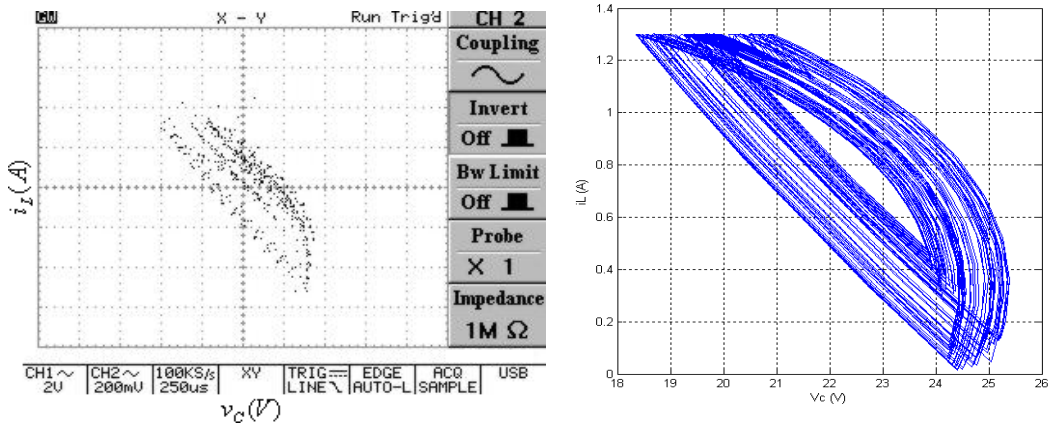

(d) Chaotic at $I_{ref} = 1.3A$

{**Left**: experimental CH2 (1A/V), **right**: simulated}.

Figure 5.9 Experimental and simulated phase portrait with $L_1 = 1mH, L_2 = 1.1mH$.

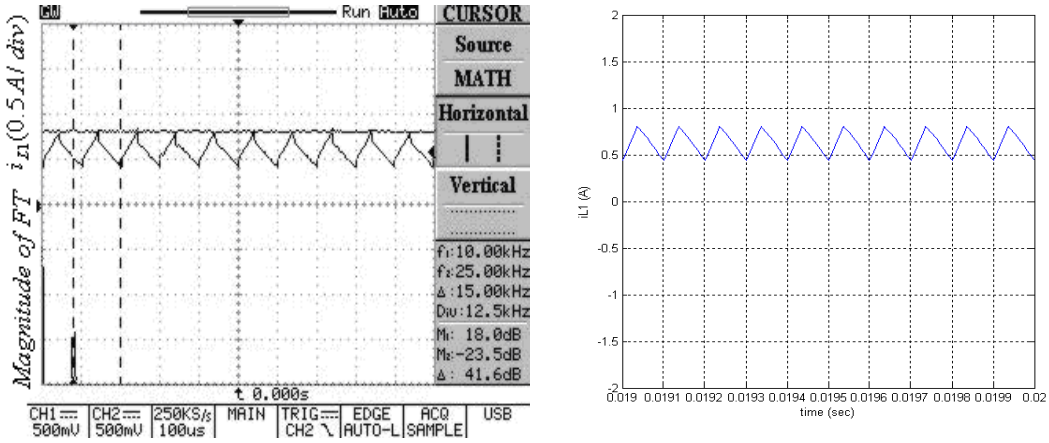

(a) Experimental and simulated results for i_{L1}.

{**Left**: experimental (1A/V), **right**: simulated}.

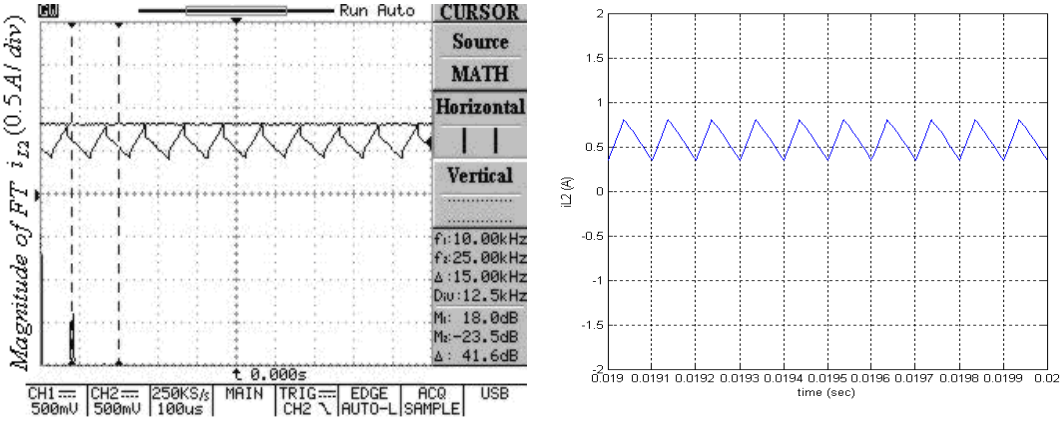

(b) Experimental and simulated results for i_{L2}.

{**Left**: experimental (1A/V), **right**: simulated}.

Figure 5.10 Period-1 with $L_1 = 1mH, L_2 = 0.9mH$ at $I_{ref} = 0.8A$.

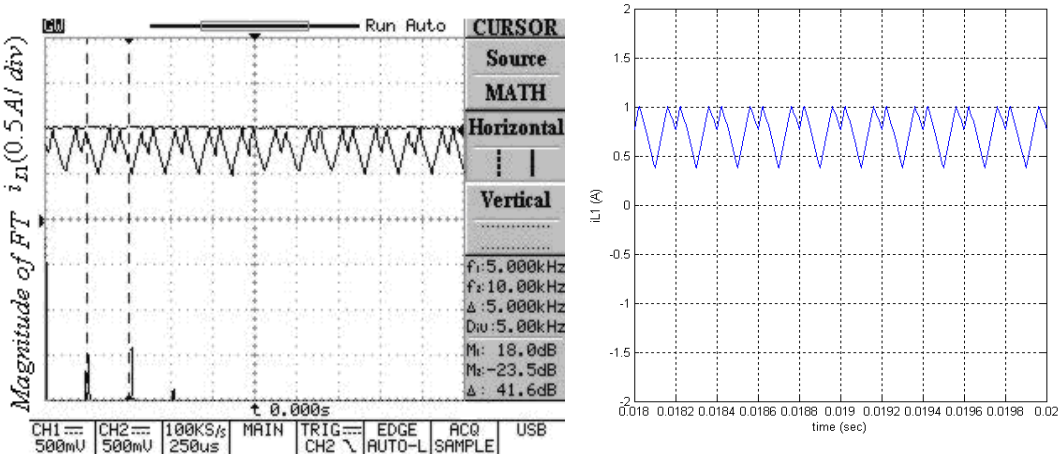

(a) Experimental and simulated results for i_{L1}.

{**Left**: experimental (1A/V), **right**: simulated}.

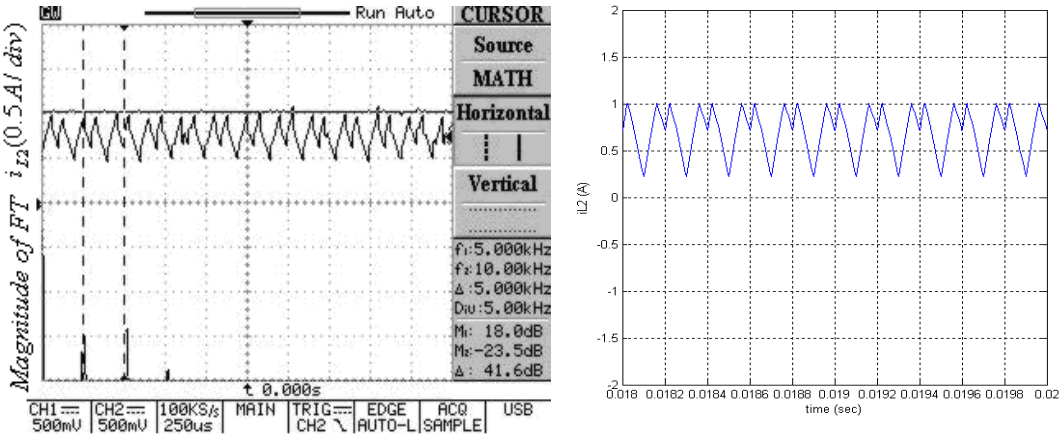

(b) Experimental and simulated results for i_{L2}.

{**Left**: experimental (1A/V), **right**: simulated}.

Figure 5.11 Period-2 with $L_1 = 1mH, L_2 = 0.9mH$ at $I_{ref} = 1A$.

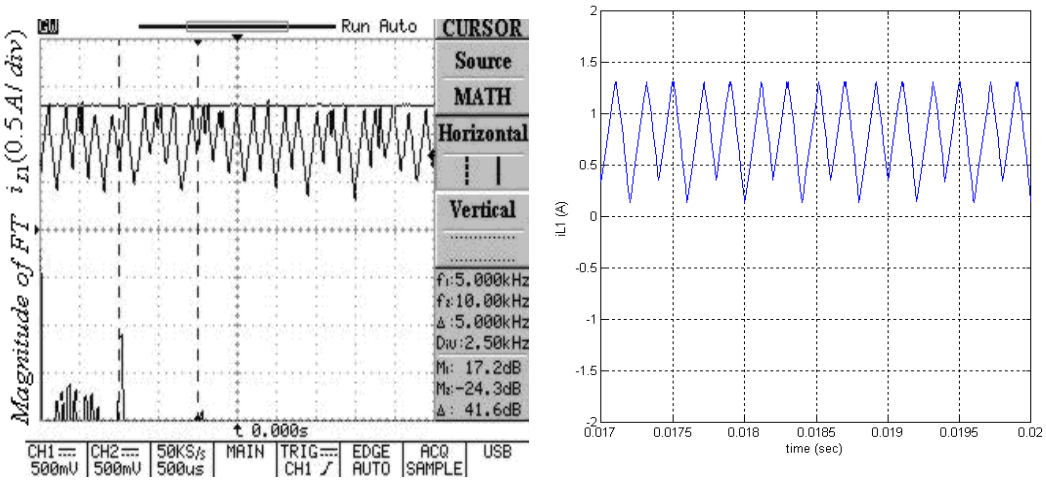

(a) Experimental and simulated results for i_{L1}.

{**Left**: experimental (1A/V), **right**: simulated}.

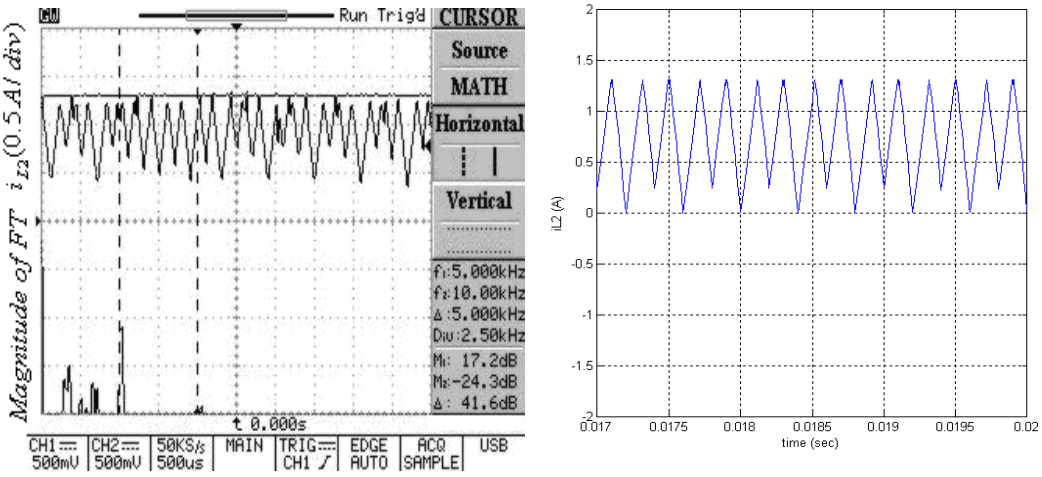

(b) Experimental and simulated results for i_{L2}.

{**Left**: experimental (1A/V), **right**: simulated}.

Figure 5.12 Chaotic with $L_1 = 1mH, L_2 = 0.9mH$ at $I_{ref} = 1.3A$.

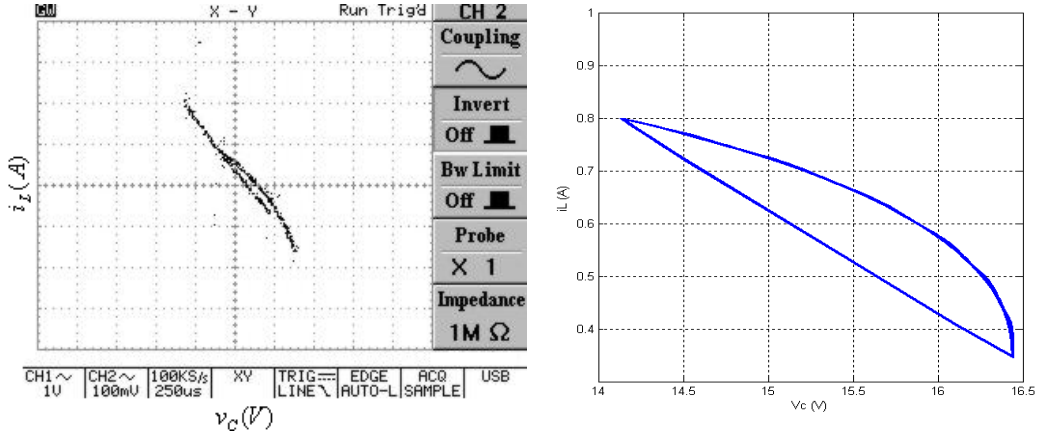

(a) Period-1 at $I_{ref} = 0.8A$

{**Left**: experimental CH2 (1A/V), **right**: simulated}.

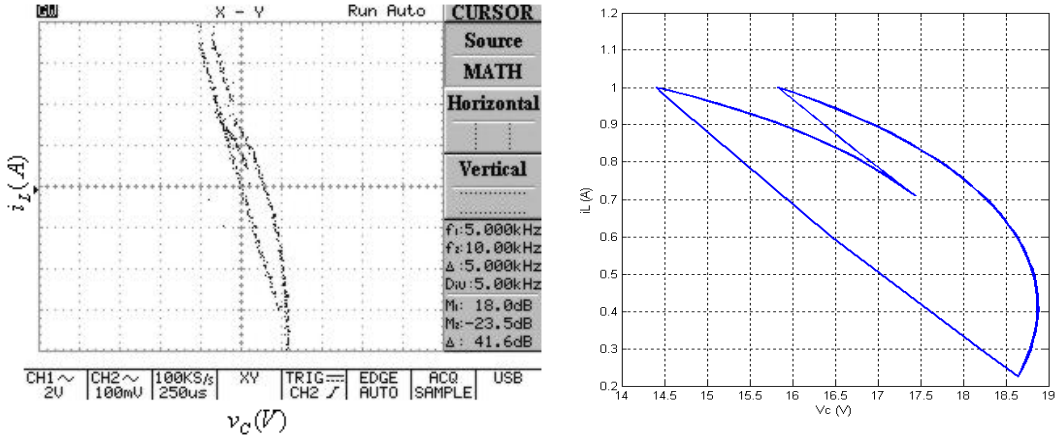

(b) Period-2 at $I_{ref} = 1A$

{**Left**: experimental CH2 (1A/V), **right**: simulated}.

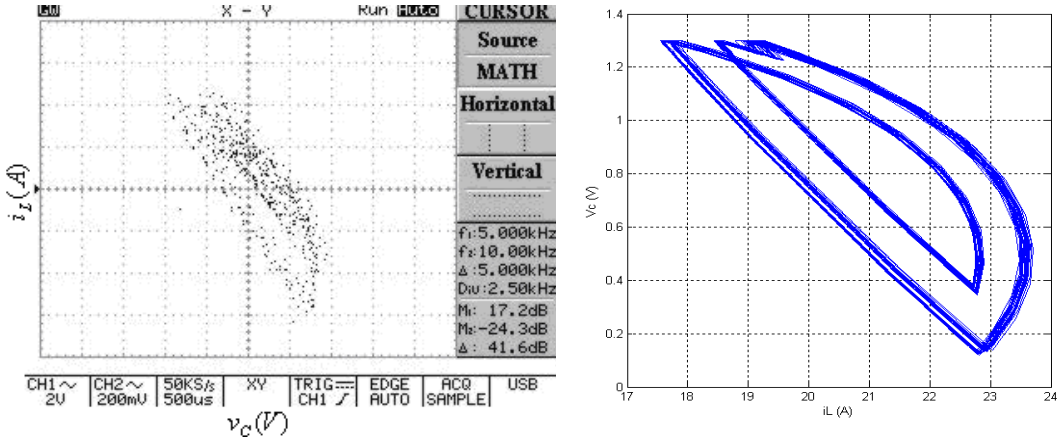

(c) Chaotic at $I_{ref} = 1.3A$

{**Left**: experimental CH2 (1A/V), **right**: simulated}.

Figure 5.13 Experimental and simulated phase portrait with $L_1 = 1mH, L_2 = 0.9mH$.

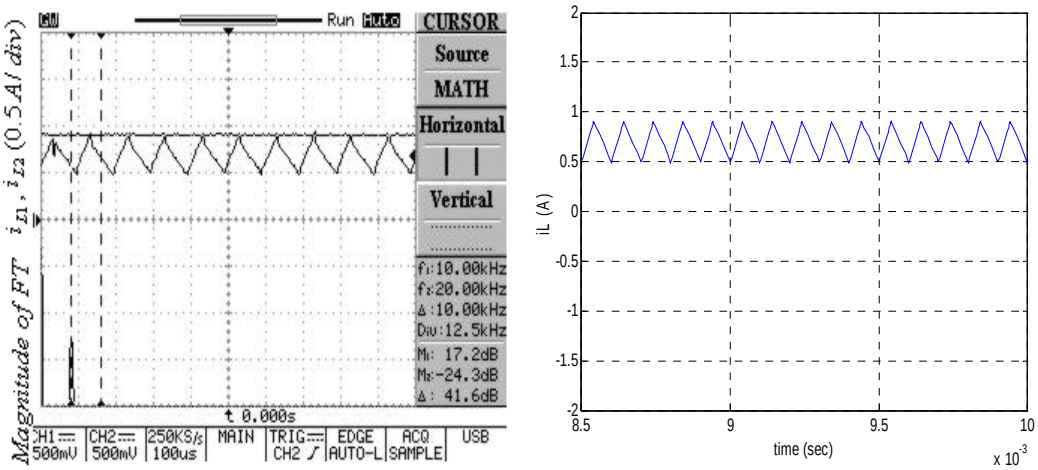

(a) Experimental and simulated inductor current for i_{L1}/i_{L2}.

{**Left**: experimental (1A/V), **right**: simulated}.

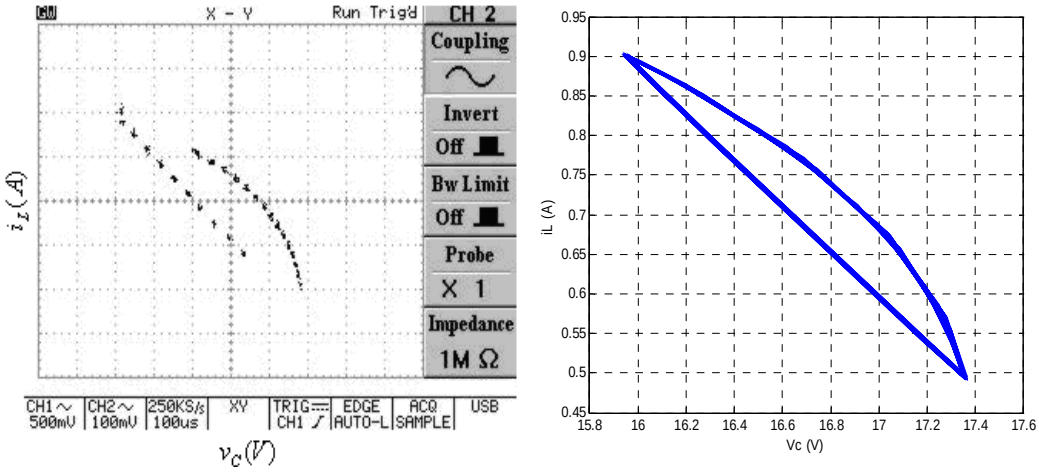

(b) Experimental and simulated phase portrait.

{**Left**: experimental CH2 (1A/V), **right**: simulated}.

Figure 5.14 Period-1 with $L_1 = L_2 = 1mH$ at $I_{ref} = 0.9A$.

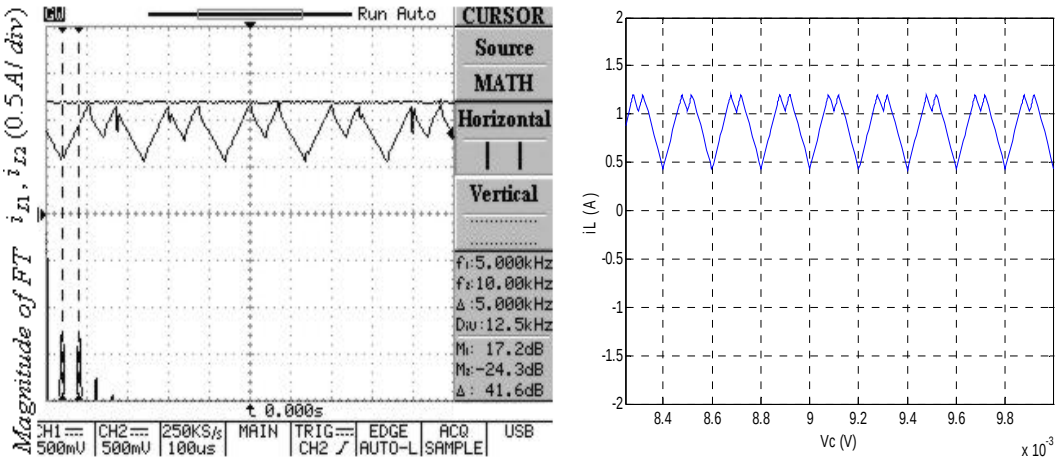

(a) Experimental and simulated inductor current for i_{L1}/i_{L2}.

{**Left**: experimental (1A/V), **right**: simulated}.

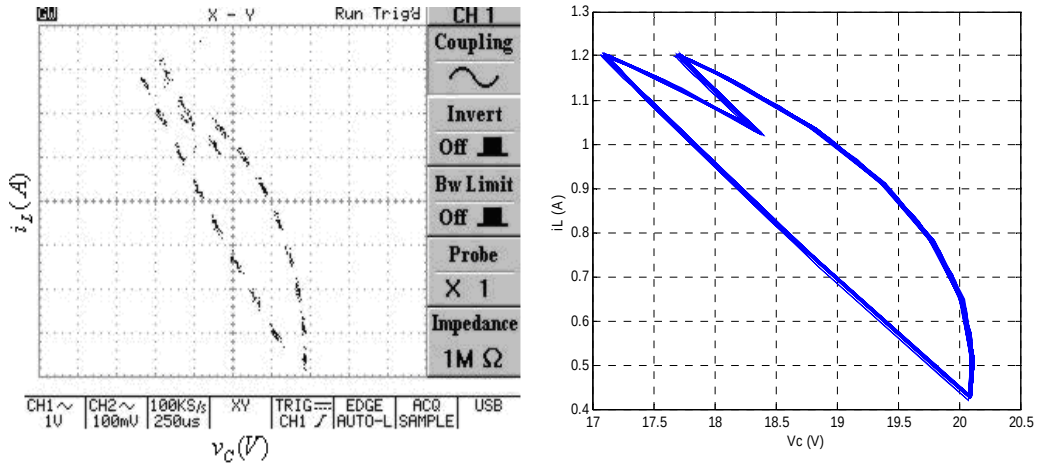

(b) Experimental and simulated phase portrait.

{**Left**: experimental (1A/V), **right**: simulated}.

Figure 5.15 Period-2 with $L_1 = L_2 = 1mH$ at $I_{ref} = 1.2A$.

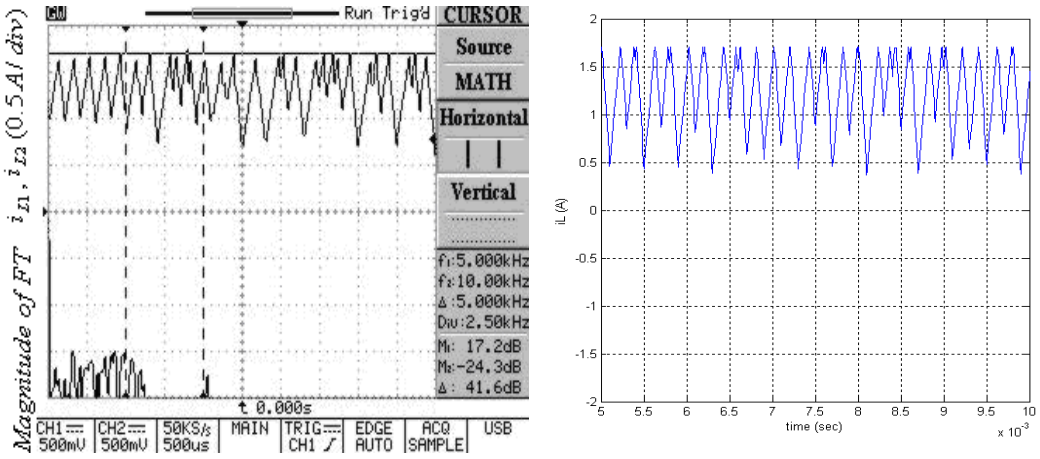

(a) Experimental and simulated inductor current for i_{L1}/i_{L2}.

{**Left**: experimental (1A/V), **right**: simulated}.

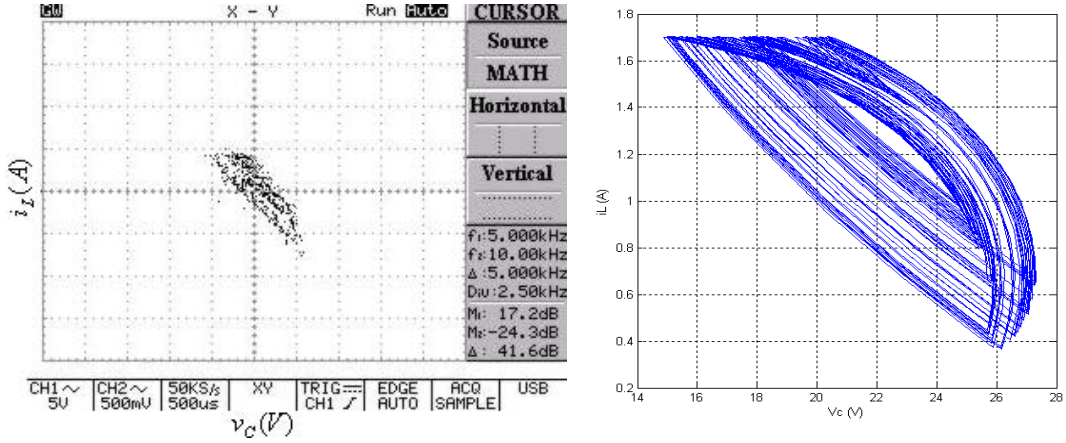

(b) Experimental and simulated phase portrait.

{**Left**: experimental CH2 (1A/V), **right**: simulated}.

Figure 5.16 Chaotic with $L_1 = L_2 = 1mH$ at $I_{ref} = 1.7A$.

CHAPTER 6
CONTROL OF CHAOS IN A DC-DC BOOST CONVERTER

The conventional method for controlling sub-harmonic oscillations and chaotic behaviour in current-controlled switched-mode power electronic converters is by slope compensation. However, in this thesis an alternative approach using delayed feedback control is investigated. The method eliminates chaos by stabilizing unstable periodic orbits that exist in the chaotic attractor [43]. A bifurcation diagram is developed on the plane of feedback parameters and this is used to identify the optimum feedback parameters for stability and robustness of control. The effectiveness and robustness of the resulting controller is demonstrated by experimental and simulated results, which are presented in Chapter 8.

In order to compare delayed feedback control with the slope compensation method, MATLAB/SIMULINK models were developed and these were used to produce the simulated results in Chapter 8.

6.1 Slope Compensation Method (SCM)

A simplified diagram for a control circuit to stabilise a DC-DC boost converter using slope compensation is given in Fig. 6.1. [10]. A compensating ramp is subtracted from the reference current I_{ref}, as shown in Fig. 6.2 and this is compared with the inductor current to control the on-time of the switch. An alternative strategy is to add the ramp to the fed-back inductor current signal i_L. The aim of the compensation ramp is to reduce the value of the reference level and since the ramp is linear, this reduction is directly proportional to the on-time of the switch. The slope of the ramp (m_c) required to ensure stability is determined by the relationship $m_C \rangle m_1(\frac{1}{2D_{off}} - 1)$, where $D_{off} = \frac{t_{off}}{T}$ and m_1 is the slope of the increasing inductor current during switch turn-on as shown in Fig. 6.2. Since $m_1 = \frac{V_{in}}{L}$, this gives $m_C \rangle \frac{V_{in}}{L}(\frac{1}{2D_{off}} - 1)$. This allows the system to operate at a larger duty cycle, without running into period doubling and chaotic regions.

6.2 Delayed Current Feedback Method (DCFM)

Ott, Grebogi and Yorke (OGY) [44] were the first researchers to propose a method for controlling chaotic systems. They determined that the behaviour of a chaotic system could be converted to a periodic system, by applying a small time-dependent feedback perturbation to one of the accessible system parameters. The changes in the system parameter are discrete in time, since they occur at each crossing of the Poincare map of the system. When applying the OGY method to control chaos in a real physical circuit, the main problem encountered was the noise introduced due to inevitable noise of the circuit elements, A/D and D/A conversion of signals (quantification), etc. The method was found to be very sensitive to the noise level - very small signals sometimes are hidden within the noise, and control is impossible [45]. Thus the method has some limitations and is sensitive to noise.

Pyragas [43] suggested that chaotic behaviour may be controlled by applying the general delayed feedback control scheme shown in Fig. 6.3. The method is based on the idea of a quasi-time-continuous self-controlling feedback, with a small perturbation calculated at a high sampling rate, which does not change the form of the desired unstable periodic orbit, but under certain conditions can stabilise it [46]. The feedback control force $F(t)$ that is applied to the system is the difference between the current value of some system variable $y(t)$, and its value τ seconds previous, multiplied by a constant K, where K is the feedback strength (Eqs.6.1 and 6.2).

$$\begin{aligned} \dot{y} &= P(y,x) + F(y,t) \\ \dot{x} &= Q(y,x) \end{aligned} \tag{6.1}$$

where

$$F(y,t) = K[y(t-\tau) - y(t)] \tag{6.2}$$

The idea behind the scheme relies on the fact that a skeleton of a chaotic attractor is formed by an infinite set of unstable periodic orbits with different periods. If the value of time delay τ is exactly equal to the period T of one of the orbits, then at the appropriate values of K the orbit can become stable, and thus chaos will be eliminated. Once control is achieved, i.e. the phase trajectory reaches the periodic orbit; the control force $F(t)$ is zero at any instant. This is called non-invasive control

and implies that virtually no power is spent in the control loop to support the desired behaviour of the system. The method has been applied successfully in many practical applications [47]. A simplified diagram for delayed current feedback applied to the boost converter is shown in Fig. 6.4.

The system performance and stability depends on both the choice of the delay τ and the feedback gain K. In order to identify the ranges of K and τ that would result in the desired periodic oscillations of i_L for various values of I_{ref}, maps of the regimes on the (τ, K) plane were generated numerically at I_{ref} = 1, 2, 3 and 4A following the method described in [48]. The process of generating the map required the production of a series of bifurcation diagrams relating i_L to *K* for a given value of τ. The process is repeated for different values of τ and the map is laboriously generated by hand. The diagrams are given in Fig. 6.5, shows areas with qualitatively distinct behaviour marked by expressions like "period-1", "chaos", etc. The contour lines define the transitions between different kinds of behaviour and these are not necessarily associated with bifurcations.

It is evident from Fig. 6.5 that a large period-1 region exists around τ = 70μs for all the maps and that this is a suitable value for the delay. To illustrate the transitions occurring in the system as its parameters are changed, two values of τ; 100μs and 70μs at $I_{ref} = 3A$ were chosen and the variation of i_L with K in the Poincaré section were obtained as shown in Fig. 6.6. At τ = 70μs the system is chaotic as K increases from zero to 0.15, after which it becomes stable "period-1" with a frequency of 10 kHz. For τ = 100μs, the system goes through a series of chaotic and periodic states up to K = 0.66, after which it becomes stable "period-2" with a frequency of 5 kHz.

6.3 MATLAB/SIMULINK Models for Control Schemes

The structure of the MATLAB/SIMULINK model for the converter controlled using slope compensation is given in Fig. 6.7 and that for the converter controlled using delayed current feedback is given in Fig. 6.8.

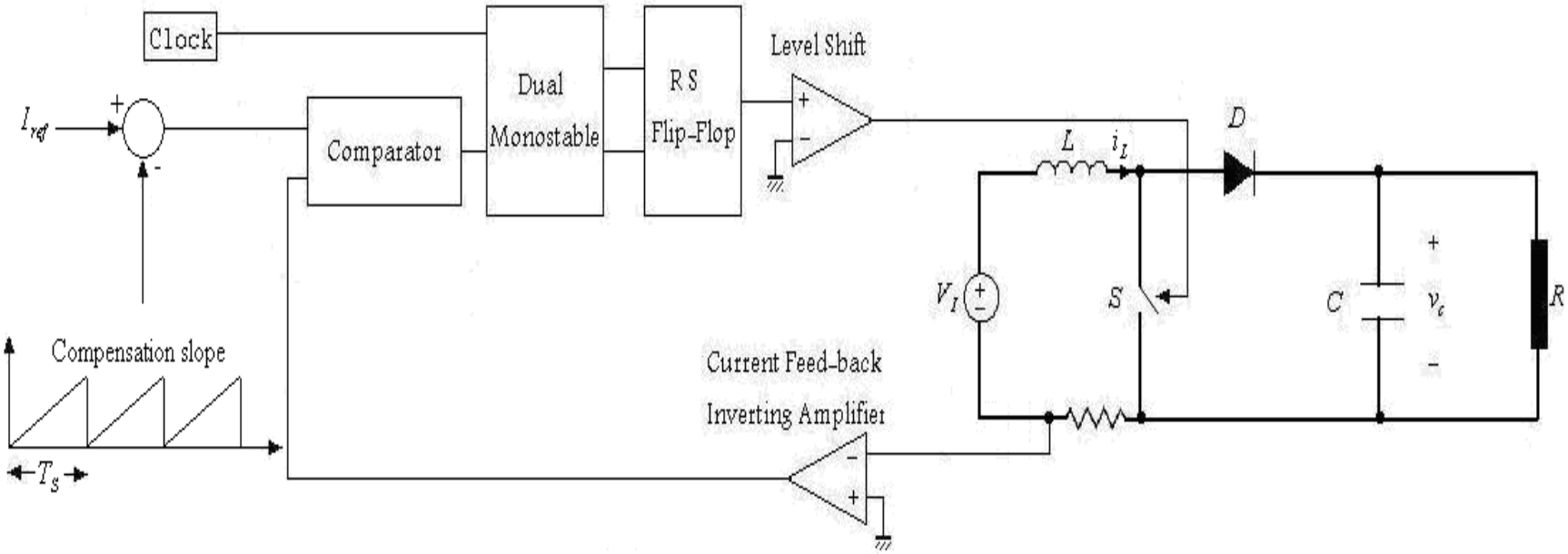

Figure 6.1 Converter circuit diagram with slope compensation.

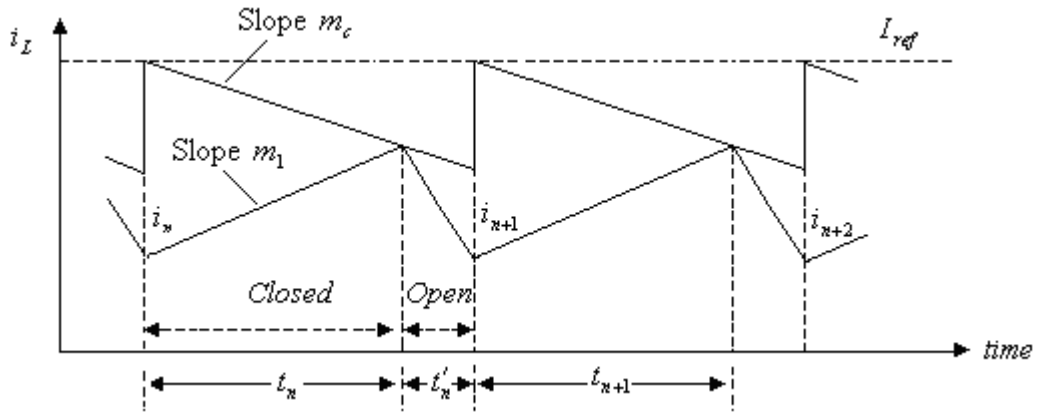

Figure 6.2 Slope compensation waveforms for Fig. 6.1.

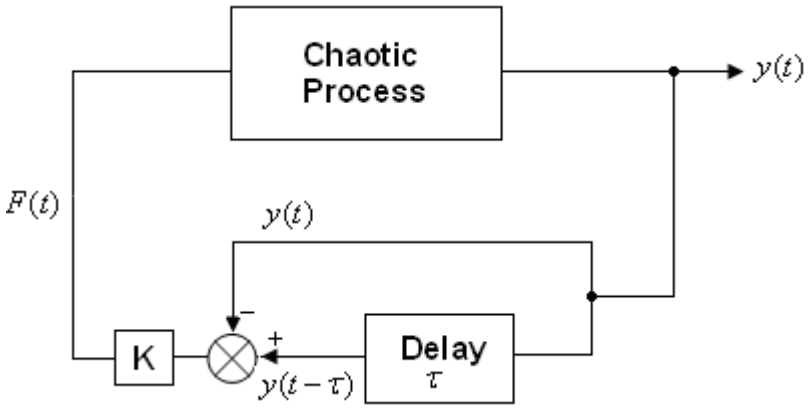

Figure 6.3 Delayed current feedback control system.

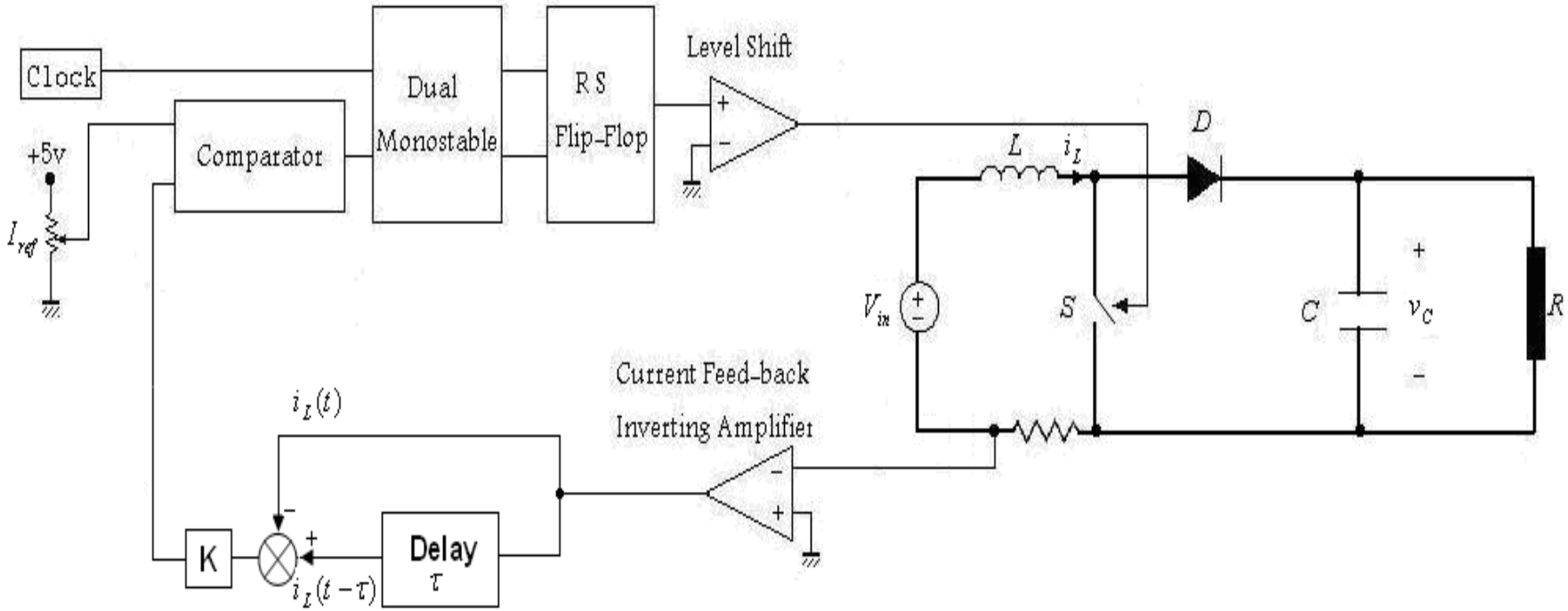

Figure 6.4 Current circuit diagram with delayed current feedback.

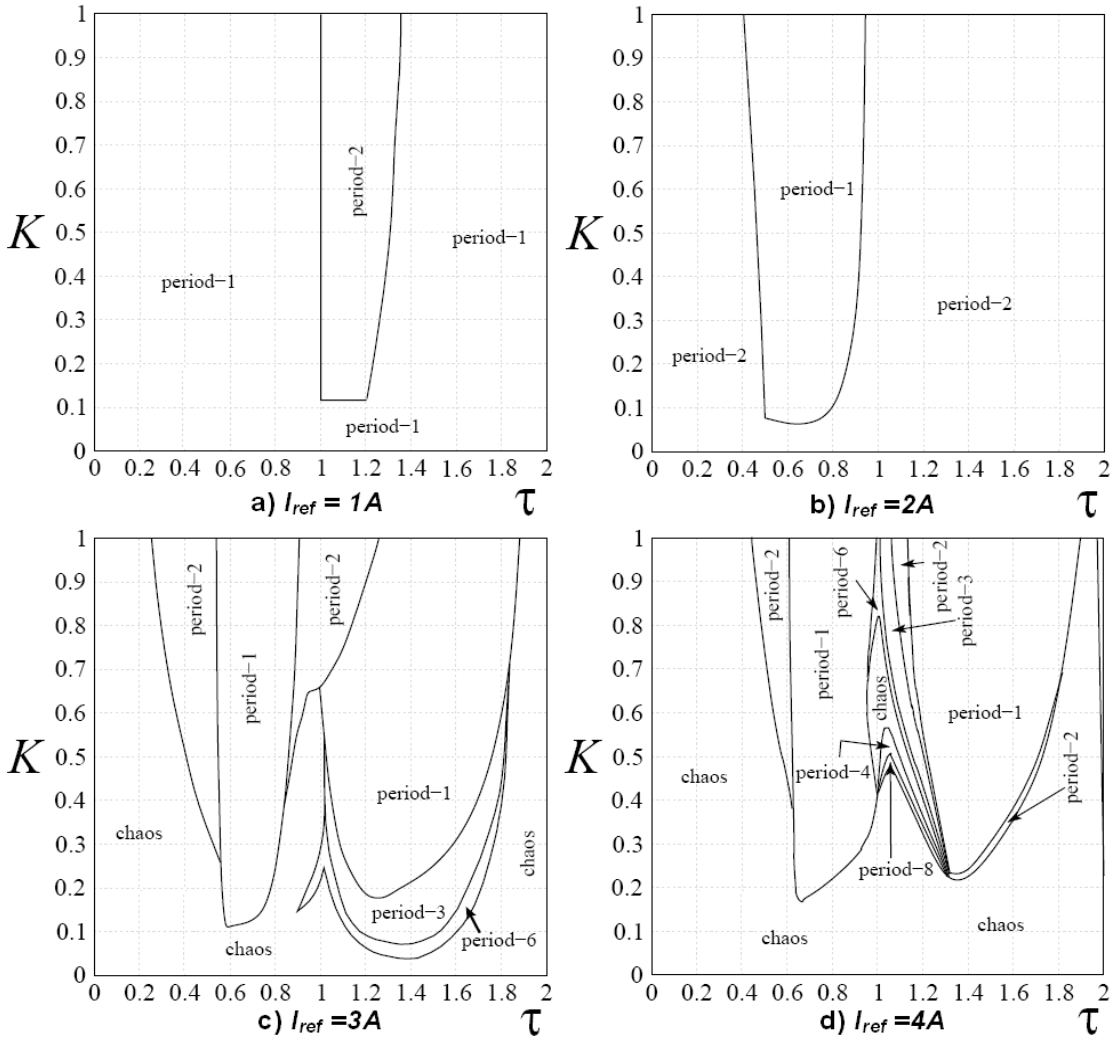

Figure 6.5 Maps of regimes on the plane (τ, K) for various I_{ref}.

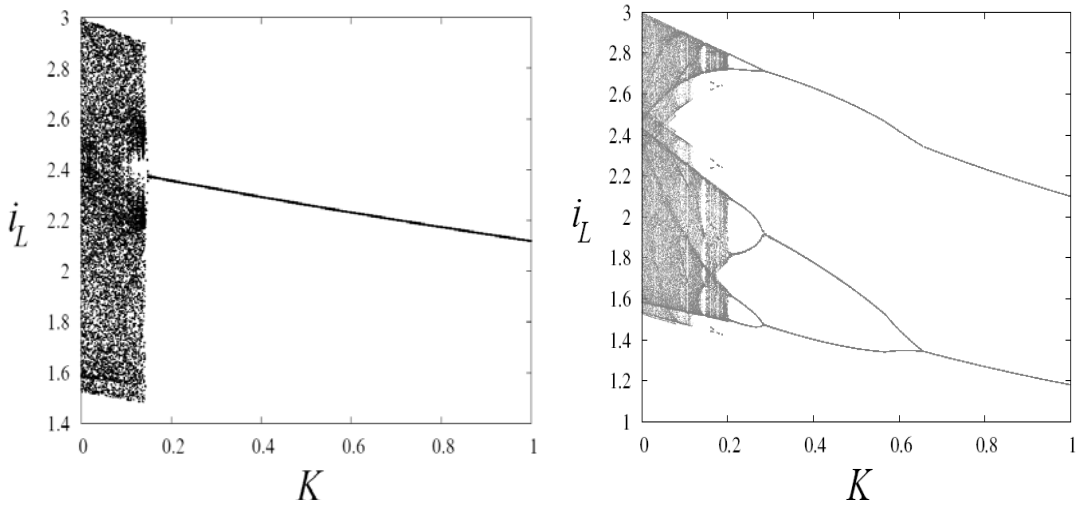

Figure 6.6 Bifurcation diagrams for i_L against K with $I_{ref} = 3A$

{**Left**: τ = 70μs, **right**: τ = 100μs}.

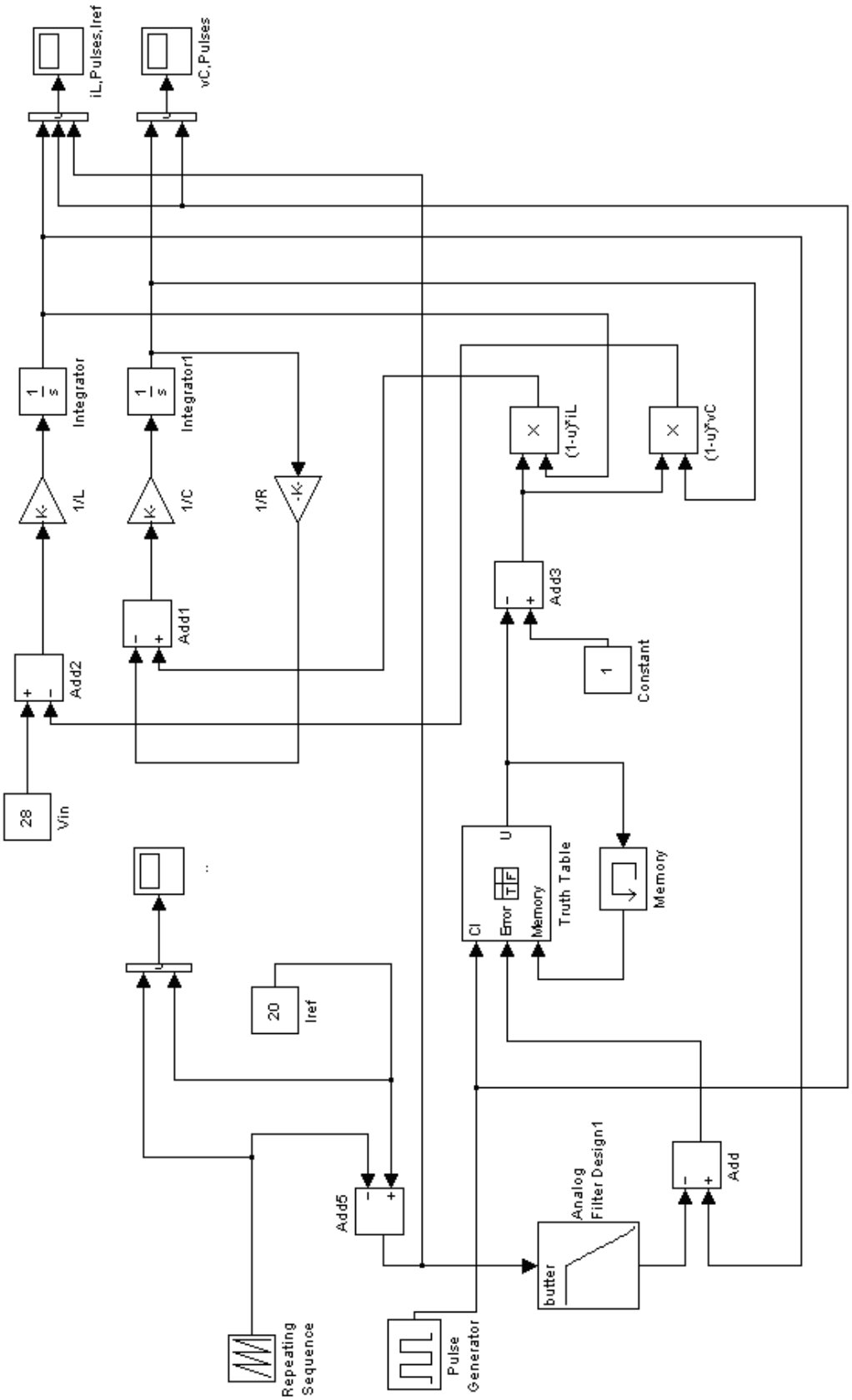

Figure 6.7 SIMULINK model using slope compensation.

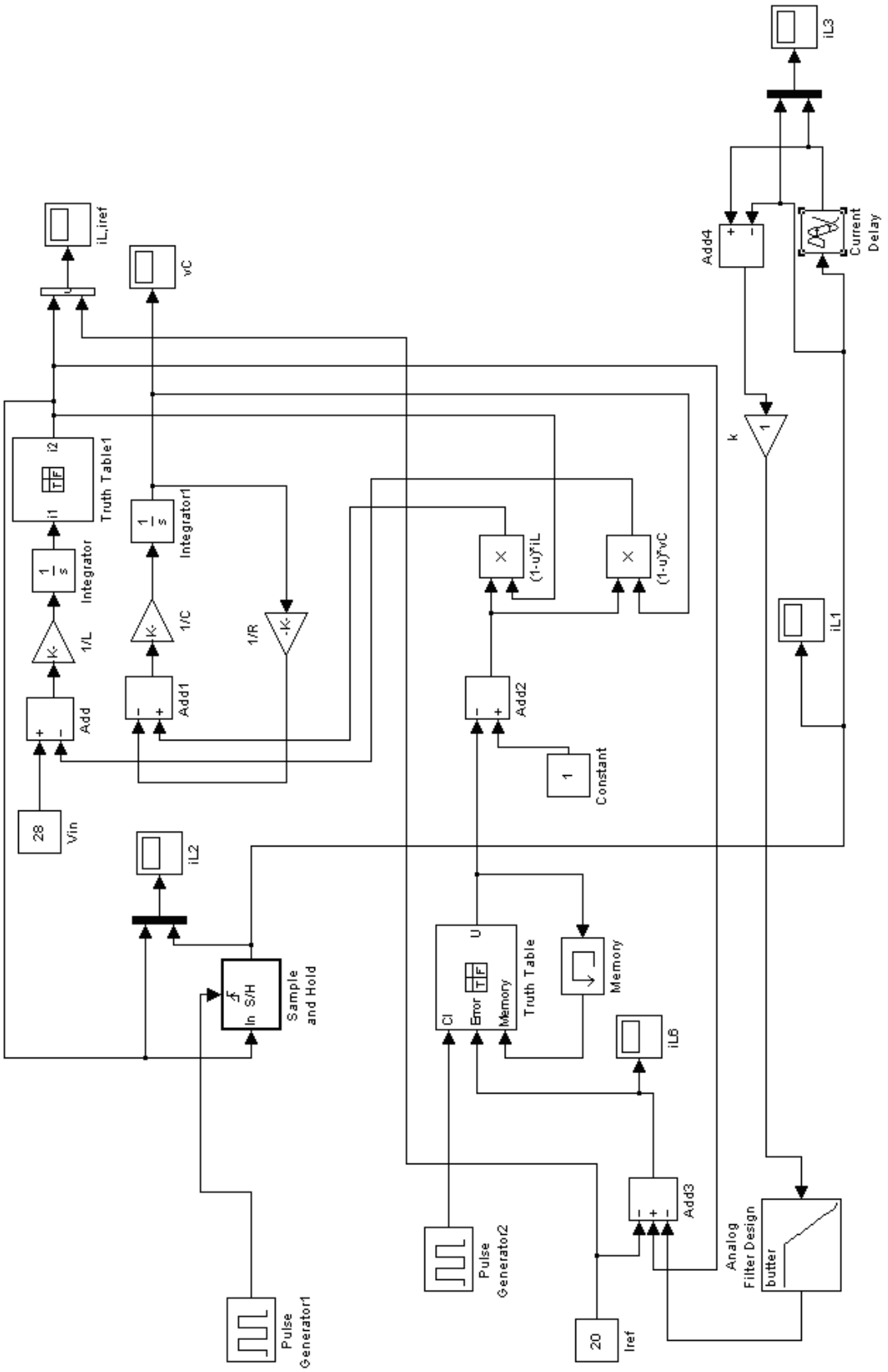

Figure 6.8 SIMULINK model with delayed current feedback.

CHAPTER 7
DC-DC BOOST CONVERTER CONTROL SCHEME

7.1 Discrete Component Control Scheme

The initial circuit, designed and built to implement the delay $i_L(t-\tau)$ in the circuit of Fig. 6.4, used the discrete analogue and digital integrated circuits shown in Fig. 7.1. The operation of the circuit is as follows. The inductor current $i_L(t)$ is converted to an 8-bit digital signal using a (MAX118) A/D converter [49]. This is loaded into the first of a series of twelve tri-state latches. A 100 kHz clock (LM555) triggers a (74HCT123) monostable on the rising edge. The $\overline{Q}$ output of the monostable simultaneously enables the "read" of the A/D converter and the "write" of the D/A converter (AD7524) [50]. It also sets into operation a "chain reaction" moving the data through the tri-state latches, starting at latch 12 and moving downwards at 10μs intervals. The chosen delay τ is selected by the switches S80-S120. eg: Closure of S100 selects the output of tri-state latch 10 to be applied to the common bus and this corresponds to a delay of 100 μs, etc. The digital signal on the common bus is converted back to an analogue signal $i_L(t-\tau)$ using the D/A converter. A photograph of the controller hardware is given in Appendix D.3.

The circuit operated satisfactorily, but it was unable to vary (τ,*K*) over a wide range. So it was decided to implement the control using a microcontroller.

7.2 Microcontroller Control

Due to the shortcomings of the discrete component control circuit, a microcontroller implementation was designed and built. An 80C51 family microcontroller was chosen as the core of the control circuit because of its proven versatility and the fact that it is still undergoing development by three major semiconductor manufacturers (Atmel, Intel and Philips) who are constantly introducing faster devices with more memory, and peripherals etc. It is an 8-bit processor which is straight forward enough to use whilst being sufficiently versatile for application to many projects. It is well supported by the department [51].

The ATMEL AT89C51 is a highly integrated semiconductor device and powerful microcontroller which provides a highly-flexible and cost-effective solution to many embedded control applications. It is referred to as a microcontroller rather than microprocessor because it contains memory and interface components. The AT89C51 is a low-power, high performance CMOS Flash version of the 80C51 microcontroller family single chip 8-bit microcontroller. It contains a 64-Kbyte Flash memory block for code and data and 256-Byte RAM for variable storage. The on-chip Flash allows the program memory to be reprogrammed by a conventional non-volatile memory programmer that is parallel programmable [52]. A simplified diagram of the hardware is given in Fig. 7.2.

The microcontroller code was written in µVision3 from KEIL Software, which is a microcontroller development tool for 80C51, 251, XC16X, ST10 and ARM microcontroller families. The KEIL µVision software was chosen since its environment supports programming in C. The binary code produced was loaded into the chip, using an advanced universal programmer (DATAMAN-48Pro). A flowchart for the program software is given in Fig. 7.3., and the program code is given in Appendix C.1.

The complete circuit diagram is given in Fig. 7.4 and a photograph of the controller hardware is given in Appendix D.4. A 10 kHz clock signal is obtained using an LM555 integrated circuit. The rising edge of the clock signal triggers a 74HCT123N monostable to enable the set input of an S-R flip flop constructed using 2-input NOR gates and 3-input AND gates. The output of the flip-flop is applied to a 311 comparator, which turns-on the gate of the MOSFET switch. The inductor current $i_L(t)$ is sensed using a 0.2Ω non-inductive resistor in series with the source of the MOSFET switch. This signal is amplified using a TL071 (A1), connected as an inverting amplifier and then converted to an 8-bit digital signal using the MAX118 A/D converter. The data output used latched three-state buffer circuitry, for direct connection to the 8-bit parallel microcontroller system input port 0. The crystal oscillator provides an external 24MHz clock signal to the microcontroller. The frequency for the timer is $1/12^{th}$ the frequency of the crystal attached to the 89C51. The controlled variable $i_L(t)$ is sampled at 10µs intervals and these are stored in a

continually updated rolling array as shown in Fig. 7.5. A pointer extracts data from this array at a delay τ, pre-programmed by the operator, to provide the value $i_L(t-\tau)$ at port 1. The 8-bit $i_L(t-\tau)$ signal is converted to an analogue signal using an AD7524 D/A converter with 2-quadrant multiplication. By setting the Vernier resistor *K* of amplifier A3, the output $K[i_L(t-\tau)-i_L(t)]$ is obtained. This output is subtracted from $i_L(t)$ and compared with the reference current I_{ref} using a 311 comparator, to generate the reset signal for the S-R flip flop, which turns-off the switch.

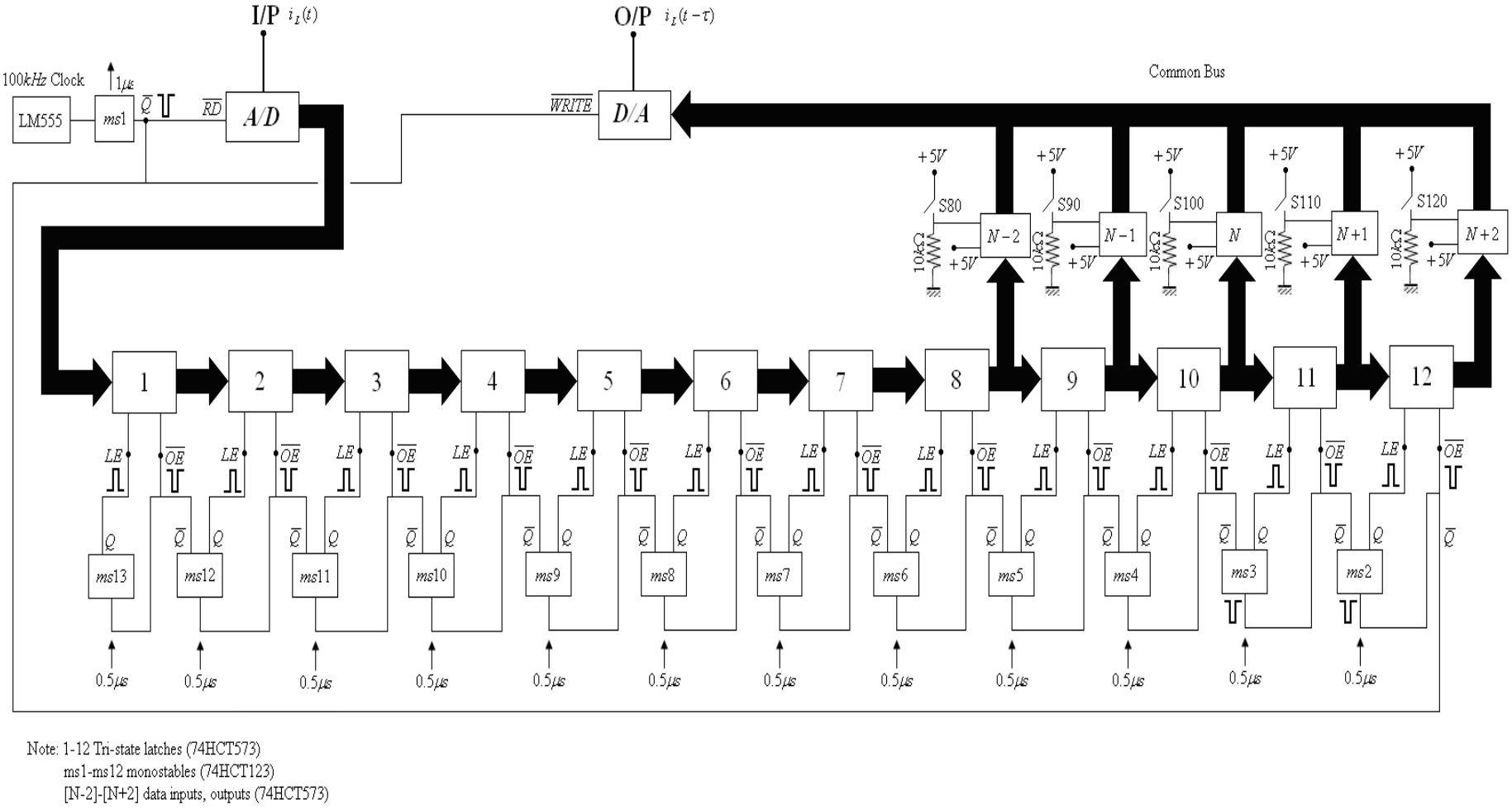

Note: 1-12 Tri-state latches (74HCT573)
ms1-ms12 monostables (74HCT123)
[N-2]-[N+2] data inputs, outputs (74HCT573)

Figure 7.1 Delayed current feedback discrete control scheme.

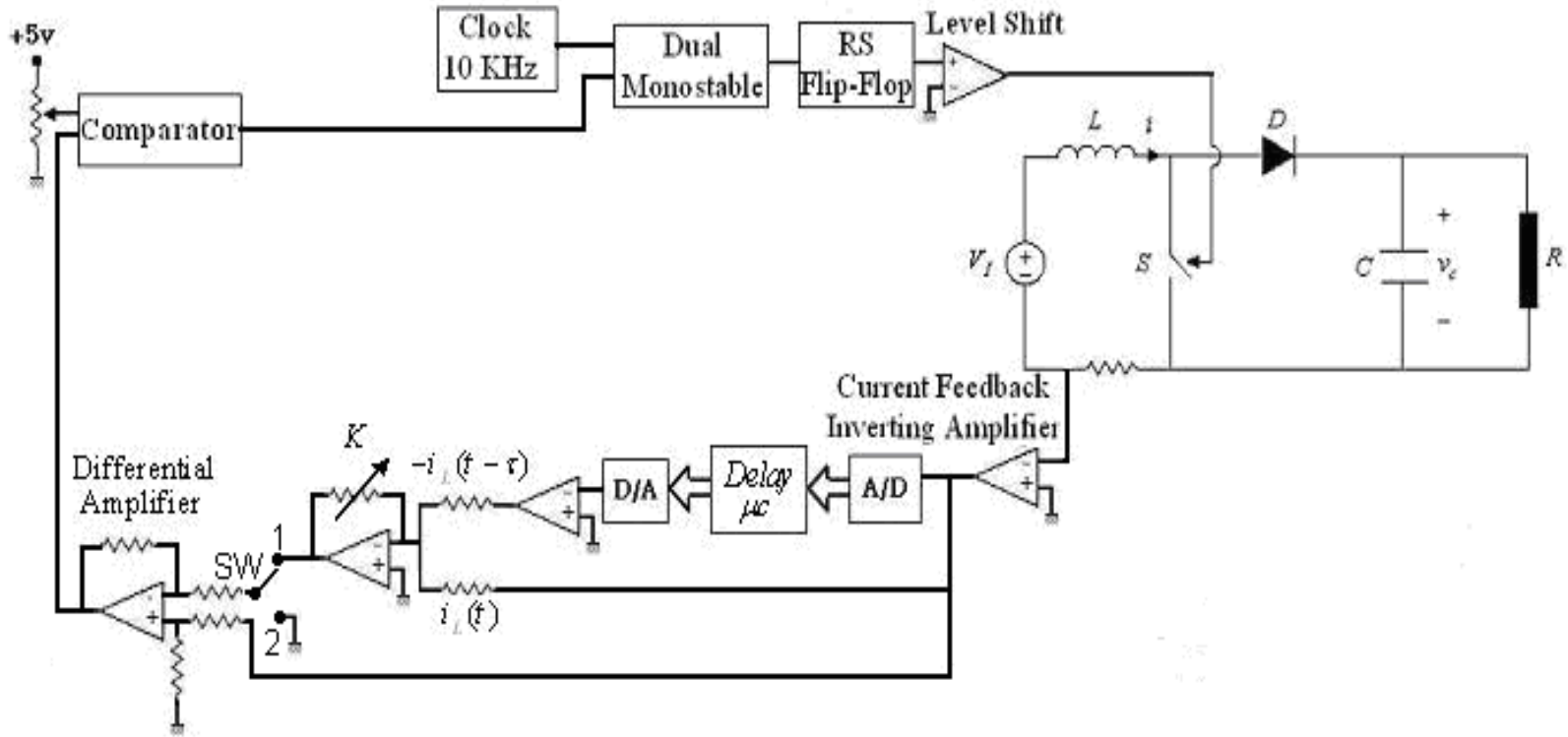

Figure 7.2 Experimental feedback control scheme.

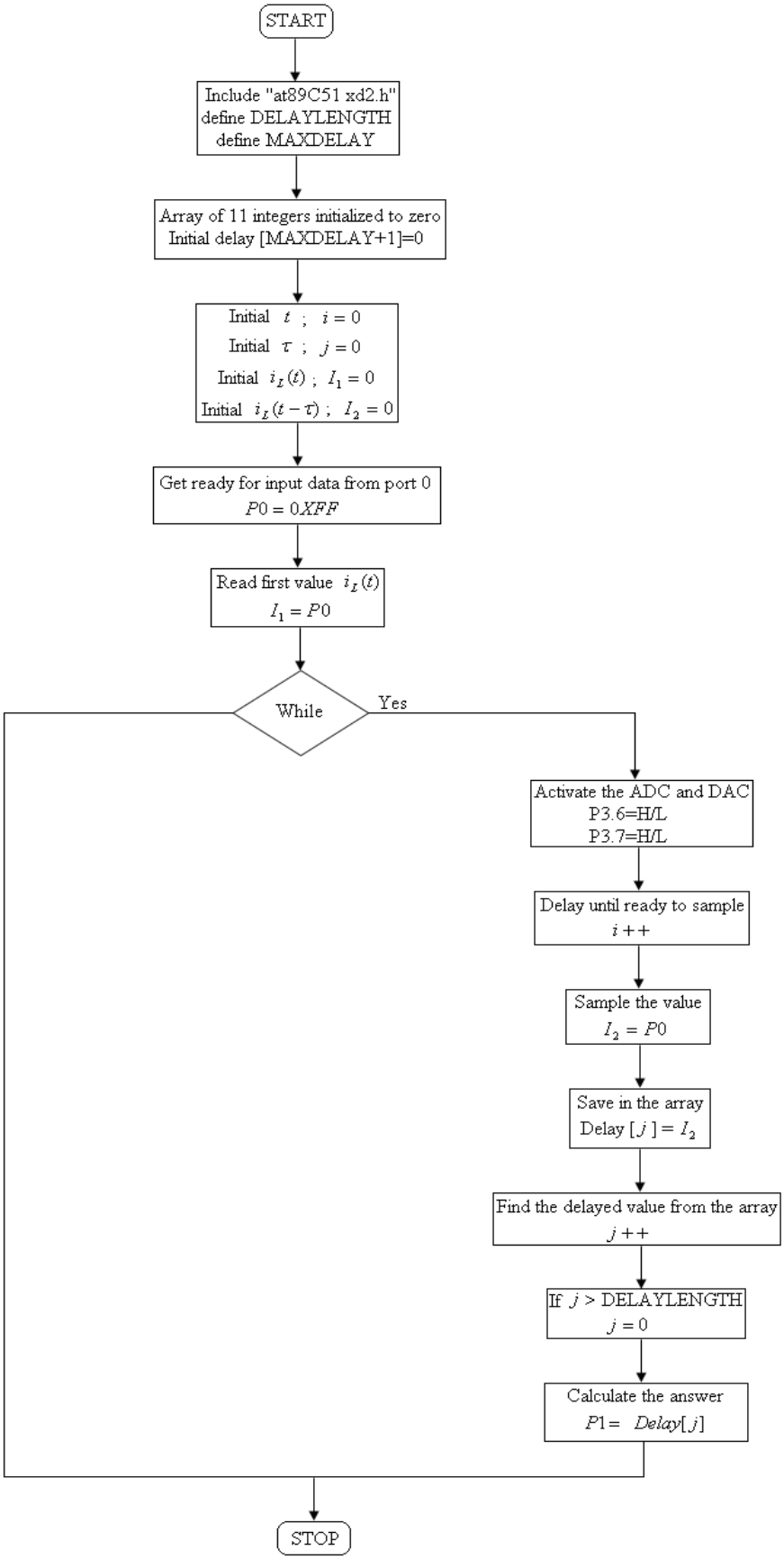

Figure 7.3 Delayed current feedback program flowchart.

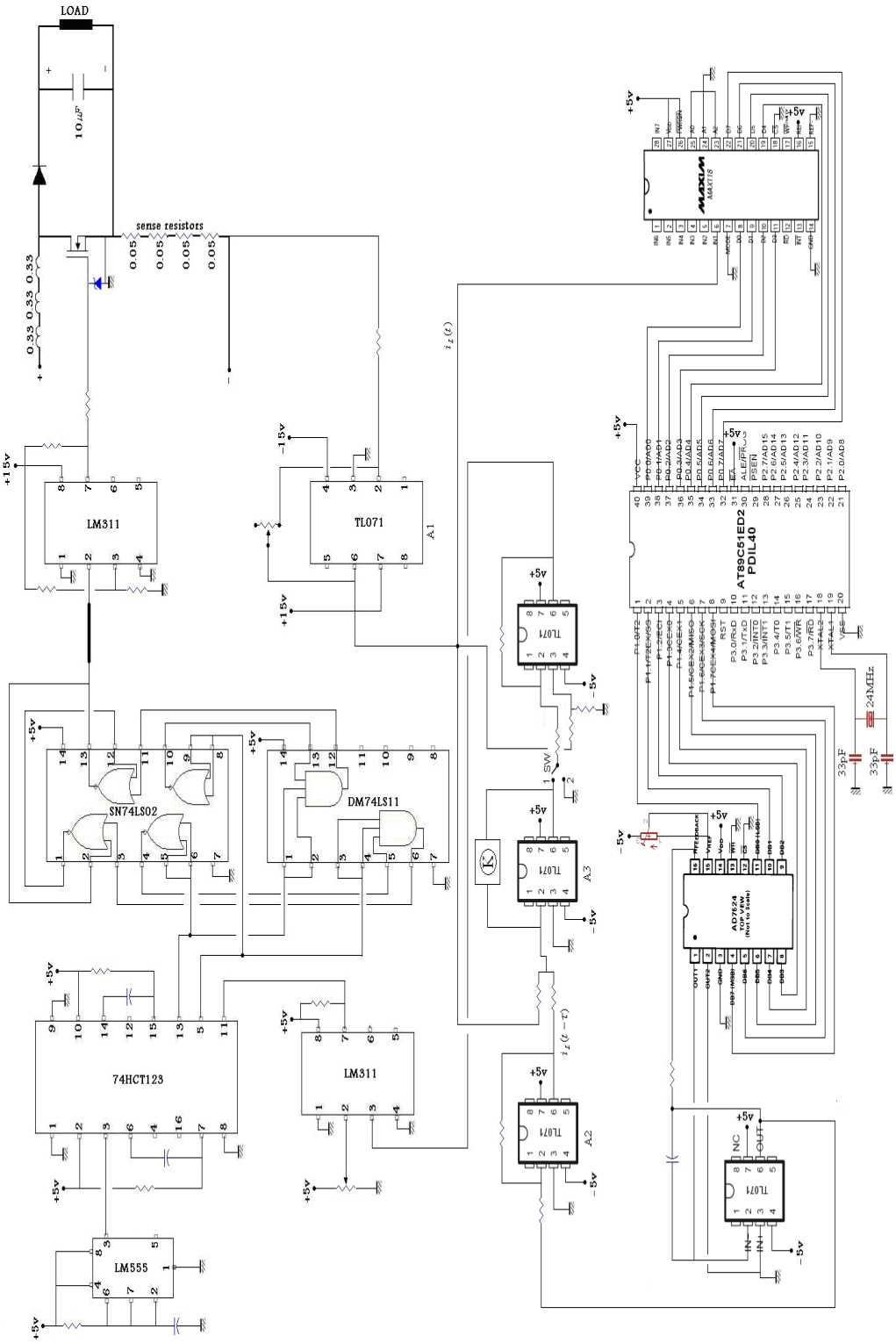

Figure 7.4 Delayed current feedback microcontroller scheme hardware.

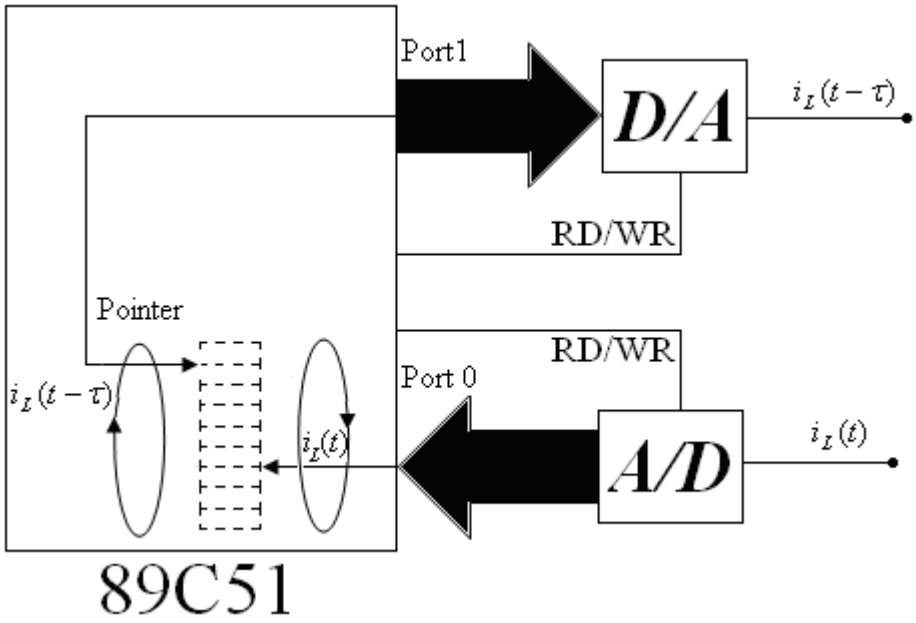

Figure 7.5 Delayed current feedback rolling array.

CHAPTER 8
EXPERIMENTAL AND SIMULATED RESULTS FOR THE CONTROLLING CHAOS SINGLE BOOST CONVERTER

This chapter presents both experimental and simulated results for the single boost converter, with delayed current feedback and investigates the improvement in performance over that of the uncontrolled converter. The simulated performance of a boost converter using slope compensation is compared to that of a converter using delayed current feedback control.

8.1 Delayed Feedback Control Results

As mentioned in Chapter 7, the controlled variable $i_L(t)$ is sampled at 10μs intervals and these are stored in a continually updated rolling array in the microcontroller and a pointer extracts data from the array at a delay τ, to provide the value $i_L(t-\tau)$.

Experimental waveforms for $i_L(t)$ and $i_L(t-\tau)$ at $I_{ref} = 1.7A$ are shown in Fig. 8.1, with the feedback switch SW of Fig. 7.2 in position 2. This disconnects the delayed current feedback from the control circuit. For this condition, it is evident from the figure that the converter is operating in a "period-2" mode. The stepped-nature of $i_L(t-\tau)$ is due to the digitisation of the waveform and the pre-programmed 100μs delay is clearly visible.

The maps of the (τ,K) plane given in Fig. 6.5, identified τ = 70μs as a stable period 1 region and τ = 100μs as a stable period 2 region, for a feedback gain K = 1. Experimental and simulated waveforms for these values of delay, with $I_{ref} = 3A$, are given in Figs. 8.2 and 8.3 respectively and show good agreement. The simulations were obtained using a FORTRAN program, which solved numerically Eqs.3.1, by setting u_S to 1 at every clock pulse and u_S to 0 when $i_L(t) - K[i_L(t-\tau) - i_L(t)] = I_{ref}$. The program listing is given in Appendix B.1.

It is clear that the waveforms are stable in both cases, and these agree with the periodic regimes predicted in Fig. 6.4. The waveforms of Fig. 8.2 have a frequency of 10 kHz ("period-1" cycles), whereas those of Fig. 8.3 have a frequency of 5 kHz ("period-2" cycles).

Although a stable "period-2" operation with a frequency of 5kHz is theoretically acceptable, the converter was designed for 10kHz operation and the system would not be performing under optimum conditions with τ = 100μs. It is important therefore, to ensure that the system is operating in a "period-1" region of Fig. 6.5, preferably far away from any bifurcation boundaries.

It is evident from Figs. 8.2(a) and 8.3(a) that the introduction of delayed current feedback is invasive, since it has reduced the value of inductor current i_L at switch turn-off from 3A. For instance, the value is 2.65A in Fig. 8.2(a) and 2.2A in Fig. 8.3(a). At first sight, this reduction in the "effective" I_{ref} is undesirable. However, inspection of the bifurcation diagram of Fig. 3.1 for the uncontrolled boost converter shows that the system would be on the verge of chaos at 2.65A and period-2 at 2.2A.

To identify the period-1/period-2 boundary for the two values of τ, I_{ref} was slowly increased until the transition occurred. For τ = 70μs, the inductor current was still stable period-1 up to $I_{ref} = 4A$ (which is the rated current), while for τ = 100μs, the boundary value was $I_{ref} = 3.5A$. Figs. 8.4 to 8.7 show the waveforms each side of the boundary for the two values of τ.

8.2 Comparison between SCM and DCFM (Simulated)

To compare the converter performance using both slope compensation and delayed current feedback, the MATLAB/SIMULINK models given in Figs. 6.7 and 6.8 were developed using parameters given in Table 8.1, which were obtained from published literature [10]. With the slope compensation method, the slope of the ramp m_C is modified according to the relationship $m_C = 0.8\frac{V_{in}}{L}(\frac{1}{2D_{off}} - 1)$, with the 0.8 factor introducing a safety margin into the relationship.

Circuit Components	Values
Switching Period T	$40\mu s$
Input Voltage V_{in}	$28V$
Inductor L	$195\mu H$
Capacitor C	$2mF$
Load Resistor R	11.2Ω

Table 8.1 Converter parameters.

Simulated inductor current waveforms for both methods of control are given in Figs. 8.8 to 8.13 using the parameters given in Table 8.1. Fig. 8.8 shows the converter inductor current without control, at a reference current value $I_{ref} = 20A$. For this condition, it is evident that the system is on the verge of chaos. Fig. 8.9 shows the inductor current and compensating ramp with slope compensation control at $I_{ref} = 20A$. It is evident that the system is now operating in stable period-1. Fig. 8.10 shows the inductor current with slope compensation control at $I_{ref} = 40A$ and for this condition, the system is chaotic. Investigations showed that the upper boundary for period-1 operation was $I_{ref} = 38A$.

Figs. 8.11 and 8.12 show inductor current waveforms for delayed current feedback control, with $I_{ref} = 20A$ and $I_{ref} = 40A$ respectively. In both cases, the system is operating in stable period-1. In fact, the system operates in period-1 up to $I_{ref} = 43A$, at which point it enters period-2 as shown in Fig. 8.13.

The above results show that a greater range of stable period-1 operation is obtained using delayed current feedback, compared with slope compensation. A further advantage with delayed current feedback is that it provides a higher output voltage for a given I_{ref} as is evident in Figs. 8.14 and 8.15.

In summary, the control strategy for delayed current feedback is simpler than that for slope compensation. This is because the slope of the compensating ramp depends on the converter input voltage, and the duty cycle which is load dependent. On the other hand, the delayed current feedback strategy is fixed, once K and τ are chosen.

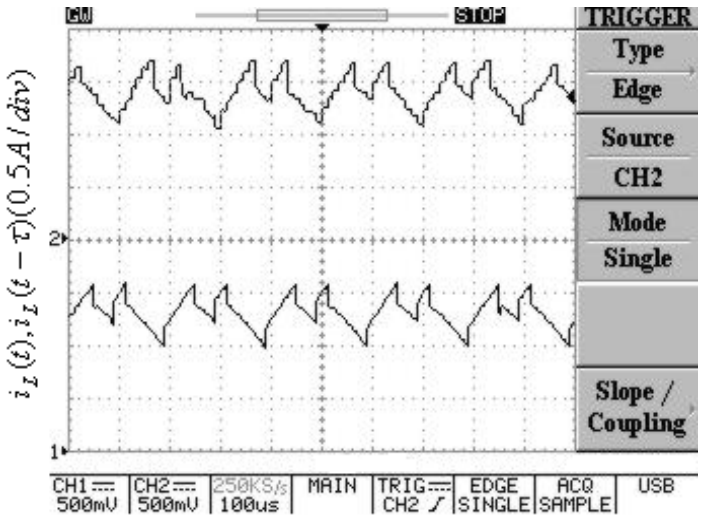

Figure 8.1 Experimental open loop waveforms (1A/V)

$I_{ref} = 1.7A$ and $\tau = 100\mu s$. $i_L(t)$ (lower) and $i_L(t-\tau)$ (upper)

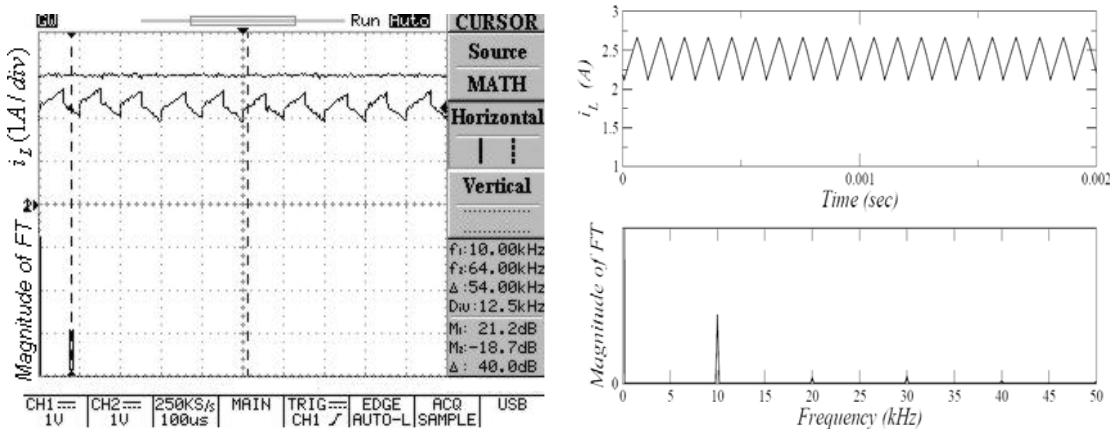

(a) Experimental and simulated inductor current.

{**Left**: experimental (1A/V), **right**: simulated}.

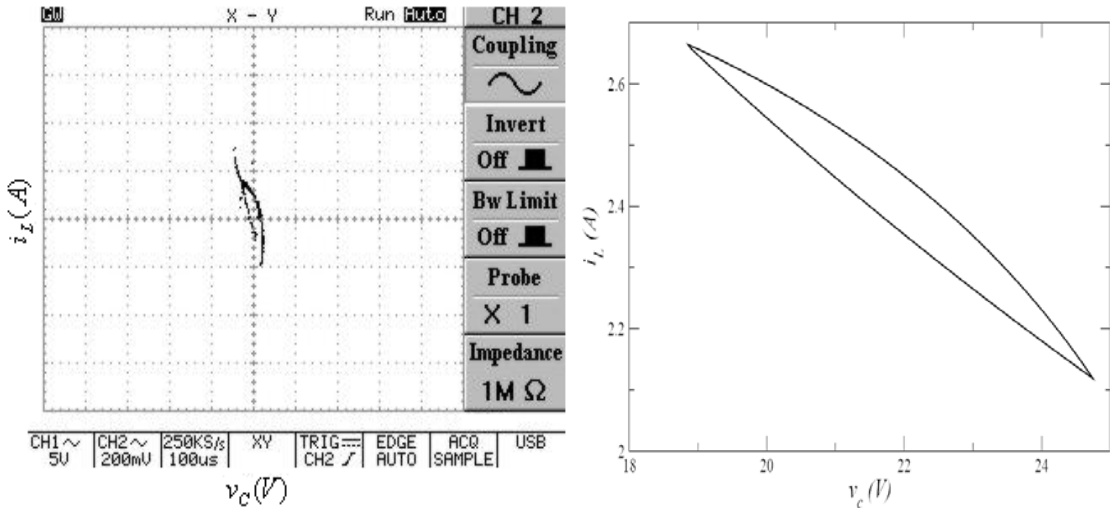

(b) Experimental and simulated phase portrait.

{**Left**: experimental, CH2 (1A/V), **right**: simulated}.

Figure 8.2 Delayed feedback control $I_{ref} = 3A$, $\tau = 70\mu s$, $K = 1$.

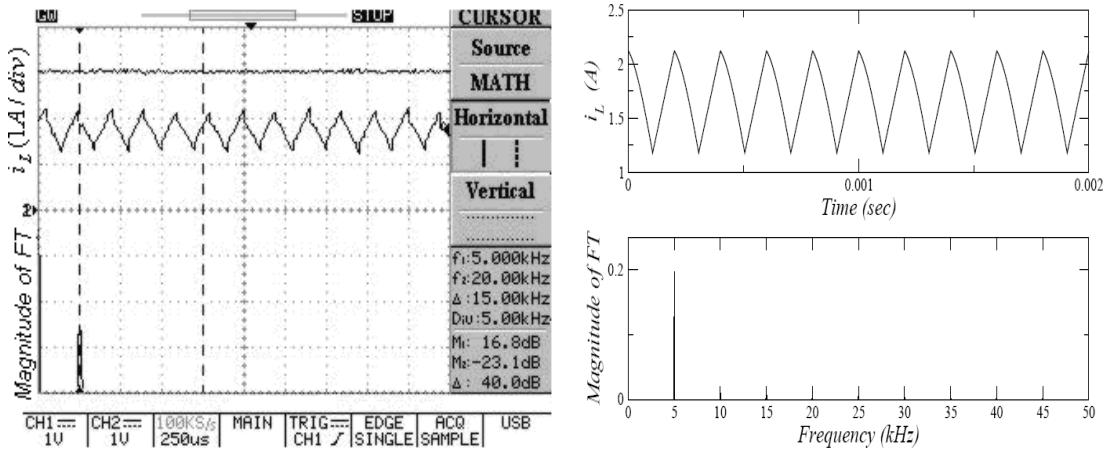

(a) Experimental and simulated inductor current.

{**Left**: experimental (1A/V), **right**: simulated}.

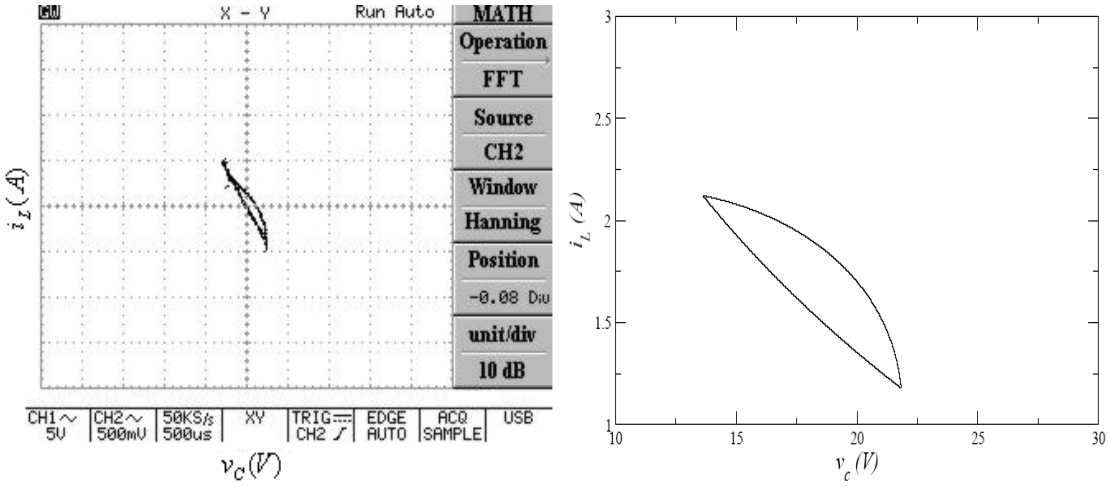

(b) Experimental and simulated phase portrait.

{**Left**: experimental, CH2 (1A/V), **right**: simulated}.

Figure 8.3 Delayed feedback control $I_{ref} = 3A,\ \tau = 100\mu s,\ K = 1$.

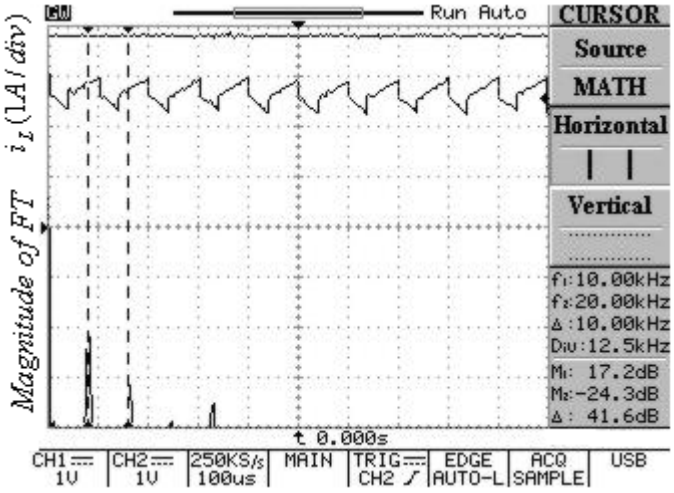

Figure 8.4 Delayed feedback control $I_{ref} = 3.8A$, $\tau = 70\mu s$, $K = 1$.

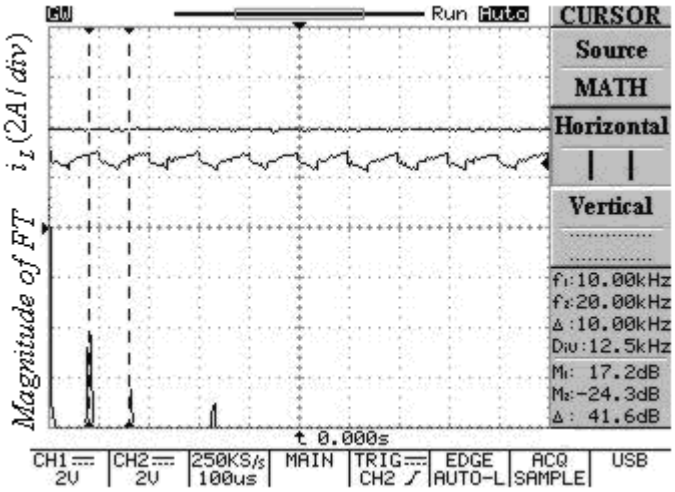

Figure 8.5 Delayed feedback control $I_{ref} = 4A$, $\tau = 70\mu s$, $K = 1$.

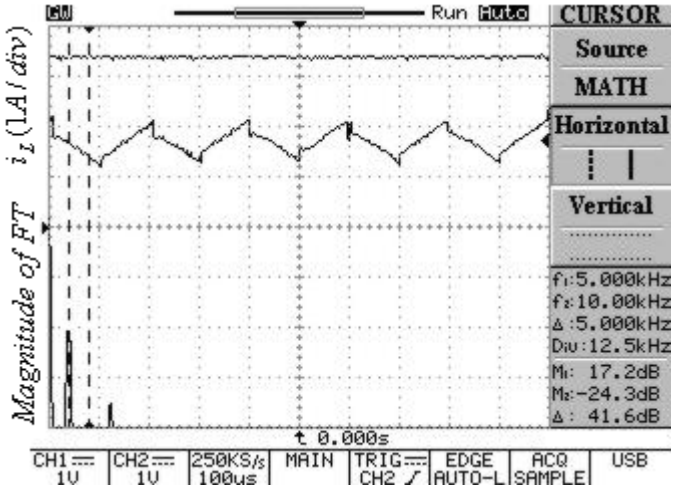

Figure 8.6 Delayed feedback control $I_{ref} = 3.4A,\ \tau = 100\mu s,\ K = 1.$

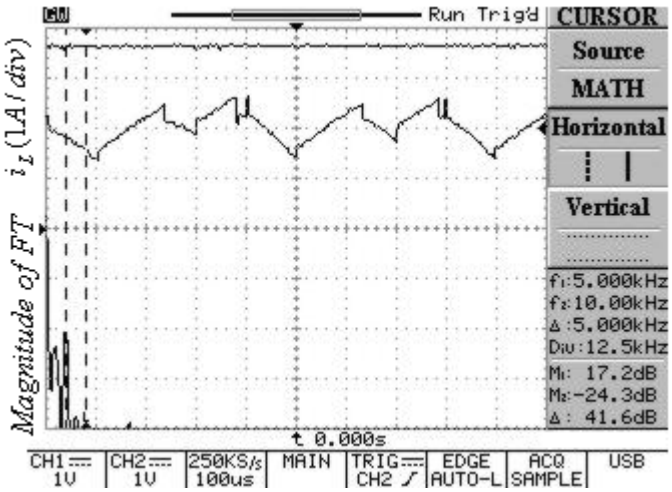

Figure 8.7 Delayed feedback control $I_{ref} = 3.6A,\ \tau = 100\mu s,\ K = 1.$

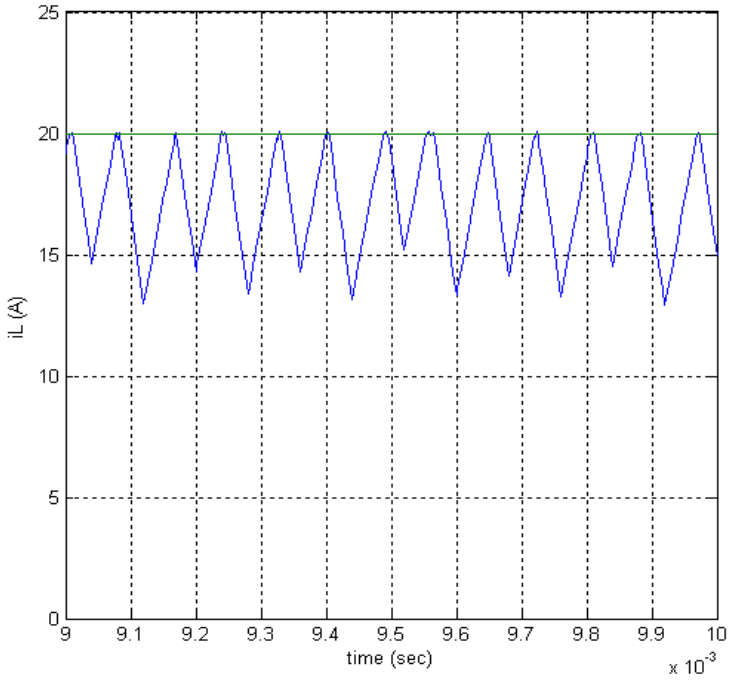

Figure 8.8 Chaotic behaviour at $I_{ref} = 20A$ without any control method.

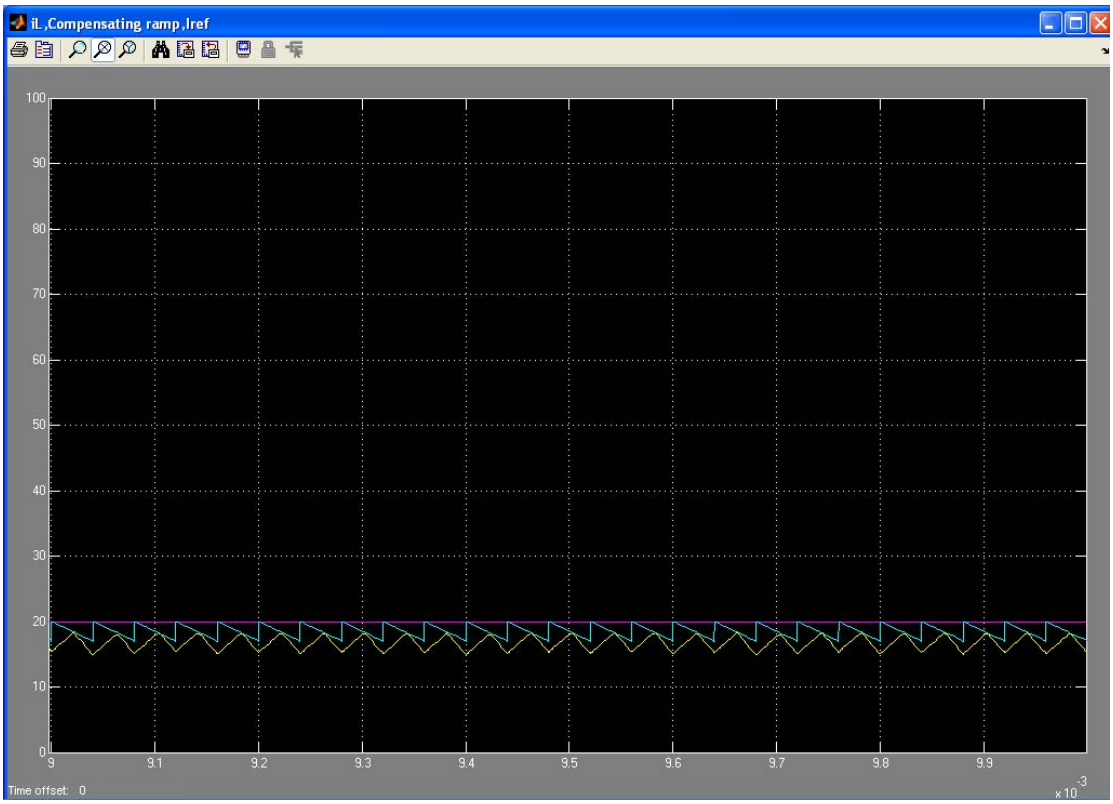

Figure 8.9 Slope compensated method control at $I_{ref} = 20A$.

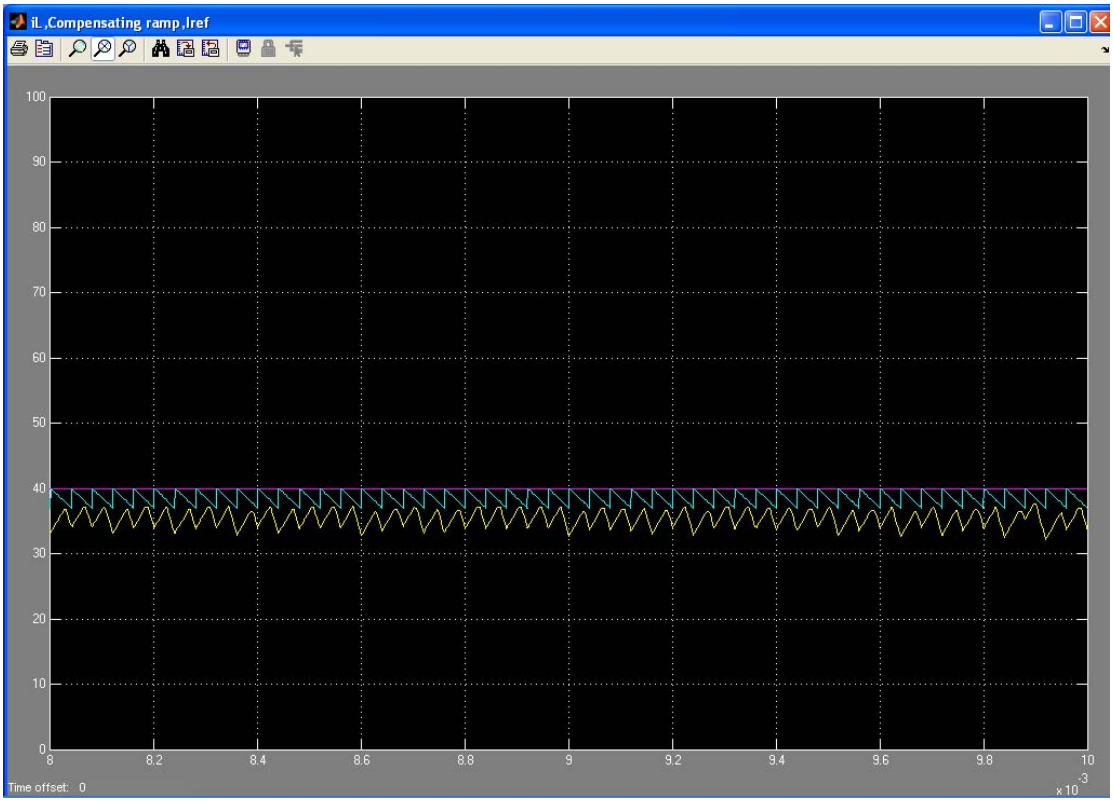

Figure 8.10 Slope compensated method control at $I_{ref} = 40A$.

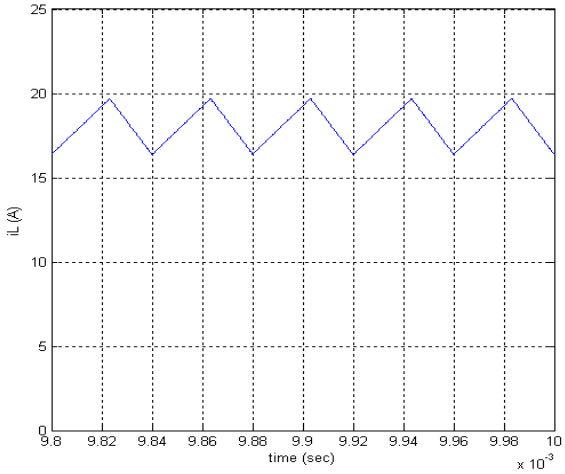

Figure 8.11 Delayed current feedback control at $I_{ref} = 20A,\ \tau = 30\mu s,\ K = 1$.

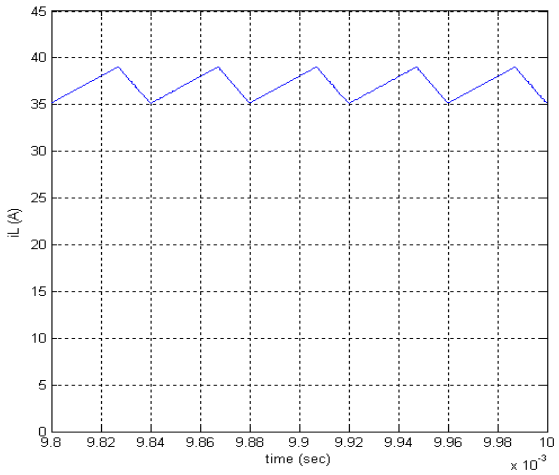

Figure 8.12 Delayed current feedback control at $I_{ref} = 40A,\ \tau = 30\mu s,\ K = 1$.

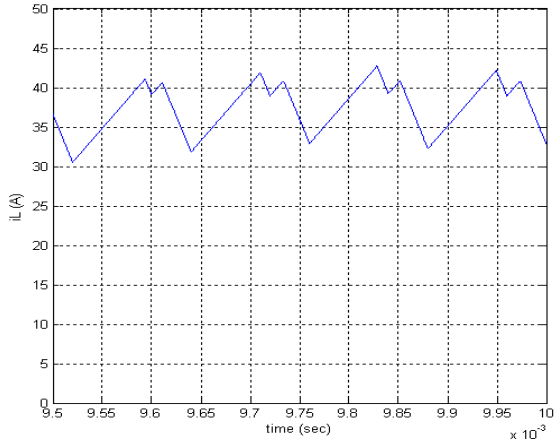

Figure 8.13 Delayed current feedback control at $I_{ref} = 45A,\ \tau = 30\mu s,\ K = 1$.

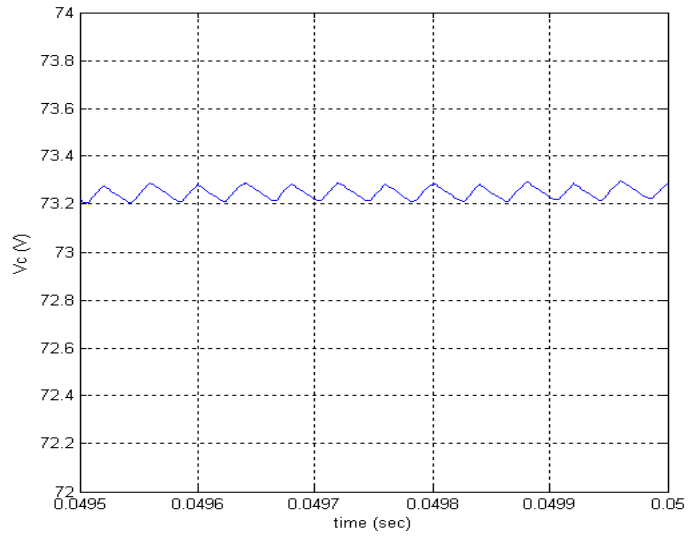

Figure 8.14 Slope compensated method control at $I_{ref} = 20A$.

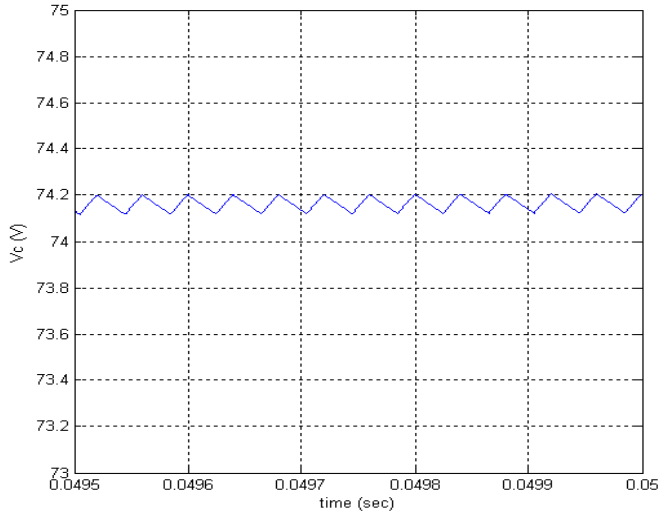

Figure 8.15 Delayed current feedback control at $I_{ref} = 20A,\ \tau = 30\mu s,\ K = 1$.

CHAPTER 9

POWER FACTOR CORRECTION BOOST CONVERTER

9.1 Introduction

The power supply quality in AC-DC power electronic converters is very important, since it can introduce both conducted and electromagnetic interference problems and affect efficiency. Consequently, the supply current must have a low harmonic content and a high power factor and these factors are enforced by national and international harmonic standards. The design of such converters, with a low harmonic content, a fast dynamic response, low voltage ripple and high efficiency is a constant challenge, which will become more difficult as the power requirements for future high-speed microprocessors, communication systems and military hardware will be more stringent.

A high frequency power factor correction (PFC) boost converter may be used to shape the input current waveform and meet these arduous requirements. Such circuits are highly nonlinear and behave in a chaotic manner through period-doubling bifurcations under certain control parameter variations. Recently, limited research has been conducted on the chaotic behaviour of this type of converter. The work presented in [36] and [38] investigated the instability of boost PFC converters with average current mode control, while that described in [37] and [39] investigated the instability under peak current mode control. Only [36] provided experimental verification of the simulated results, whereas none of the papers provide experimental verification for the peak current mode control.
This work presents both simulated and experimental results for peak current mode control.

9.2 Converter Operation

A simplified circuit diagram for the converter is shown in Fig. 9.1. The rectifier output voltage $V_{in}|\sin\theta|$ is the converter input voltage. The switch is controlled by a feedback loop comprising a comparator and a flip-flop. The comparator compares the

inductor current i_L with a reference current I_{ref}, where I_{ref} is a rectified sine wave in-phase with the supply voltage. Control of the switch S is similar to that described for the DC-DC boost converter in section 2.2.

9.3 Iterative Map

An iterative map was developed, using a difference equation of the form

$$x_{n+1} = f(x_n, I_{ref}) \tag{9.1}$$

where

$$x = [i_L \quad v_C]^T \tag{9.2}$$

with i_L is the inductor current and v_C the capacitor voltage.

The circuit operation has two configurations or states, according to the condition of the switch. Assuming that the switch is initially closed and neglecting circuit resistance, the inductor current i_L increases linearly until $i_L = I_{ref}$ and any clock pulses arriving prior to this time are ignored. When $i_L = I_{ref}$, the switch opens, and remains open until the arrival of the next clock pulse, whereupon it re-closes. A portion of the waveforms for I_{ref} and i_L are given in Fig. 9.2.

The two circuit states are treated separately:

S ***Closed***

Diode D is reverse biased and blocks at $t = 0$, giving the circuit shown in Fig. 9.3 (a). Again, assuming that the circuit resistance is negligible, the circuit equations are

$$L\frac{di_L}{dt} = \hat{V}_{in}\left|\sin\theta\right| \tag{9.3}$$

and

$$C\frac{dv_C}{dt} = -\frac{v_C}{R} \tag{9.4}$$

Defining the inductor current i_n at time $t = 0$ and I_{ref} at $t = t_n$, the solution of equation 9.3 is

$$t_n = \frac{L(I_{ref} - i_n)}{\hat{V}_{in}|\sin\theta|} \tag{9.5}$$

Defining the capacitor voltage v_n at $t = 0$, the solution of Eq.9.4 at $t = t_n$ is

$$v_c(t_n) = v_n e^{-t_n/\tau_{RC}} \tag{9.6}$$

where $\tau_{RC} = RC$ and t_n is the time during which S is closed.

S ***Open***

The switch opens at t_n and a voltage is induced in L to try to maintain the inductor current. This forward biases D, which conducts as shown in Fig. 9.3(b). The circuit equations are now

$$L\frac{di_L}{dt} + v_C = \hat{V}_{in}|\sin\theta| \tag{9.7}$$

$$C\frac{dv_C}{dt} + \frac{v_C}{R} = i_L \tag{9.8}$$

Substituting for v_C and $\frac{dv_C}{dt}$ derived from Eq.9.7 into Eq.9.8 gives

$$\frac{d^2 i_L}{dt^2} + (\frac{1}{RC})\frac{di_L}{dt} + (\frac{1}{LC})i_L = \frac{\hat{V}_{in}|\sin\theta|}{(RLC)} \tag{9.9}$$

The general solution of Eq.9.9 has two terms, the homogeneous equation and a particular solution. The particular solution, obtained by assigning a final value (i_L = constant) in Eq.9.9 after all derivative quantities become zero is

$$i_{Lp}(t) = \frac{\hat{V}_{in}|\sin\theta|}{R} \tag{9.10}$$

The solution of the homogeneous equation depends on the roots of the characteristic equation

$$\lambda_{1,2} = -\frac{1}{2RC} \pm \sqrt{\frac{1}{4R^2C^2} - \frac{1}{LC}}$$

or

$$\lambda_{1,2} = -\frac{1}{2\tau_{RC}} \pm j\omega \tag{9.11}$$

where

$$\omega = \sqrt{\frac{1}{LC} - \frac{1}{(2\tau_{RC})^2}} \tag{9.12}$$

Thus, the homogeneous solution is

$$i_{Lh}(t) = e^{-t/2\tau_{RC}}(A_1 \sin \omega t + A_2 \cos \omega t) \tag{9.13}$$

giving the general solution

$$i_L(t) = e^{-t/2\tau_{RC}}(A_1 \sin \omega t + A_2 \cos \omega t) + \frac{\hat{V}_{in}|\sin\theta|}{R} \tag{9.14}$$

where the constants A_1 and A_2 are defined by the boundary conditions.

The circuit is described by Eq.9.14 until the next clock pulse arrives, causing the switch to close at time t_n', where

$$t_n' = T[1 - (t_n / T)] \tag{9.15}$$

Setting $t = 0$ immediately after the switch has opened gives

$$i_L(0) = A_2 + \frac{\hat{V}_{in}|\sin\theta|}{R} = I_{ref} \tag{9.16}$$

Thus

$$A_2 = I_{ref} - \frac{\hat{V}_{in}|\sin\theta|}{R} \tag{9.17}$$

and

$$v_C(0) = v_n e^{-t_n/\tau_{RC}} = \hat{V}_{in}|\sin\theta| - L\frac{di_L}{dt}\Big|_{t=0} \tag{9.18}$$

Taking the time derivative of Eq.7.14 gives

$$\frac{di_L}{dt}\Big|_{t=o} = A_1\omega - \frac{A_2}{2\tau_{RC}} \tag{9.19}$$

Solving for A_1

$$A_1 = \frac{\frac{L}{2\tau_{RC}}(I_{ref}') + \hat{V}_{in}|\sin\theta| - v_n e^{-t_n/\tau_{RC}}}{\omega L} \tag{9.20}$$

where

$$I'_{ref} = I_{ref} - \frac{\hat{V}_{in}|\sin\theta|}{R} \tag{9.21}$$

By definition, $i_{n+1} = i_L(t'_n)$, so Eqs.9.14, 9.17, and 9.20 give

$$i_L(t) = e^{-t'_n/2\tau_{RC}}\left[\frac{\frac{L}{2\tau_{RC}} I'_{ref} + \hat{V}_{in}|\sin\theta| - v_n e^{-t_n/\tau_{RC}}}{\omega L}\sin\omega t'_n + I'_{ref}\cos\omega t'_n\right] + \frac{\hat{V}_{in}|\sin\theta|}{R} \tag{9.22}$$

The derivative $\frac{di_L}{dt}$ is obtained from Eq.9.8 and substituted into Eq.9.7, to give

$$\frac{d^2 v_C}{dt^2} + \left(\frac{1}{RC}\right)\frac{dv_C}{dt} + \left(\frac{1}{LC}\right)v_C = \frac{\hat{V}_{in}|\sin\theta|}{(LC)} \tag{9.23}$$

The general solution of Eqn.9.23 again has two terms, the homogeneous equation and a particular solution. The particular solution, obtained by putting a final value (v_C = constant) in Eq.9.23 after all derivative quantities become zero is

$$v_{Cp}(t) = \hat{V}_{in}|\sin\theta| \tag{9.24}$$

The solution of the homogeneous equation depends on the roots of the characteristic equation

$$\begin{aligned} \lambda_{1,2} &= -\frac{1}{2RC} \pm \sqrt{\frac{1}{4R^2C^2} - \frac{1}{LC}} \\ \lambda_{1,2} &= -\frac{1}{2\tau_{RC}} \pm j\omega \end{aligned} \tag{9.25}$$

where:

$$\omega = \sqrt{\frac{1}{LC} - \frac{1}{(2\tau_{RC})^2}} \tag{9.26}$$

Thus, the homogeneous solution is

$$v_{Ch}(t) = e^{-t/\tau_{RC}}(B_1\sin\omega t + B_2\cos\omega t) \tag{9.27}$$

giving the general solution

$$v_C(t) = e^{-t/\tau_{RC}}(B_1\sin\omega t + B_2\cos\omega t) + \hat{V}_{in}|\sin\theta| \tag{9.28}$$

where the constants B_1 and B_2 are set by boundary conditions.

Setting $t = 0$ immediately after the switch opens gives

$$v_C(0) = B_2 + \hat{V}_{in}\left|\sin\theta\right| = v_n e^{-t_n/\tau_{RC}} \tag{9.29}$$

so

$$B_2 = v_n e^{-t_n/\tau_{RC}} - \hat{V}_{in}\left|\sin\theta\right| \tag{9.30}$$

and

$$i_L(0) = C\frac{dv_C}{dt}\Big|_{t=0} + \frac{v_C}{R} = I_{ref} \tag{9.31}$$

Taking the time derivative of Eq.9.28 at $t = 0$ gives

$$\frac{dv_C}{dt}\Big|_{t=0} = B_1\omega - \frac{B_2}{2\tau_{RC}} \tag{9.32}$$

from which

$$B_1 = \frac{[\dfrac{v_n e^{-t_n/\tau_{RC}}}{2\tau_{RC}} - \dfrac{\hat{V}_{in}\left|\sin\theta\right|}{2\tau_{RC}} - I'_{ref}/C]}{\omega} \tag{9.33}$$

Since $v_{C(n+1)} = v_C(t'_n)$, from Eqs.9.28, 9.30, and 9.33

$$\begin{aligned} v_C(t) = {} & \hat{V}_{in}\left|\sin\theta\right| - e^{-t'_n/2\tau_{RC}}[(\frac{v_n e^{-t_n/\tau_{RC}}}{2\tau_{RC}} - \frac{\hat{V}_{in}\left|\sin\theta\right|}{2\tau_{RC}} - \frac{I'_{ref}}{C})\frac{\sin\omega t'_n}{\omega} \\ & + (\hat{V}_{in}\left|\sin\theta\right| - v_n e^{-t_n/\tau_{RC}})\cos\omega t'_n] \end{aligned} \tag{9.34}$$

Eqns.9.22 and 9.34 comprise one form of mapping for the boost converter, which will be described in greater detail in chapter 10.

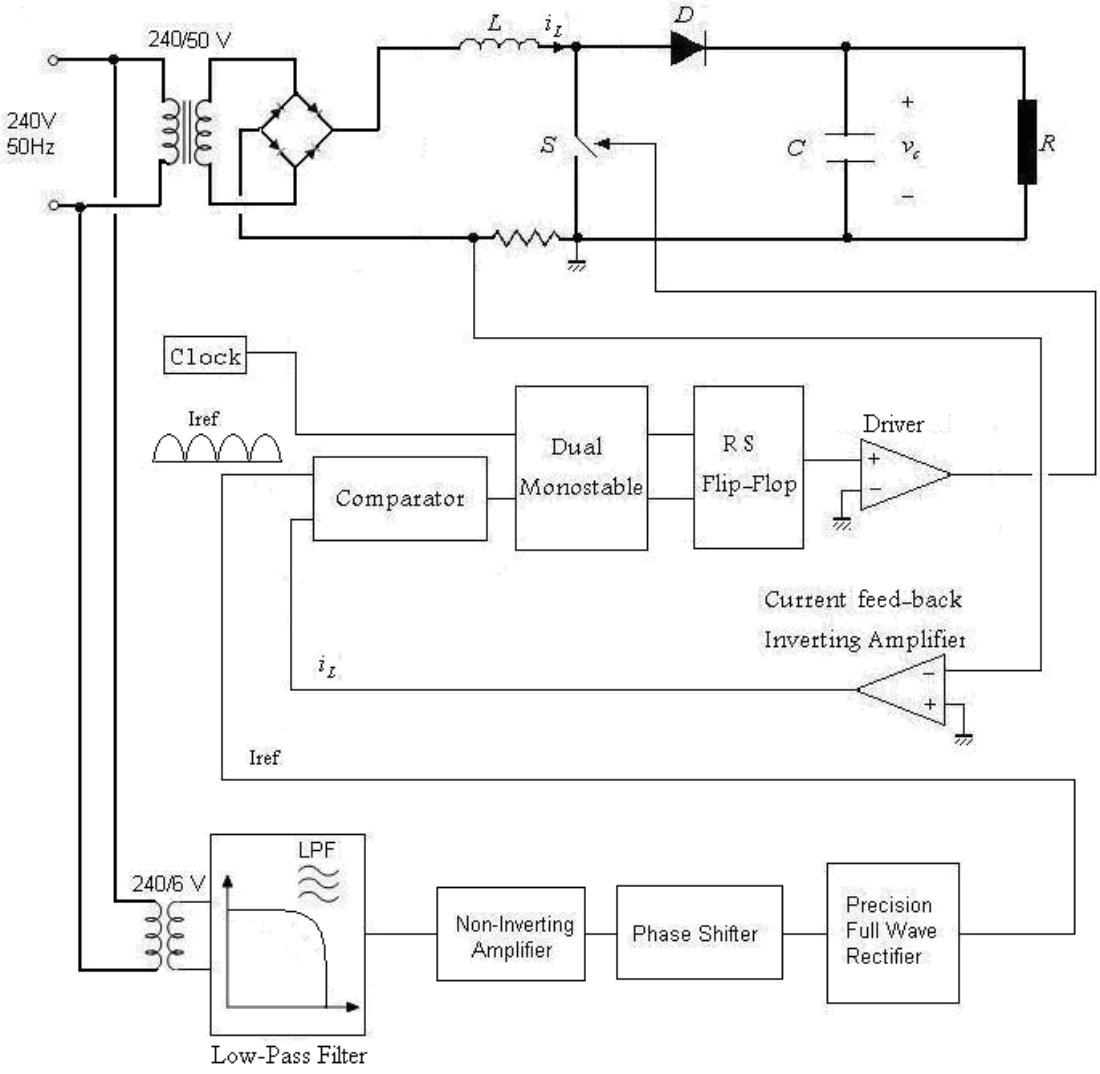

Figure 9.1 Converter circuit diagram.

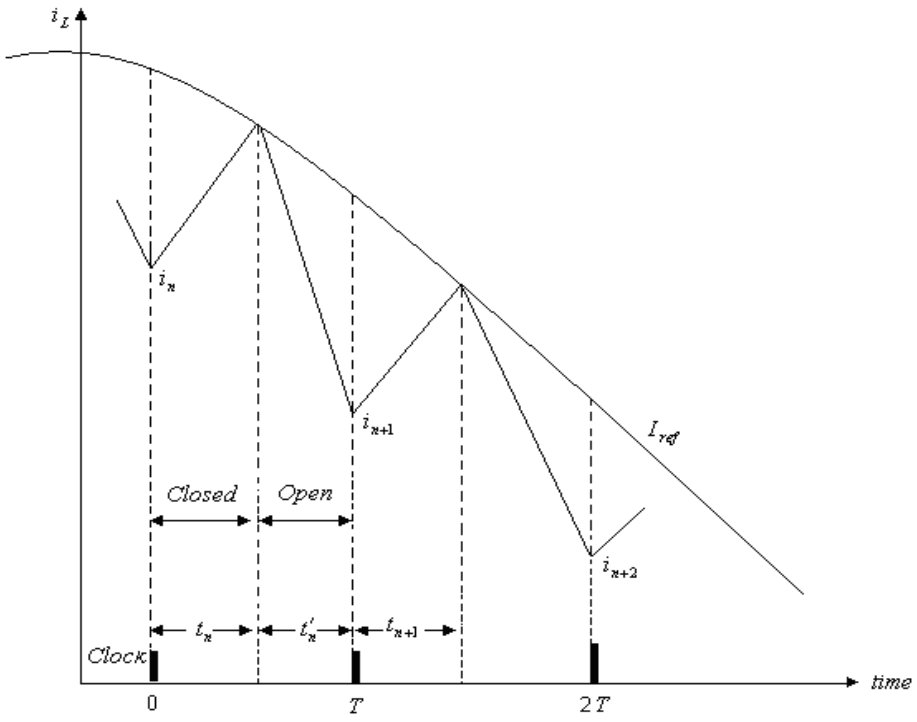

Figure 9.2 I_{ref} and i_L waveforms.

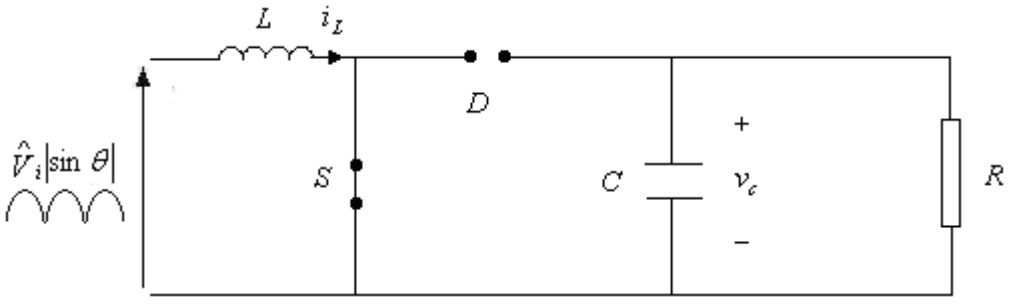

(a) S closed

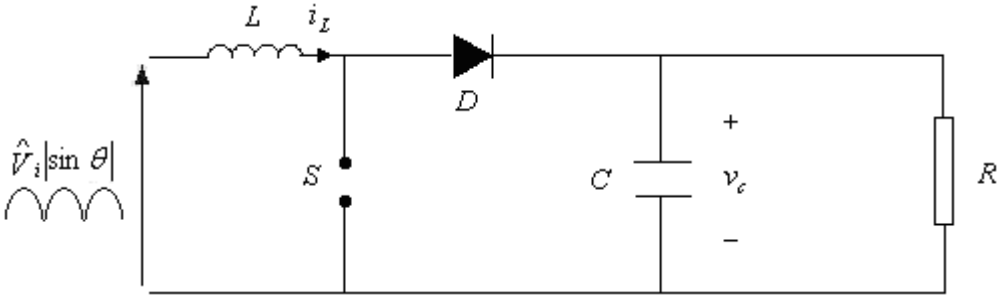

(b) S open.

Figure 9.3 Converter circuit states.

CHAPTER 10
CHAOS IN A POWER FACTOR CORRECTION BOOST CONVERTER

10.1 Numerical Analysis

A MATLAB program was written to generate bifurcation diagrams for the PFC boost converter, and these were used to investigate the system dynamics. A flowchart for the program is given in Fig. 10.1 and the program listing is given in Appendix A.3. The bifurcation diagrams relate the capacitor voltage or inductor current vectors $(v_{C(n)} \text{ or } i_{L(n)})$ sampled at one clock pulse, to the vector $(v_{C(n)} \text{ or } i_{L(n)})$ at the previous clock pulse. To obtain the bifurcation diagrams, initial conditions $(v_{C(0)}$ and $i_{L(0)})$ were specified and $\hat{I}_{ref}$ was defined, where $I_{ref} = \hat{I}_{ref} \sin\theta$. Eqs.9.22 and 9.34 were iterated 12000 times. The first 11000 iterations were discarded, to eliminate transient conditions and the last 1000 were plotted, taking $\hat{V}_{in}$ as the bifurcation parameter. $\hat{V}_{in}$ was swept from 5 to $80V$ in $0.5V$ steps with $I_{ref} = 3|\sin\theta|A$. The parameters used for the simulations are given in Table 10.1.

Circuit Components	Values
Switching Period T	$100\mu s$
Input Voltage $\hat{V}_{in}$	$5\text{-}80V$
Line Frequency	$50Hz$
Inductor L	$15mH$
Capacitor C	$220\mu F$
Load Resistor R	$300\,\Omega$

Table 10.1 System parameters.

The bifurcation diagram relating the inductor current i_L with the bifurcation parameter $\hat{V}_{in}$ is shown in Fig. 10.2 at $\hat{I}_{ref} = 3A$. It is evident that the system is stable until $\hat{V}_{in}$ is reduced to about $63V$. Over this region, the inductor current i_L at $\hat{I}_{ref} = 3A$, has a single unique value at the instant of every switch turn-on. As an

example, consider $\hat{V}_{in} = 65V$ in Fig. 10.2. The single value of i_L at switch turn-on is $i_L = 2.3$A. At $\hat{V}_{in}=63V$ one of the Floquet multipliers leaves the unit circle through -1, producing a period-doubling bifurcation (period-2). During period-2, the inductor current has two unique values at alternate instants of turn-on. For example, with $\hat{V}_{in} = 60V$, i_L alternates between 1.85 and 2.85A at switch turn-on. As $\hat{V}_{in}$ decreases further, the system undergoes stable period-3 operation. Further bifurcations occur as $\hat{V}_{in}$ is reduced and the system eventually becomes chaotic at $\hat{V}_{in} = 45V$, with the value of i_L at each turn-on having many values.

Figs. 10.3 to 10.5 show bifurcation diagrams relating the inductor current to the bifurcation parameter $\hat{I}_{ref}$ for fixed values of $\hat{V}_{in}$. These diagrams show that the period-doubling route to chaos is from left to right, as opposed to the one obtained when the control parameter was $\hat{V}_{in}$. As with the bifurcation diagrams of Figs. 3.2 and 3.3(a) for the single DC-DC boost converter, the bifurcation diagrams of Figs. 10.3 to 10.5 are orthogonal with Fig. 10.2, forming a 3-dimensional state-control space.

10.2 Experimental Implementation

The experimental converter shown in Fig. 10.6 was designed and built to verify the theoretical model. The 10 kHz clock signal is obtained using an LM555 integrated circuit. The rising edge of the clock signal triggers a 74HCT123N monostable to drive the set input of an S-R flip-flop, constructed using 2-input NOR gates and 3-input AND gates. The output of the flip-flop is applied to a 311 comparator, which turns-on the MOSFET switch.

The inductor current i_L is sensed using a small non-inductive sense resistor as shown. Comparing this signal with the reference current I_{ref}, generates the reset pulse for the S-R flip-flop, which turns-off the switch as explained in section 9.2. The reference current I_{ref} is obtained from a step-down transformer connected to the power supply. The output of the transformer is filtered and then rectified using a precision full-wave

rectifier. An active filter UAF42 eliminates switching harmonics. The natural frequency ω_n and the Q-factor of the pole pair are designed according to the Blackadder filter type and cut-off frequency. The low-pass transfer function is

$$\frac{V_o(s)}{V_1(s)} = \frac{A_{LP}\omega_n^2}{s^2 + s\omega_n / Q + \omega_n^2} \tag{10.1}$$

where the filter gain is set by the equation

$$A_{LP} = \frac{1 + \frac{R_1}{R_2}}{R_G[\frac{1}{R_G} + \frac{1}{R_Q} + \frac{1}{R_4}]} \tag{10.2}$$

and the second order cut-off frequency is governed by R_{F1} and R_{F2} according to

$$\omega_n^2 = \frac{R_2}{R_1 R_{F1} R_{F2} C_1 C_2} \tag{10.3}$$

The Q-factor of the filter is set by the resistor R_Q. Eq. 10.4 gives the relationship between Q, R_Q and other circuit values.

$$Q = \frac{1 + \frac{R_4(R_G + R_Q)}{R_G R_Q}}{1 + \frac{R_2}{R1}}[\frac{R_2 R_{F1} C_1}{R_1 R_{F2} C_2}]^{1/2} \tag{10.4}$$

The phase shifter shown in Fig. 10.6 eliminates the phase shift produced by the step-down transformer and the active filter and ensures that I_{ref} is in phase with $\hat{V}_{in}|\sin\theta|$. A photograph of the converter hardware is shown in Appendix D.5.

10.3 MATLAB/SIMULINK Model

A MATLAB/SIMULINK model was developed based on the system equations:

$$\begin{aligned} \frac{di_L}{dt} &= \frac{1}{L}[\hat{V}_{in}|\sin\theta| - v_C(1-u_S) - i_L\{R_1 u_S + R_2(1-u_S)\}] \\ \frac{dv_C}{dt} &= \frac{1}{C}[-\frac{v_C}{R} + i_L(1-u_S)] \end{aligned} \tag{10.5}$$

where u_S takes the value 0 or 1 depending on whether the switch is closed or open. R_1 and R_2 are circuit loop resistances for the converter, which were measured experimentally. The structure of the SIMULINK model is given in Fig. 10.7.

10.4 Experimental and Simulated Results

The experimental and simulated inductor current waveforms and harmonic spectra for $\hat{V}_{in}$ = 65V**,** 60V and 20V are given in Figs. 10.8 to 10.10. In Fig. 10.8, it is evident that the system is stable period-1 at $\hat{V}_{in} = 65V$, with a 10kHz fundamental and a series of higher harmonics. As $\hat{V}_{in}$ decreases to 60V, the system becomes period-2, with an appreciable 5kHz component in the frequency spectrum as shown in Fig. 10.9. Fig. 10.10 shows that as $\hat{V}_{in}$ reduces to 20V, the system becomes chaotic and the frequency spectrum is continuous. The experimental and simulated results are in good agreement and also show good agreement with the bifurcation diagram of Fig. 10.2.

Phase portraits relating the capacitor voltage to the inductor current at the bifurcation parameters $\hat{V}_{in}$ = 65V, 60V and 20V are given in Figs. 10.11 to 10.13 respectively. The phase portraits corresponding to these cases demonstrate period-1, period- 2 and chaotic behaviour. There was a small differences between simulated and experimental results phase portraits are due to the practical difficulties in the digital oscilloscope.

The capacitor voltage waveforms with the three different values of the bifurcation parameter $\hat{V}_{in}$ and a fixed reference current $\hat{I}_{ref}$ = 3A are given in Figs. 10.14 to 10.16. Again, the experimental and simulated results are in good agreement.

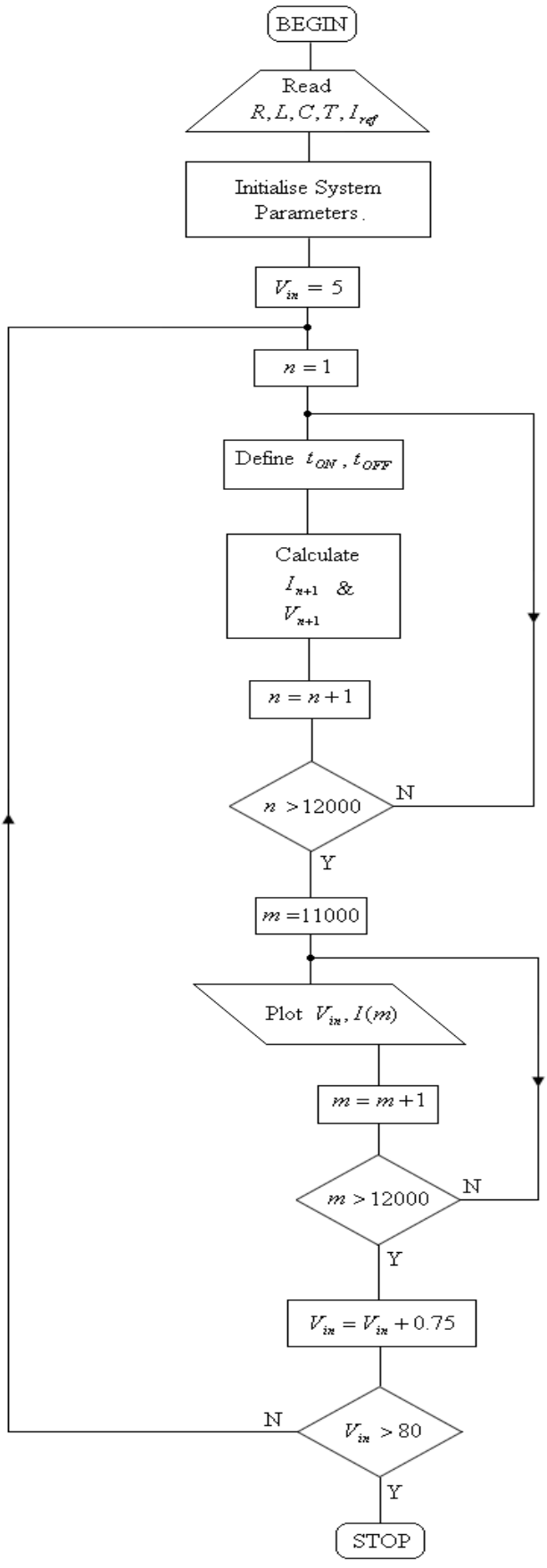

Figure 10.1 Bifurcation program flowchart.

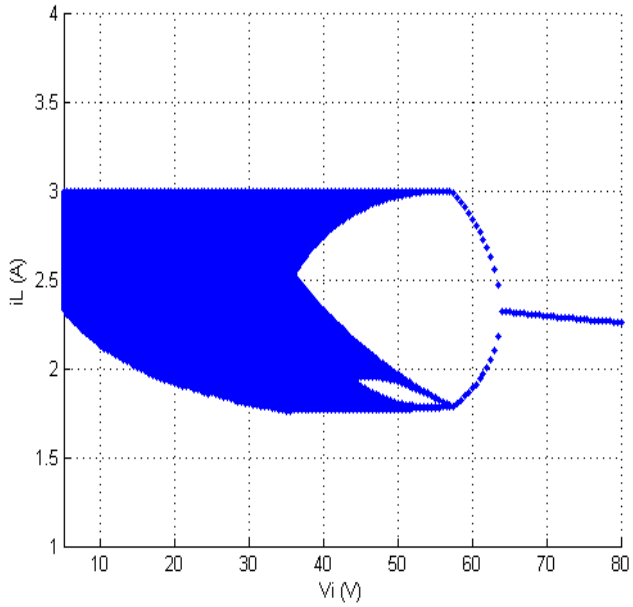

Figure 10.2 Bifurcation diagram with $\hat{V}_{in}$ as the control parameter. ($\hat{I}_{ref}$ = 3A)

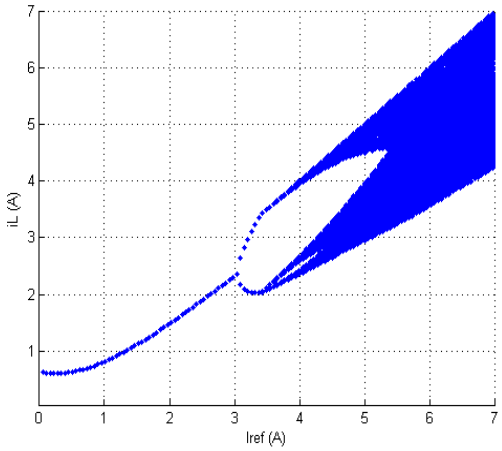

Figure 10.3 Bifurcation diagram with $\hat{I}_{ref}$ as the control parameter at $\hat{V}_{in} = 65V$.

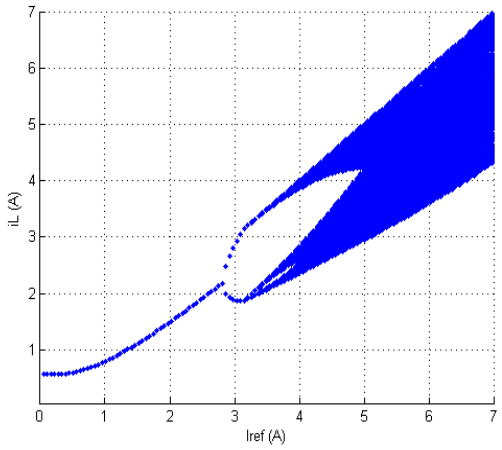

Figure 10.4 Bifurcation diagram with $\hat{I}_{ref}$ as the control parameter at $\hat{V}_{in} = 60V$.

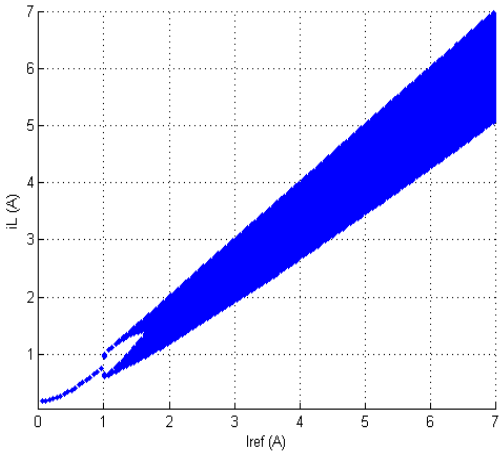

Figure 10.5 Bifurcation diagram with $\hat{I}_{ref}$ as the control parameter at $\hat{V}_{in} = 20V$.

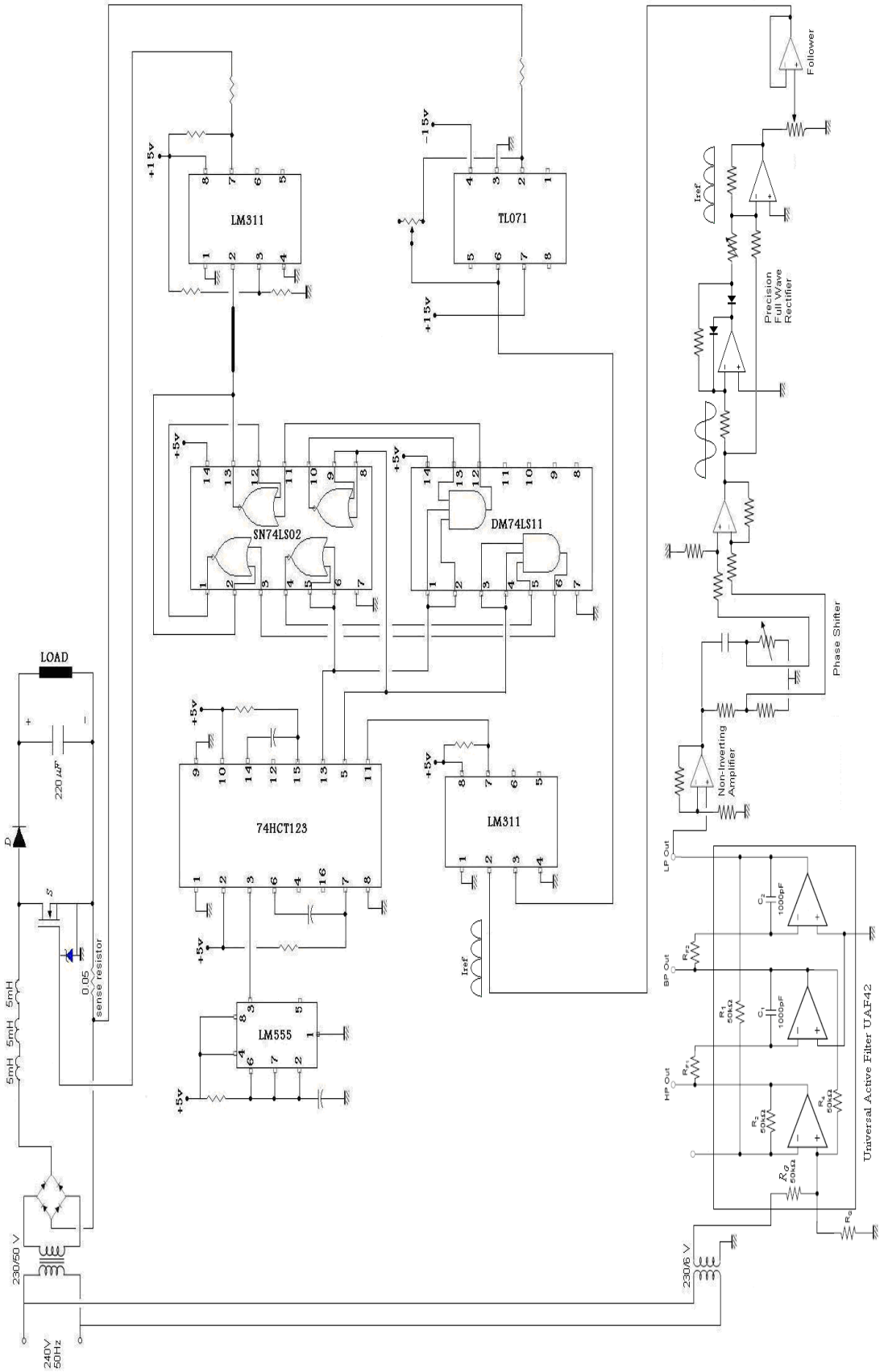

Figure 10.6 PFC boost converter hardware.

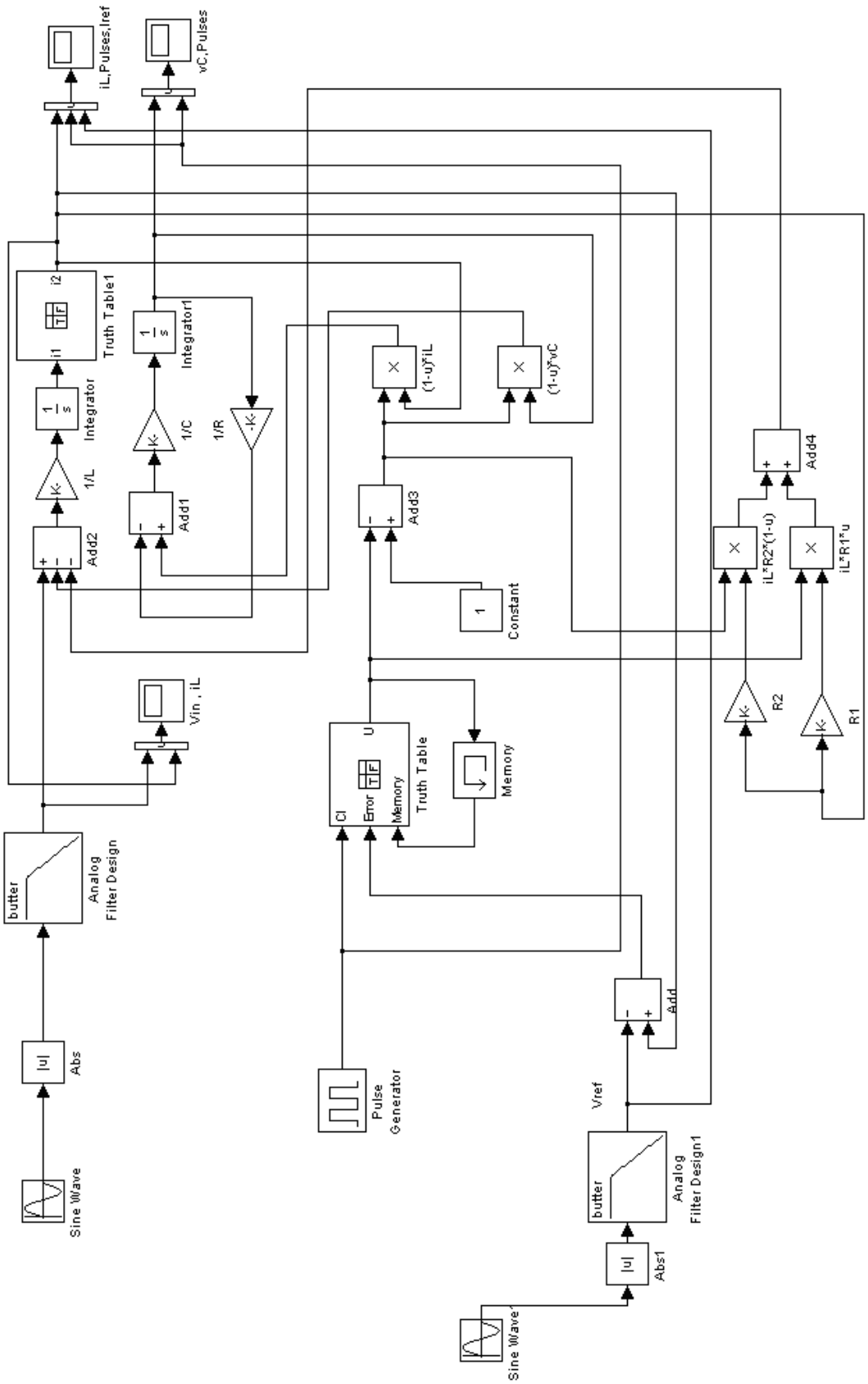

Figure 10.7 MATLAB/SIMULINK model for a PFC boost converter.

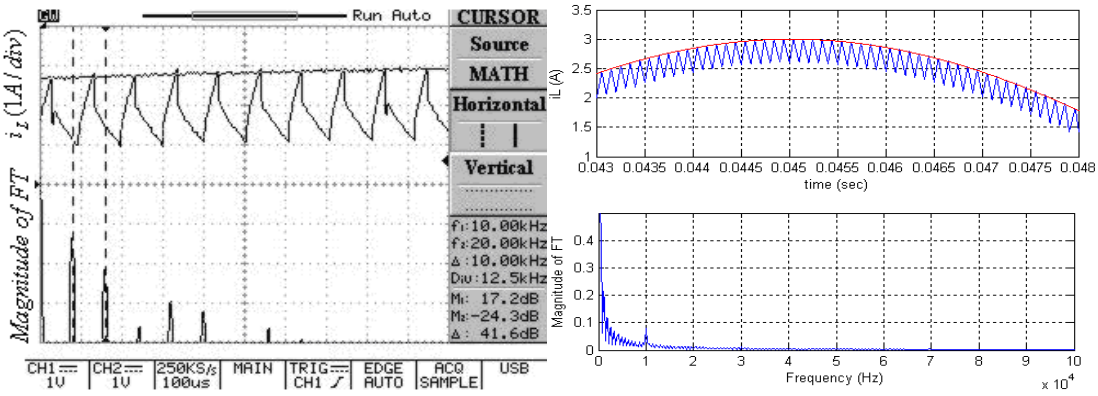

Figure 10.8 Experimental and simulated inductor current at $\hat{V}_{in} = 65V$.

{**Left**: experimental (1A/V), **right**: simulated}.

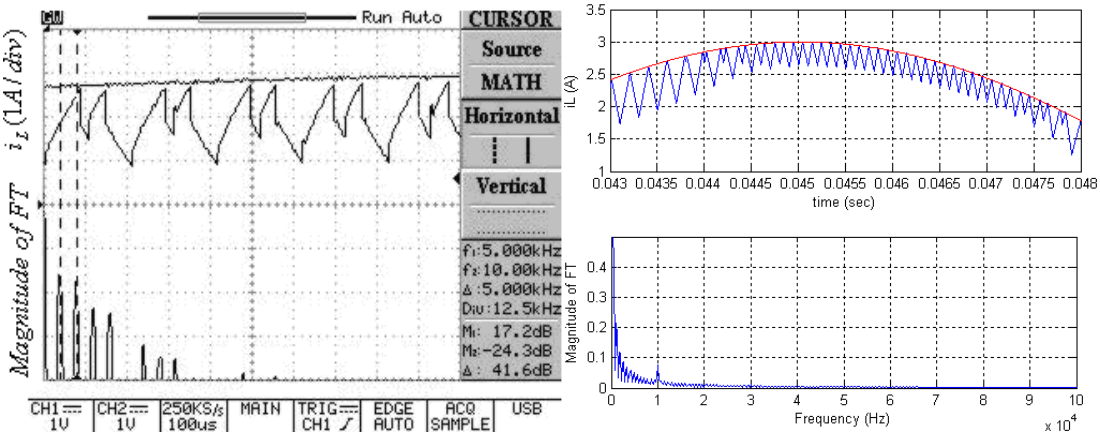

Figure 10.9 Experimental and simulated inductor current at $\hat{V}_{in} = 60V$.

{**Left**: experimental (1A/V), **right**: simulated}.

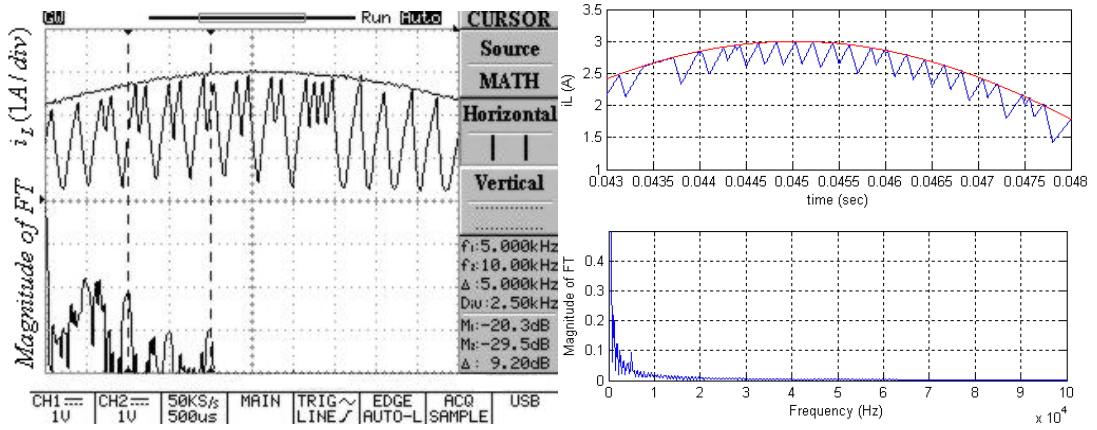

Figure 10.10 Experimental and simulated inductor current at $\hat{V}_{in} = 20V$.

{**Left**: experimental (1A/V), **right**: simulated}.

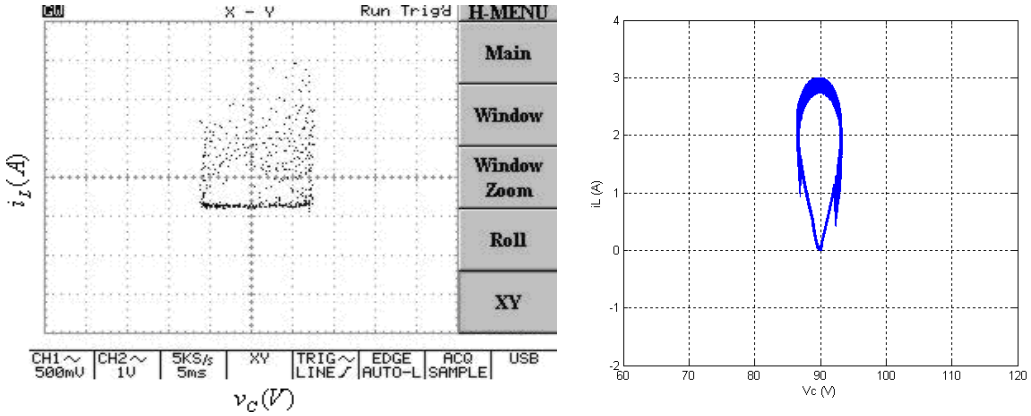

Figure 10.11 Experimental and simulated phase portrait at $\hat{V}_{in} = 65V$.

{**Left**: experimental (CH2 1A/V), **right**: simulated}.

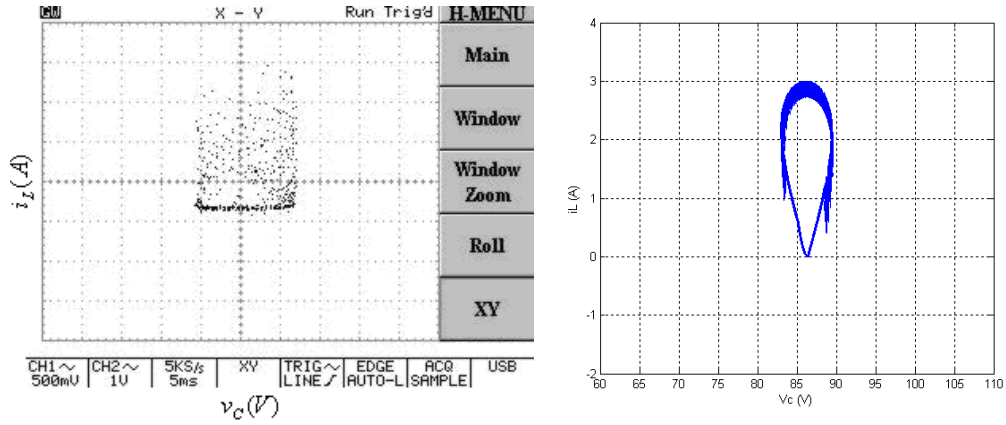

Figure 10.12 Experimental and simulated phase portrait at $\hat{V}_{in} = 60V$.

{**Left**: experimental (CH2 1A/V), **right**: simulated}.

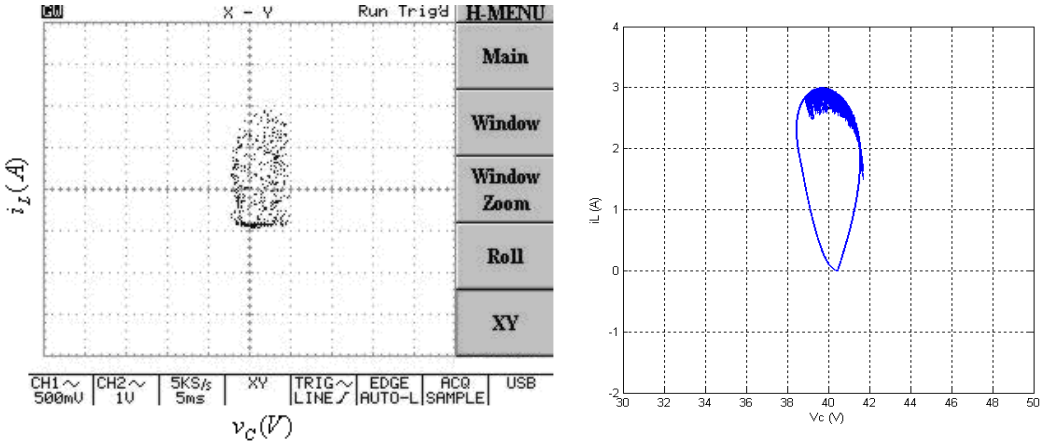

Figure 10.13 Experimental and simulated phase portrait at $\hat{V}_{in} = 20V$.

{**Left**: experimental (CH2 1A/V), **right**: simulated}.

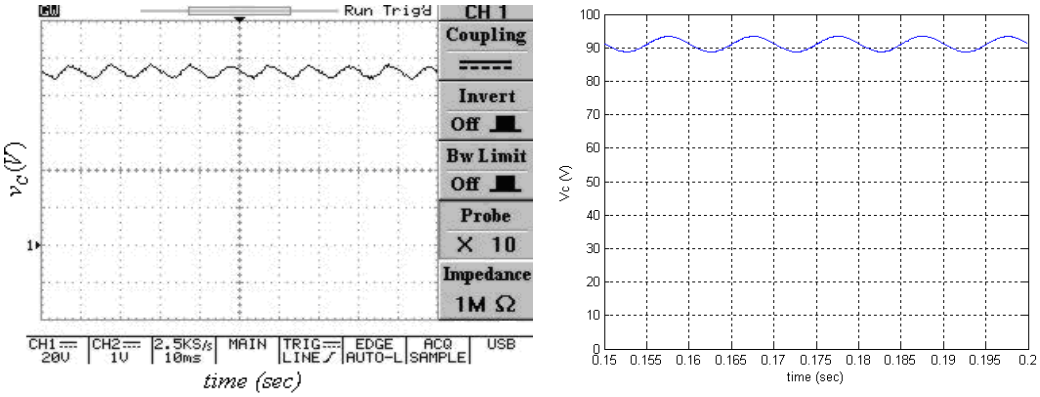

Figure 10.14 Experimental and simulated capacitor voltage at $\hat{V}_{in} = 65V$.

{**Left**: experimental, **right**: simulated}.

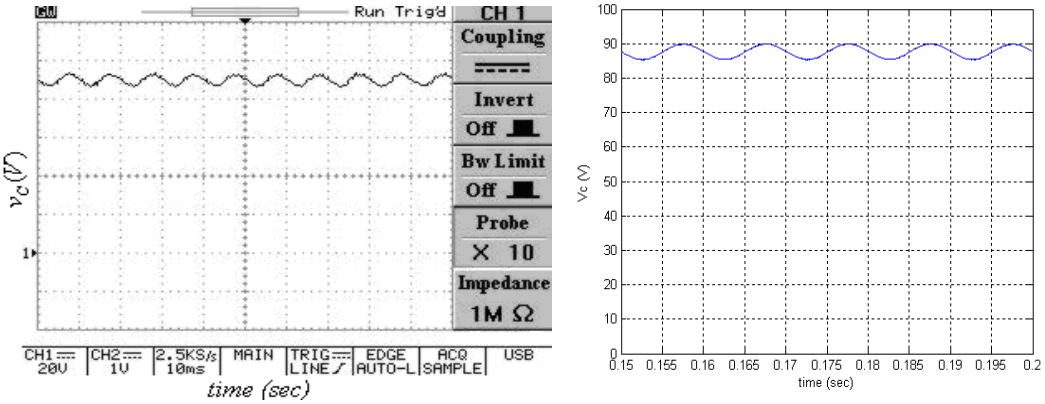

Figure 10.15 Experimental and simulated capacitor voltage at $\hat{V}_{in} = 60V$.

{**Left**: experimental, **right**: simulated}.

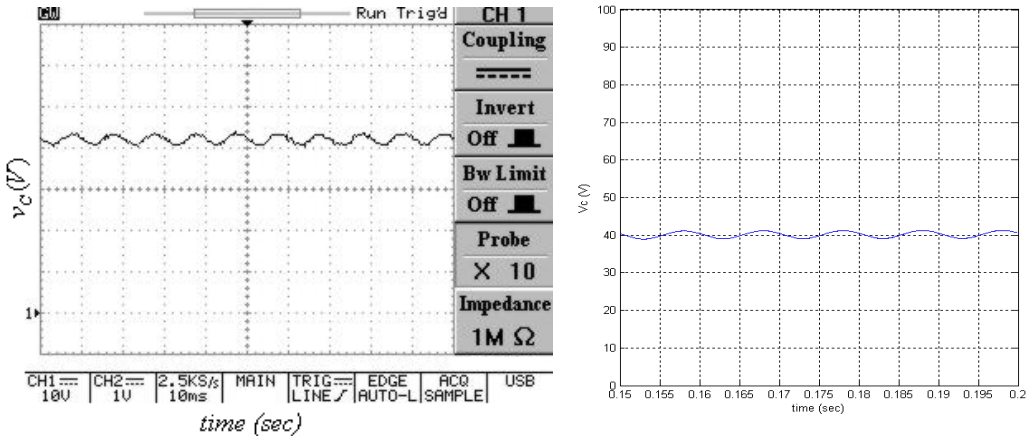

Figure 10.16 Experimental and simulated capacitor voltage at $\hat{V}_{in} = 20V$.

{**Left**: experimental, **right**: simulated}.

CHAPTER 11
CONTROL OF CHAOS IN A PFC BOOST CONVERTER

11.1 Introduction

As with the single boost converter described in Chapter 6 to 8, a delayed feedback controller is used to eliminate chaos in the PFC boost converter. The effectiveness and robustness of the controller is demonstrated by experimental and simulated results.

The simulated performance of the PFC boost converter using both slope compensation and delayed feedback control are compared.

11.2 Experimental Implementation

Practical implementation of delayed feedback control is achieved using an 89C51 microcontroller. The controlled variable $i_L(t)$ is sampled at 10μs intervals and the values are stored in a continually updated rolling array. A pointer extracts data from the array at a delay τ, pre-programmed by the operator, to provide the value $i_L(t-\tau)$. A simplified diagram for the scheme is shown in Fig. 11.1 and a photograph of the controller hardware is given in Appendix D.6.

The experimental waveforms for $i_L(t)$ and $i_L(t-\tau)$ at $\hat{V}_{in} = 50V$ and $\hat{I}_{ref} = 3A$ are shown in Fig. 11.2, with the feedback switch SW in position 2 disconnecting the delayed current feedback from the control circuit. For this condition, the converter is operating in a chaotic mode.

11.3 MATLAB/SIMULINK Models

11.3.1 Slope Compensation Method (SCM)

The circuit arrangement for the converter using slope compensation is shown in Fig. 11.3. The comparator compares the inductor current i_L with a reference level, which is equal to the reference current I_{ref} minus the compensation ramp signal. Typical waveforms for I_{ref}, i_L and the compensating ramp are given in Fig. 11.4. Control of

the converter switch is similar to that of the conventional boost converter described in Section 2.1.

The structure of the MATLAB/SIMULINK model of the converter, using slope compensation is given in Fig. 11.5.

11.3.2 Delayed Current Feedback Method (DCFM)

Simulated results were obtained for the closed-loop system by solving numerically Eqs.10.5 using the MATLAB/SIMULINK model shown in Fig. 11.6. The control function u_S was set to 1 at every clock pulse and to 0 when $i_L(t) = I_{ref} - K[i_L(t-\tau) - i_L(t)]$.

11.4 Experimental and Simulated Results (Delayed Current Feedback)

Over a practical range for τ from 10μs-150μs in 10μs steps, experimental and simulated results for τ = 70μs and 100μs are presented in Figs. 11.7 and 11.8, respectively, for a feedback gain K=1 and $\hat{I}_{ref} = 3A$. In accordance with the results described in Section 8.1 for the single boost converter, the periodic regimes in both cases are stable, with the waveforms of Fig. 11.7 having a frequency of 10 kHz ("period-1" cycles) and those of Fig. 11.8 having a frequency of 5 kHz ("period-2" cycles). Again, the converter was designed for 10 kHz operation and the system would not be performing under optimum conditions with τ = 100μs.

The experimental and simulated capacitor voltage waveforms with delayed feedback control at τ = 70μs, $\hat{V}_{in} = 20V$ and a peak reference current $\hat{I}_{ref} = 3A$ are given in Fig. 11.9. It is evident that the capacitor voltage has reduced by a small amount compared with the capacitor voltage waveforms without delayed feedback control shown in Fig. 10.16.

11.5 Comparison between SCM and DCFM (Simulated)

Simulated inductor current waveforms for both the slope compensation and delayed current feedback methods are given in Fig. 11.7(a) and Figs. 11.10 using the parameters given in Table 10.1. Fig. 11.10 shows the inductor current with slope

compensation control at $\hat{V}_{in} = 20V$. It is evident that the system is operating in stable period-1.

Control is lost when the supply voltage approaches zero, since there is insufficient voltage to maintain period-1 operation.

The capacitor voltage waveforms with ramp compensation at $\hat{V}_{in} = 20V$ and a peak reference current I_{ref} = 3A are given in Fig. 11.11.

The above results show that both methods provides a robust controller but there is an advantage with delayed current feedback rather than the slope compensated controller is that it provides a higher output voltage for a given $\hat{V}_{in}$ as evident in Figs. 11.9 and 11.11.

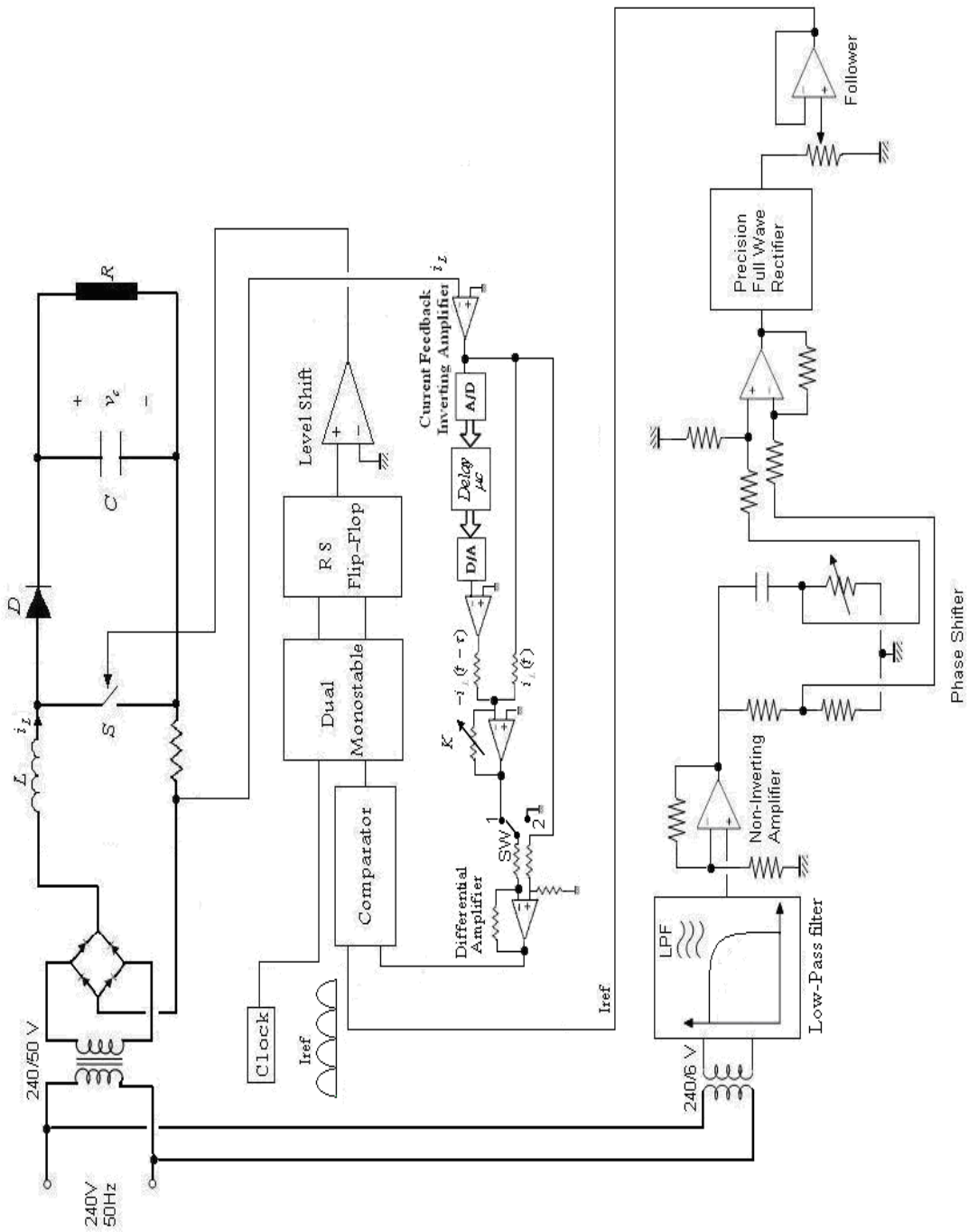

Figure 11.1 Experimental feedback control scheme.

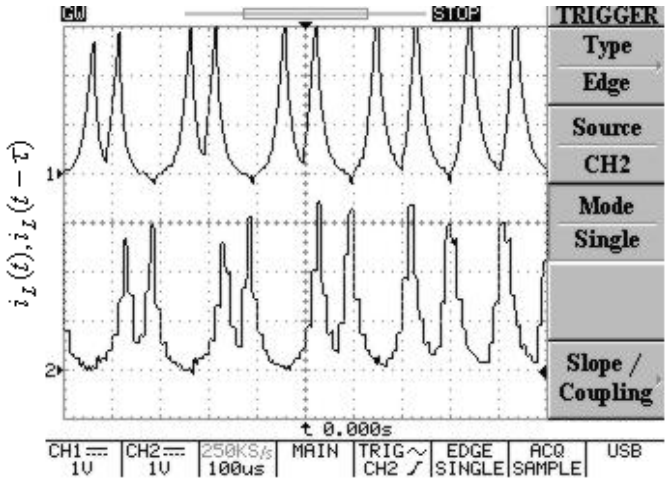

Figure 11.2 Experimental open loop waveforms (1A/V)

$\hat{V}_{in} = 50V$, $\hat{I}_{ref} = 3A$, $\tau = 70\mu s$. $i_L(t)$ (upper) and $i_L(t-\tau)$ (lower)

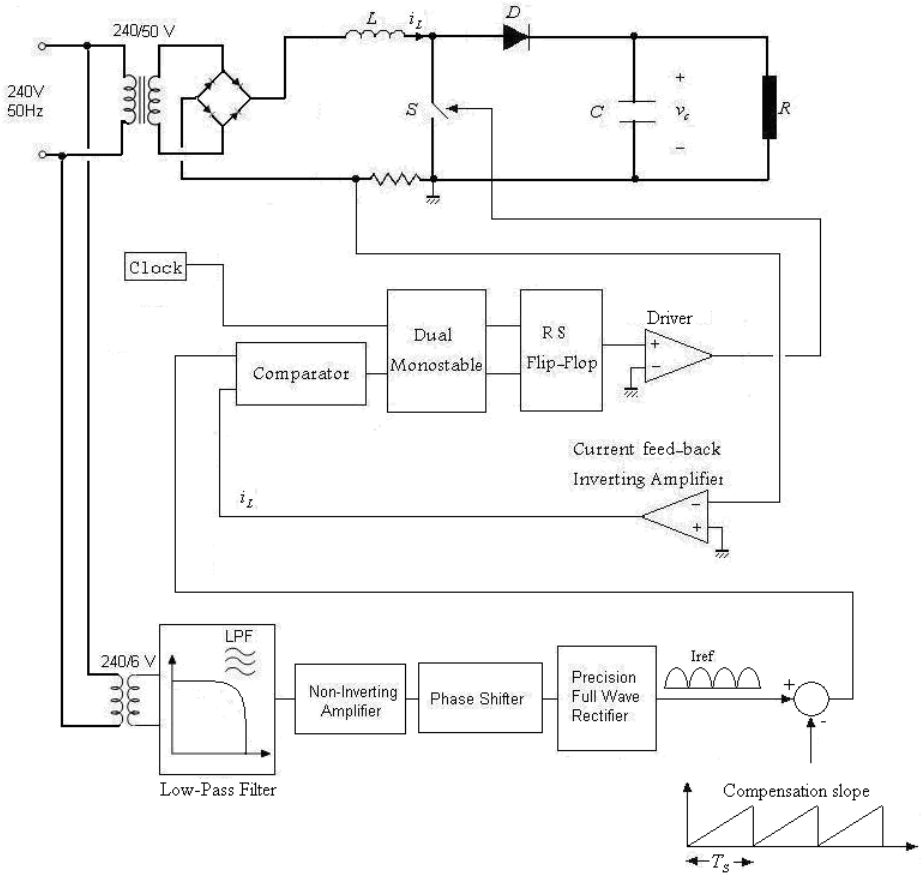

Figure 11.3 Converter circuit diagram with compensating ramp.

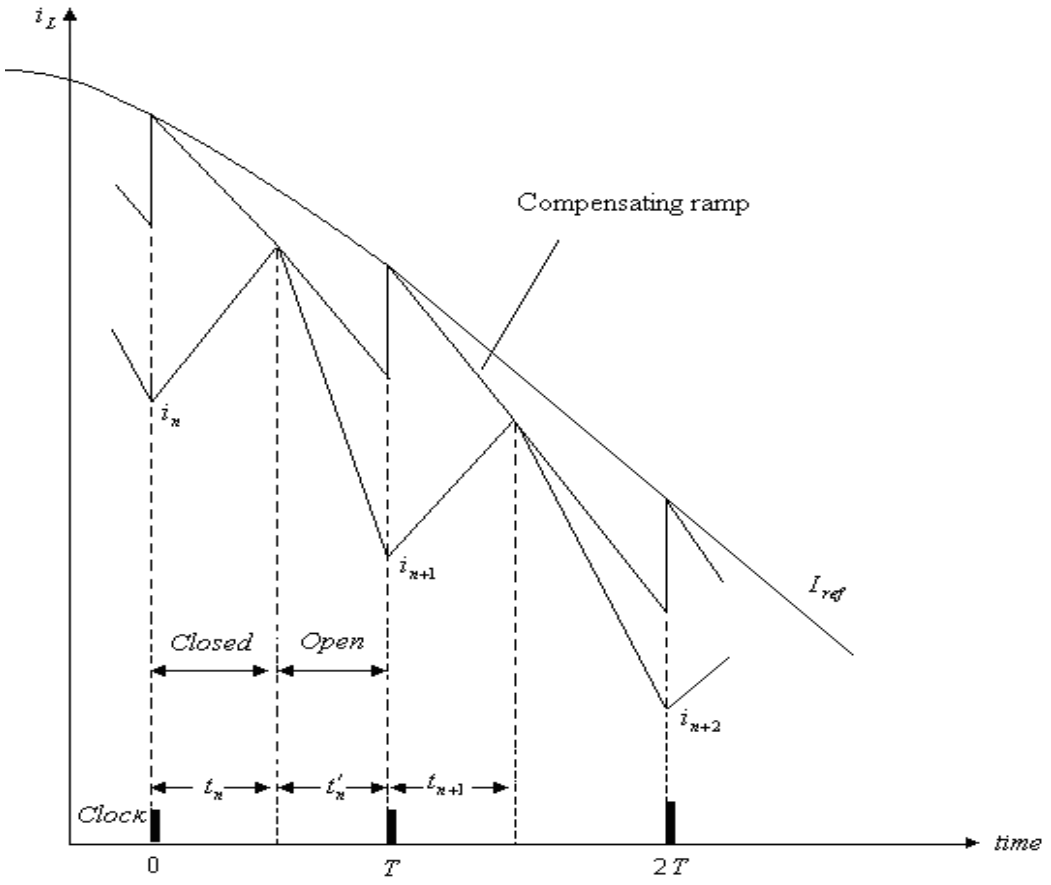

Figure 11.4 I_{ref} and i_L waveforms with compensating ramp.

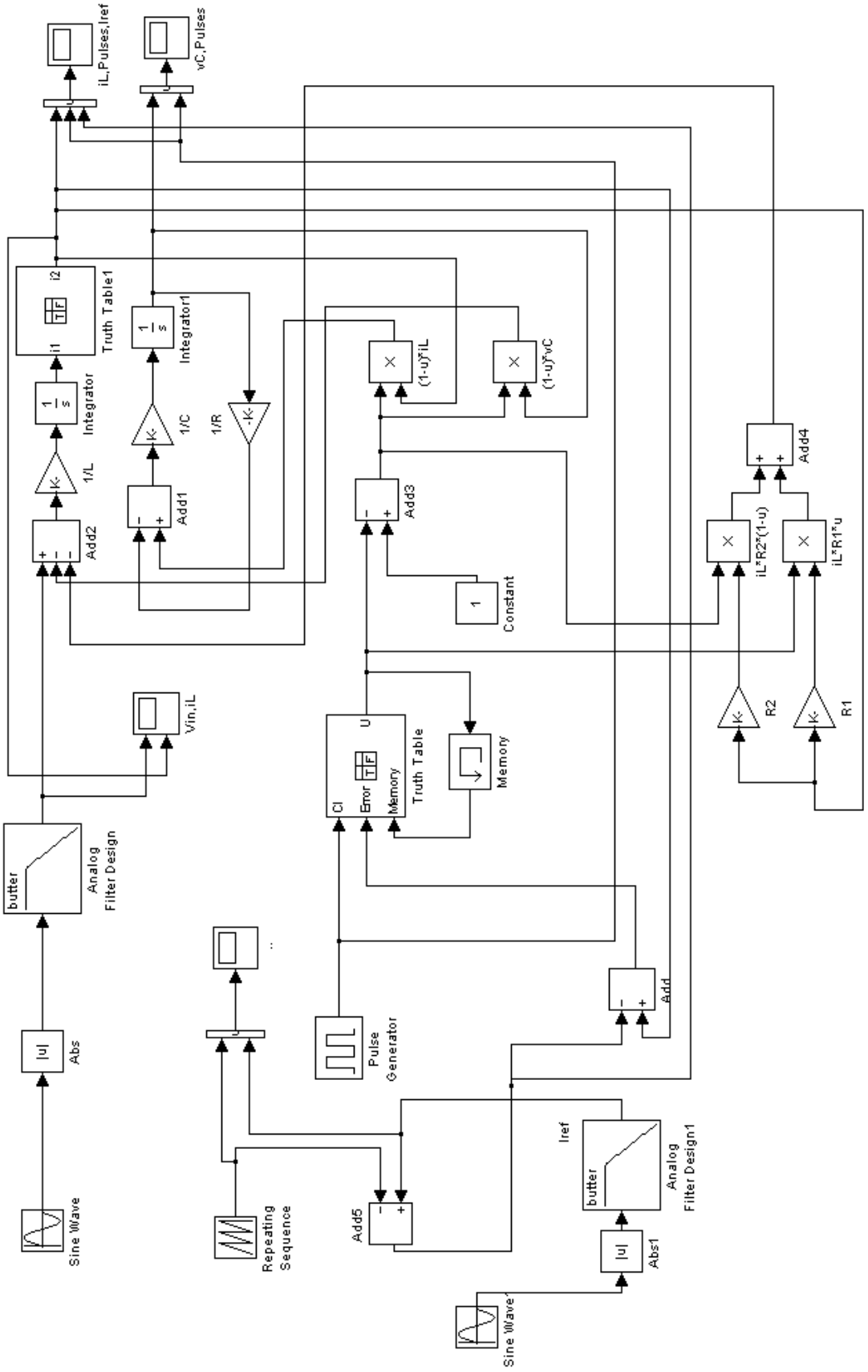

Figure 11.5 MATLAB/SIMULINK model with ramp compensation.

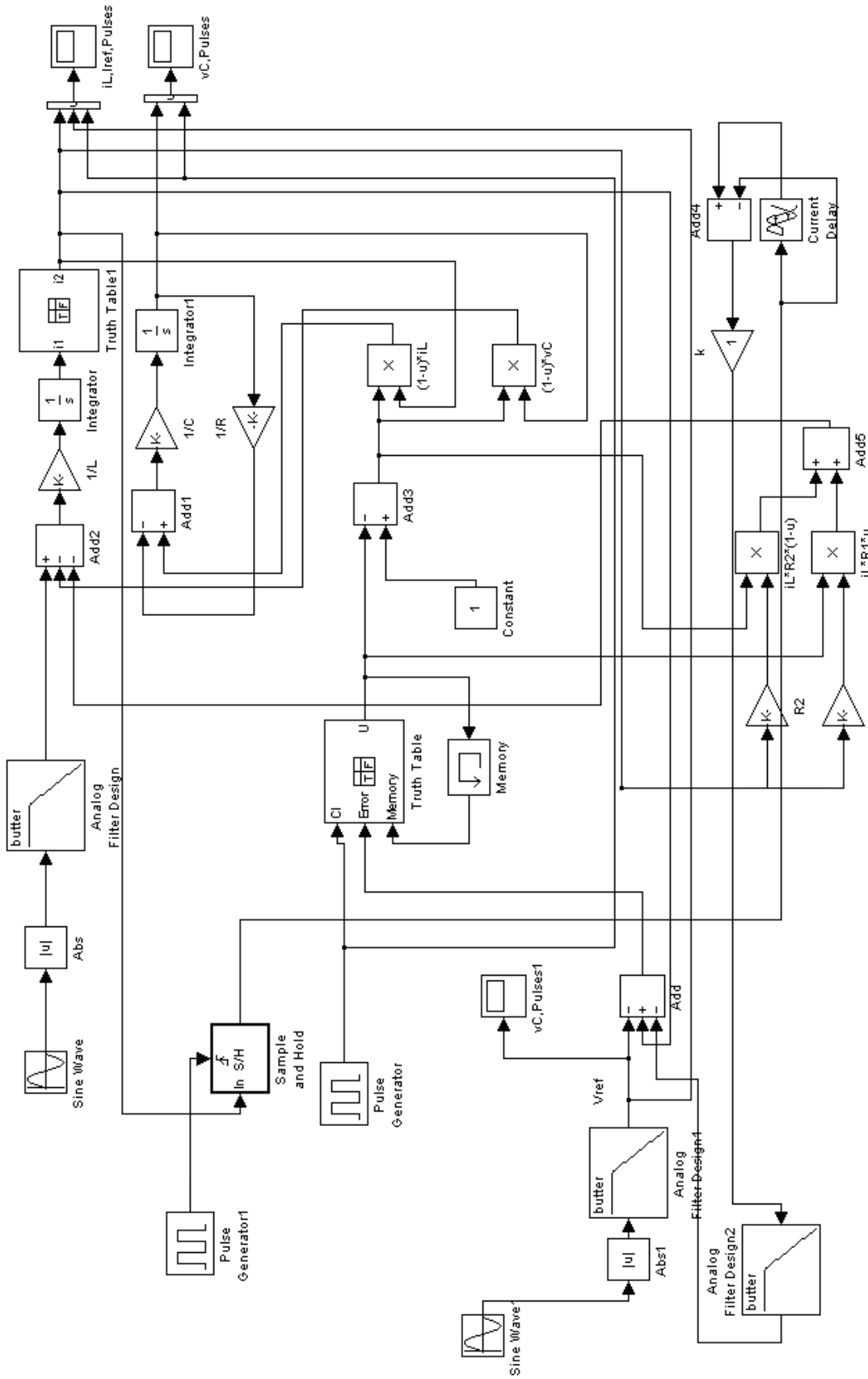

Figure 11.6 MATLAB/SIMULINK model with delayed current feedback.

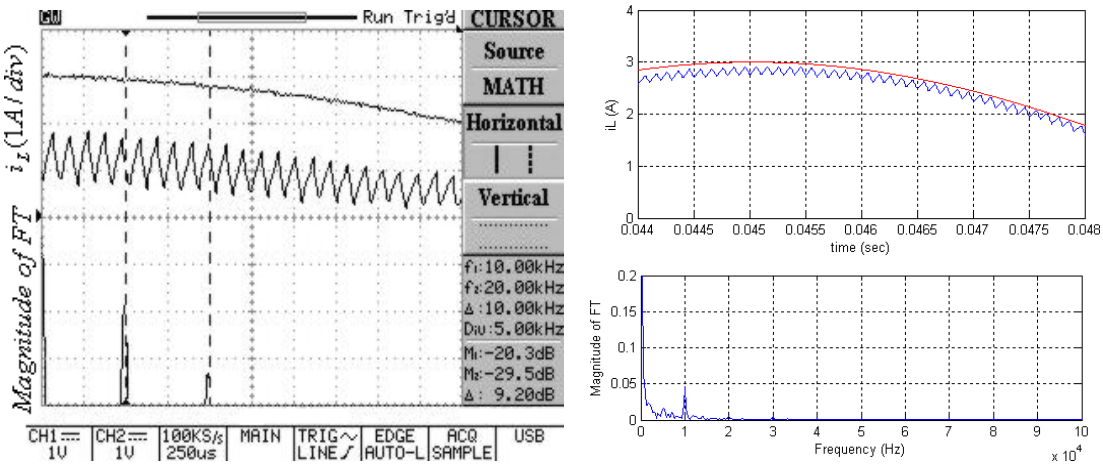

(a) Experimental and simulated inductor current.

{**Left**: experimental (1A/V), **right**: simulated}

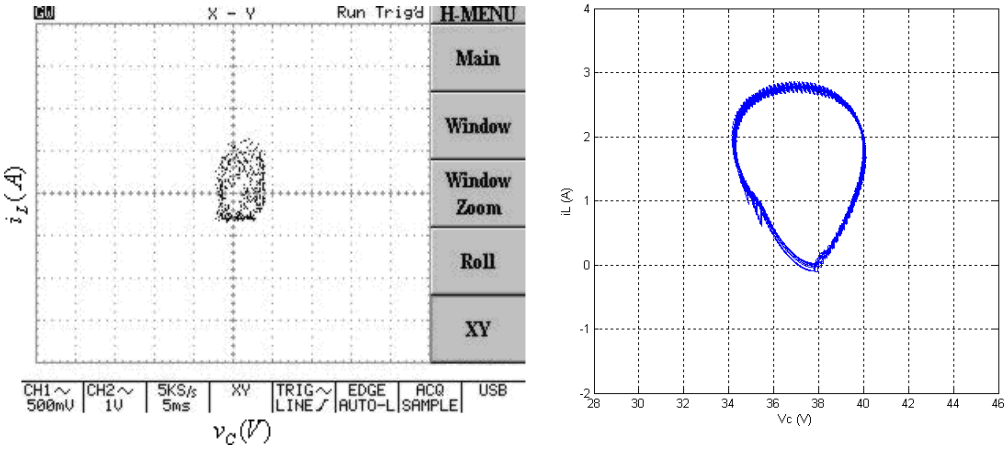

(b) Experimental and simulated phase portrait.

{**Left**: experimental CH2 (1A/V), **right**: simulated}

Figure 11.7 Delayed feedback control, $\tau = 70\mu s$, $\hat{V}_{in} = 20V$, $\hat{I}_{ref} = 3A$, and K=1.

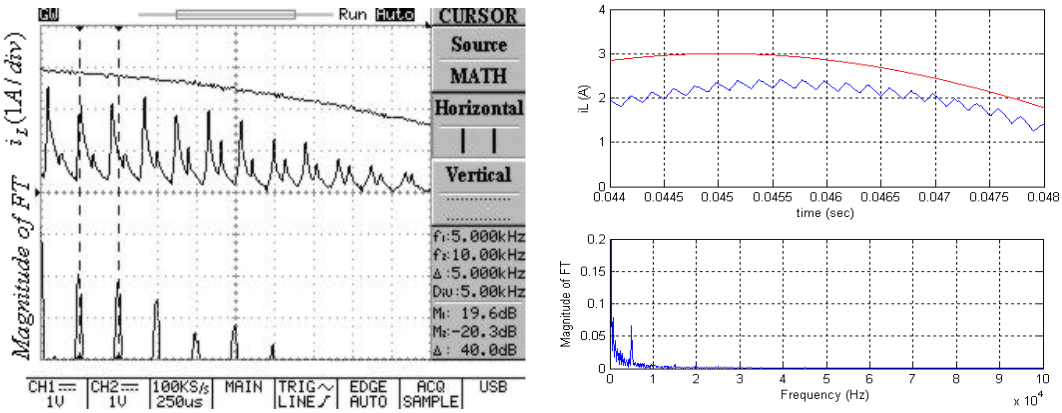

(a) Experimental and simulated inductor current.

{**Left**: experimental (1A/V), **right**: simulated}

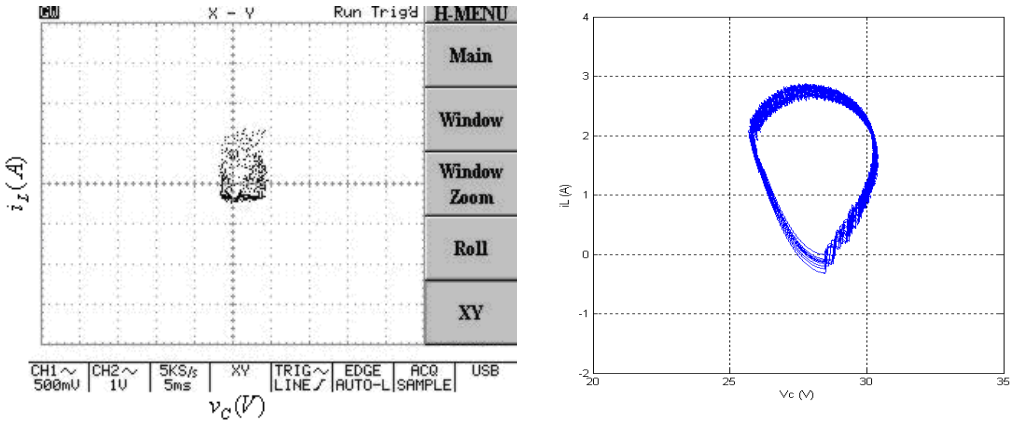

(b) Experimental and simulated phase portrait.

{**Left**: experimental CH2 (1A/V), **right**: simulated}

Figure 11.8 Delayed feedback control, $\tau = 100\mu s$, $\hat{V}_{in} = 20V$, $\hat{I}_{ref} = 3A$, and K=1.

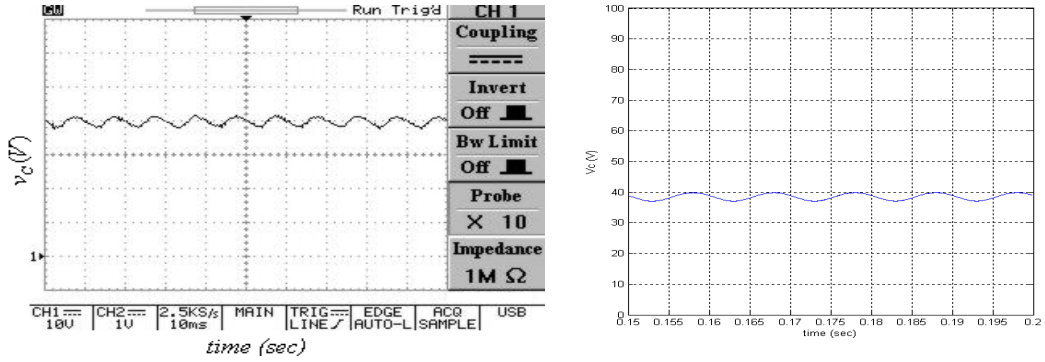

Figure 11.9 Experimental and simulated output voltage (delayed feedback control), $\tau = 70\mu s$, $\hat{V}_{in} = 20V$, $\hat{I}_{ref} = 3A$, and K=1.{**Left**: experimental, **right**: simulated}

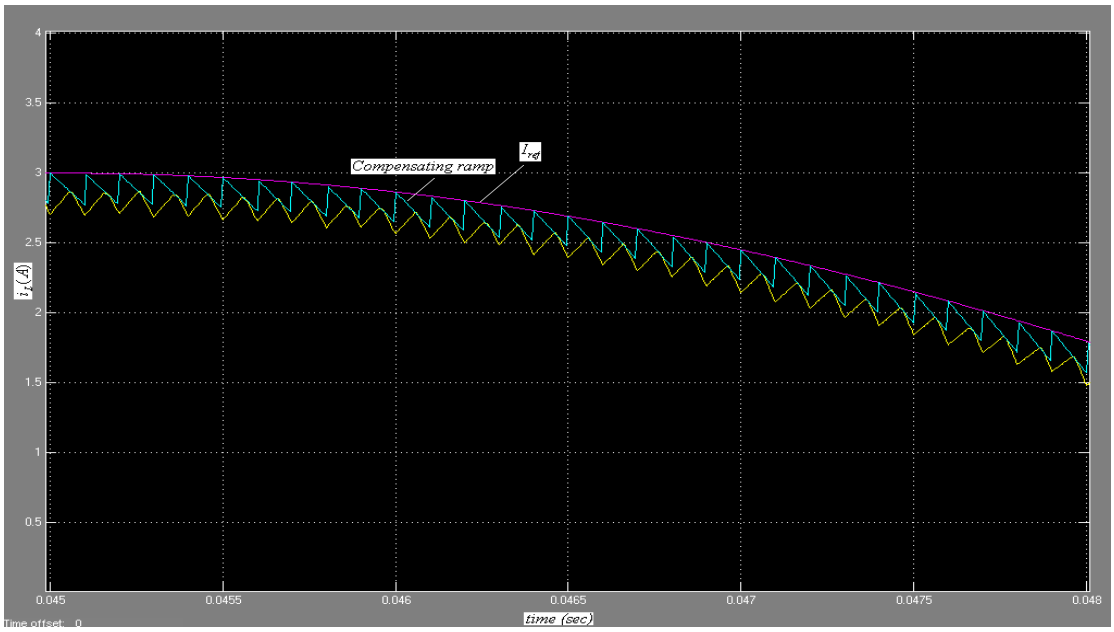

Figure 11.10 Inductor current (slope compensated control), $\hat{V}_{in} = 20V$ and $\hat{I}_{ref} = 3A$.

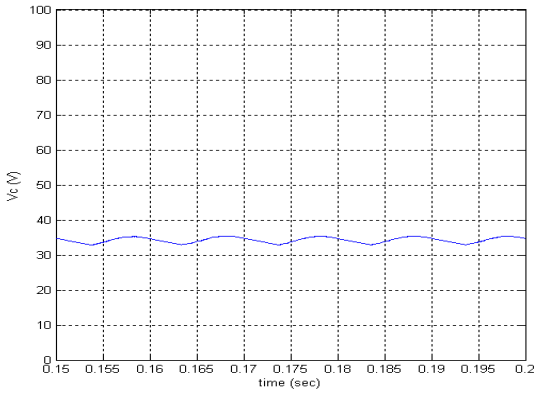

Figure 11.11 Output voltage (slope compensated control), $\hat{V}_{in} = 20V$ and $\hat{I}_{ref} = 3A$.

CHAPTER 12
CONCLUSION AND FUTURE WORK

This chapter presents conclusions on the work described in the thesis and makes a number of suggestions for future work in this field.

12.1 Concluding Remarks

The thesis is concerned with the analysis and control of chaotic behaviour in DC-DC boost converters and PFC boost converters. Bifurcation diagrams were generated for a single boost converter, a parallel two-module boost converter and a PFC boost converter, and these were used to investigate the converter behaviour as one of its parameters was varied. In every case, it was observed that as the bifurcation parameter I_{ref} increased, the system underwent period-doubling bifurcations, from a stable periodic solution with a single value for the inductor current at switch turn-on, to chaos, where the inductor current had many values at switch turn-on. Since I_{ref} increases with increased load, this indicates that the converters could become chaotic under heavy load conditions. When the input voltage V_{in} was chosen as the bifurcation parameter, the period-doubling route to chaos occurred as V_{in} was reduced. This indicates that the converters could become chaotic during supply voltage dips, which are common in applications where boost converters are connected to photovoltaic arrays for power conditioning.

MATLAB/SIMULINK models were developed to predict the circuit waveforms for each of the converters. These models were validated by comparison with waveforms obtained from experimental converters. The models were then used to verify the bifurcation points predicted by the bifurcation diagrams.

The simulated waveforms showed excellent agreement with experimental waveforms and the changes in state of the waveforms corresponded closely to the transition points of the bifurcation diagrams. Each waveform for period-1 operation predicted a single point on the bifurcation diagram, two points for period-2 operation and

multiple points for chaotic regions. Both the MATLAB/SIMULINK models and the bifurcation diagrams will provide useful design tools when designing new boost converter topologies.

During the investigation of bifurcation in the two-module paralleled converter, a "synchronisation" phenomenon was observed. This occurred over the range investigated of ± 10% of the nominal inductance value, which is much larger than the manufacturing tolerances for these inductors. The synchronisation behaviour may be beneficial in the control of chaos in paralleled converters, since the paralleled units could then be considered as a single entity.

The thesis describes the first application of a robust scheme for controlling chaos in DC-DC and PFC boost converters using the delayed feedback control method developed by Pyragas. Initially, a discrete component control circuit was developed to implement the control, but this was replaced by an ATMEL89C51 microcontroller, which provided more flexibility. When developing the delayed feedback control strategy, this ensured that the appropriate delay value could easily be varied by simple software alterations.

The control system performance and its stability using delayed feedback control depends on both the choice of the delay τ and the feedback gain K. Maps of the regimes on the (τ, K) plane were generated numerically for different values of I_{ref}. This, in effect provided a 3-dimensional τ, K, I_{ref} space. This was used to identify a large period-1 region in which the system may operate. Appropriate values of τ and K were then used in the practical control scheme.

MATLAB/SIMULINK models were developed for a DC-DC boost converter and a PFC boost converter, controlled using both the popular slope compensation method and delayed current feedback. The simulated performance of the converters controlled using delayed feedback control and the slope compensation method were compared. The results indicated that delayed current feedback results in a greater range of stable period-1 operation, compared with that obtained using slope compensation. Another advantage with delayed current feedback is that it provides a

higher output voltage for a given I_{ref}, and the control strategy is simpler than that for slope compensation. This is because the compensating ramp depends on both the converter input voltage, and the duty cycle which is load dependent. On the other hand, the delayed current feedback strategy is fixed, once K and τ are chosen.

Irrespective of the control method used with the AC-DC converter, control is lost when the supply voltage approaches zero, since there is insufficient voltage to maintain period-1 operation.

12.2 Future Work

DC-DC boost converters are often used in power conditioning circuits for photovoltaic (PV) systems, to step the voltage up for energy storage or for export to the electricity grid. Converters used for these applications have a higher than normal failure rate. The output voltage of a PV array can vary considerably, according to the amount of light incident on the array, and rapid changes in the voltage may cause transient chaotic behaviour in the power conditioning converter connected to the array. This may cause mal-functioning of the control system and possibly result in the converter failure. A thorough investigation is required into the interaction between a PV array and its power conditioning boost converter, to establish whether transient chaotic behaviour is responsible for the high failure rate.

PV arrays may be connected in series/parallel combinations to increase the output voltage and current of the overall unit and power conditioning may be achieved either at the individual array level, using many small converters, or at the overall system level, using one large converter. The economics of both approaches is currently being investigated. The effects of chaos on series/parallel combinations of converters will also need to be investigated.

REFERENCES

[1] Middlebrook, R. D. and Cuk, S., "A General Unified Approach to Modelling Switching-Converter Power Stages," in Proceeding IEEE Power Electronics Specialists Conference, June 1976, pp. 73-86.

[2] Lee, F. C. Y., Iwens, R. P. and Yu, Y., "Generalized Computer-Aided Discrete Time-Domain Modelling and Analysis of DC-DC Converters," IEEE Transactions on Industrial Electronics and Control Instrumentation, Vol. 26, No. 2, May 1979, pp. 58-69.

[3] Hamill, D. C. and Jeffries, D. J., "Subharmonic and Chaos in a Controlled Switched-Mode Power Converter," IEEE Transactions on Circuits and Systems, Vol. 35, No. 8, August 1988, pp. 1059-1061.

[4] Krein, P. T. and Bass, R. M., "Multiple Limit Cycle Phenomena In Switching Power Converters," in Proceeding IEEE Applied Power Electronics Conference, 1989, pp. 143-148.

[5] Deane, J. H. B. and Hamill, D. C., "Analysis, Simulation and Experimental Study of Chaos in the Buck Converter," in Proceeding IEEE Power Electronics Specialists Conference, June 1990, pp. 491-498.

[6] Deane, J. H. B. and Hamill, D. C., "Instability, Subharmonic, and Chaos in Power Electronic Systems," IEEE Transactions on Power Electronics, Vol. 5, No. 3, July 1990, pp. 260- 268.

[7] Hamill, D. C., Deane, J. H. B., and Jefferies D. J., "Modelling of Chaotic DC-DC Converters by Iterated Nonlinear Mappings," IEEE Transactions on Power Electronics, Vol. 7, No. 1, January 1992, pp. 25-36.

[8] Deane, J. H. B. and Hamill, D. C., “Chaotic Behaviour in Current-Mode Controlled DC-DC Converter,” Electronics Letters, Vol. 27, No. 13, June 1991, pp. 1172-1173.

[9] Deane, J. H. B., “Chaos in a Current-Mode Controlled Boost DC-DC Converter,” IEEE Transactions on Circuits and systems-I: Fundamental Theory and Applications, Vol. 39. No. 8, August 1992, pp. 680-683.

[10] Zafrany, I. and Ben-Yaakov, S., “A Chaos Model of Subharmonic Oscillations in Current Mode PWM Boost Converters,” in Proceeding IEEE Power Electronics Specialists Conference, 1995, pp. 1111-1117.

[11] Marrero, J. L. R., Font, J. M. and Verghese, G. C., “Analysis of the Chaotic Regime for DC-DC Converters Under Current-Mode Control,” in Proceeding IEEE Power Electronics Specialists Conference, 1996, pp. 1477-1483.

[12] Chan, W. C. Y. and Tse, C. K., “Study of Bifurcations in Current-Programmed DC/DC Boost Converters: From Quasi-Periodicity to Period-Doubling,” IEEE Transactions on Circuits and Systems-II: Fundamental Theory and Applications, Vol. 44, No. 12, December 1997.

[13] Banerjee, S., “Nonlinear Modelling and Bifurcations in the Boost Converter,” IEEE Transactions on Power Electronics, Vol. 13, No. 2, March 1998, pp. 252-260.

[14] Banerjee, S., Karthik, M. S., Yuan, G. and York, J. A., “Bifurcations in One-Dimensional Piecewise Smooth Maps-Theory and Applications in Switching Circuits,” IEEE Transactions on Circuits and systems-I: Fundamental Theory and Applications, Vol. 47. No. 3, March 2000, pp. 389-394.

[15] Tse, C. K. and Lai, Y. M., “Control of Bifurcation in Current-Programmed DC/DC Converters: A Reexamination of Slope Compensation,” IEEE International Symposium on Circuits and Systems, May 2000, pp. 671-674.

[16] Bernardo, M. and Vasca, F., "Discrete-Time Maps for the Analysis of Bifurcations and Chaos in DC/DC Converters," IEEE Transactions on Circuits and Systems-I: Fundamental Theory and Applications, Vol. 47. No. 2, February 2000, pp. 130-143.

[17] Lai, Y. M., Tse, C. K. and Chow, M. H. L., "Control of Bifurcation in Current-Programmed DC/DC Converters: An Alternative Viewpoint of Ramp Compensation," Circuits Systems Signal Processing, Vol. 20, No. 6, 2001, pp. 695-707.

[18] MA, Y., Kawakami, H., Tse, C. K. and Kousaka, T., "General Consideration for Modeling and Bifurcation Analysis of Switched Dynamical Systems," International Journal of Bifurcation and Chaos. Vol. 16, No. 3, 2006, pp. 693-700.

[19] Chen, Y., Tse, C. K., Wong, S. and Qiu, S., "Interaction of Fast-Scale and Slow-Scale Bifurcations in Current-Mode Controlled DC/DC Converters," International Journal of Bifurcation and Chaos. Vol. 17, No. 5, 2007, pp. 1609-1622.

[20] Tse, C. K., "Flip Bifurcation and Chaos in Three-State Boost Switching Regulators," IEEE Transactions on Circuits and Systems-I: Fundamental Theory and Applications, Vol. 41. No. 1, January 1994.

[21] Aston P. J., Deane, J. H. B. and Hamill, D. C., "Targeting in Systems with Discontinuities, with Application to Power Electronics," IEEE Transactions on Circuits and Systems-I: Fundamental Theory and Applications, Vol. 44. No. 10, October 1997.

[22] Banerjee, S. and Grebogi, C., "Border Collision Bifurcations in Two-Dimensional Piecewise Smooth Maps," Physical Review Letters, Vol. 59, Number 4, 1999, pp. 4052-4061.

[23] Banerjee, S., Parui, S. and Gupta, A., "Dynamical Effects of Missed Switching in Current-Mode Controlled DC-DC Converters," IEEE Transactions on Circuits and systems-II: Express Briefs, Vol. 51. No. 12, December 2004, pp. 649-654.

[24] Al-Mothafar, M. R., "Small-Signal and Transient Behaviour of Two-Module DC-DC Converter Using Mutually Coupled Output Filter Inductors," International Journal of Electronics, Vol. 79, No. 6, 1995, pp. 917-932.

[25] Iu, H. H. C., Tse, C. K. and Lai, Y. M., "Bifurcation in Current-Sharing Parallel-Connected Boost Converters," Power electronics and Motion Control Conference, PIEMC 2000, pp 921-924.

[26] Iu, H. H. C., Tse, C. K., Pajevalica, V. and Lai, Y. M., "Bifurcation Behaviour in Parallel-Connected Boost Converters," International Journal of Circuit Theory and Applications. Vol. 29, No. 3, 2001, pp. 281-298.

[27] Iu, H. H. C. and Tse, C. K., "Study of Low-Frequency Bifurcation Phenomena of a Parallel-Connected Boost Converter System Via Simple Averaged Models," IEEE Transactions on Circuits and Systems-I: Fundamental Theory and Applications, Vol. 50. No. 5, May 2003.

[28] Schlecht, M. F., "A Line Interfaced Inverter with Active Control of the Output Current Waveform," in Proceeding IEEE Power Electronics Specialists Conference, 1980, pp. 234-241.

[29] Kosher, M. J. and Steigerwald, R. L., "An AC to DC Converter with High Quality Input Waveforms," IEEE Transactions on Industry Applications, Vol.19, No. 4, July/August 1983, pp. 586-599.

[30] Williams, J. B., "Design of Feedback Loop in Unity Power Factor AC-to-DC Converter," in Proceeding IEEE Power Electronics Specialists Conference, 1989, pp. 959-967.

[31] Dixon, L. H., "High Power Factor Preregulator for Off-Line Power Supplies," Unitrode Power Supply Design Seminar Manual, SEM-600, 1988.

[32] Dixon, L. H., “High Power Factor Switching Preregulator Design Optimization,” Unitrode Power Supply Design Seminar Manual, SEM-700, 1990.
[33] Dixon, L. H., “Average Current Mode Control of Switching Power Supplies,” Unitrode Power Supply Design Seminar Manual, SEM-700, 1990, pp. 356-369.

[34] Noon, J. P. and Dalal, D., “Practical Design Issues for PFC Circuits,” in Proceeding IEEE Applied Power Electronics Conference, 1997, pp. 51-58.

[35] Noon, J. P., “Designing High-Power Factor Off-Line Power Supplies,” 2003 Unitrode Design Seminar Manual, SEM 1500, Texas Instruments, 2003.

[36] Orabi, M. and Ninomiya, T., “Nonlinear Dynamics of Power-Factor-Correction Converter,” IEEE Transactions on Industrial Electronics, Vol. 50, No. 6, December 2003, pp. 1116-1125.

[37] Tse, C. K., Dranga, O. and Iu, H. H. C., “Bifurcation Analysis of a Power-Factor-Correction Boost Converter: Uncovering Fast-Scale Instability,” IEEE International Symposium Circuits and Systems, 2003, Vol. 3, pp. 312-315.

[38] Iu, H. H. C., Zhou, Y. and Tse, C. K., “Fast Scale Instability in a PFC Boost Converter under Average Current-Mode Control,” International Journal of Circuit Theory and Applications, Vol. 31, 2003, pp. 611-624.

[39] ElAroudi, A., Orabi, M., Martinez-Salamero, L. and Ninomiya, T., “Investigating stability and bifurcations of a boost PFC circuit under peak current mode control,” IEEE International Symposium on Circuits and Systems, 2005, pp. 2835-2838.

[40] Nayfeh, A. H., and Balachandran B., Applied Nonlinear Dynamics, John Willy, New York, 1995.

[41] Khalil, H., Nonlinear Systems, Third Edition, Prentice Hall, Upper Saddle River, New Jersey, 2002.

[42] Tse, C. K. and Chan W. C. Y., "Chaos from a Current Programmed Cuk Converter," International Journal of Circuit Theory Applications, Vol. 23, May-June 1995, pp. 217-225.
[43] Pyragas, K., "Continuous Control of Chaos by Self-Controlling Feedback," Physics Letters, A 170, 1992, pp 421-428.

[44] Ott, E., Grebogi, C. and Yorke, J. A., "Controlling Chaos," Physical Review Letters, Vol. 64, Number 11, 1990, pp. 1196-1199.

[45] Ogorzalek, M. J., "Taming Chaos: Part II–Control," IEEE Transactions on Circuits and Systems-I; Fundamental Theory and Applications, Vol. 40, No. 10, October 1993, pp. 700-706.

[46] Kapitaniak, T, Controlling Chaos, Theoretical and Practical Methods in Non-Linear Dynamics, Academic Press, 1996.

[47] Pyragas, K., "Delayed Feedback Control of Chaos," Philosophical Transactions of the Royal society, 2006, Vol. 364, 2309-2334.

[48] Balanov, A. G., Janson, N. B. and Scholl, E., "Delayed Feedback Control of Chaos: Bifurcation Analysis," Physical Review, Vol. 71, 2005.

[49] MAXIM, 8-Bit ADCs User's Guide, August 1996.

[50] ANALOG DEVICES, 8-Bit Buffered Multiplying DAC User's Guide.

[51] Gabb, W. C., "89C51 Laboratory notes-Outputs, Timing and Assembly Language," Department of Electronic and Electrical Engineering, Loughborough University.

[52] ATMEL, 8-Bit Flash Microcontroller AT89C51ED2 User's Guide, December 2003.

[53] Natsheh, A. N., Kettleborough, J. G. and Nazzal, J. M., "Analysis, Simulation and Experimental Study of Chaotic Behaviour in Parallel-Connected DC–DC Boost Converters," Chaos, Solitons & Fractals, in Press, Corrected Proof, Available Online 14 August 2007.

[54] Natsheh, A. N., Janson, N. B. and Kettleborough, J. G., "Experimental Study of Controlling Chaos in a DC–DC Boost Converter," Chaos, Solitons & Fractals, in Press, Corrected Proof, Available Online 26 December 2007.

[55] Natsheh, A. N., Janson, N. B. and Kettleborough, J. G., "Control of chaos in a DC-DC boost converter," in Proceedings of the IEEE International Symposium on Industrial Electronics (ISIE08), Cambridge, UK, June/July 2008, pp. 317-322.

APPENDICES

APPENDIX A

A LISTING OF THE SOFTWARE PROGRAMMED BY MATLAB

A.1 MATLAB Program for Bifurcation Diagram of a Single Boost Converter

```
%This MATLAB program is for single boost converter
R=20;
L=1e-3;
C=10e-6;
T=100e-6;
Vi=10;
%Iref=3;

K=1/(2*R*C);
W=sqrt((1/(L*C))-K^2);

I(1)=0;
V(1)=0;

for Iref=0:0.05:5.5

   for n=1:750

t(n)=L*(Iref-I(n))/Vi;

tprime(n)=T*(1-((t(n)/T)-fix(t(n)/T)));

Irefprime=Iref-(Vi/R);

I(n+1)=expm(-K*tprime(n))*(((K*L*Irefprime+Vi-V(n)*expm(-
2*K*t(n)))/(W*L))*sin(W*tprime(n))+Irefprime*cos(W*tprime(n)))+(Vi/R)
;

V(n+1)=Vi-(expm(-K*tprime(n))*((K*V(n)*expm(-2*K*t(n))-K*Vi-
(Irefprime/C))*(sin(W*tprime(n))/W)+(Vi-V(n)*expm(-
2*K*t(n)))*cos(W*tprime(n))));
```

```
end

    hold on
    plot(Iref,I(500:750),'b.')
    hold off
    xlabel('Iref (A)')
    ylabel('iL (A)')
    grid

End
```

A.2 MATLAB Program for Bifurcation Diagram of a Two-Module Boost Converter

```
%This MATLAB program is for two-module boost converter
R=20;
L1=1e-3;
L2=1.2e-3;
C=24e-6;
T=100e-6;
Vi=10;

Vc(1)=0;
I1(1)=0;
I2(1)=0;

for Iref=0:0.01:1.4

   for n=1:750

tc1(n)=L1*(Iref-I1(n))/Vi;
td1=T*(1-((tc1(n)/T)-fix(tc1(n)/T)));
d1=tc1(n)/T;

tc2(n)=L2*(Iref-I2(n))/Vi;
td2(n)=T*(1-((tc2(n)/T)-fix(tc2(n)/T)));
d2=tc2(n)/T;

f1=1-(td2(n)/(R*C))+(((td2(n)^2)/2)*((1/((R^2)*(C^2)))-(1/(L1*C))-
(1/(L2*C))));
g1=1-((tc2(n)-tc1(n))/(R*C))+((((tc2(n)-
tc1(n))^2)/2)*((1/((R^2)*(C^2)))-(1/(L1*C))));
h1=-((tc2(n)-tc1(n))/L1)+(((tc2(n)-tc1(n))^2)/(2*R*L1*C));
f2=-(td2(n)/L1)+((td2(n)^2)/(2*R*L1*C));
f3=-(td2(n)/L2)+((td2(n)^2)/(2*R*L2*C));
g2=((tc2(n)-tc1(n))/C)-(((tc2(n)-tc1(n))^2)/(2*R*(C^2)));
h2=1-(((tc2(n)-tc1(n))^2)/(2*L1*C));

K13=(td2(n)/C)-((td2(n)^2)/(2*R*C^2));
K23=-(td2(n)^2)/(2*L1*C);
K33=1-((td2(n)^2)/(2*L2*C));
```

```
K11=(f1*g1)+(K13*h1);
K12=(f1*g2)+(K13*h2);
K21=(f2*g1)+((1+K23)*h1);
K22=(f2*g2)+((1+K23)*h2);
K31=(f3*g1)+((K33-1)*h1);
K32=(f3*g2)+((K33-1)*h2);

NN1=-((tc2(n)^2-tc1(n)^2)/(2*L1*C))-(((tc2(n)^3)-
(tc1(n)^3))/(6*R*L1*(C^2)));
NN2=((tc2(n)-tc1(n))/L1)-(((tc2(n)^3)-(tc1(n)^3))/(6*(L1^2)*C));
NN3=(tc2(n)-tc1(n))/L2;

N1=(K11*NN1)+(K12*NN2)+(K13*NN3);
N2=(K21*NN1)+(K22*NN2)+(K23*NN3);
N3=(K31*NN1)+(K32*NN2)+(K33*NN3);

Q1=-((td2(n)^2)/(2*L1*C))-((td2(n)^3)/(6*R*L1*(C^2)))-
((td2(n)^2)/(2*L2*C))-((td2(n)^2)/(6*R*L2*C));
Q2=(td2(n)/L1)-((td2(n)^3)/(6*(L1^2)*C))-((td2(n)^3)/(6*L1*L2*C));
Q3=(td2(n)/L2)-((td2(n)^3)/(6*(L2^2)*C))-((td2(n)^3)/(6*L1*L2*C));

M1=(f1*Q1)+(K13*Q2)+(K13*Q3);
M2=(f2*Q1)+((1+K23)*Q2)+(K23*Q3);
M3=(f3*Q1)+((K33-1)*Q2)+(K33*Q3);

u1=((K12*(tc1(n)/L1))+(K13*(tc1(n)/L2)))+N1+M1;
u2=((K22*(tc1(n)/L1))+(K23*(tc1(n)/L2)))+N2+M2;
u3=((K32*(tc1(n)/L1))+(K33*(tc1(n)/L2)))+N3+M3;

KK=1-(tc1(n)/(R*C))+((tc1(n)^2)/(2*(R^2)*(C^2)));

KKK1=(K11*KK);
KKK2=(K21*KK);
KKK3=(K31*KK);

Vc(n+1)=KKK1*Vc(n)+K12*I1(n)+K13*I2(n)+u1*Vi;
I1(n+1)=KKK2*Vc(n)+K22*I1(n)+K23*I2(n)+u2*Vi;
I2(n+1)=KKK3*Vc(n)+K32*I1(n)+K33*I2(n)+u3*Vi;
```

```
I = I1+I2;

    end

    hold on
    plot(Iref,I1(500:750),'b.')
    hold off
    xlabel('Iref (A)')
    ylabel('iL1 (A)')
    grid

end
```

A.3 MATLAB Program for Bifurcation Diagram of a PFC Boost Converter

```
%This MATLAB program is for power factor correction boost converter
R=300;
L=15e-3;
C=220e-6;
T=100e-6;
Iref=3;



K=1/(2*R*C);
W=sqrt((1/(L*C))-K^2);

I(1)=0;
V(1)=0;

for theta=pi:pi/2:2*pi;

for Vi=5:0.5:80

for n=1:12000

t(n)=L*((Vref*abs(sin(theta)))-I(n))/((sqrt(2)*Vi)*abs(sin(theta)));

tprime(n)=T*(1-((t(n)/T)-fix(t(n)/T)));

Irefprime=(Iref*abs(sin(theta)))-(((sqrt(2)*Vi)*abs(sin(theta)))/R);

I(n+1)=expm(-
K*tprime(n))*(((K*L*Irefprime+((sqrt(2)*Vi)*abs(sin(theta)))-
V(n)*expm(-
2*K*t(n)))/(W*L))*sin(W*tprime(n))+Irefprime*cos(W*tprime(n)))+(((sqr
t(2)*Vi)*abs(sin(theta)))/R);

V(n+1)=((sqrt(2)*Vi)*abs(sin(theta)))+(expm(-
K*tprime(n))*((K*V(n)*expm(-2*K*t(n))-
K*((sqrt(2)*Vi)*abs(sin(theta)))+(((Iref*abs(sin(theta)))-
((V(n)*expm(-2*K*t(n)))/(R)))/C))*(sin(W*tprime(n))/W)+(-
```

```
((sqrt(2)*Vi)*abs(sin(theta)))+V(n)*expm(-
2*K*t(n)))*cos(W*tprime(n))));

end

   hold on
   plot(Vi,I(11000:12000),'b.')
   hold off
   xlabel('Vi (V)')
   ylabel('iL (A)')
   axis([5 80 1 4])
   grid

end
end
```

APPENDIX B
THE SOFTWARE PROGRAMMED BY FORTRAN

B.1 Delayed Feedback FORTRAN Program

```
c This programme ingtegrates a CIRCUIT system produced by Ammar Natsheh.

c The delayed feedback here is the traditional one, where the feedback term is
c added to the equation in the way realized in the real electronic circuit.

c CIRCUIT is with noise and delayed feedback, both applied to x

      implicit real*8 (a-h,o-z)
      PARAMETER (NM=10,NLAG=500000,KLAG=10,nn=1000000)
      DIMENSION RK(4,10),F(10),YY1(10),FB(10),YN(10)
      dimension y(10), y0(10), tau(KLAG),NLM(KLAG),LCUR(KLAG),
     ,XLAG(KLAG),kl(KLAG), flag(KLAG,NLAG),
     ,t_poi1(50000),poi1(2,50000),pp(2,50000),v(2,50000),
     ,for(50000),
     ,ylag(50000)

      character*40 fout,froot
      character*20 name_dir,aaa
      character*60 name_res
      character*20 name_dir_BD
      character*3 k_rand,key_wr_poi,key_wr_pp,key_wr_bif
      character*4 apar(10)

      real gasdev

      COMMON/NOISE/IX1
      common/par/pa(10),tt
      common/prev/u
```

```
c===== "reading parameters">
      open(1,file='cir_cont_BD_agr.in')
       read(1,*)fout
       read(1,*)name_res
          read(1,*)aaa
       read(1,*)name_dir_BD
          read(1,*)name_dir
          read(1,*)key_wr_poi,key_wr_bif,key_wr_pp,t_ini,t_end
          read(1,*)n,m
          read(1,*)aaa
          read(1,*)(pa(ii), ii=1,m+1)!  L, C, vi, R, iref, T,  K, D
          read(1,*)(y0(jj), jj=1,n)
          read(1,*)t_rel,t_int,h,kti,n_poi
          read(1,*)ipar
          read(1,*)spa,fpa,stpa
          read(1,*) ndel   ! number of delayes
          read(1,*) (kl(ii),ii=1,ndel)
          read(1,*) (tau(ii),ii=1,ndel)
          read(1,*)k_rand,nIX1
      close(1)
          print *,'Parameters read.'
c===== "reading parameters"<

c====== "naming parameters" ========>
c   for FHN>>>>
          goto 1
       apar(1)="eps1"
       apar(2)="a1"
       apar(3)="K"
       apar(4)="D1"
c for CIRCUIT >>>>>
1      continue
       apar(1)="L"
       apar(2)="C"
```

```
      apar(3)="vi"
      apar(4)="R"
      apar(5)="iref"
      apar(6)="T"
      apar(7)="K"
      apar(8)="D"
c====== "naming parameters" ========<

      open(3,file=name_res,access='append')
      write(3,*)'# ',(apar(j),': ',pa(j),', ',j=1,4)
      write(3,*)'# ',(apar(j),': ',pa(j),', ',j=5,m)
      write(3,*)'# kl:',(kl(ii),ii=1,ndel),
     ,          ' tau:',(tau(ii),ii=1,ndel)
      write(3,*)'# t_rel:',t_rel,' t_int:',t_int,' h:',h,
     ,   ' kti:',kti,' n_poi:',n_poi
      write(3,*)'   '
      write(3,*)"# a(ipar),av_for,sqav_for,var_for,"//
     *          " av_isi, sqav_isi, var_isi"
      close(3)



c========== "initialising random variables generator"
     if (k_rand.eq.'yes'.and.pa(m+1).gt.0.) then
         itime=time()
            if (itime.lt.0) then
c**********************************************************************
***********
               print*, "Warning! The function 'time' was compiled with errors!"
               print*,"Please, change the string 'itime = (integer) time_();' "
               print*, "on the string 'itime = (integer) time();' in C(!)-source file,"
               print*,"and then recompile it typing 'g77 -o myfile.x myfile.c' "
c**********************************************************************
***********
               stop
```

```
            end if
c           print *,itime
          do while (abs(itime).gt.300)
             itime=abs(itime)-327
          end do
                IX1=-itime
              else
              IX1=nIX1
      end if
      print*, "Seed for gasdev is ",IX1
      do i=1, 1.D07
        xxx=gasdev(ix1)
      end do
          print *,'gasdev initialized'
c========== "initialising random variables generator"<

c========"setting parameter values">
      if(t_rel.le.0.0)t_rel=h*kti
      npstep=(fpa-spa)/stpa +1
      pi=4.0*datan(1.d0)
      pi2=pi*2.0
      h2=dsqrt(h)
      dt=h*kti
      n1=t_int/h/kti
          print *,'Parameter values set'
c========"setting parameter values"<

c====== setting initial conditions ====>
          if(ipar.eq.5)then
                  y(1)=0.5*spa
          else
                  y(1)=pa(5)*0.5
          end if
          u=1.
```

```
c       x_il_prev=y(1)*0.9
c          x_dif_prev=y(1)*0.9
           x_dif_prev=0.
           x_il_prev=y(1)*0.9-x_dif_prev*pa(7)

c------ to prevent an error if lag=0 >
        do ii=1, ndel
          flag(ii,1)=y(kl(ii))
        end do
c------ to prevent an error if lag=0 <

      call INILAG(ndel,tau,h,flag,NLM,LCUR,XLAG)
           print *,'INILAG executed'
c====== setting initial conditions ====<

c//   PARAMETRIZATION LOOP---------------------------------
c//      do pa(ipar)=spa,fpa,stpa
c//      if  number of control parameter <=m+1 then
c//      parameters or noise intensity are varied with iteration,
c//      else the delay of number  ipar-m-1 is varied.

      do k=0,npstep
         open(16,file="numBD")
         if (ipar.le.m+1) then
            pa(ipar)=spa +k*stpa
            write(16,'(f8.4)')pa(ipar)
               print *,pa(ipar)
         else
            tau(ipar-m-1)=spa+k*stpa
            write(16,'(f8.4)') tau(ipar-m-1)
            print *, tau(ipar-m-1)
         end if
         close(16)
```

```
c         do i=1,n
c                   y(i)=y0(i)
c         end do
          pa_iref=pa(5)
          t_per=pa(6)

      av_for=0.
      sqav_for=0.
      t=0.
      tp=0.
      D=pa(m+1)
c============= "relaxation" >
      do while (t.lt.t_rel)
        t=t+h
      CALL
EMMN(ndel,N,y,h,h2,T,m,RK,F,YY1,FB,YN,FLAG,NLM,KL,LCUR,XLAG)

c         pa_iref=pa_iref0+pa(7)*(xlag(1)-y(1))

c         if((y(1).lt.pa_iref).and.(y(1).gt.x_il_prev))then
          x_dif=pa(7)*(xlag(1)-y(1))
          x_il=y(1)-x_dif
c         if((x_dif.lt.pa_iref).and.(x_dif.gt.x_dif_prev))then
          if((x_il.lt.pa_iref).and.(x_il.gt.x_il_prev))then
                    u=1.
          else
                    u=0.
          end if
        if(t-tp.ge.t_per) then
          u=1.
          tp=t
        end if
c       x_il_prev=y(1)
           x_dif_prev=(xlag(1)-y(1))*pa(7)
```

```
          x_il_prev=y(1)-x_dif_prev
      end do
          print *,'Relaxation over, t=',t
c============= "relaxation" <

      print *,'Relaxation over:',t
      if (ipar.le.m+1) then
          print *,apar(ipar),": ",pa(ipar)
      else
          print *,"tau: ", tau(ipar-m-1)
      end if

c====== temporary line to check if feedback induces cycle ==>
c       pa(m+1)=0.
c====== temporary line to check if feedback induces cycle ==<

c========== "integration">
c       open(10,file='tmp.pp')
       i_poi1=0
       i_wr=0
       n1_true=0
       x1_prev=y(1)
       y1_prev=y(2)
       f1_prev=f(1)
       sec_prev=10.*x1_prev-y1_prev
       do i=1,n1
        do ii=1,kti
         t=t+h
         CALL
     *   EMMN(ndel,N,y,h,h2,T,m,RK,F,YY1,FB,YN,FLAG,NLM,KL,LCUR,XLAG)
c          pa_iref=pa_iref0+pa(7)*(xlag(1)-y(1))
c       if((y(1).lt.pa_iref).and.(y(1).gt.x_il_prev))then

          x_dif=pa(7)*(xlag(1)-y(1))
```

```
          x_il=y(1)-x_dif
c         if((x_dif.lt.pa_iref).and.(x_dif.gt.x_dif_prev))then
          if((x_il.lt.pa_iref).and.(x_il.gt.x_il_prev))then
                    u=1.
          else
                    u=0.
          end if
        if(t-tp.ge.t_per) then
          u=1.
          tp=t
        end if
c         x_il_prev=y(1)
          x_dif_prev=(xlag(1)-y(1))*pa(7)
          x_il_prev=y(1)-x_dif_prev
c          if(y(1).ge.0..and.x1_prev.lt.0.)then  ! section il=0
           if(f(1).ge.0..and.f1_prev.lt.0.)then  ! section d il/dt=0
c          sec=10.*y(1)-y(2)
c          if(sec.ge.0..and.sec_prev.lt.0.)then  ! section vc=10 il

           i_poi1=i_poi1+1
c====="linear interpolation"====>
c         call lin_int(t,h,x1_prev,y(1),tp1)        ! section il=0
c           call poi_int(t,h,tp1,y1_prev,y(2),y1p)   ! section il=0

         call lin_int(t,h,f1_prev,f(1),tp1)          ! section d il/dt=0
           call poi_int(t,h,tp1,x1_prev,y(1),x1p)   ! section d il/dt=0
           call poi_int(t,h,tp1,y1_prev,y(2),y1p)   ! section d il/dt=0

c         call lin_int(t,h,sec_prev,sec,tp1)          ! section vc=10 il
c           call poi_int(t,h,tp1,x1_prev,y(1),x1p)   ! section vc=10 il
c           call poi_int(t,h,tp1,y1_prev,y(2),y1p)   ! section vc=10 il
c====="linear interpolation"====<
           t_poi1(i_poi1)=tp1
c===== "storing the poincare map"======>
```

```
         if(key_wr_poi.eq.'yes'.or.key_wr_bif.eq.'yes')then
            poi1(1,i_poi1)=x1p
            poi1(2,i_poi1)=y1p
c           print *,'Poincare points:',(poi1(j,i_poi1),j=1,n)
c           pause ' '
            end if
c===== "storing the poincare map"======<
           if(i_poi1.ge.n_poi)goto 3
           end if
        x1_prev=y(1)
        y1_prev=y(2)
        f1_prev=f(1)
           sec_prev=10.*x1_prev-y1_prev
        end do
c==== for ordinary delayed feeback ====>
           force=xlag(1)-y(1)
c==== for ordinary delayed feeback ====<
        av_for=av_for+pa(7)*force
           sqav_for=sqav_for+pa(7)*force*pa(7)*force
c       print *, y(2), xlag(1) , av_for, sqav_for
c       pause "
c==== "storing the phase variables and continuous phases" ====>
           if(t.ge.t_ini.and.t.le.t_end.and.i_wr+1.le.n1)then
           i_wr=i_wr+1
c          print *,'i_wr:',i_wr
           do j=1,n
          pp(j,i_wr)=y(j)
             v(j,i_wr)=f(j)
           end do
           for(i_wr)=force*pa(7)
           ylag(i_wr)=XLAG(1)
c       print *, y(2), xlag(1)
c       pause "
        end if
```

```
c==== "storing the phase variables and continuous phases" ====<
      end do
3     continue
      n1_true=i
      n_wr_pp=i_wr
      n_poi1=i_poi1
      print *,'                          Time:',t
      print *,' Planned number of integration steps:',n1
      print *,'    True number of integration steps:',n1_true
      print *,'Number of phase port points to write:',n_wr_pp
      print *,'Total number of Poincare points:',n_poi1
c      close(10)
c========== "integration"<

      av_for=av_for/n1_true
      sqav_for=sqav_for/n1_true
      var_for=sqrt(sqav_for-av_for*av_for)
c     print *, av_for,  sqav_for,   var_for
c     pause ' '

          open(7,file="numBD")
       read(7,*)froot
          close(7)
          kspc=index(froot," ")
          kspc1=index(fout,"")
c//       print *, froot(1:kspace-1)//".dat"

c======== "writing Poincare map">
          if(key_wr_poi.eq.'yes')then
          open(5, file=name_dir//froot(1:kspc-1)//".poi")
            print *,'Writing phase portraits to: '//
     .    name_dir//froot(1:kspc-1)//".poi"
          write(5,*)'# ',(apar(j),': ',pa(j),', ',j=1,4)
            write(5,*)'# ',(apar(j),': ',pa(j),', ',j=5,m)
```

```
          write(5,*)'# kl:',(kl(ii),ii=1,ndel),
     ,         ' tau:',(tau(ii),ii=1,ndel)
          write(5,*)'# t_poi1(i_poi)-t_rel,'//
     *       '(poi1(j,i_poi),j=1,n),t_isi'
           do i_poi=2,n_poi1
            t_isi=t_poi1(i_poi)-t_poi1(i_poi-1)
            write(5,200)t_poi1(i_poi)-t_rel,(poi1(j,i_poi),j=1,n),
     *       t_isi
c          write(5,*)t_isi
           end do
           close(5)
           end if

           if(key_wr_bif.eq.'yes'.and.n_poi1.ge.2)then
          open(5,file=name_dir_BD//froot(1:kspc-1)//".bd")
          if (ipar.le.m+1) then
             do i_poi=2,n_poi1
                t_isi=t_poi1(i_poi)-t_poi1(i_poi-1)
                write(5,200) pa(ipar),(poi1(j,i_poi),j=1,n),
     *                       t_isi
             end do
          else
             do i_poi=2,n_poi1
                t_isi=t_poi1(i_poi)-t_poi1(i_poi-1)
              write(5,200) tau(ipar-m-1),(poi1(j,i_poi),j=1,n),
     *                       t_isi
             end do
           end if
         write(5,*)'      '
           close(5)
           end if
c======== "writing Poincare map"<

c====== "writing phase portraits">
```

```
        if(key_wr_pp.eq.'yes')then
            open(4, file=name_dir//"pp_"//froot(1:kspc-1))
            print *,'Writing phase portraits to: '//
     .     name_dir//froot(1:kspc-1)//".pp"
          write(4,*)'# ',(apar(j),': ',pa(j),', ',j=1,4)
            write(4,*)'# ',(apar(j),': ',pa(j),', ',j=5,m)
          write(4,*)'# kl:',(kl(ii),ii=1,ndel),
     ,         ' tau:',(tau(ii),ii=1,ndel)
          write(4,*)'# t, y(j),j=1,n'
            do i_wr=1,n_wr_pp
             write(4,200)t_ini-t_rel+i_wr*dt,(pp(j,i_wr),j=1,n),
     *      (v(j,i_wr),j=1,n),ylag(i_wr),for(i_wr)
            end do
            close(4)
            end if
c===== "writing phase potraits"<

c========= "calculating mean ISI">
        av_isi=0.
           sqav_isi=0.
        do i_poi=2,n_poi1
          t_isi=t_poi1(i_poi)-t_poi1(i_poi-1)
             av_isi=av_isi+t_isi
             sqav_isi=sqav_isi+t_isi*t_isi
           end do
           av_isi=av_isi/real(n_poi1-1)
           sqav_isi=sqav_isi/real(n_poi1-1)
           var_isi=sqav_isi-av_isi*av_isi
c========= "calculating mean ISI"<

c======== "writing statistical averages">
         open(3,file=name_res,access='append')
         if (ipar.le.m+1) then
           write(3,200) pa(ipar),av_for,sqav_for,var_for,
```

```
     *          av_isi,sqav_isi,var_isi
                print *,pa(ipar),av_for,sqav_for,var_for,
     *          av_isi,sqav_isi,var_isi
           else
             write(3,200) tau(ipar-m-1),av_for,sqav_for,var_for,
     *          av_isi,sqav_isi,var_isi
                print *,tau(ipar-m-1),av_for,sqav_for,var_for,
     *          av_isi,sqav_isi,var_isi
           end if
           close(3)
c======== "writing statistical averages"<
              print *,"   "
         end do

         call system("rm numBD")
200      format(1x,20(g12.5,1x))
         print *,char(7)
         end



c= THESE ARE CIRCUIT EQS with telegraph signal feedback=
c feedback and noise are both applied to a fast x-variable.
         subroutine fu(t,y,f,FB,K,N, XLAG)
         implicit real*8(a-h,o-z)
         common/par/pa(10),tt
         COMMON/NOISE/IX1
         common/prev/u
         dimension y(N),f(N),FB(N),XLAG(10)

              pa_L=pa(1)
              pa_C=pa(2)
              pa_vi=pa(3)
              pa_R=pa(4)
              pa_iref=pa(5)
```

```
      pa_T=pa(6)
      pa_K=pa(7)
      pa_D=pa(8)

      x_il=y(1)
      x_vc=y(2)
      ff=xlag(1)-x_il

c     print *,t,x_il,pa_iref,u

c     f(1)=1./pa_L*(pa_vi-x_vc*(1.-u)+ pa_K*ff)
      f(1)=1./pa_L*(pa_vi-x_vc*(1.-u))
      f(2)=1./pa_C*(-x_vc/pa_R+x_il*(1.-u))
      fb(1)=pa_D

c     print *,'fdbk:',xlag(1),x_il,ff,pa_K*ff
c     pause ' '

    return
    end
c feedback and noise are both applied to a fast x-variable.
c= THESE ARE CIRCUIT EQS with telegraph signal feedback=

c= THESE ARE CUBIC EQUATIONS OF FHN SYSTEM with telegraph signal
feedback=
c feedback and noise are both applied to a fast x-variable.
    subroutine fu_fhn(t,y,f,FB,K,N, XLAG)
    implicit real*8(a-h,o-z)
    common/par/pa(10),tt
    COMMON/NOISE/IX1
    dimension y(N),f(N),FB(N),XLAG(10)

c===== calculating feedback force===>
      ff=xlag(1)-y(1)
```

```
c===== calculating feedback force===<

      f(1)=(y(1)-y(1)*y(1)*y(1)/3.d0-y(2))/pa(1)
     *     + pa(3)*ff
      f(2)=y(1)+pa(2)
      fb(1)=pa(4)

     return
     end
c feedback and noise are both applied to a fast x-variable.
c= THESE ARE CUBIC EQUATIONS OF FHN SYSTEM with telegraph signal
feedback=

     SUBROUTINE FUNS(X,Y,F,K,N,XLAG)
     IMPLICIT REAL*8(A-F,O-Z)
     REAL GASDEV
     common/par/pa(10),tt
     COMMON/NOISE/IX1
     DIMENSION F(N),Y(N),XLAG(10)

     F(1)=gasdev(IX1)

     RETURN
     END




      SUBROUTINE EMMN(NDEL,N,Y,H,H2,T,K,RK,F,Y1,FB,YN,FLAG,
     ,                              NLM,KL,LCUR,XLAG)
*
********** EULER-MARUYAMA METHOD FOR ITO DELAY STOCHASTIC
EQUATION ***
** dX(t)=f(X(t),X(t-tau))dt+g(X(t),X(t-tau))dW(t), t \in [0,T] *****
```

```
********** N - NUMBER OF EQUATIONS **********
********** FU - DETERMINISTIC PART, FUNS - NOISY PART ********
**********          H2=DSQRT(H)        **********
********** NDEL - NUMBER OF DELAYS **************************
********** FLAG -ARRAY OF DELAYED VARIABLE  **********
********** KL - NUMBER OF DELAYED VARIABLE IN THE
INEQUATION *********
********** NLM - NUMBER OF ELEMENTS IN ARRAY FLAG
**********
********** LCUR - CURRENT ELEMENT OF ARRAY FLAG
**********
********** XLAG - CURRENT VALUE X(T-TAU) **********
*


      IMPLICIT double precision (A-H,O-Z)
      PARAMETER (NM=100,NLAG=500000,KLAG=10)
      DIMENSION Y(nm),RK(4,nm),F(nm),Y1(nm),FB(Nm),YN(Nm),KL(KLAG),
     ,          FLAG(KLAG,NLAG),NLM(KLAG),LCUR(KLAG),XLAG(KLAG)
c     COMMON/NOISE/DD
      COMMON/NOISE/IX1
      common/pars/pi2,pi,ro_0,ro_0_k_B_T,
     *           ak_B_T,e_h,G11,G12
      CALL FU(T,Y,F,FB,K,N,XLAG)
      CALL FUNS(T,Y,YN,K,N,XLAG)
      DO 1 I=1,N
        RK(1,I)=H*F(I)+YN(I)*FB(I)*H2
    1   Y1(I)=Y(I)+RK(1,I)/2

      DO J=1,NDEL
        FLAG(J,LCUR(J))=Y(KL(J))
        LCUR(J)=LCUR(J)+1
        IF(LCUR(J).GT.NLM(J)) LCUR(J)=1
        XLAG(J)=FLAG(J,LCUR(J))
```

```
 END DO

 CALL FU(T+H/2,Y1,F,FB,K,N,XLAG)
 DO 2 I=1,N
   RK(2,I)=H*F(I)+YN(I)*FB(I)*H2
2   Y1(I)=Y(I)+RK(2,I)/2
 CALL FU(T+H/2,Y1,F,FB,K,N,XLAG)
 DO 3 I=1,N
   RK(3,I)=H*F(I)+YN(I)*FB(I)*H2
3  Y1(I)=Y(I)+RK(3,I)

 DO J=1,NDEL
   FLAG(J,LCUR(J))=Y(KL(J))
   LCUR(J)=LCUR(J)+1
   IF(LCUR(J).GT.NLM(J)) LCUR(J)=1
   XLAG(J)=FLAG(J,LCUR(J))
 END DO

 CALL FU(T+H,Y1,F,FB,K,N,XLAG)
 DO 4 I=1,N
   RK(4,I)=H*F(I)+YN(I)*FB(I)*H2
4  Y(I)=Y(I)+(RK(1,I)+2*(RK(2,I)+RK(3,I))+RK(4,I))/6
 RETURN
 END



 SUBROUTINE INILAG(ndel,tau,h,flag,NLM,LCUR,XLAG)
  IMPLICIT REAL*8(A-h,O-Z)
  PARAMETER (NM=100, NLAG=500000,KLAG=10)
  DIMENSION FLAG(KLAG,NLAG),tau(KLAG),NLM(KLAG),LCUR(KLAG),
,          XLAG(KLAG)
  do ii=1,ndel
    NLM(ii)=tau(ii)*2/h
```

```
********* inital conditions for each delayed variable**************
        DO I=1,NLM(ii)
          flag(ii,I)=0.
        end do
*********************************************************************
        LCUR(ii)=1
        XLAG(ii)=FLAG(ii,1)
      end do
      return
      end
     FUNCTION gasdev(idum)
     INTEGER idum
     REAL gasdev
CU    USES ran1
     INTEGER iset
     REAL fac,gset,rsq,v1,v2,ran3
     SAVE iset,gset
     DATA iset/0/
     if (iset.eq.0) then
1      v1=2.*ran3(idum)-1.
       v2=2.*ran3(idum)-1.
       rsq=v1**2+v2**2
       if(rsq.ge.1..or.rsq.eq.0.)goto 1
       fac=sqrt(-2.*log(rsq)/rsq)
       gset=v1*fac
       gasdev=v2*fac
       iset=1
     else
       gasdev=gset
       iset=0
     endif
     return
     END
```

```
      FUNCTION ran3(idum)
      INTEGER idum
      INTEGER MBIG,MSEED,MZ
C     REAL MBIG,MSEED,MZ
      REAL ran3,FAC
      PARAMETER (MBIG=1000000000,MSEED=161803398,MZ=0,FAC=1./MBIG)
C     PARAMETER (MBIG=4000000.,MSEED=1618033.,MZ=0.,FAC=1./MBIG)
      INTEGER i,iff,ii,inext,inextp,k
      INTEGER mj,mk,ma(55)
C     REAL mj,mk,ma(55)
      SAVE iff,inext,inextp,ma
      DATA iff /0/
      if(idum.lt.0.or.iff.eq.0)then
        iff=1
        mj=MSEED-iabs(idum)
        mj=mod(mj,MBIG)
        ma(55)=mj
        mk=1
        do 11 i=1,54
          ii=mod(21*i,55)
          ma(ii)=mk
          mk=mj-mk
          if(mk.lt.MZ)mk=mk+MBIG
          mj=ma(ii)
11      continue
        do 13 k=1,4
          do 12 i=1,55
            ma(i)=ma(i)-ma(1+mod(i+30,55))
            if(ma(i).lt.MZ)ma(i)=ma(i)+MBIG
12        continue
13      continue
        inext=0
        inextp=31
        idum=1
```

```
      endif
      inext=inext+1
      if(inext.eq.56)inext=1
      inextp=inextp+1
      if(inextp.eq.56)inextp=1
      mj=ma(inext)-ma(inextp)
      if(mj.lt.MZ)mj=mj+MBIG
      ma(inext)=mj
      ran3=mj*FAC
      return
      END



c=== "finding a precise moment of crossing by linear interpolation">>>
       subroutine lin_int(t,h,x_prev,x,tp)
       implicit real*8(a-h,o-z)
       a=(x-x_prev)/h
       b=x-a*t
       tp=-b/a

       return
       end
c=== "finding a precise moment of crossing by linear interpolation"<<<

c===== "finding more precise Poincare section for other variables">>>
      subroutine poi_int(t,h,tp,x_prev,x,xp)
      implicit real*8(a-h,o-z)
      a=(x-x_prev)/h
      b=x-a*t
      xp=a*tp+b
      return
      end
c===== "finding more precise Poincare section for other variables"<<<
```

B.2 Delayed Feedback FORTRAN Software Parameters

"sp0.0dat" !output file

"RES/cir.tmp" name_res

"==========" 20th pos

"CIR_INV/BD/////////////" name_dir_BD

"CIR_INV/BD/////////////////////////////////" name_dir

'yes' 'no' 'no' 5.e-2 6.e-2 ! key_wr_poi, key_wr_bif, key_wr_pp, t_ini,t_end

2 7 !dimension of system, number of parameters

" 1-L 2-C 3-vi 4-R 5-iref 6-T 7-K 8-D "

1.e-3, 1.e-5, 10.0, 20., 3., 1.e-4, 0.0, 0. ! L, C, vi, R, iref, T, K, D

0.1 0.1 !initial conditions

5.e-2 1.e-2 2.e-8 50 100000 !t_rel,t_int,h,kti, n_poi

7 !number of parameter to vary

0., 1. ,0.001 !starting value, final value, step of parameter

1 ! numbers of delays

1 ! numbers of delayed variables

1.1e-4 !delays

'no' , -201 !random seed for GASDEV?, nIX1 for manual manipulation

========= For FHN_cubic in excitable regime: ======

"sp0.0dat" !output file

"RES/fhn_tel.tmp" name_res

"==========" 20th pos

"FHN_TEL/////////////////" name_dir

'no', 'yes', 100. 200. ! key_wr_poi, key_wr_pp, t_ini,t_end

2 3 !dimension of system, number of parameters

" 1 2 3 4 "

.001, 1.05, 5.0, 0.5 !parameters (eps,a,K), D

0. 0. !initial conditions

100. 100. 0.0005 200 10000 !t_rel,t_int,h,kti, n_poi

5 !number of parameter to vary

0., 10. , 1. !starting value, final value, step of parameter

1 ! numbers of delays

```
1                ! numbers of delayed variables
2.9              !delays
'no' , -201      !random seed for GASDEV?, nIX1 for manual manipulation
```

APPENDIX C

THE SOFTWARE PROGRAMMED INTO THE ATMEL AT89C51

C.1 C Programming Code

```
#include "at89c51xd2.h"

#define DELAYLENGTH 7   //for a different delay time
                        //1=30us.....2=40us.....3=60us......4=70us.....5=80us….6=90us.....
                        //7=100us....8=120us.....9=130us....10=140us.....11=150us

#define MAXDELAY 10

void main()
{
        int delay[MAXDELAY+1] = {0};     //array of 11 integers initialized to 0

        int * first = &delay[0];
        int * last = &delay[DELAYLENGTH];
        int * pDelay = first;

        int I1 = 0;
        int I2 = 0;
        int i=0;
        int j = 0;
        int k = 1;

   CKCON0 |= 0x01;      //enable X2 mode
        P0 = 0xFF;      //port 0 as input
        I1 = P0;        //reading first value

        while(1)
        {
        P3_6 = 1;
```

```
        P3_7 = 1;

        P3_6 = 0;
        P3_7 = 0;
                i++;        //delay until ready to sample

        I2 = P0;            // sampling the value

        delay[j] = I2;      // saving in the array
                j++;        // finding the delayed value we want from the array
                if (j > DELAYLENGTH)
                {
                        j = 0;
                }

                P1 = delay[j];    // calculating the output answer
        }
}
```

C.2 AT89C51XD2 Header

```
/*H*********************************************************************
*********
* NAME: AT89C51XD2.h
*-------------------------------------------------------------------------
* PURPOSE: SFR Description file for AT89C51xD2 products
*                                   ON KEIL compiler
**********************************************************************
********/

#define Sfr(x, y)                   sfr x = y
#define Sbit(x, y, z)   sbit x = y^z
#define Sfr16(x,y)          sfr16 x = y

/*--------------------------------------*/
/* Include file for 8051 SFR Definitions  */
/*--------------------------------------*/

/*  BYTE Register  */
Sfr (P0 , 0x80);

Sbit (P0_7 , 0x80, 7);
Sbit (P0_6 , 0x80, 6);
Sbit (P0_5 , 0x80, 5);
Sbit (P0_4 , 0x80, 4);
Sbit (P0_3 , 0x80, 3);
Sbit (P0_2 , 0x80, 2);
Sbit (P0_1 , 0x80, 1);
Sbit (P0_0 , 0x80, 0);

Sfr (P1 , 0x90);

Sbit (P1_7 , 0x90, 7);
```

```
Sbit (P1_6 , 0x90, 6);
Sbit (P1_5 , 0x90, 5);
Sbit (P1_4 , 0x90, 4);
Sbit (P1_3 , 0x90, 3);
Sbit (P1_2 , 0x90, 2);
Sbit (P1_1 , 0x90, 1);
Sbit (P1_0 , 0x90, 0);
Sfr (P2 , 0xA0);
Sbit (P2_7 , 0xA0, 7);
Sbit (P2_6 , 0xA0, 6);
Sbit (P2_5 , 0xA0, 5);
Sbit (P2_4 , 0xA0, 4);
Sbit (P2_3 , 0xA0, 3);
Sbit (P2_2 , 0xA0, 2);
Sbit (P2_1 , 0xA0, 1);
Sbit (P2_0 , 0xA0, 0);


Sfr (P3 , 0xB0);

Sbit (P3_7 , 0xB0, 7);
Sbit (P3_6 , 0xB0, 6);
Sbit (P3_5 , 0xB0, 5);
Sbit (P3_4 , 0xB0, 4);
Sbit (P3_3 , 0xB0, 3);
Sbit (P3_2 , 0xB0, 2);
Sbit (P3_1 , 0xB0, 1);
Sbit (P3_0 , 0xB0, 0);

Sbit (RD , 0xB0, 7);
Sbit (WR , 0xB0, 6);
Sbit (T1 , 0xB0, 5);
Sbit (T0 , 0xB0, 4);
Sbit (INT1 , 0xB0, 3);
```

```
Sbit (INT0 , 0xB0, 2);
Sbit (TXD , 0xB0, 1);
Sbit (RXD , 0xB0, 0);

Sfr (P4 , 0xC0);
Sbit (P4_7 , 0xC0, 7);
Sbit (P4_6 , 0xC0, 6);
Sbit (P4_5 , 0xC0, 5);
Sbit (P4_4 , 0xC0, 4);
Sbit (P4_3 , 0xC0, 3);
Sbit (P4_2 , 0xC0, 2);
Sbit (P4_1 , 0xC0, 1);
Sbit (P4_0 , 0xC0, 0);

Sfr (P5 , 0xE8);
Sbit (P5_7 , 0xE8, 7);
Sbit (P5_6 , 0xE8, 6);
Sbit (P5_5 , 0xE8, 5);
Sbit (P5_4 , 0xE8, 4);
Sbit (P5_3 , 0xE8, 3);
Sbit (P5_2 , 0xE8, 2);
Sbit (P5_1 , 0xE8, 1);
Sbit (P5_0 , 0xE8, 0);
Sfr (PSW , 0xD0);

Sbit (CY  , 0xD0  , 7);
Sbit (AC  , 0xD0  , 6);
Sbit (F0  , 0xD0  , 5);
Sbit (RS1 , 0xD0  , 4);
Sbit (RS0 , 0xD0  , 3);
Sbit (OV  , 0xD0  , 2);
Sbit (UD  , 0xD0  , 1);
Sbit (P   , 0xD0  , 0);
```

```
Sfr (ACC , 0xE0);
Sfr (B , 0xF0);
Sfr (SP , 0x81);
Sfr (DPL , 0x82);
Sfr (DPH , 0x83);

Sfr (PCON , 0x87);
Sfr (CKCON0 , 0x8F);
Sfr (CKCON1 , 0xAF);

/*------------------ TIMERS registers ----------------------*/
Sfr (TCON , 0x88);
Sbit (TF1 , 0x88, 7);
Sbit (TR1 , 0x88, 6);
Sbit (TF0 , 0x88, 5);
Sbit (TR0 , 0x88, 4);
Sbit (IE1 , 0x88, 3);
Sbit (IT1 , 0x88, 2);
Sbit (IE0 , 0x88, 1);
Sbit (IT0 , 0x88, 0);

Sfr (TMOD , 0x89);

Sfr  (T2CON , 0xC8);
Sbit (TF2   , 0xC8, 7);
Sbit (EXF2  , 0xC8, 6);
Sbit (RCLK  , 0xC8, 5);
Sbit (TCLK  , 0xC8, 4);
Sbit (EXEN2 , 0xC8, 3);
Sbit (TR2   , 0xC8, 2);
Sbit (C_T2  , 0xC8, 1);
Sbit (CP_RL2, 0xC8, 0);

Sfr (T2MOD , 0xC9);
```

```
Sfr (TL0 , 0x8A);
Sfr (TL1 , 0x8B);
Sfr (TL2 , 0xCC);
Sfr (TH0 , 0x8C);
Sfr (TH1 , 0x8D);
Sfr (TH2 , 0xCD);
Sfr (RCAP2L , 0xCA);
Sfr (RCAP2H , 0xCB);
Sfr (WDTRST , 0xA6);
Sfr (WDTPRG , 0xA7);


/*------------------- UART registers ----------------------*/
Sfr (SCON , 0x98);
Sbit (SM0  , 0x98, 7);
Sbit (FE   , 0x98, 7);
Sbit (SM1  , 0x98, 6);
Sbit (SM2  , 0x98, 5);
Sbit (REN  , 0x98, 4);
Sbit (TB8  , 0x98, 3);
Sbit (RB8  , 0x98, 2);
Sbit (TI   , 0x98, 1);
Sbit (RI   , 0x98, 0);

Sfr (SBUF , 0x99);
Sfr (SADEN , 0xB9);
Sfr (SADDR , 0xA9);

/*-------------------- Internal Baud Rate Generator --------*/
Sfr (BRL         , 0x9A);
Sfr (BDRCON , 0x9B);
/*-------------------- IT registers ----------------------*/
Sfr (IEN0  , 0xA8);
Sfr (IEN1  , 0xB1);
```

```
Sfr (IPH0 , 0xB7);
Sfr (IPH1 , 0xB3);
Sfr (IPL0 , 0xB8);
Sfr (IPL1 , 0xB2);



/*  IEN0  */
Sbit (EA   , 0xA8, 7);
Sbit (EC   , 0xA8, 6);
Sbit (ET2  , 0xA8, 5);
Sbit (ES   , 0xA8, 4);
Sbit (ET1  , 0xA8, 3);
Sbit (EX1  , 0xA8, 2);
Sbit (ET0  , 0xA8, 1);
Sbit (EX0  , 0xA8, 0);


/*---------------------- PCA registers -----------------------------*/
Sfr (CCON , 0xD8);
Sfr (CMOD , 0xD9);
Sfr (CH , 0xF9);
Sfr (CL , 0xE9);
Sfr (CCAP0H  , 0xFA);
Sfr (CCAP0L  , 0xEA);
Sfr (CCAPM0  , 0xDA);
Sfr (CCAP1H  , 0xFB);
Sfr (CCAP1L  , 0xEB);
Sfr (CCAPM1  , 0xDB);
Sfr (CCAP2H  , 0xFC);
Sfr (CCAP2L  , 0xEC);
Sfr (CCAPM2  , 0xDC);
Sfr (CCAP3H  , 0xFD);
Sfr (CCAP3L  , 0xED);
```

```
Sfr (CCAPM3  , 0xDD);
Sfr (CCAP4H  , 0xFE);
Sfr (CCAP4L  , 0xEE);
Sfr (CCAPM4  , 0xDE);
/* CCON */
Sbit (CF   , 0xD8, 7);
Sbit (CR   , 0xD8, 6);

Sbit (CCF4   , 0xD8, 4);
Sbit (CCF3  , 0xD8, 3);
Sbit (CCF2  , 0xD8, 2);
Sbit (CCF1  , 0xD8, 1);
Sbit (CCF0  , 0xD8, 0);


/*------------------ T W I registers ------------------------------*/
Sfr ( SSCON , 0x93);
Sfr ( SSCS , 0x94);
Sfr ( SSDAT , 0x95);
Sfr ( SSADR , 0x96);
Sfr ( PI2          , 0xF8);
Sbit (PI2_1  , 0xF8, 1);
Sbit (PI2_0  , 0xF8, 0);

/*-------------------- OSC control registers ----------------------*/
Sfr ( CKSEL , 0x85 );
Sfr ( OSCCON , 0x86 );
Sfr ( CKRL , 0x97 );

/*-------------------- Keyboard control registers -----------------*/
Sfr ( KBLS , 0x9C );
Sfr ( KBE , 0x9D );
Sfr ( KBF , 0x9E );
/*-------------------- SPI ---------------------- -----------------*/
```

```
Sfr ( SPCON, 0xC3 );
Sfr ( SPSTA, 0xC4 );
Sfr ( SPDAT, 0xC5 );
/*------ Misc ----------------------------------------------------*/
Sfr       ( AUXR , 0x8E);
Sfr ( AUXR1, 0xA2);
Sfr ( FCON, 0xD1);


/*------ E data ----------------------------------------------------*/

Sfr ( EECON,  0xD2 );
```

APPENDIX D

A LISTING OF THE HARDWARE PHOTOGRAPHS

D.1 Single Boost Converter Circuit.

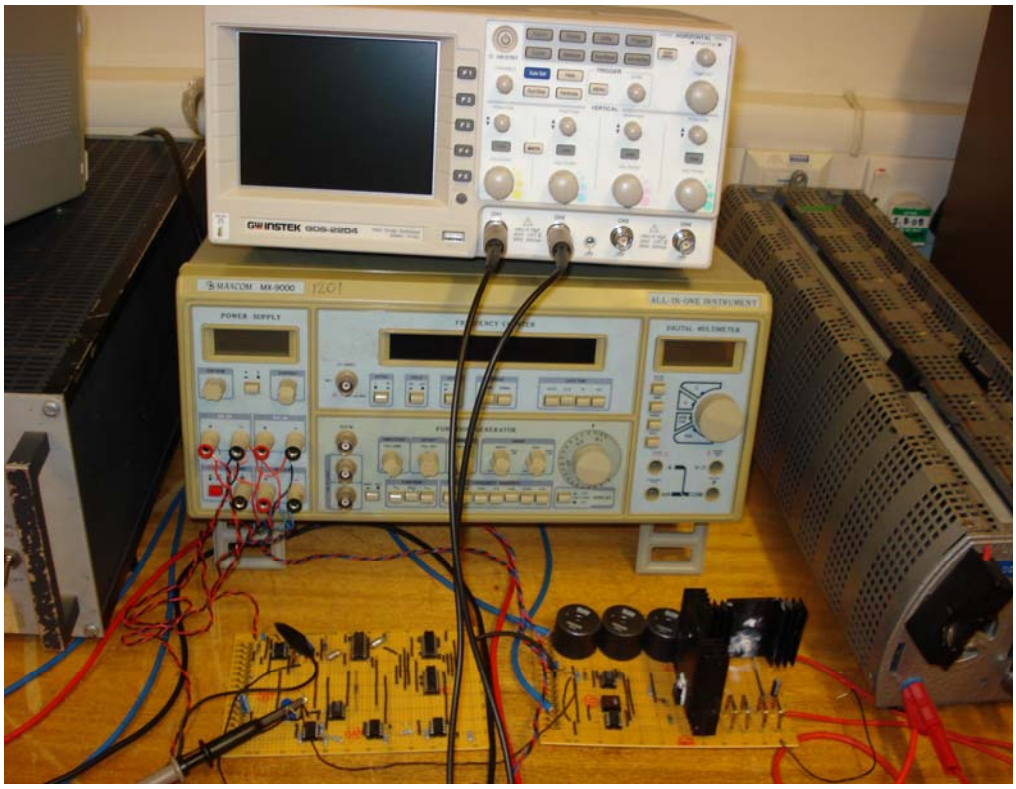

D.2 Two-Module Boost Converter Circuit.

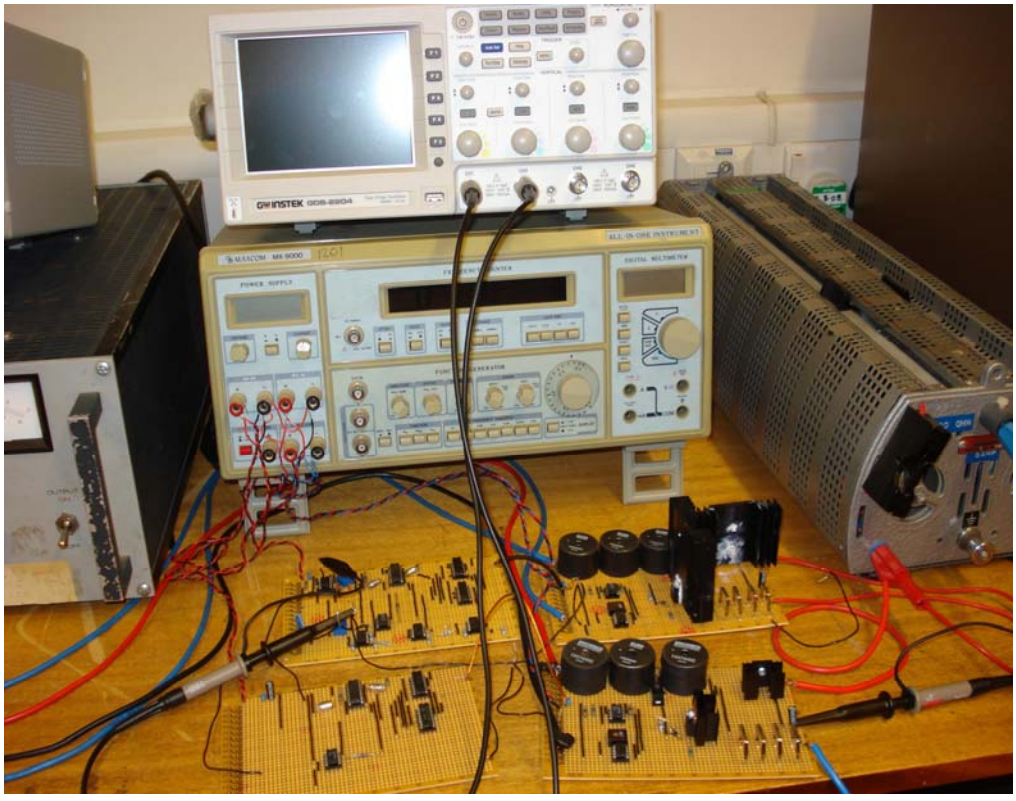

D.3 Delayed Current Feedback Discrete Control Scheme Circuit.

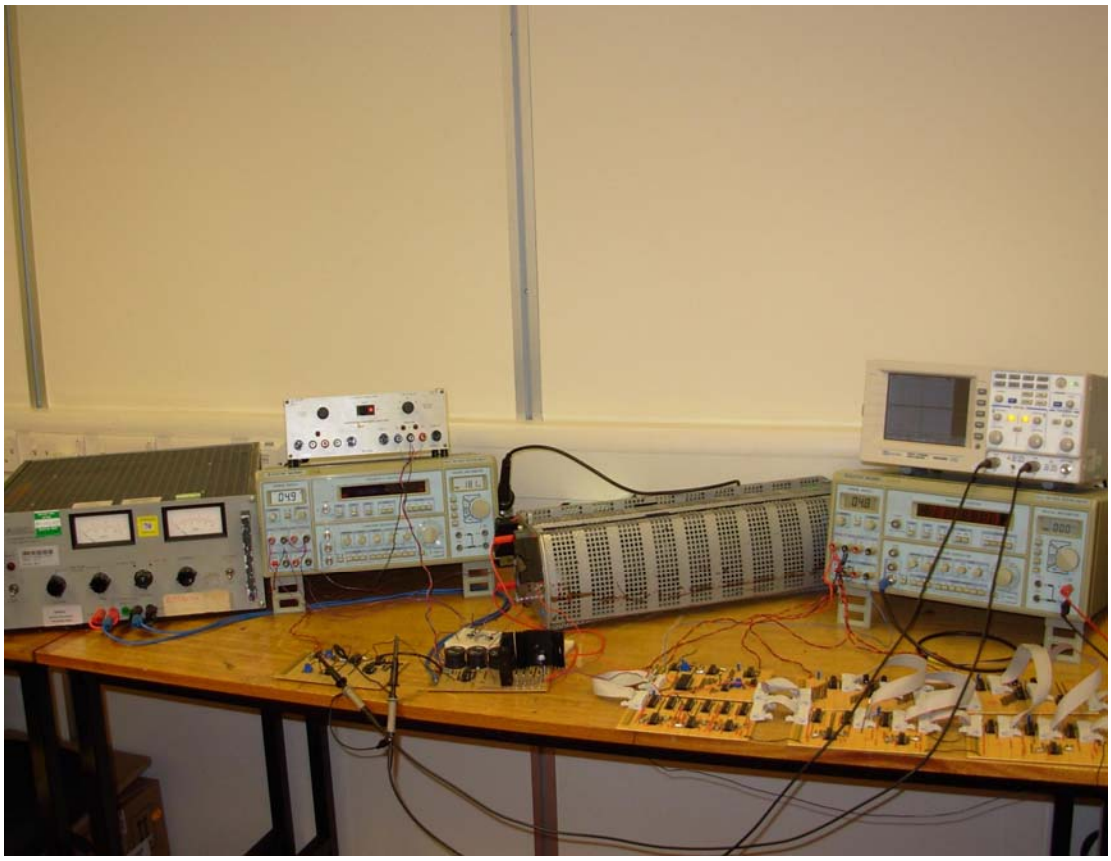

D.4 Delayed Current Feedback Microcontroller Control Scheme Circuit.

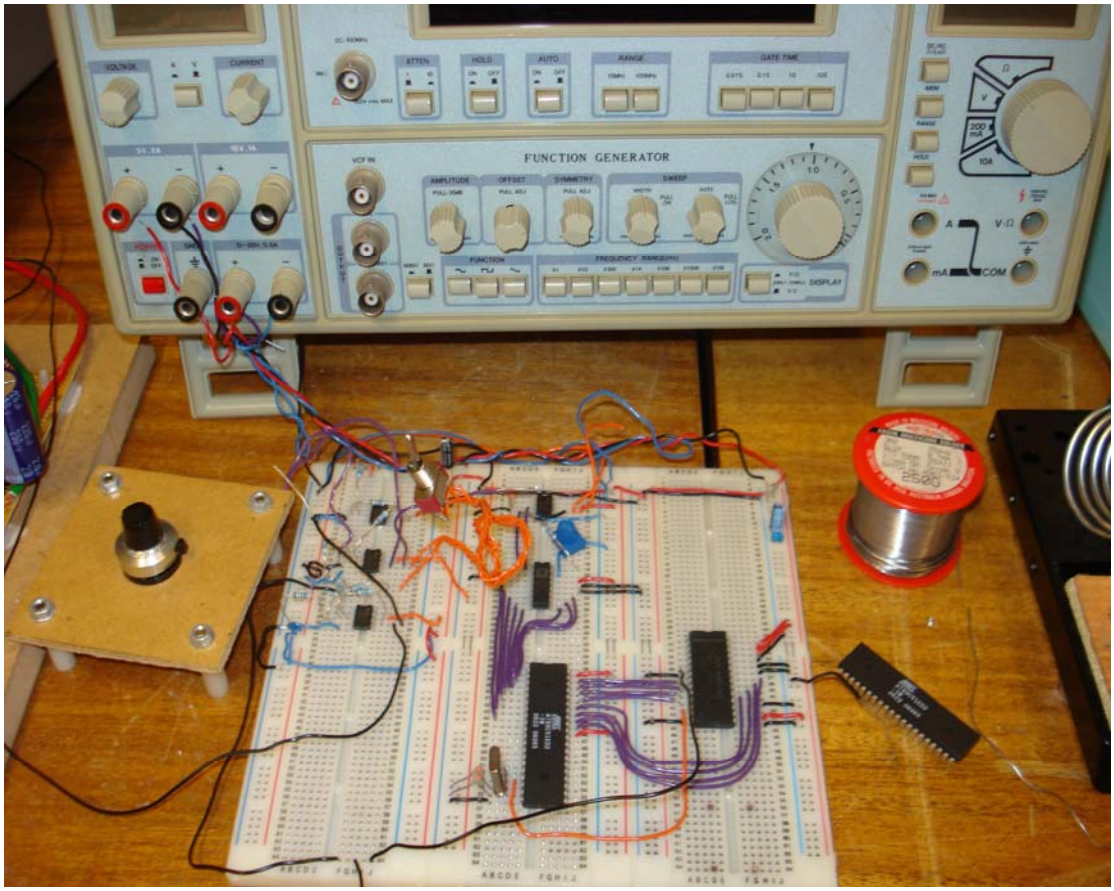

D.5 Power Factor Correction (PFC) Boost Converter Circuit.

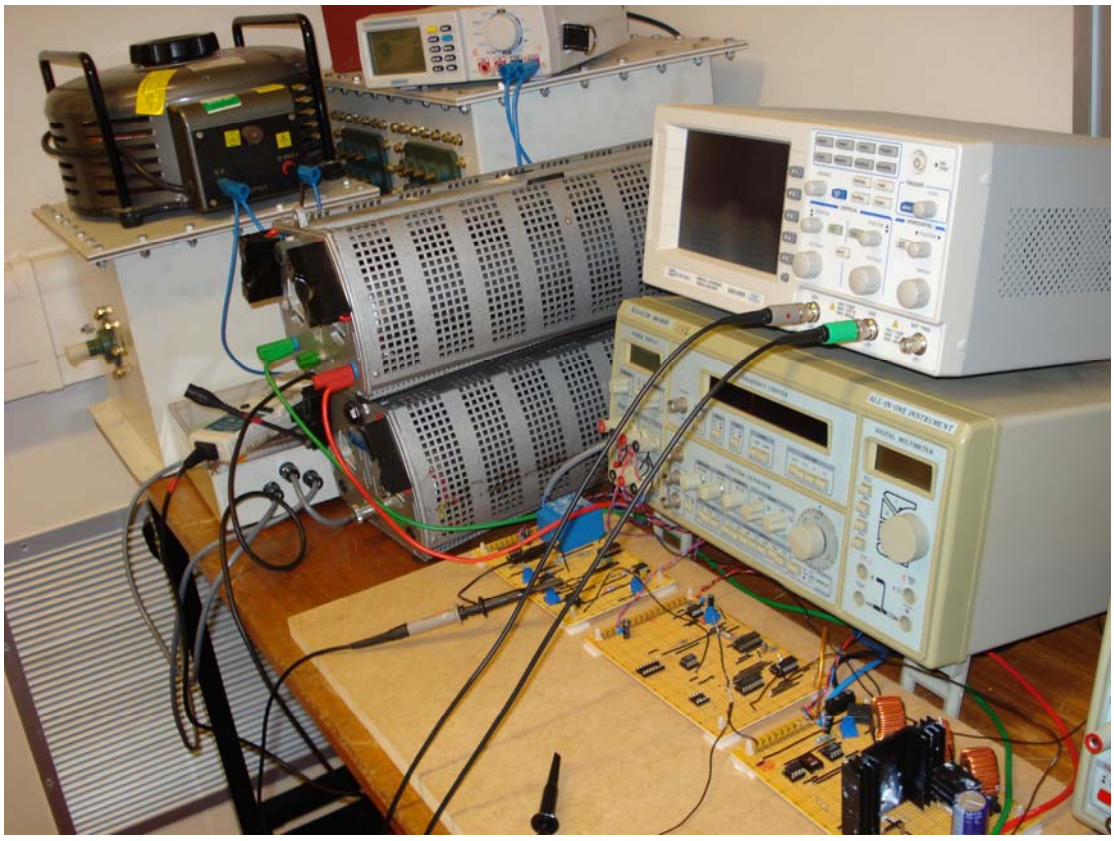

D.6 PFC Boost Converter Circuit with Delayed Current Feedback Control.

APPENDIX E

PUBLISHED WORK

E.1 ***Elsevier Journal Paper, Chaos, Solitons & Fractals***

‘‘Analysis, simulation and experimental study of chaotic behaviour in parallel-connected DC–DC boost converters’’

Available online at www.sciencedirect.com
ScienceDirect
Chaos, Solitons and Fractals xxx (2007) xxx–xxx
CHAOS SOLITONS & FRACTALS
www.elsevier.com/locate/chaos

Analysis, simulation and experimental study of chaotic behaviour in parallel-connected DC–DC boost converters

Ammar N. Natsheh [a], J. Gordon Kettleborough [a], Jamal M. Nazzal [b,*]

[a] *Department of Electronic and Electrical Engineering, Loughborough University, Loughborough, Leicestershire LE11 3TU, UK*
[b] *Faculty of Engineering, Al-Ahliyya Amman University, Post Code 19328 Amman, Jordan*

Accepted 5 July 2007

Communicated by Professor G. Iovane

Abstract

The paper describes an experimental study of the bifurcation behaviour of a modular peak current-mode controlled DC–DC boost converter. The parallel-input/parallel-output converter comprises two identical boost circuits and operates in the continuous-current conduction mode. A comparison is made between the results obtained from an experimental converter with those obtained from bifurcation diagrams generated from previous work and waveforms from a new MATLAB/SIMULINK simulation presented in this paper. Another comparison is made between the modular converter diagrams with those of the single boost converter.

1. Introduction

DC–DC switch-mode converters are non-linear devices and recently it has been observed that they may behave in a chaotic manner. This has generated much interest, particularly in single-stage topologies such as the buck, boost, and buck-boost converters [1–7].

The connection of several DC–DC converters in parallel, with the load shared between modules, reduces current stress on the switching devices and increases system reliability. However, despite the growing popularity of these modular converters, their bifurcation phenomena have rarely been studied. The work presented in [8] describes the bifurcation phenomena in a parallel system of two boost converters under a master-slave current-sharing control scheme. One converter has voltage feedback control, while the other has an additional inner current loop which adjusts the voltage feedback loop, to ensure equal sharing of the load current.

This paper investigates chaotic behaviour in a two-module parallel input/parallel-output boost converter operating under a peak current-mode control scheme, where each module has its own current feedback loop. The converter consists of two identical boost circuits and operates in the continuous-current conduction mode. A comparison is made between waveforms obtained from an experimental converter and both a MATLAB/SIMULINK model

* Corresponding author. Tel.: +962 79 5261 490; fax: +962 65 3351 69.
E-mail address: jnazzal@ammanu.edu.jo (J.M. Nazzal).

0960-0779/$ - see front matter © 2007 Elsevier Ltd. All rights reserved.
doi:10.1016/j.chaos.2007.07.020

and results obtained from bifurcation diagrams generated from a nonlinear mapping in closed form using MATLAB [9].

2. Bifurcation and chaos theory

Bifurcation theory, originally developed by Poincare, is used to indicate the qualitative change in behavior of a system in terms of the number and the type of solutions, under the variation of one or more parameters on which the system depends [10].

In bifurcation problems, in addition to state variables, there are control parameters. The relationship between any of these controls parameters and any state variable is called the state-control space. In this space, locations at which bifurcations occur are called bifurcation points. Bifurcations of an equilibrium or fixed-point solution are classified as either

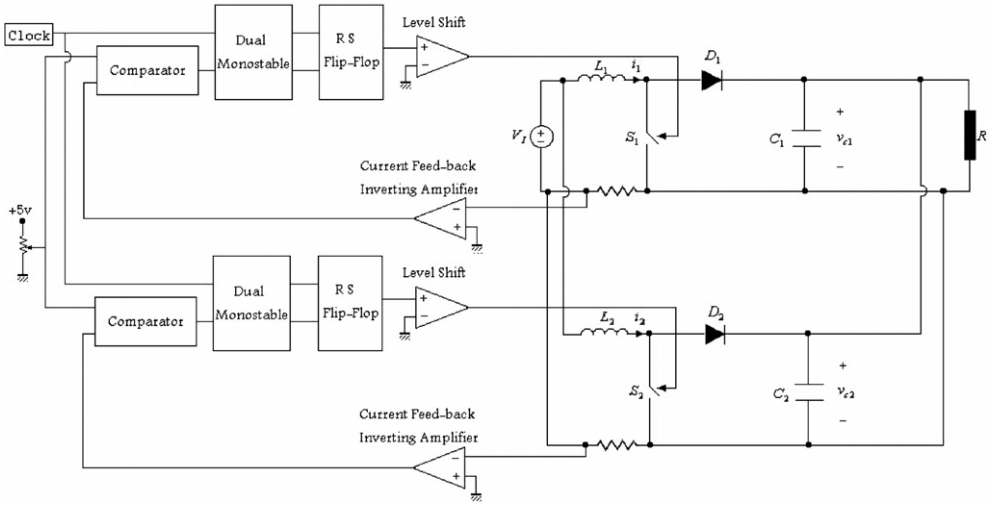

Fig. 1. Simplified circuit diagram for the two-module converter.

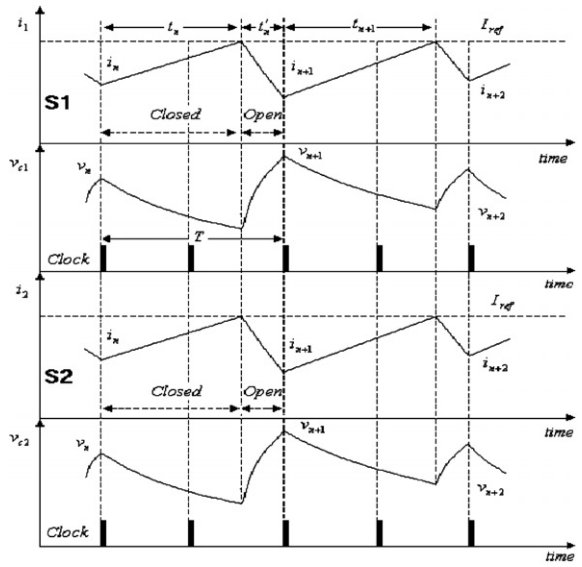

Fig. 2. Module current voltage waveforms for the circuit of Fig. 1.

Please cite this article in press as: Natsheh AN et al., Analysis, simulation and experimental study of chaotic ..., Chaos, Solitons & Fractals (2007), doi:10.1016/j.chaos.2007.07.020

static bifurcations, such as saddle-node, pitch fork, or transcritical bifurcations; or as *dynamic bifurcations* which are also known as the Hopf bifurcation that exhibits periodic solutions. For the fixed-point solutions, the local stability of the system is determined from the eigenvalues of the Jacobian matrix of the linearized system. On the other hand, with periodic-solutions, the system stability depends on what is known as the Floquet theory and the eigenvalues of the Monodromy matrix that are known in the literature as Floquet or characteristic multipliers. The types of bifurcation are determined from the manner in which the Floquet multipliers leave the unit circle. There are three possible ways for this to happen [10]:

(i) If the Floquet multiplier leaves the unit circle through +1, then three possible bifurcations may occur: transcritical, symmetry-breaking, or cyclic-fold bifurcation.
(ii) If the Floquet multiplier leaves through −1, the period-doubling (Flip bifurcation) occurs.
(iii) If the Floquet multipliers are complex conjugate and leave the unit circle from the real axis, the system exhibits secondary Hopf bifurcation.

To observe the system dynamics under all the above possible bifurcations, a complete diagram known as a *bifurcation diagram* is constructed. A bifurcation diagram shows the variation of one of the state variables with one of the system parameters, otherwise known as a control parameter.

3. Mathematical modelling and numerical analysis

A simplified diagram for the proposed converter is shown in Fig. 1. It consists of two peak current-mode controlled DC–DC boost converters whose outputs are connected in parallel to feed a common resistive load. Each converter has its own current feedback loop comprising a comparator and a flip-flop. Each comparator compares its respective peak inductor current with a reference value, to determine the on-time of the switch.

The current and voltage waveforms for the circuit of Fig. 1 are shown in Fig. 2. Switches S_1 and S_2 are controlled such that they close at the same time. When they are closed, diodes D_1 and D_2 are non-conducting, and inductor

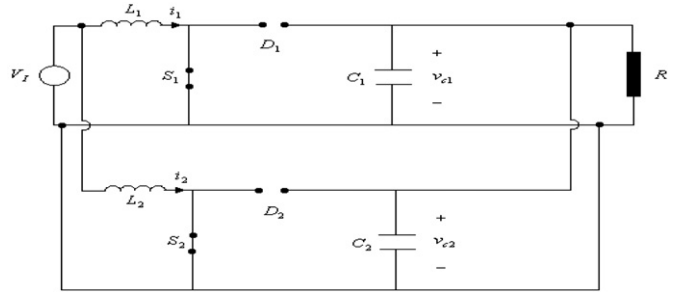

Fig. 3. Circuit diagram for the two-module converter with S_1, S_2 closed and D_1, D_2 open.

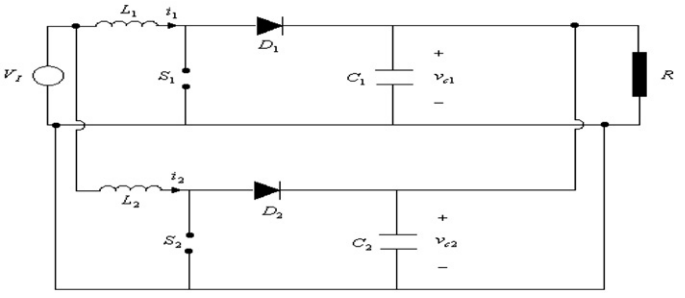

Fig. 4. Circuit diagram of the two-module converter with S_1, S_2 open and D_1, D_2 conducting.

Please cite this article in press as: Natsheh AN et al., Analysis, simulation and experimental study of chaotic ..., Chaos, Solitons & Fractals (2007), doi:10.1016/j.chaos.2007.07.020

currents i_1 and i_2 increase linearly. S_1 and S_2 open respectively when $i_1 = I_{ref}$ and $i_2 = I_{ref}$, whereupon D_1 and D_2 conduct and the inductor currents decay linearly. S_1 and S_2 close again when the next clock pulse arrives.

The iterative map describing the system takes the form:

$$x_{n+1} = f(x_n, I_{ref}) \tag{1}$$

where subscript n denotes the value at the beginning of the nth cycle and x is the state vector

Table 1
The set of circuit parameter

Circuit components	Values
Switching period T	100 μs
Input voltage V_I	10 V
Inductance L_1	1 mH
Inductance L_2	1 mH
Capacitance C_1	10 μF
Capacitance C_2	10 μF
Load resistance R	20 Ω

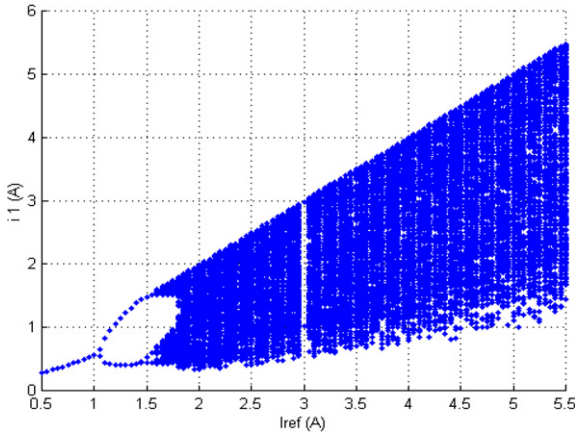

Fig. 5. Bifurcation diagram of i_1 for the two-module converter.

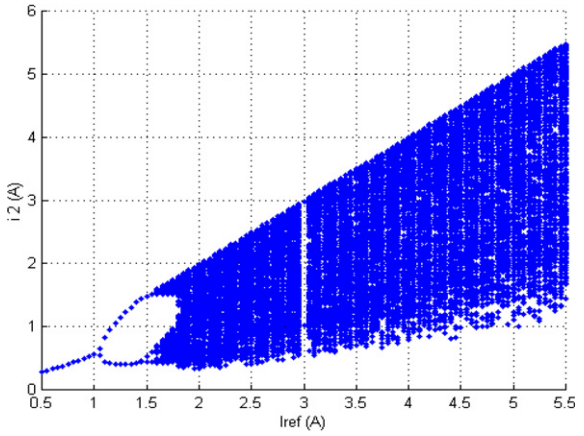

Fig. 6. Bifurcation diagram of i_2 for the two-module converter.

Please cite this article in press as: Natsheh AN et al., Analysis, simulation and experimental study of chaotic ..., Chaos, Solitons & Fractals (2007), doi:10.1016/j.chaos.2007.07.020

$$x = \begin{bmatrix} i_1 \\ v_{c1} \\ i_2 \\ v_{c2} \end{bmatrix} \tag{2}$$

with i_1, i_2, the currents through inductors L_1 and L_2, respectively, v_{c1}, v_{c2}, the voltages across capacitors C_1 and C_2, respectively, and v_{c1}, v_{c2}, considered as separate states for clarity.

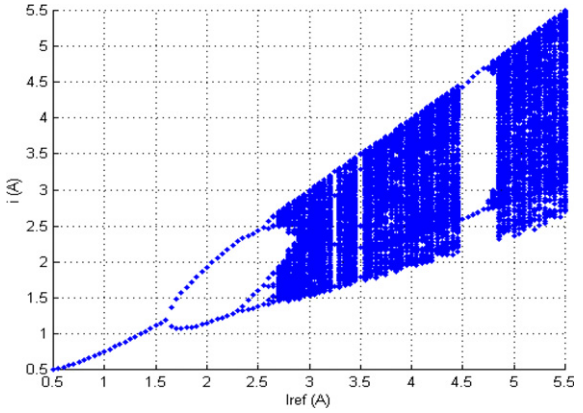

Fig. 7. Bifurcation diagram for a single boost converter with I_{ref} as the bifurcation parameter.

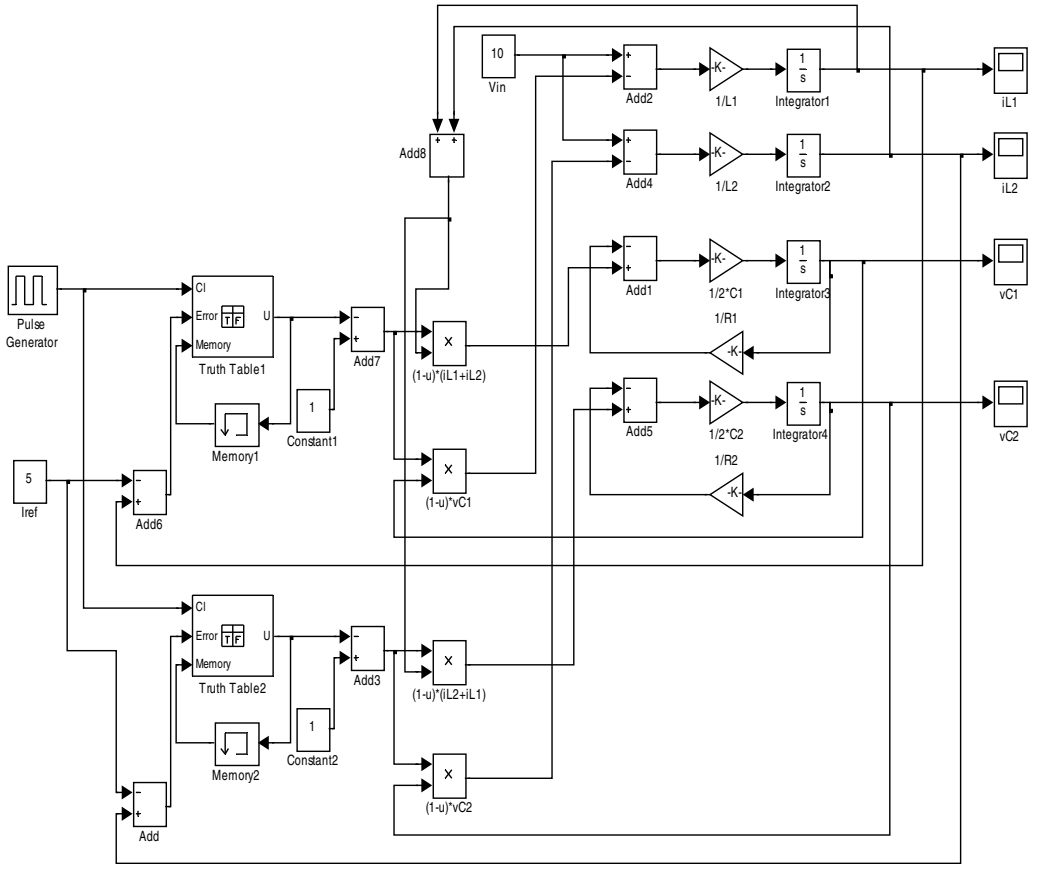

Fig. 8. MATLAB/SIMULINK module for the two-module converter.

Please cite this article in press as: Natsheh AN et al., Analysis, simulation and experimental study of chaotic ..., Chaos, Solitons & Fractals (2007), doi:10.1016/j.chaos.2007.07.020

3.1. S_1 and S_2 closed

Diodes D_1 and D_2 block at $t = 0$ and the circuit is as shown in Fig. 3. Assuming that $L_1 = L_2 = L$ and $C_1 = C_2 = C$, the circuit can be described by the following set of first-order differential equations:

$$\frac{di_1}{dt} = \frac{di_2}{dt} = \frac{V_I}{L} \tag{3}$$

$$\frac{dv_{c1}}{dt} = -\frac{1}{2RC} v_{c1} \tag{4}$$

$$\frac{dv_{c2}}{dt} = -\frac{1}{2RC} v_{c2} \tag{5}$$

Assuming that initially the module inductor current is i_n and the capacitor voltage is v_n, and that the inductor current is I_{ref} at time t_n, the solution of these equations gives

$$t_n = \frac{L(I_{\text{ref}} - i_n)}{V_I} \tag{6}$$

$$v_{c1}(t) = v_{c2}(t) = v_n e^{-2kt} \tag{7}$$

where

$$k = \frac{1}{4RC} \tag{8}$$

and t_n is the time at which switches S_1 and S_2 open.

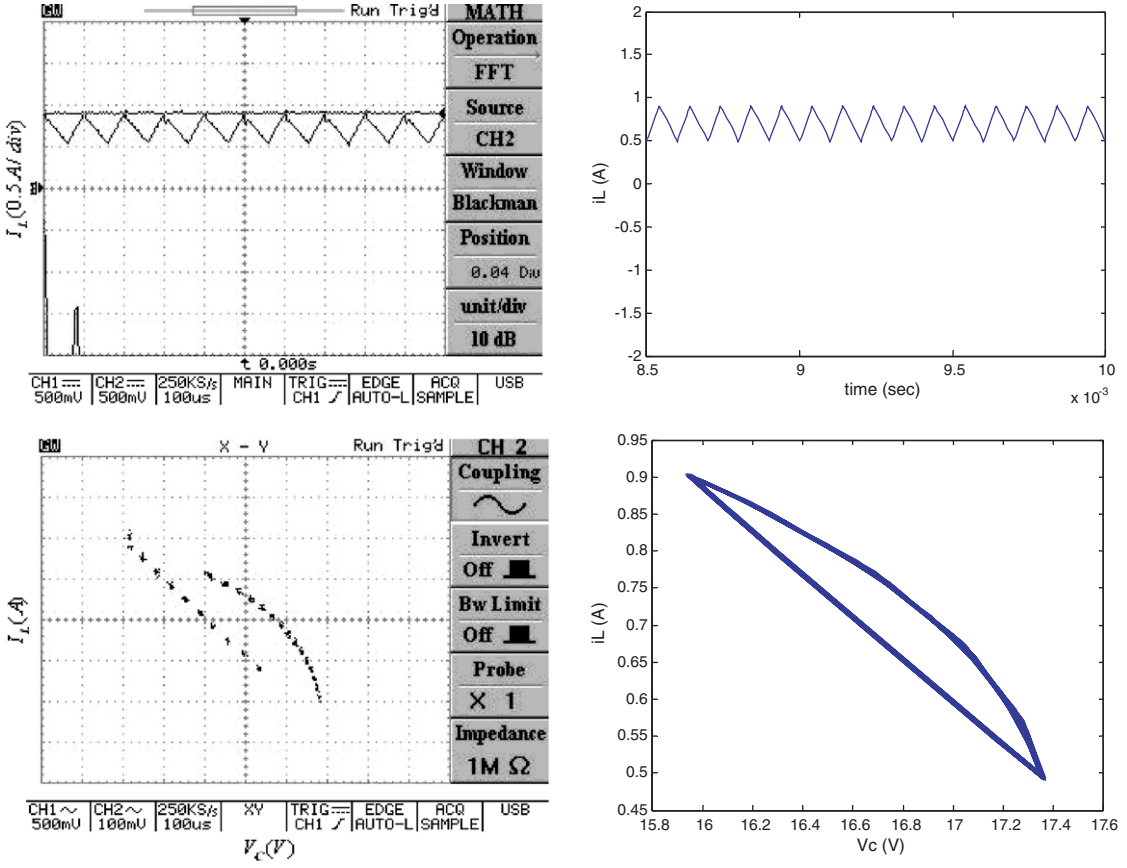

Fig. 9. Period-1 (experimental waveforms 1A/V) at $I_{\text{ref}} = 09$ A {left: practical, right: SIMULINK.}.

Please cite this article in press as: Natsheh AN et al., Analysis, simulation and experimental study of chaotic ..., Chaos, Solitons & Fractals (2007), doi:10.1016/j.chaos.2007.07.020

3.2. S_1 and S_2 open

When S_1 and S_2 open, D_1 and D_2 conduct. The circuit is as shown in Fig. 4, and is described by the following differential equations:

$$\frac{di_1}{dt} = -\frac{v_{c1}}{L} + \frac{V_I}{L} \tag{9}$$

$$\frac{di_2}{dt} = -\frac{v_{c2}}{L} + \frac{V_I}{L} \tag{10}$$

$$\frac{dv_{c1}}{dt} = -\frac{v_{c1}}{2RC} + \frac{i_1}{2C} + \frac{i_2}{2C} \tag{11}$$

$$\frac{dv_{c2}}{dt} = -\frac{v_{c2}}{2RC} + \frac{i_1}{2C} + \frac{i_2}{2C} \tag{12}$$

whose general solution is

$$i_1(t) = i_2(t) = e^{-kt}(A_1 \sin \omega t + A_2 \cos \omega t) + \frac{V_I}{2R} \tag{13}$$

where

$$\omega = \sqrt{\frac{1}{LC} - k^2} \tag{14}$$

and k is given in Eq. (8).

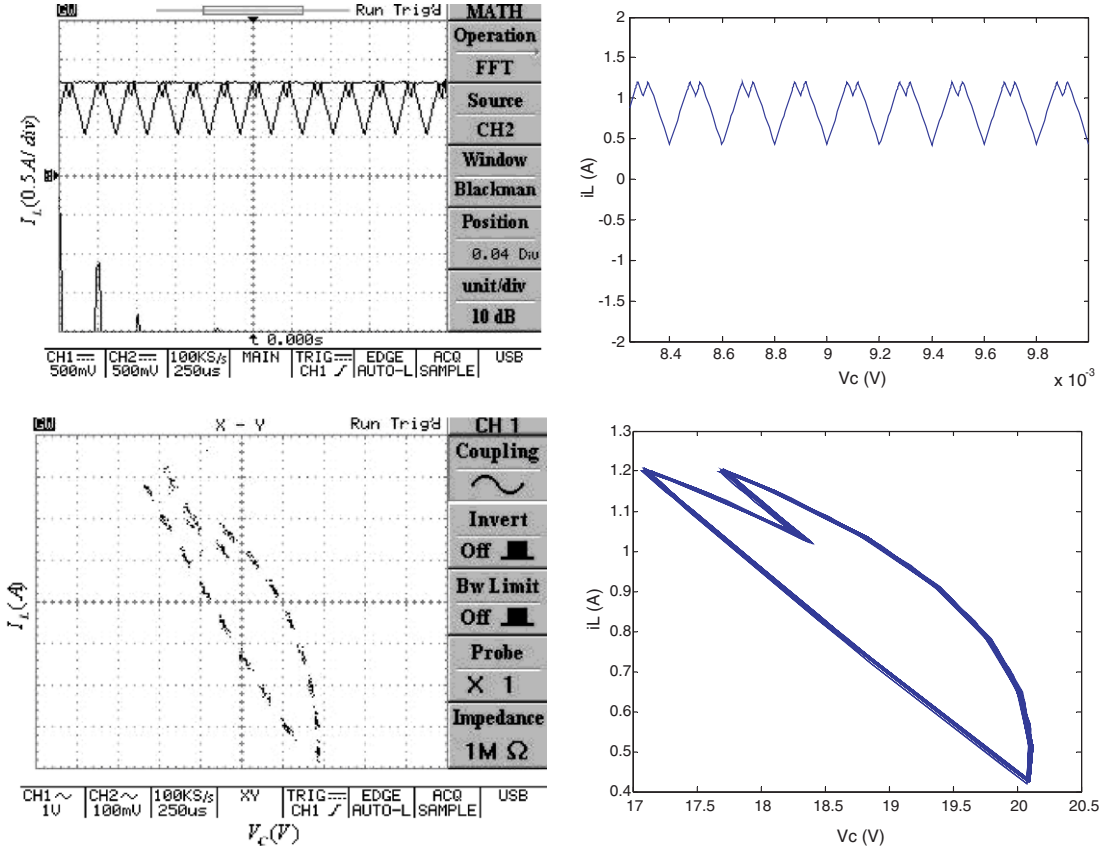

Fig. 10. Period-2 (experimental waveforms 1A/V) at $I_{ref} = 1.2$ A {left: practical, right: SIMULINK.}.

Please cite this article in press as: Natsheh AN et al., Analysis, simulation and experimental study of chaotic ..., Chaos, Solitons & Fractals (2007), doi:10.1016/j.chaos.2007.07.020

The constants A_1 and A_2 are set by the boundary conditions.

The circuit is defined by these equations until the next set of clock pulses arrives, causing S_1 and S_2 to close. This happens at a time t'_n, where

$$t'_n = T[1 - (t_n/T)] \tag{15}$$

Setting $t = 0$ immediately after S_1 and S_2 have opened gives

$$i_1(0) = i_2(0) = A_2 + \frac{V_I}{2R} = I_{\text{ref}} \tag{16}$$

and

$$v_{c1}(0) = v_{c2}(0) = v_n e^{-2kt_n} = V_I - L\frac{di_1}{dt_{t=0}} = V_I - L\frac{di_2}{dt_{t=0}} \tag{17}$$

Using Eq. (13), and solving gives

$$A_1 = \frac{V_I - v_n e^{-2kt_n} + LI'_{\text{ref}}k}{\omega L} \tag{18}$$

$$A_2 = I_{\text{ref}} - \frac{V_I}{2R} \tag{19}$$

where

$$I'_{\text{ref}} = I_{\text{ref}} - \frac{V_I}{2R} \tag{20}$$

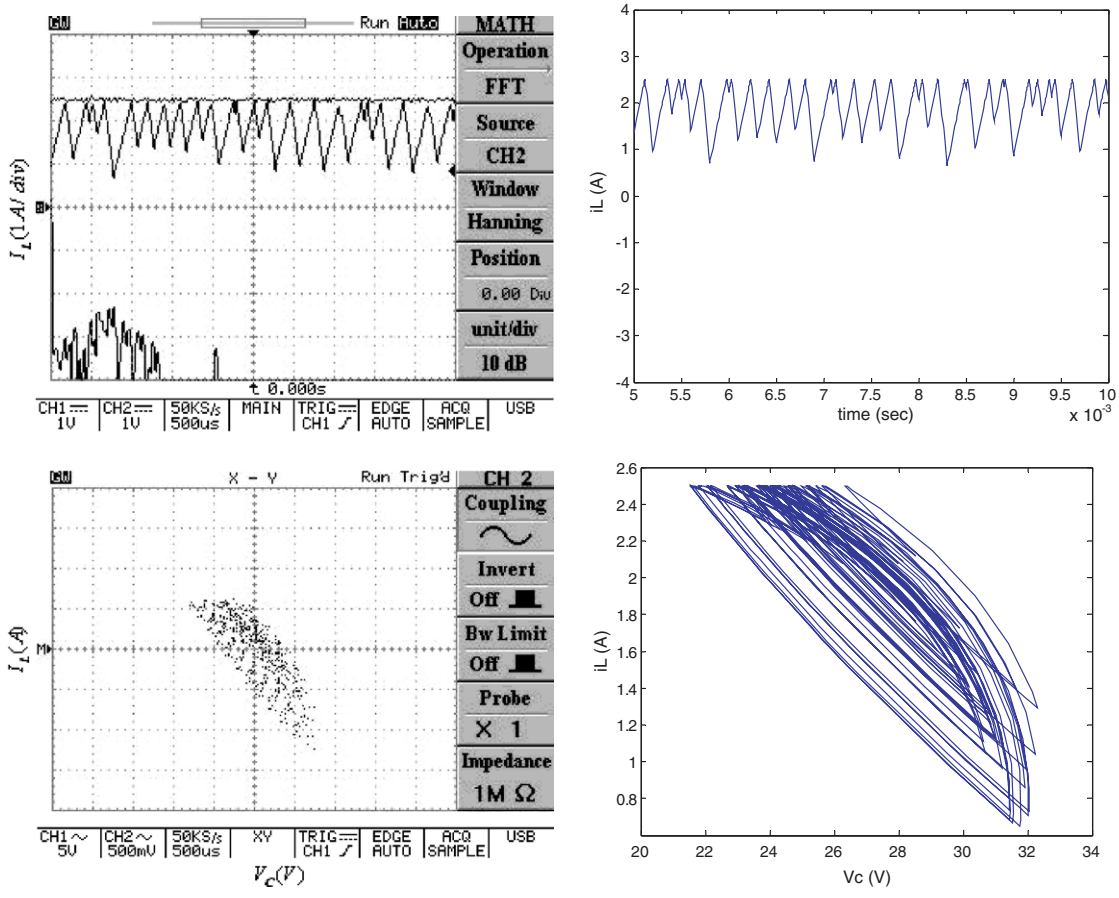

Fig. 11. Chaotic (experimental waveforms 1A/V) at $I_{\text{ref}} = 2.5$A {left: practical, right: SIMULINK.}.

Please cite this article in press as: Natsheh AN et al., Analysis, simulation and experimental study of chaotic ..., Chaos, Solitons & Fractals (2007), doi:10.1016/j.chaos.2007.07.020

Since $i_{1(n+1)} = i_1(t'_n)$, and $i_{2(n+1)} = i_2(t'_n)$, using Eq. 13 gives

$$i_{1(n+1)} = i_{2(n+1)} = \mathrm{e}^{-kt'_n}\left[\frac{kLI'_{\mathrm{ref}}V_I - v_n\,\mathrm{e}^{-2kt_n}}{\omega L}\sin\omega t'_n + I'_{\mathrm{ref}}\cos\omega t'_n\right] + \frac{V_I}{2R} \tag{21}$$

Similarly,

$$v_{c1(n+1)} = v_{c2(n+1)} = V_I\,\mathrm{e}^{-kt'_n}\left[\frac{kv_n\,\mathrm{e}^{-2kt_n} - kV_I - I'_{\mathrm{ref}}/C}{\omega}\sin\omega t'_n + \left(V_I - v_n e^{-2kt_n}\right)\cos\omega t'_n\right] \tag{22}$$

Eqs. (21) and (22) were programmed into MATLAB.

The mapping (refer to Eqs. 21 and 22 above) is a function that relates the voltage and current vector (v_{n+1}, i_{n+1}) sampled at one instant, to the vector (v_n, i_n) at a previous instant, with numerical analysis carried out using MATLAB. To obtain the bifurcation diagrams, initial conditions $(i_{1(0)}, v_{c1(0)}, i_{2(0)}, v_{c2(0)})$ are specified, together with a given I_{ref}. The equations are iterated 750 times, with the first 500 values discarded. The last 250 values are plotted taking I_{ref} as the bifurcation parameter (I_{ref} was swept from 0.5 to 5.5) with the set of circuit parameters listed in Table 1.

Figs. 5 and 6 show the inductor current bifurcation diagrams for the two parallel converters. It is evident that period-1 is stable until a critical bifurcation point $I_{\mathrm{refo}} = 1.05A$. A further increase in I_{refo} results in one of the Floquet multipliers leaving the unit circle through -1, which causes a period-doubling bifurcation. A further increase in I_{ref} beyond I_{ref} results in the system undergoing stable period-2, and a route to chaos. For $I_{\mathrm{ref}} > I_{\mathrm{refo}}$, the period-1 solution will continue to be an unstable period-1 solution.

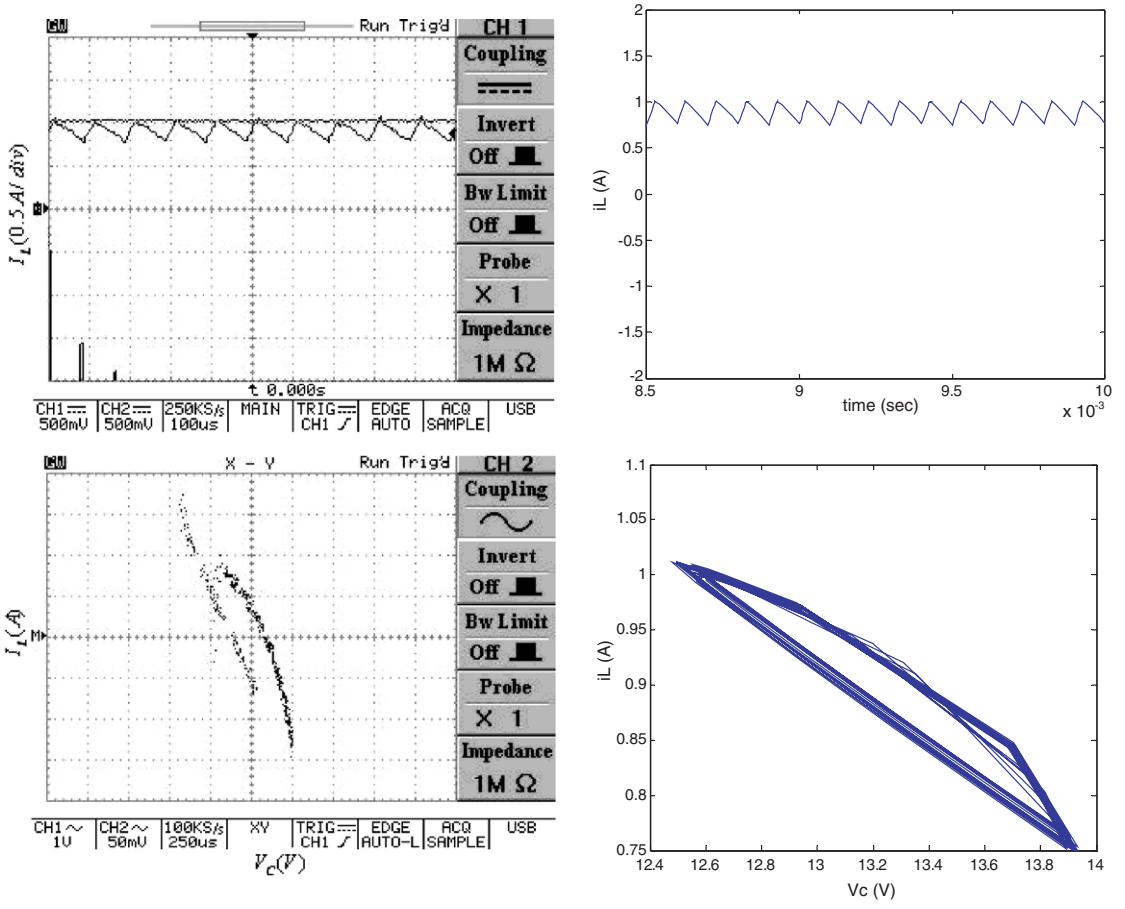

Fig. 12. Period-1 (experimental waveforms 1A/V) at $I_{\mathrm{ref}} = 1$A {left: practical, right: SIMULINK.}.

Please cite this article in press as: Natsheh AN et al., Analysis, simulation and experimental study of chaotic ..., Chaos, Solitons & Fractals (2007), doi:10.1016/j.chaos.2007.07.020

To compare the inductor current bifurcation behaviour in the two-module system with that of a single-unit boost converter, which has the same parameter values of Table (1), the bifurcation diagram of the latter is plotted in Fig. 7. It is clear that the critical bifurcation point of the modular converter takes place at a lower value of reference current compared to that of the single-boost converter.

To check the validity of these findings, experimental results and a MATLAB/SIMULINK model were employed and the results are discussed in the following section.

4. Experimental implementation and MATLAB/SIMULINK simulation

To verify the theoretical model, an experimental two-module boost converter was built, according to the block diagram of Fig. 1. Also a MATLAB/SIMULINK model was developed and this is shown in Fig. 8.

Figs. 9–11 show both experimental and MATLAB/SIMULINK inductor current waveforms, phase portraits showing the relationship between inductor current and capacitor voltage, and power spectral densities for different values of the bifurcation parameter I_{ref}. The figures are in good agreement and clearly demonstrate period-1, period-2, and chaotic behavior. The power spectrum in the chaotic region has a wide band, unlike that for period-1, which contains a fundamental switching frequency component, together with higher order harmonics at multiples of the switching frequency. Comparing the results obtained from the bifurcation diagrams of Figs. 5 and 6 with those given in Figs. 9–11 show good agreements in terms of operating region.

Figs. 12–14 show the steady-state waveforms for the single converter inductor current, the phase portraits, and power spectral densities for different values of the bifurcation parameter I_{ref}. Again, the figures are in good agreement and clearly demonstrate period-1, period-2, and chaotic behavior. The bifurcation diagram of Fig. 7 also agrees with the experimental results and those obtained from the MATLAB/SIMULINK model.

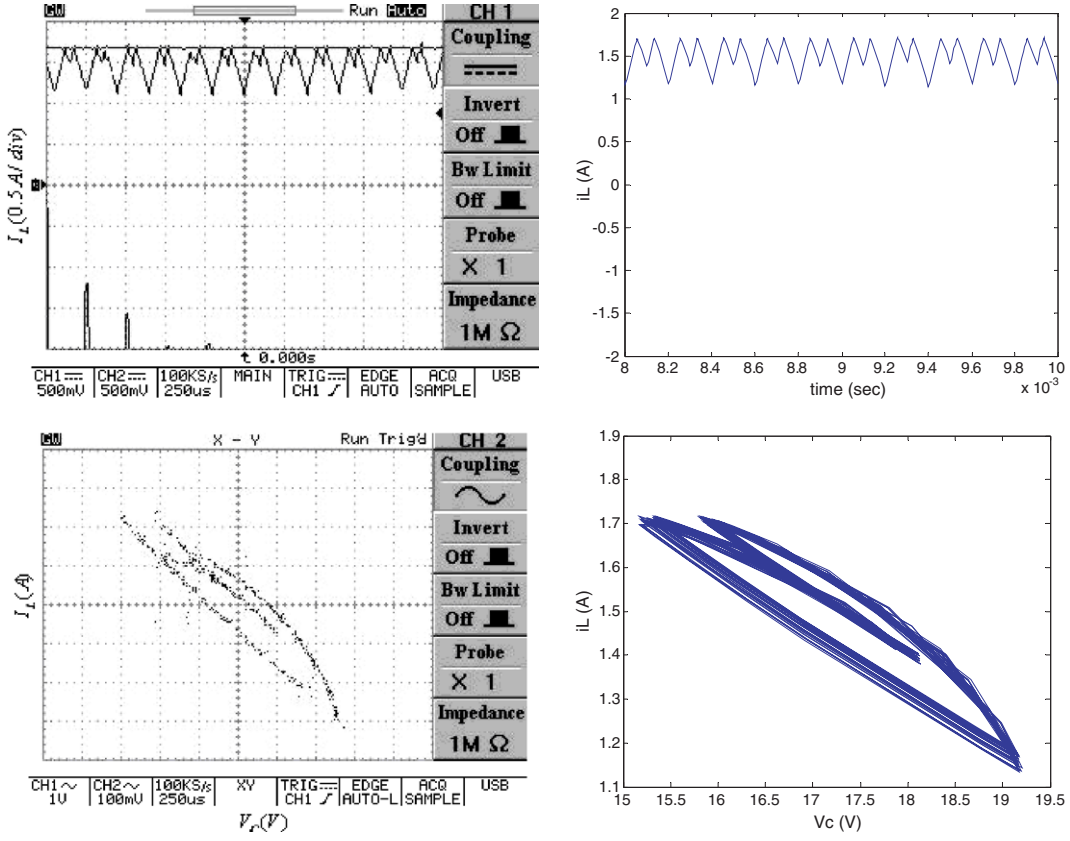

Fig. 13. Period-2 (experimental waveforms 1A/V) at $I_{ref} = 2.5$A {left: practical, right: SIMULINK.}.

Please cite this article in press as: Natsheh AN et al., Analysis, simulation and experimental study of chaotic ..., Chaos, Solitons & Fractals (2007), doi:10.1016/j.chaos.2007.07.020

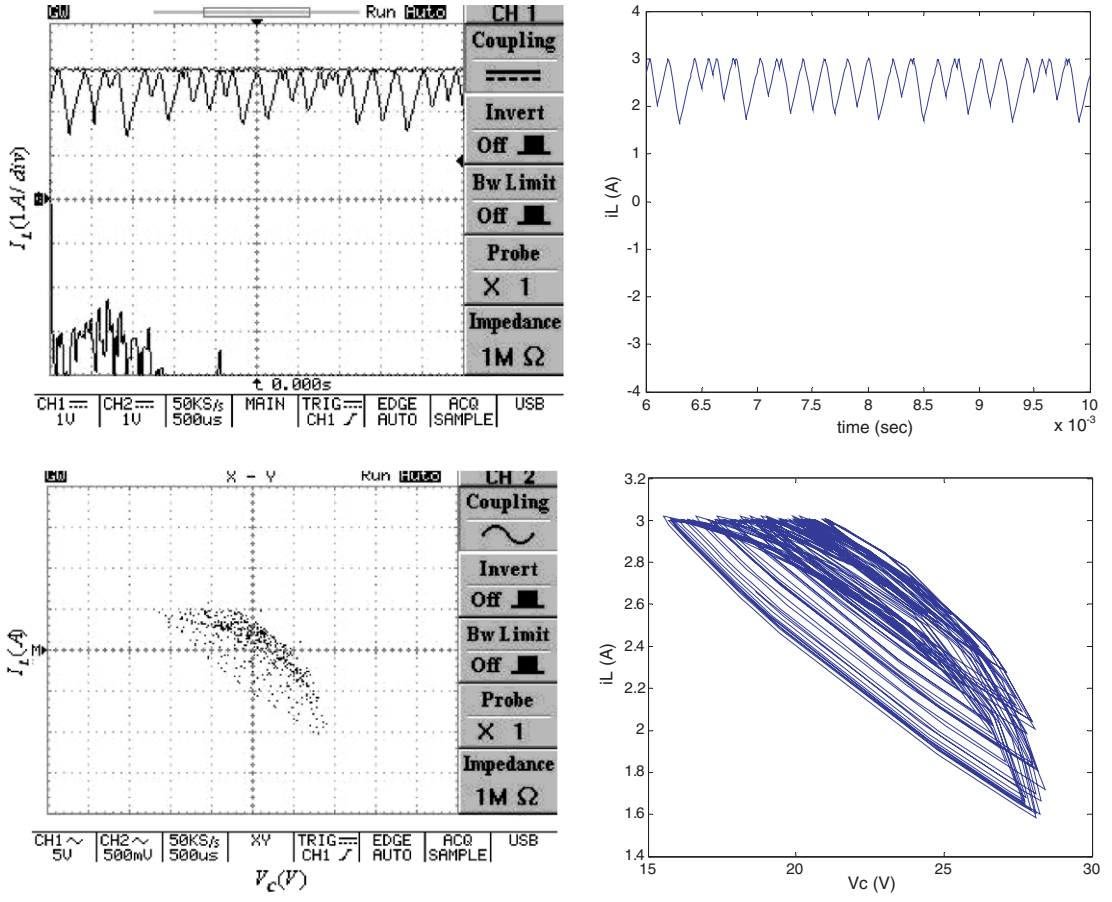

Fig. 14. Chaotic (experimental waveforms 1A/V) at $I_{ref} = 3A$ {left: practical, right: SIMULINK.}.

5. Conclusion

The waveforms produced by the MATLAB/SIMULINK models for both the two-module and the single converters show excellent agreement with experimental waveforms. They also agree with the transition points predicted by the bifurcation diagrams. These models will be used in an on-going research programme which will investigate methods of controlling and ultimately eliminating chaotic behaviour.

References

[1] Deane JHB, Hamill DC. Instability, subharmonic and chaos in power electronic circuits. IEEE Trans Power Electron 1990;5:260–8.
[2] Deane JHB. Chaos in a current-mode controlled boost DC–DC converter. IEEE Trans Circ Syst1: Fundam Theory Appl 1992;39(8):680–3.
[3] Hamill DC, Deane JHB, Jefferies DJ. Modeling of chaotic DC–DC converters by iterated nonlinear mapping. IEEE Trans Power Electron 1992;7(1):25–36.
[4] Tse CK. Flip bifurcation and chaos in three-state boost switching regulators. IEEE Trans Circ Syst1: Fundam Theory Appl 1994;41(1):16–21.
[5] Tse CK, Chan WCY. Chaos from a current programmed Cuk converter. Int J Circ Theory Appl 1995;23:217–25.
[6] Marrero JLR, Font JM, Verghese GC. Analysis of the chaotic regime for DC–DC converters under current-mode control. In: Power Electronics Specialists Conference, PESC; 1996.p. 1477–83.
[7] Banerjee S. Nonlinear modeling and bifurcation in boost converter. IEEE Trans Power Electron 1998;13(2):25–260.

Please cite this article in press as: Natsheh AN et al., Analysis, simulation and experimental study of chaotic ..., Chaos, Solitons & Fractals (2007), doi:10.1016/j.chaos.2007.07.020

[8] Iu HHC, Tse CK, Lai YM. Bifurcation in current-sharing parallel-connected boost converters. In: Power electronics and motion control conference, PIEMC; 2000. p. 921–24.
[9] Natsheh A, Nazzal J. Application of bifurcation theory to current mode controlled parallel-connected DC–DC boost converters with multi bifurcation parameters. Chaos, Solitons & Fractals 2007;33(4):1135–56.
[10] Nayfeh AH, Balachandran B. Applied nonlinear dynamics. New York: John Wiley; 1995.

Please cite this article in press as: Natsheh AN et al., Analysis, simulation and experimental study of chaotic ..., Chaos, Solitons & Fractals (2007), doi:10.1016/j.chaos.2007.07.020

E.2 ***Elsevier Journal Paper, Chaos, Solitons & Fractals***

‘‘Experimental study of controlling chaos in a DC–DC boost converter’’

Available online at www.sciencedirect.com
ScienceDirect
Chaos, Solitons and Fractals xxx (2007) xxx–xxx
CHAOS SOLITONS & FRACTALS
www.elsevier.com/locate/chaos

Experimental study of controlling chaos in a DC–DC boost converter

Ammar N. Natsheh [a,*], J. Gordon Kettleborough [a], Natalia B. Janson [b]

[a] Department of Electronic and Electrical Engineering, Loughborough University, Loughborough, Leicestershire LE11 3TU, UK
[b] Department of Mathematical Sciences, Loughborough University, Loughborough, Leicestershire LE11 3TU, UK

Accepted 29 October 2007

Communicated by Prof. L. Marek-Crnjac

Abstract

This paper presents a delayed feedback control scheme for eliminating chaotic behaviour in a peak current-mode controlled DC–DC boost converter operating in the continuous current conduction mode. Experimental results and FORTRAN simulations show the effectiveness and robustness of the scheme.

1. Introduction

The phenomenon of chaos, which has become very popular, rejuvenated interest in non-linear dynamics. Many researchers are used this theory to investigate and analyze the stability problem in electrical circuits [1–3].

The current-controlled DC–DC switch-mode boost converter is a highly non-linear circuit which behaves in a chaotic manner through period-doubling bifurcations under certain control parameter variations [4–11]. This undesirable behaviour results in switching, copper and dielectric losses, together with undesirable acoustic noise and may cause catastrophic failure of the unit.

Recently, research is been devoted to bifurcation and chaos control of such above-mentioned systems. The current paper investigates the control of chaotic behaviour in a DC–DC boost converter, operating under a peak current-mode control scheme, using delayed feedback control. The control strategy is based on the idea of stabilization of unstable periodic orbits that exist in the chaotic attractor [12]. A comparison is made between waveforms obtained from an experimental converter, and a model implemented in FORTRAN which integrates numerically the system state-variable equations. A bifurcation diagram is obtained numerically on the plane of feedback parameters and is confirmed experimentally. This bifurcation diagram enables one to choose the optimum feedback parameters for stability and robustness.

* Corresponding author.
E-mail address: A.N.Natsheh2@lboro.ac.uk (A.N. Natsheh).

0960-0779/$ - see front matter
doi:10.1016/j.chaos.2007.10.048

Please cite this article in press as: Natsheh AN et al., Experimental study of controlling chaos in a DC–DC boost ..., Chaos, Solitons & Fractals (2007), doi:10.1016/j.chaos.2007.10.048

2. Converter operation

A conventional boost converter is shown in Fig. 1, with a feedback path comprising a comparator and a flip-flop. The comparator compares the inductor current with a reference value, to control the state of switch S.

Fig. 2 shows the inductor current and the capacitor voltage waveforms. The circuit has two states, depending on whether the controlled switch S is open or closed. When S is closed, diode D is reverse biased and is non-conducting. Neglecting the resistance of inductor L, i_L rises linearly and energy is stored in the magnetic field of the inductor. S is opened when $i_L = I_{ref}$ at which instant, as a result of Lenz's law, a voltage $L\mathrm{d}i_L/\mathrm{d}t$ is induced in the inductor, to try to maintain the current flow. This voltage forward biases the diode and the current decays linearly, accompanied by a transferral of energy from the inductor to capacitor C. Increasing I_{ref} increases the energy transfer and consequently the output voltage of the converter.

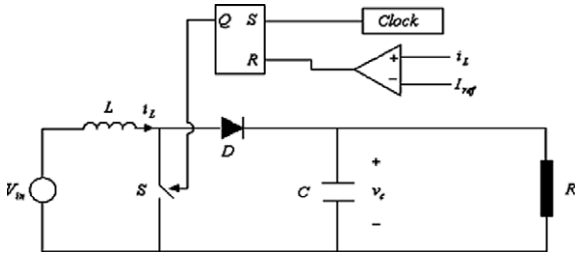

Fig. 1. Current-mode controlled DC–DC boost converter circuit.

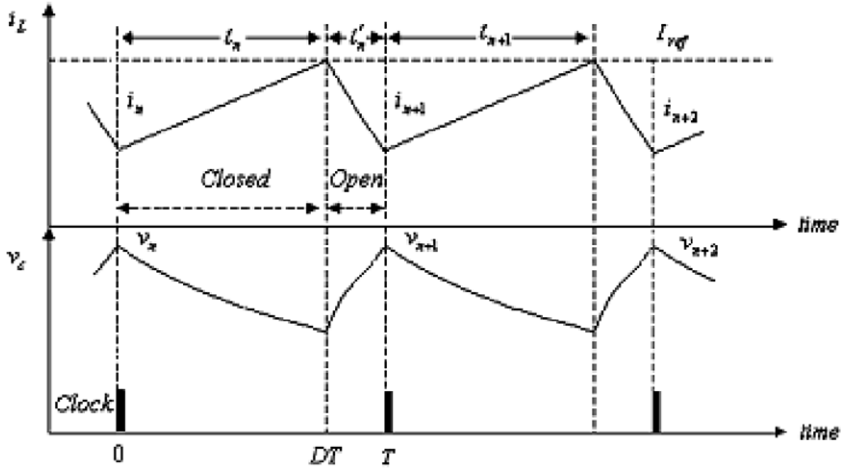

Fig. 2. Converter current and voltage waveforms.

Table 1
Circuit parameters

Circuit component	Value
Switching period	100 μs
Input voltage V_{in}	10 V
Inductance L	1 mH
Capacitance C	10 μF
Load resistance R	20 Ω

Please cite this article in press as: Natsheh AN et al., Experimental study of controlling chaos in a DC–DC boost ..., Chaos, Solitons & Fractals (2007), doi:10.1016/j.chaos.2007.10.048

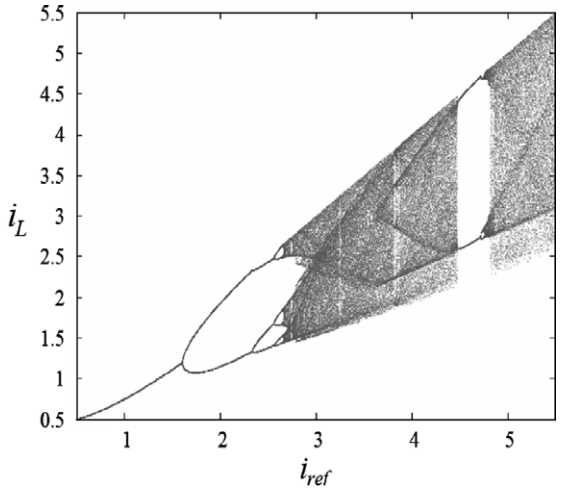

Fig. 3. Bifurcation diagram with I_{ref} as the bifurcation parameter.

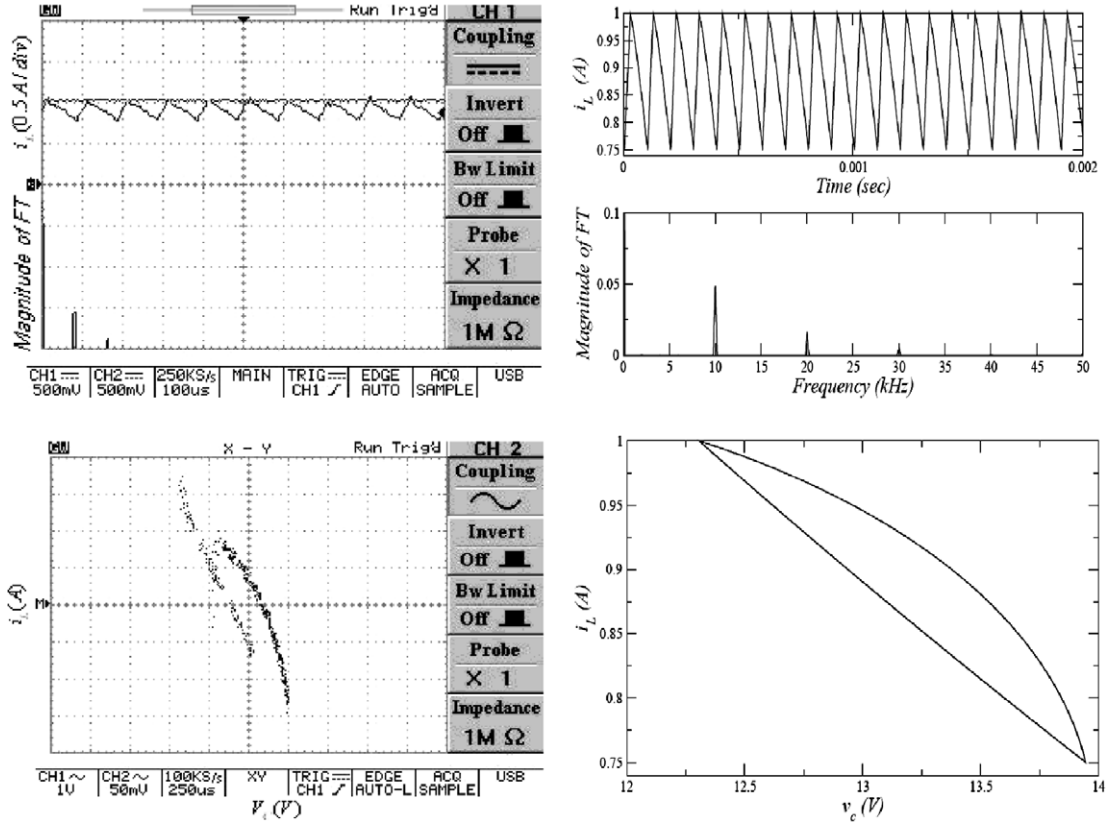

Fig. 4. "Period-1" regime at $I_{ref} = 1$ A. Left: experimental waveforms (1 A/V) and right: simulated.

Please cite this article in press as: Natsheh AN et al., Experimental study of controlling chaos in a DC–DC boost ..., Chaos, Solitons & Fractals (2007), doi:10.1016/j.chaos.2007.10.048

3. Open-loop performance

The model equations that describe the operation of the circuit shown in Fig. 1 are

$$\begin{aligned}\frac{di_L}{dt} &= \frac{1}{L}[v_i - v_C(1-u_S)]\\ \frac{dv_C}{dt} &= \frac{1}{C}\left[-\frac{v_C}{R} + i_L(1-u_S)\right]\end{aligned} \tag{1}$$

where u_S takes the value 0 or 1 depending on whether the switch is closed or open. A diagram relating the values of i_L in the Poincaré section defined by $di_L/dt = 0$ and $d^2i_L/dt^2 < 0$, as I_{ref} is varied was obtained numerically using the parameters listed in Table 1 and is given in Fig. 3.

It is evident from the diagram that the first period-doubling bifurcation occurs at $I_{ref} \approx 1.68$ A, and a few more period-doubling bifurcations occur at values close to 2.35 A, 2.55 A and 2.7 A. At $I_{ref} > 2.75$ A the system is chaotic.

To check the validity of this bifurcation diagram, the open-loop performance of a converter designed and built to the specification of Table 1 was investigated experimentally, and by means of simulation with a program written in FORTRAN. This solved numerically the system differential equations, setting u_S to 1 at every clock pulse and u_S to 0 when $i_L = I_{ref}$. Results for period-1, period-2 and chaotic regimes are presented in Figs. 4–6. Inductor current i_L waveforms, their Fourier amplitude spectra and the phase portraits between inductor current i_L and capacitor voltage v_C show good agreement between experimental and simulated results and also agree with the bifurcation diagram in Fig. 3. Further investigations also verified the bifurcation points, but these have not been shown for reasons of brevity.

It is worth noting that, as seen from Figs. 4–6, the frequency of periodic "period-1" oscillations at $I_{ref} = 1$ A is 10 kHz but the frequency of "period-2" oscillations at $I_{ref} = 1.7$ A is only 5 kHz, the dominating frequency of chaotic

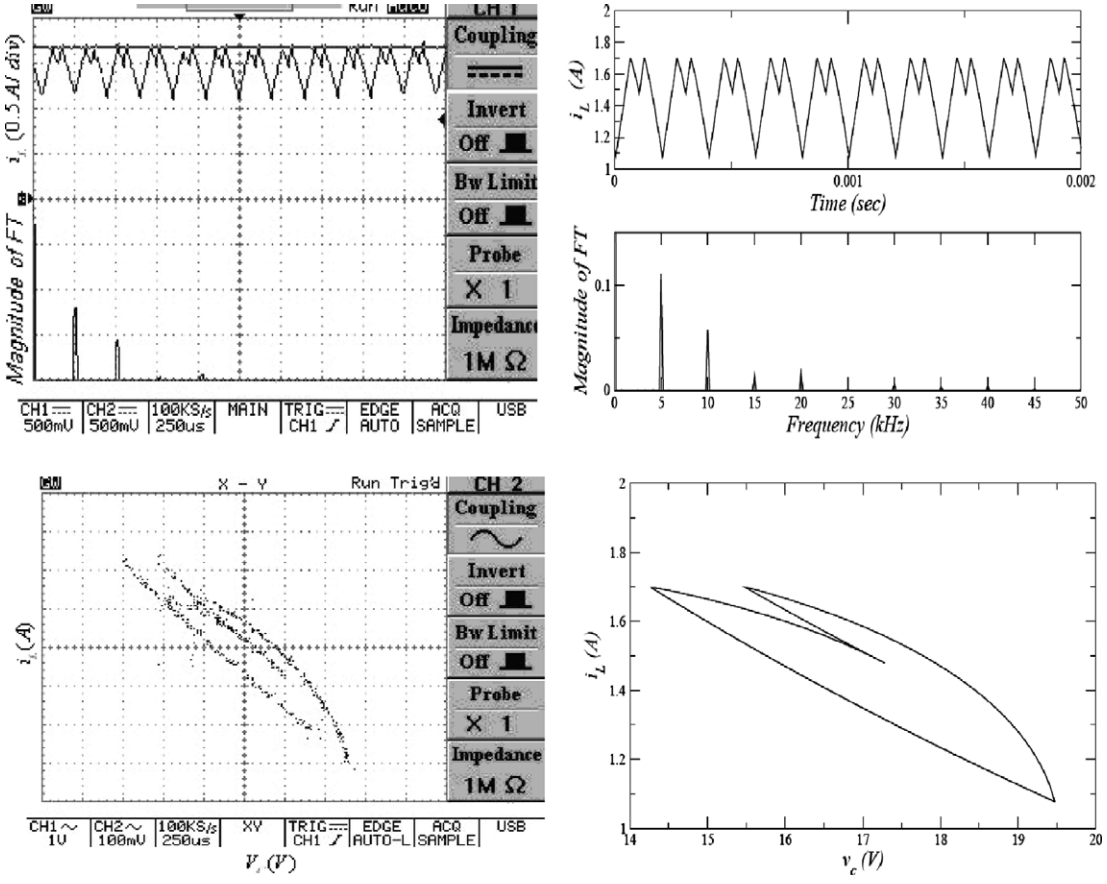

Fig. 5. "Period-2" regime at $I_{ref} = 1.7$ A. Left: experimental waveforms (1 A/V) and right: simulated.

Please cite this article in press as: Natsheh AN et al., Experimental study of controlling chaos in a DC–DC boost ..., Chaos, Solitons & Fractals (2007), doi:10.1016/j.chaos.2007.10.048

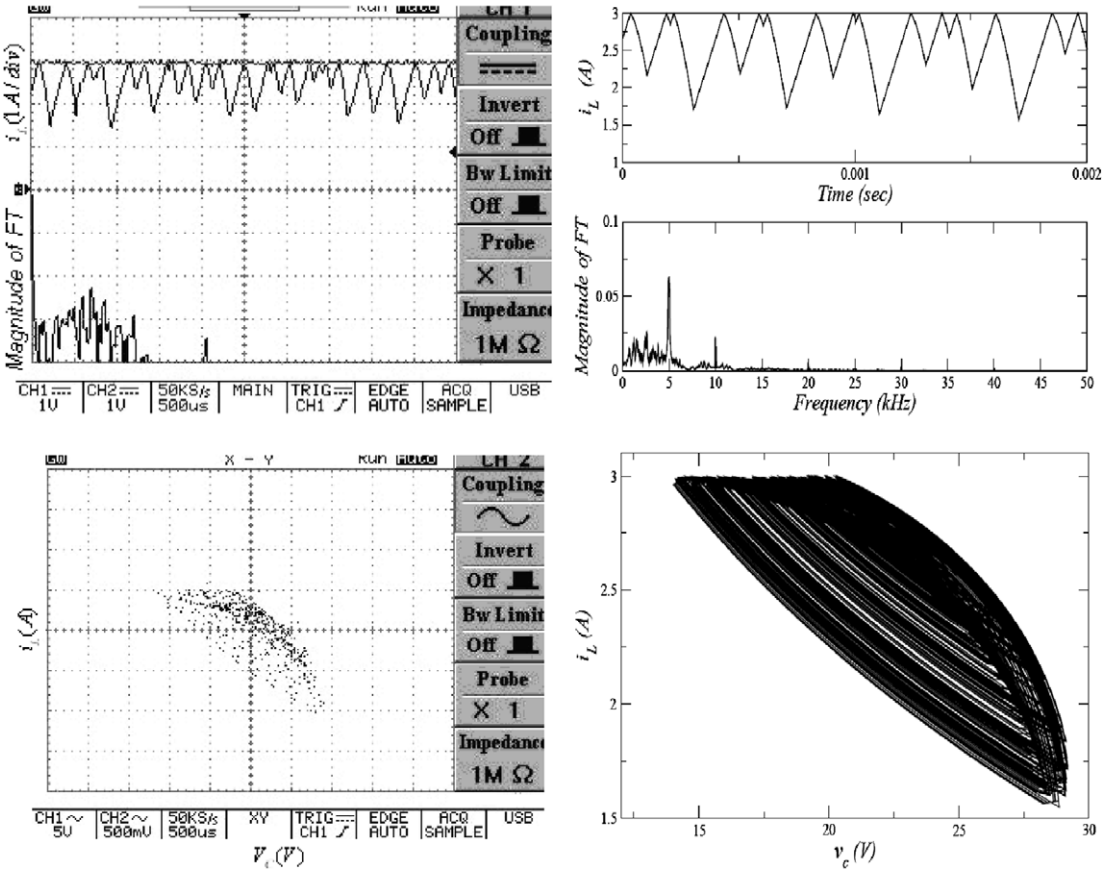

Fig. 6. Chaotic regime at $I_{ref} = 3$ A. Left: experimental waveforms (1 A/V) and right: simulated.

oscillations at $I_{ref} = 3$ A is also 5 kHz, which means that the frequency of oscillations has halved as a result of the cascade of period-doubling bifurcations as compared to the desired frequency 10 kHz.

4. Control of chaos

Pyragas [12] has suggested that chaotic behaviour may be eliminated from the system if one applies the delayed feedback control scheme shown in Fig. 7. The feedback control force $F(t)$ that is applied to the system is the difference between the current value of some system variable $y(t)$, and its value τ seconds before, multiplied by a constant K, where

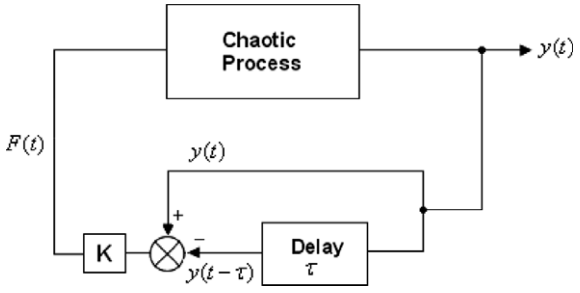

Fig. 7. Delayed current feedback control system.

Please cite this article in press as: Natsheh AN et al., Experimental study of controlling chaos in a DC–DC boost ..., Chaos, Solitons & Fractals (2007), doi:10.1016/j.chaos.2007.10.048

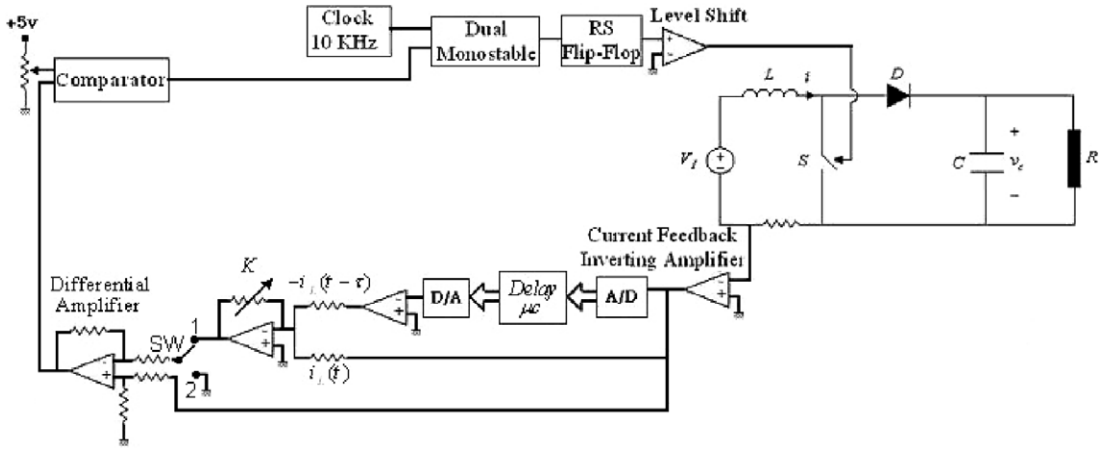

Fig. 8. Experimental feedback control scheme.

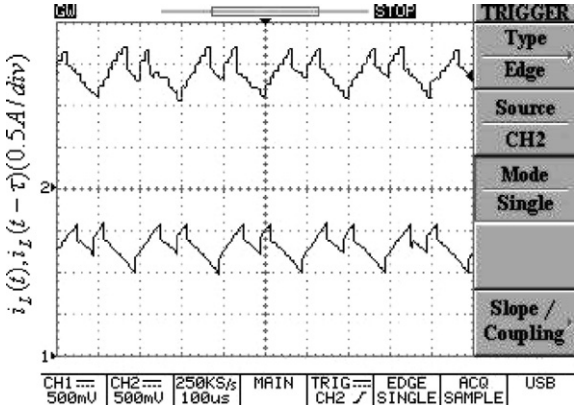

Fig. 9. Experimental open-loop waveforms $i_L(t)$ (lower) and $i_L(t-\tau)$ (upper) for $I_{ref} = 1.7$ A and $\tau = 100$ μs.

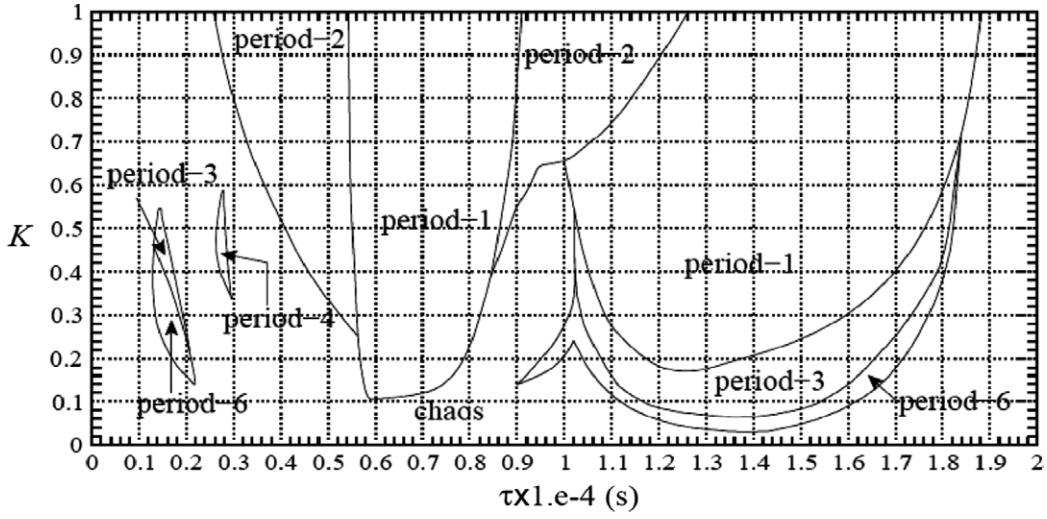

Fig. 10. Map of regimes relating K to τ for $I_{ref} = 3$ A.

Please cite this article in press as: Natsheh AN et al., Experimental study of controlling chaos in a DC–DC boost ..., Chaos, Solitons & Fractals (2007), doi:10.1016/j.chaos.2007.10.048

K is the feedback strength. The idea behind the scheme relies on the fact that a skeleton of a chaotic attractor is formed by an infinite (countable) set of unstable periodic orbits with different periods. If the value of time delay τ is exactly equal to the period T of one of the orbits, then at the appropriate values of K the orbit can become stable, and chaos will thus be eliminated. Once control is achieved, i.e. the phase trajectory reaches the periodic orbit, the control force $F(t)$ is zero at any instant. This is called non-invasive control and implies that virtually no power is spent in the control loop to support the desired behaviour of the system.

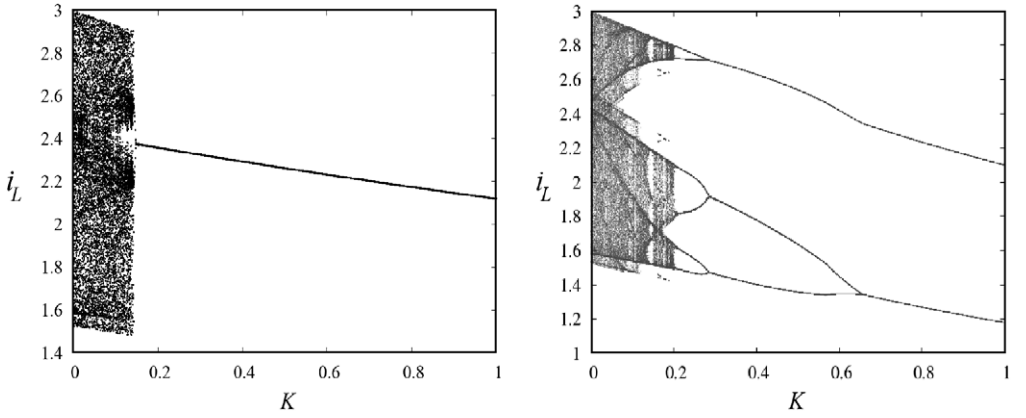

Fig. 11. Bifurcation diagrams with delayed feedback control at $I_{ref} = 3$ A (values of i_L in the Poincaré section are shown against K). Left: $\tau = 70$ μs and right: $\tau = 100$ μs.

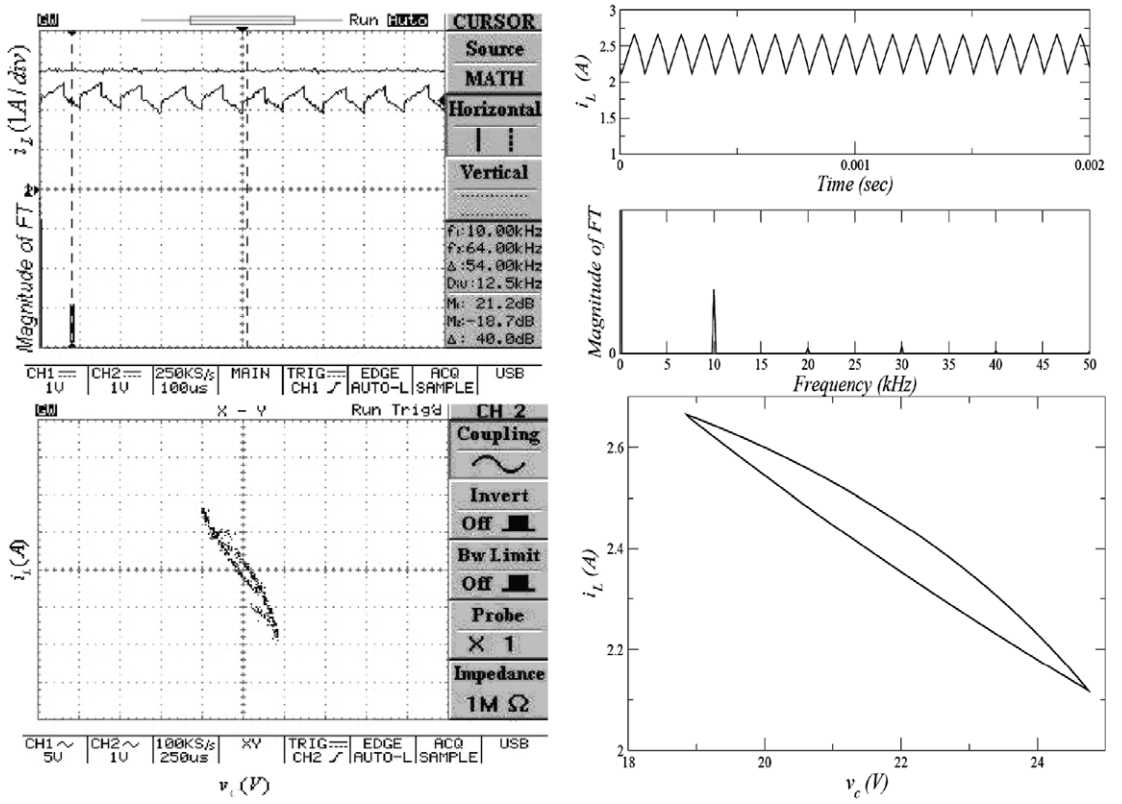

Fig. 12. Delayed feedback control $I_{ref} = 3$ A, $\tau = 70$ μs, $K = 1$. Left: experimental waveforms (1 A/V) and right: simulated.

Please cite this article in press as: Natsheh AN et al., Experimental study of controlling chaos in a DC–DC boost ..., Chaos, Solitons & Fractals (2007), doi:10.1016/j.chaos.2007.10.048

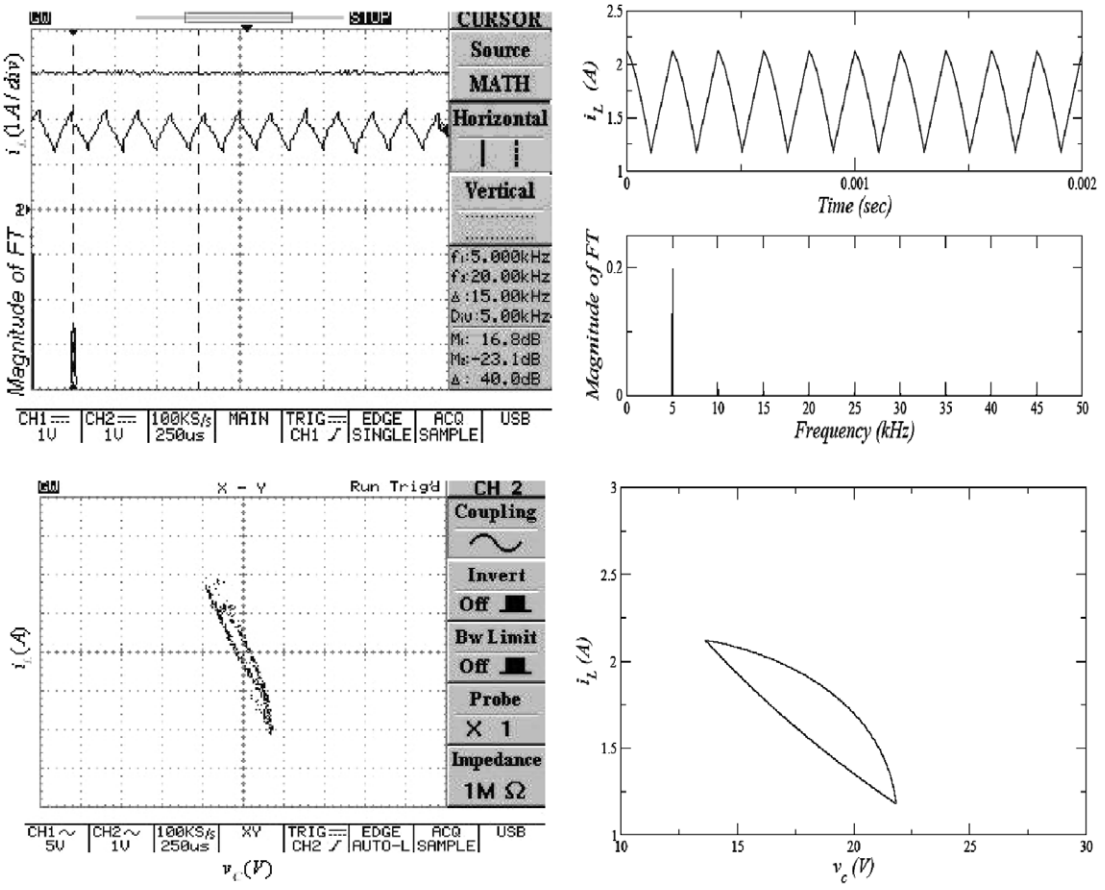

Fig. 13. Delayed feedback control $I_{ref} = 3$ A, $\tau = 100$ μs, $K = 1$. Left: experimental waveforms (1 A/V) and right: simulated.

Practical implementation of delayed feedback control was achieved using an 89C51 microcontroller, which sampled the controlled variable $i_L(t)$ at 10 μs intervals and stored the values in a continually updated rolling array. A pointer extracts data from this array at a delay τ, pre-programmed by the operator, to provide the value $i_L(t-\tau)$. A simplified diagram of the scheme is shown in Fig. 8.

The experimental waveforms for $i_L(t)$ and $i_L(t-\tau)$ at $I_{ref} = 1.7$ A are shown in Fig. 9, with the feedback switch SW in position 2 disconnecting the delayed current feedback from the control circuit. The converter is operating in a "period-2" mode. The stepped nature of $i_L(t-\tau)$ is due to the digitisation of the waveform, and the pre-programmed 100 μs delay is clearly visible.

The system performance and stability depends on both the choice of the delay τ and the feedback gain K. In order to identify the ranges of K and τ that would result in the desired periodic oscillations of i_L, a map of the regimes on the (τ, K) plane was generated numerically at $I_{ref} = 3$ A following [13]. The diagram is given in Fig. 10 and shows areas with qualitatively distinct behaviour marked by expressions like "period-1", "chaos", etc. On the solid lines which separate different areas, the transitions between different kinds of behaviour occur.

To illustrate the transitions occurring in the system as its parameters are changed, two values of τ, 100 μs and 70 μs, were chosen and the variation of i_L with K in the Poincaré section were obtained as shown in Fig. 11. At $\tau = 70$ μs the system is chaotic as K increases from zero to 0.15, after which it acquires a stable "period-1" cycle with a frequency of 10 kHz. For $\tau = 100$ μs, the system goes through a series of chaotic and periodic states up to $K = 0.66$, after which it becomes stable "period-2" with a frequency of 5 kHz.

Experimental and simulated results for $\tau = 70$ μs and 100 μs are compared in Figs. 12 and 13, respectively, at $K = 1$. Simulations were obtained by solving numerically Eq. (1), setting u_S to 1 at every clock pulse and u_S to 0 when $i_L(t) = I_{ref} - K[i_L(t-\tau) - i_L(t)]$. It is clear that the periodic regimes observed are stable in both cases, and these agree with the bifurcation diagrams of Fig. 11. The waveforms of Fig. 12 have a frequency of 10 kHz ("period-1" cycles), whereas those of Fig. 13 have a frequency of 5 kHz ("period-2" cycles).

Please cite this article in press as: Natsheh AN et al., Experimental study of controlling chaos in a DC–DC boost ..., Chaos, Solitons & Fractals (2007), doi:10.1016/j.chaos.2007.10.048

5. Conclusions

The paper describes a robust scheme for controlling chaos in a current-controlled DC–DC boost converter, with the results of Figs 12 and 13 both exhibiting stable operation. However, although a stable "period 2" operation with a frequency of 5 kHz is theoretically acceptable, the converter was designed for 10 kHz operation and the system would not be performing under optimum conditions with $\tau = 100$ μs. It is important therefore, to ensure that the system is operating in a "period 1" region of Fig. 10, preferably far away from any bifurcation boundaries.

Originally, the idea was to prevent chaos in the system by stabilizing the periodic orbit with the help of the feedback force that would become zero once the desired regime is achieved, i.e. to implement the non-invasive control. However, the chosen way of introducing the feedback loop into the system has made the control force non-zero at any feedback parameters τ or K, thus rendering the control invasive. This happened because the feedback has led to the effective variation of control parameter I_{ref} in time, which destroyed the original periodic orbits and created the new ones instead. As a result, the most suitable value of τ appears to be considerably different from the periods 100 or 200 μs of the periodic orbits in the original system.

Acknowledgements

We are grateful to A.G. Balanov for the help with producing the software. N.B. Janson acknowledges the support from EPSRC (UK).

References

[1] Abed EH, Varaiya PP. Nonlinear oscillations in power systems. Int J Electr Power Energy Syst 1989;6:37–43.
[2] Abdellah AG, El-Nadi AM. Experimental observation of chaotic properties in a system of two coupled Wien–Bridge oscillators. Chaos, Solitons & Fractals 2007;32(3):988–95.
[3] Harb B, Harb A. Chaos and bifurcation in a third-order phase locked loop. Chaos, Solitons & Fractals 2004;19(3):667–72.
[4] Deane JHB, Hamill DC. Instability, subharmonic and chaos in power electronic circuits. IEEE Trans Power Electron 1990;5:260–8.
[5] Deane JHB. Chaos in a current-mode controlled boost DC–DC converter. IEEE Trans Circuit Syst-1: Fundam Theory Appl 1992;39(8):680–3.
[6] Hamill DC, Deane JHB, Jefferies DJ. Modelling of chaotic DC–DC converters by iterated nonlinear mapping. IEEE Trans Power Electron 1992;7(1):25–36.
[7] Tse CK. Flip bifurcation and chaos in three-state boost switching regulators. IEEE Trans Circuit Syst-1: Fundam Theory Appl 1994;41(1):16–21.
[8] Tse CK, Chan WCY. Chaos from a current programmed Cuk converter. Int J Circuit Theory Appl 1995;23(May–June):217–25.
[9] Marrero JLR, Font JM, Verghese GC. Analysis of the chaotic regime for DC–DC converters under current-mode control. In: Power electronics specialists conference, PESC; 1996. p. 1477–83.
[10] Banerjee S. Nonlinear modelling and bifurcation in boost converter. IEEE Trans Power Electron 1998;13(2):253–60.
[11] Natsheh AN, Kettleborough JG, Nazzal JM. Analysis, simulation and experimental study of chaotic behaviour in parallel-connected DC–DC boost converters. Chaos, Solitons & Fractals [in press]. doi:10.1016/j.chaos.2007.07.020.
[12] Pyragas K. Continuous control of chaos by self-controlling feedback. Phys Lett A 1992;170:421–8.
[13] Balanov AG, Janson NB, Scholl E. Delayed feedback control of chaos: bifurcation analysis. Phys Rev E 2005;71:016222.

Please cite this article in press as: Natsheh AN et al., Experimental study of controlling chaos in a DC–DC boost ..., Chaos, Solitons & Fractals (2007), doi:10.1016/j.chaos.2007.10.048

E.3 ***IEEE Conference Paper, Cambridge University-UK***

‘‘Control of Chaos in a DC-DC Boost Converter’’

Control of Chaos in a DC-DC Boost Converter

Ammar N. Natsheh*, Natalia B. Janson** and J. Gordon Kettleborough*
* Department of Electronic and Electrical Engineering
** Department of Mathematical Sciences
Loughborough University
Loughborough, Leicestershire, LE11 3TU, UK

***Abstract*-A delayed feedback control scheme is described, for eliminating chaotic behaviour in a peak current-mode controlled DC-DC boost converter operating with continuous inductor current. Contour maps, which relate important feedback parameters to the converter performance, are used to identify the best combination of these parameters. Experimental results and FORTRAN simulations show the effectiveness and robustness of the scheme.**

I. Introduction

A current-controlled DC-DC switch-mode boost converter behaves in a chaotic manner through period doubling bifurcations under certain control parameter variations [1-7]. This behaviour is undesirable, since it results in increased losses, together with undesirable acoustic noise and may cause catastrophic failure of the unit.

This paper investigates the control of chaotic behaviour using delayed feedback control, which is based on the idea of stabilization of unstable periodic orbits that exist in the chaotic attractor [8]. We numerically reveal the maps of regimes on the plane of the feedback parameters following [9]. The knowledge of these maps enables one to choose the optimum feedback parameters to ensure the stability and robustness of the required periodic behaviour.

A comparison is made between waveforms obtained from an experimental converter, and a model implemented in FORTRAN which integrates numerically the system state-variable equations. The experiment reproduces the numerical findings with very good accuracy.

II. Converter Operation

A conventional boost converter is shown in Fig. 1(a), with a feedback path comprising a comparator and a flip-flop. The comparator compares the inductor current with a reference value (I_{ref}), to control the state of switch S.

The circuit has two states, depending on whether the controlled switch S is open or closed. When S is closed, diode D is reverse biased and is non-conducting. Neglecting the resistance of inductor L, i_L rises linearly (Fig. 1(b)) and energy is stored in the magnetic field of the inductor. S is opened when $i_L = I_{ref}$ at which instant, a voltage Ldi_L/dt is induced in the inductor, to try to maintain the current flow. This voltage forward biases the diode and the current decays linearly, accompanied by a transferral of energy from the inductor to capacitor C. The switch closes each time a pulse arrives from the clock with the period T. Increasing I_{ref} increases the energy transfer and consequently the output voltage of the converter.

III. Open-Loop Operation

The model equations that describe the operation of the circuit shown in Fig. 1 are

$$\frac{di_L}{dt} = \frac{v_i - v_C(1-u_S)}{L}, \quad \frac{dv_C}{dt} = \frac{-v_C/R + i_L(1-u_S)}{C}, \qquad (1)$$

where u_S takes the value 0 or 1 depending on whether the switch is closed or open. A bifurcation diagram relating the values of i_L in the Poincaré section defined by $di_L/dt = 0$ and $d^2i_L/dt^2 < 0$ (local maxima of i_L), as I_{ref} is varied was obtained numerically using the parameters listed in Table 1 and is given in Fig. 2.

It is evident from the diagram that the first period-doubling bifurcation occurs at $I_{ref} \approx 1.68$A, and a few more period-doubling bifurcations occur at values close to 2.35A, 2.55A and 2.7A. At $I_{ref} > 2.75$A the system is chaotic.

To check the validity of this bifurcation diagram, the open-loop performance of a converter designed and built to the specification of Table 1 was investigated experimentally, and by means of simulation with a program written in FORTRAN. This solved numerically the system differential equations, setting u_S to 1 at every clock pulse and u_S to 0 when $i_L = I_{ref}$. Results for period-1, period-2 and chaotic regimes were obtained for the inductor current waveform, its Fourier amplitude spectra and the phase portraits between inductor current and capacitor voltage v_C, and these showed good agreement between experimental and simulated results and also agree with the bifurcation diagram in Fig. 2. The results for chaotic conditions ($I_{ref}=3A$) are given in Fig. 3. Further investigations also verified the locations of the bifurcation points in the Poincare section.

TABLE I
CIRCUIT PARAMETERS

Circuit Component	Value
Switching period	100μs
Input voltage V_{in}	10V
Inductance L	1mH
Capacitance C	10μF
Load resistance R	20Ω

It is worth noting that, as seen in Fig. 3, the dominating frequency of chaotic oscillations at $I_{ref}=3A$ is 5kHz, which means that the frequency of oscillations has halved as a result of the cascade of period-doubling bifurcations as compared to the desired frequency 10kHz.

IV. Control of Chaos

Pyragas [8] has suggested that chaotic behaviour may be eliminated from the system if one applies the delayed feedback control scheme shown in Fig. 4. The feedback control force *F(t)*, applied to the system is the difference between the current value of some system variable *y(t),* and its value τ seconds previously, multiplied by a constant *K*, where *K* is the feedback strength. The idea behind the scheme relies on the fact that a skeleton of a chaotic attractor is formed by an infinite (countable) set of unstable periodic orbits with different periods. If the value of time delay τ is exactly equal to the period *T* of one of the orbits, then at the appropriate values of *K* the orbit can become stable, and chaos will thus be eliminated. Once control is achieved, i.e. the phase trajectory reaches the periodic orbit, the control force *F(t)* is zero at any instant. This is called non-invasive control and implies that virtually no power is spent in the control loop to support the desired behaviour of the system.

Practical implementation of delayed feedback control was achieved using an 89C51 microcontroller, which sampled the controlled variable $i_L(t)$ at 10μs intervals and stored the values in a continually updated rolling array. A pointer extracts data from this array at a delay τ, pre-programmed by the operator, to provide the value $i_L(t-\tau)$. A simplified diagram of the scheme is shown in Fig. 5.

The system performance and stability depends on both the choice of the delay τ and the feedback gain *K*. In order to identify the ranges of *K* and τ that would result in the desired periodic oscillations of i_L for various values of I_{ref}, maps of the regimes on the (τ,*K*) plane were generated numerically at I_{ref} = 1, 2, 3 and 4A, following [9]. The diagrams are given in Fig. 6 and show areas with qualitatively distinct behaviour marked by expressions like "period-1", "chaos", etc. On the lines which separate different areas, the transitions between different kinds of behaviour occur.

It is evident from Fig. 6 that a large period-1 region exists around τ = 70μs for all the maps and that this is a suitable value for the delay. To illustrate the transitions occurring in the system for τ = 70μs and $I_{ref}=3A$, the variation of i_L with *K* in the Poincaré section were obtained as shown in Fig. 7. The system is chaotic as *K* increases from zero to 0.13, after which it acquires a stable "period-1" cycle with a frequency of 10 kHz.

Experimental and simulated results for $I_{ref}=3A$, τ=70μs and *K*=1, are compared in Fig. 8. The simulations were obtained by solving numerically Eqs. (1), setting u_S to 1 at every clock pulse and u_S to 0 when $i_L(t) = I_{ref} - K[i_L(t-\tau) - i_L(t)]$. It is clear that the periodic regime observed is stable and this agrees with the bifurcation diagram of Fig. 7. The waveforms of Fig. 8 have the desired frequency of 10 kHz ("period-1" cycles).

V. Conclusions

The paper describes a robust scheme for controlling chaos in a current-controlled DC-DC boost converter, with the results of Fig.8 exhibiting stable “period-1” operation. It is important to ensure that the system operates in a “period-1” and not a “period-2” region of Fig. 6, since the converter was designed for optimum operation at 10 kHz. Also, it is preferable that operation is far away from any bifurcation boundaries.

Originally, the idea was to prevent chaos in the system by stabilizing the periodic orbit with the help of the feedback force that would become zero once the desired regime is achieved, i.e. to implement the non-invasive control. However, the chosen way of introducing the feedback loop into the system has made the control force non-zero at any feedback parameters τ or *K*, thus rendering the control invasive. This happened because the feedback has led to the effective variation of control parameter I_{ref} in time, which destroyed the original periodic orbits and created the new ones instead. As a result, the most suitable value of τ appears to be considerably different from the 100μs of the periodic orbit in the original system.

VI. Acknowledgments

We are grateful to A.G. Balanov for the help with producing the software. N.B. Janson acknowledges the support from EPSRC (UK).

References

[1] Deane, J. H. B. and Hamill, D. C., “Instability, Subharmonic and Chaos in Power Electronic Circuits,” IEEE Transactions on Power Electronics, Vol. 5, 1990, pp. 260-268.

[2] Deane, J. H. B., “Chaos in a Current-Mode Controlled Boost DC-DC Converter,” IEEE Transactions on Circuits and systems-1: Fundamental Theory and Applications, Vol. 39. No. 8, August 1992, pp. 680-683.

[3] Hamill, D. C., Deane, J. H. B., and Jefferies D. J., “Modelling of Chaotic DC-DC Converters by Iterated Nonlinear Mapping,” IEEE Transactions on Power Electronics, Vol. 7, No. 1, 1992, pp. 25 – 36.

[4] Tse, C. K.,” Flip Bifurcation and Chaos in Three-State Boost Switching Regulators,” IEEE Transactions on Circuits and systems-1: Fundamental Theory and Applications, Vol. 41, No. 1, January 1994, pp. 16-21.

[5] Tse, C. K., and Chan W. C. Y., “Chaos from a current programmed Cuk converter,” Int. J. Circuit Theory Applications, Vol. 23, May-June 1995, 217-225.

[6] Marrero, J. L. R., Font, J. M., and Verghese, G. C., "Analysis of the chaotic regime for DC-DC converters under current-mode control," Power Electronics Specialists Conference, PESC 1996, pp. 1477-1483.
[7] Banerjee, S., "Nonlinear Modelling and Bifurcation in Boost Converter," IEEE Transactions on Power Electronics, Vol. 13, No. 2, 1998, pp. 253 – 260.
[8] Pyragas, K., "Continuous control of chaos by self-controlling feedback," Physics Letters, A 170, 1992, pp 421-428.
[9] Balanov, A. G., Janson, N. B., and Scholl, E., "Delayed feedback control of chaos: Bifurcation Analysis" Physical Review E.71, 016222.(2005)

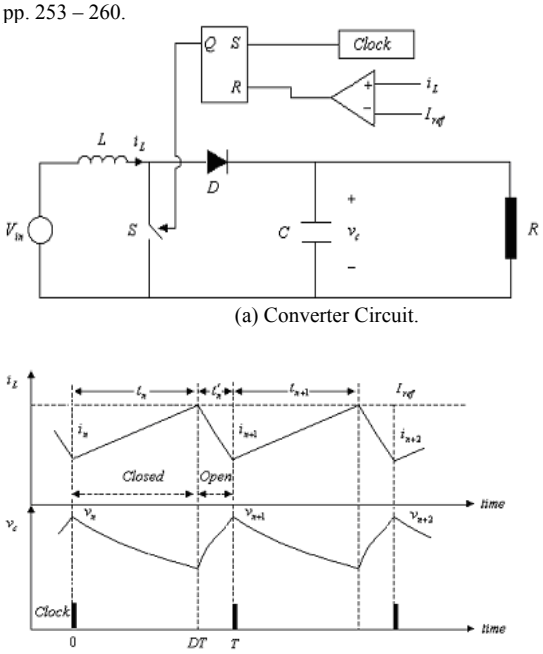

(a) Converter Circuit.

(b) Current and voltage waveforms.

Fig.1 Boost Converter Circuit.

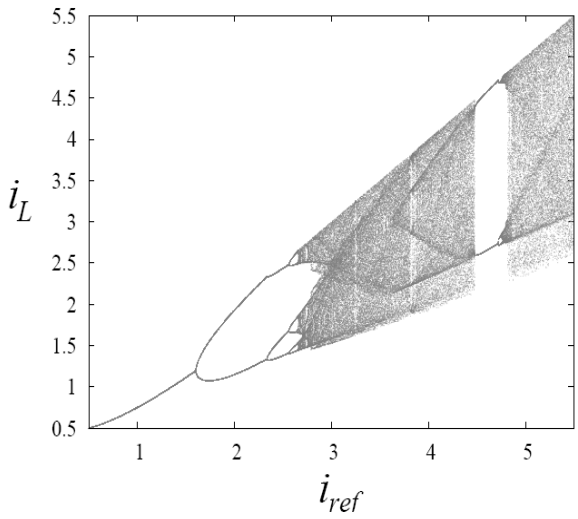

Fig. 2. Bifurcation diagram.

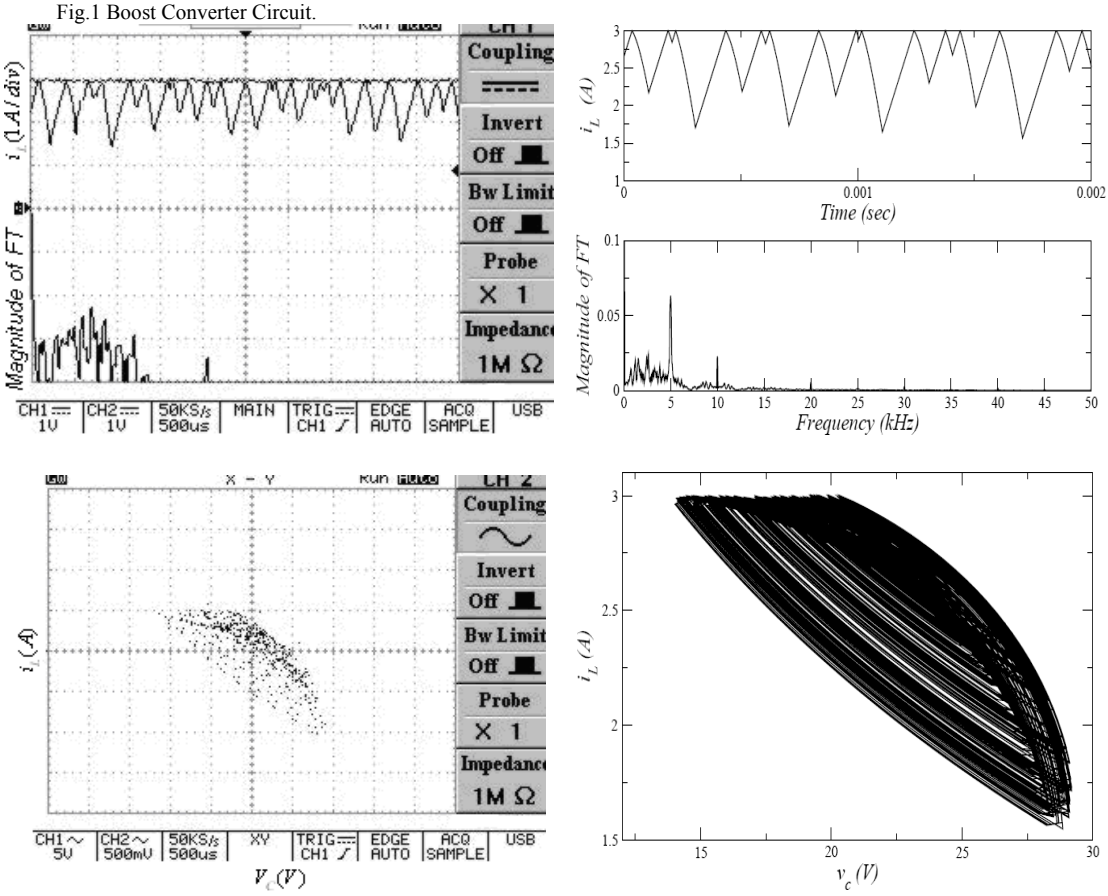

Fig. 3. Chaotic regime at I_{ref}=3A. Waveforms, Fourier amplitude spectra and phase portraits: experimental with 1A/V (left) and simulated (right).

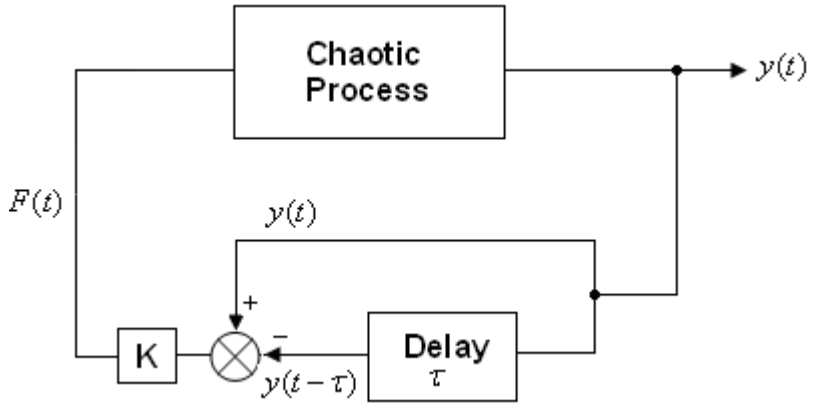

Fig. 4. Delayed-current feedback control system.

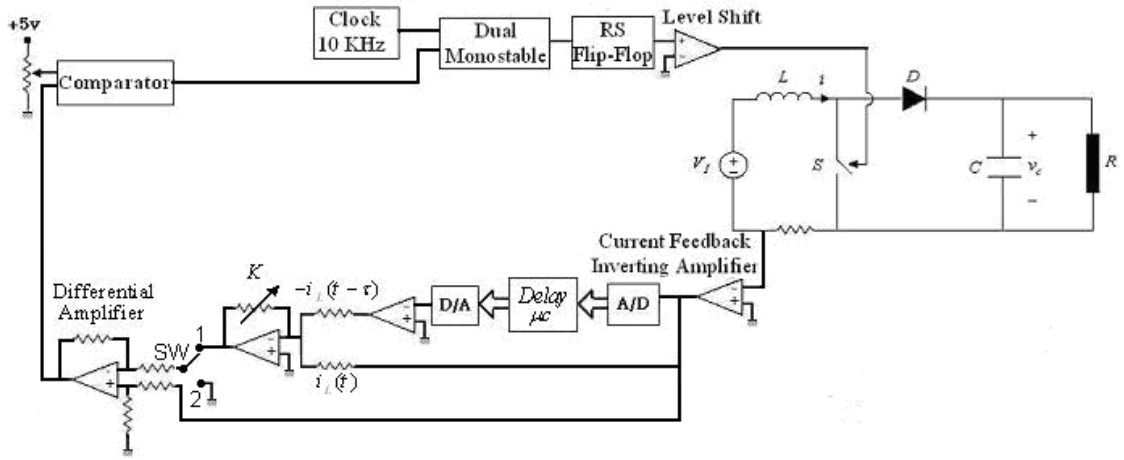

Fig. 5. Experimental feedback control scheme.

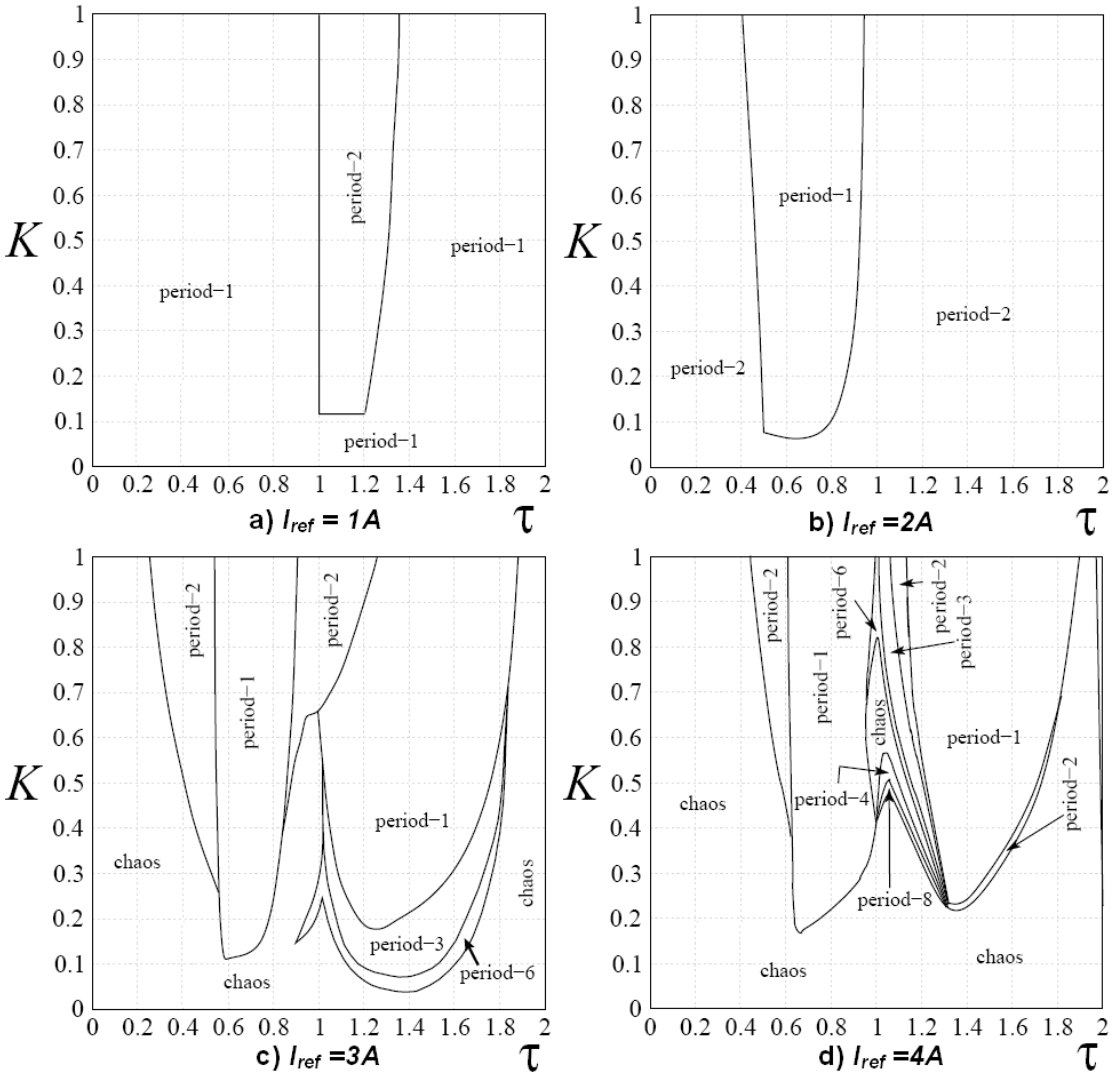

Fig. 6. Maps of regimes on the plane (τ,K) for various I_{ref}.

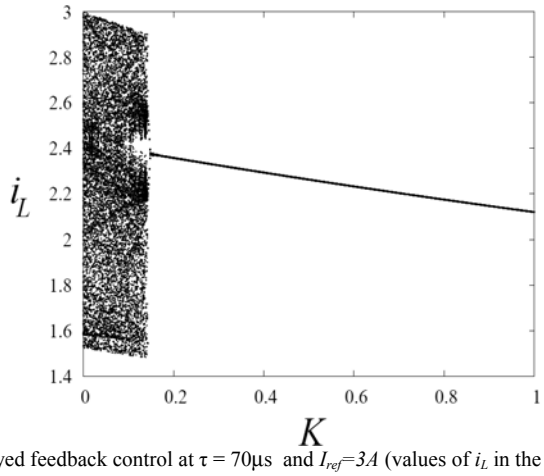

Fig. 7. Bifurcation diagram with delayed feedback control at τ = 70μs and I_{ref}=3A (values of i_L in the Poincaré section are shown against K).

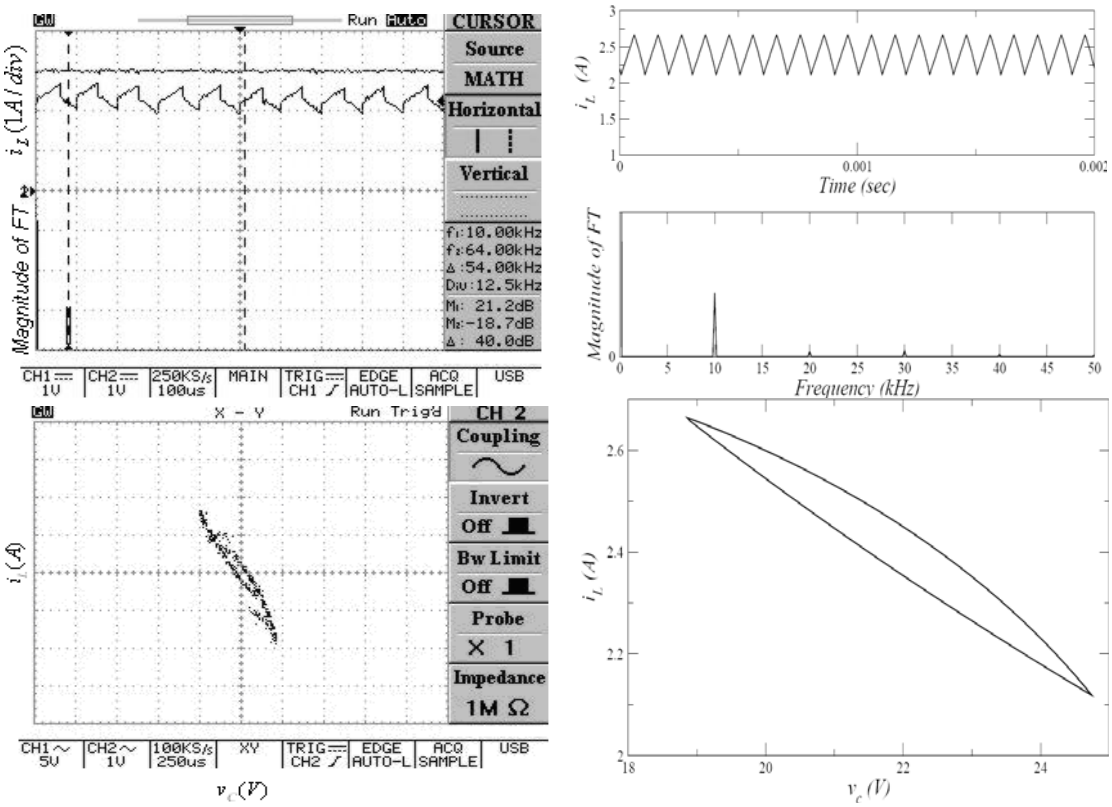

Fig. 8. Delayed feedback control at τ = 70μs, $I_{ref}=3A$, and K=1. Waveforms, Fourier amplitude spectra and phase portraits: experimental with 1A/V (left) and simulated (right).